

EXPERIMENTAL ANALYSIS AND
SIMULATION OF BACTERIA
CHEMOTACTIC BEHAVIOR IN
RESPONSE TO ANTIBACTERIALS

EXPERIMENTAL ANALYSIS AND SIMULATION
OF BACTERIA CHEMOTACTIC BEHAVIOR IN
RESPONSE TO ANTIBACTERIALS

By:

SARA JAHROMI, B.Sc.

Submitted to the School of Graduate Studies
in Partial Fulfillment of the Requirements for the Degree
Master of Applied Science in Biomedical Engineering

McMaster University

Winter 2019



BIOMEDICAL ENGINEERING

Masters in Applied Science in Biomedical Engineering

McMaster University, Hamilton, Ontario

TITLE: EXPERIMENTAL ANALYSIS AND SIMULATION OF
 BACTERIA CHEMOTACTIC BEHAVIOR IN RESPONSE TO
 ANTIBACTERIALS

AUTHOR: Sara Jahromi

SUPERVISOR: Dr. Zeinab Hosseini-Doust

 (Chemical Engineering, Faculty of Engineering)

Abstract

Bacteria plays an important role in a great number of biological reactions in living species, such as food digestion [1] or in natural environments, such as lakes and soil [2]. As bacteria's natural predators, bacteriophages target bacterial cells with high specificity. Co-discovered by Frederick Twort (1915) and Felix d'Hérelle (1917), bacteriophages (or for short "phage") were used as the sole antimicrobial for treatment of infectious disease, before they were overshadowed by antibiotics in 1940 [3]. However, the rising concern over antibiotic resistance in the past decade resulted in a renewed interest towards phage antimicrobials [4].

In this study I designed microfluidic devices for studying bacteria interaction with antibiotics and viruses. Motile bacteria cells can move toward chemo-attractant or away from chemo-repellents. Hence, I quantified bacteria response to these 2 stressors in term of total displacement of cells. In addition to the experimental results, I calculated bacteria displacement for control experiment and 2 stressors by simulation of bacteria chemotaxis. Comparing the simulation and experimental results in the experiments, I identified bacteria chemotactic sensitivity, X_0 , that relates chemical gradient concentration to chemotactic velocity.

For future direction of this study, we suggest designing and develop a microfluidic device able to separate bacteria by exerting different drag forces to different cells. Discrepancy in the chemotactic properties of a single bacterium, such as resistance

of the cell to a specific antibacterial, results in different chemotactic velocity of the cell. This distinct cell will move in a different chemotactic velocity compared to the rest of the homogenous population and hence will be exerted to a different drag force. With a proper design, different drag forces can direct cells to different chambers and hence separate cells with respect to their chemotactic response. Such a device can be used for detection of resistant bacteria to a specific antibacterial.

Acknowledgements

I would like to express my sincerest gratitude to Dr. Carlos Filipe and Dr. P. Ravi Selvaganapathy for their invaluable help and support. They both helped me a lot at a very challenging time and generously assisted me in this research.

I would like to thank my friend and colleague, Amid Shakeri (PhD candidate, Didar Lab, McMaster University), for kindly sparing his time to train me on microfabrication steps.

I also like to acknowledge Leticia Monteiro Gonçalves (Master's student, department of engineering physics, McMaster university) and Doris Stevanovic (research engineer, CEDT clean room facility, McMaster university) for training me on using the “ μ PG 101” direct writing system and clean room safety and operation and Dr. Marta Princz (research lab technician, Biointerfaces Institute, McMaster university) for helping me troubleshoot my work with the equipment and training me on many equipment in the Biointerfaces Institute, including the fluorescence microscope for imaging of the bacteria in my project.

I also like to take the chance to appreciate Mohmmadhossein Dabaghi (PhD Candidate, school of biomedical engineering, McMaster university), Neda Saraei (research assistant, school of biomedical engineering, McMaster university) and Alireza Shahin PhD Candidate, school of biomedical engineering, McMaster university), for helping me for the fabrication of my master mold and microfluidic devices.

I would also like to thank my friends in Biohybrids lab for their emotional support and all the memorable moments we had together.

To My Dad

There were days,

only thinking of you

would make me smile

days that nothing else could make me smile

Table of Contents

Abstract	iv
Acknowledgment	iv
List of Figures	x
List of Tables	xiii
List of Symbols and Abbreviations	xiv
Chapter 1. Motivation and Organization	1
1.1. Motivation and Objectives	1
1.2. Sequence of the Chapters	2
Chapter 2. Introduction	4
2.1. Introduction to Bacteria, Bacteriophages, Antibiotics and Their Interactions	5
2.2. Microfluidics for Studying Bacteria	8
2.3. Introduction to Photolithography and Soft Lithography	13
2.4. Introduction to Chemotaxis in Bacteria	17
2.5. Experimental Studies on Bacteria Chemotaxis	19
Chapter 3. Materials and Methods	28
3.1. Source of Chemicals and Reagents	28
3.1.1 Silicon Wafers	28
3.1.2 Photoresist	28
3.1.3 PDMS	29
3.1.4 LB media, BSA and PBS	29
3.1.5 Tetracycline and Ampicillin	29
3.1.6 <i>E. coli</i> Strain	30
3.1.7 T4 Phage Strain	30
3.2. Device Design and Fabrication	30
3.3. Device Preparation and Filling	35
3.4. Imaging and Sampling Method	36
3.5. Image Processing	39

3.6. Challenges.....	41
Chapter 4. Results and Discussion.....	45
4.1. Effect of Bovine Serum Albumin on Cell Adhesion to PDMS Walls	45
4.2. Bacteria Response to Antibiotic Challenge.....	47
4.3. Bacteria Response to Phage Challenge	54
4.4. Effect of Orientation on Bacteria Total Displacement	56
4.5. Statistical Analysis of the Results	59
Chapter 5. Simulations	64
5.1. Modeling of Chemotaxis.....	64
5.2. Geometry, Particle Properties and Initial Conditions	66
5.3. Effect of Convection on Bacteria Displacement	74
5.4. Calculation of Total Force Effective on Cells in <i>E. coli</i> -water System.....	77
5.5. Identification of X0 for <i>E. coli</i> -Ampicillin System.....	81
5.6. Identification of X0 for <i>E. coli</i> -T4 Phage System.....	83
5.7. Error Sources in Identification of X0, Chemotactic Sensitivity	86
Chapter 6 – Summary and Future Work.....	88
References.....	91
Appendix.....	103
A.1. Microscopy Images Control Experiments with and without BSA.....	103
A.2. Microscopy Images of Control Experiments (Water Treatment)	106
A.3. Microscopy images of Antibiotic Treatment Experiments	135
A.4. Microscopy images of PT_E1 and PT_E2.....	163
A.5. Governing Equations for the Simulation of Particle Tracing, Transport of Species and Fluid Flow	190
A.6. Bacteria Displacement According to Time.....	193

List of Figures

Figure 2.1. The structure of a bacterial cell. Adapted from [9] with permission granted from copyright clearance center.	5
Figure 2.2. An array of multi-colored squares	10
Figure 2.3. Schematic of photolithography and soft lithography steps. Adapted from [7] with permission granted from copyright clearance center.	14
Figure 2.4. Signal transduction pathways in an E. coli cell. adapted from reference [43] with permission granted from copyright clearance center.	18
Figure 2.5. Schematic of microfluidic experiment geometries and their methods for quantification of chemotaxis	26
Figure 3.1. Designed geometry of the device	32
Figure 3.2. Sampling spots for bacteria movement analysis	37
Figure 3.3. Different imaging areas	38
Figure 3.4. Modification of microscopy images and measurement of bacteria displacement using ImageJ	40
Figure 4.1. Total displacement of bacteria suspended in pbs (nbsa_c) and bsa 5% in pbs (bsa_c) after 60 minutes	45
Figure 4.2. Bacteria total displacement after 60 minutes in response to antibiotic and DI water at different positions	48
Figure 4.3. Different regions of bacteria movement analysis	50
Figure 4.4. a) Device before filling with pressurized flow. b) Exaggerated deformation pattern of the device due to pressurized flow	

	51
Figure 4.5. Bacteria total displacement after 60 minutes in PT_E compared to C_E at different positions	55
Figure 4.6. Bacteria total displacement at different positions and orientations, antibiotic and phage treatment experiments	57
Figure 4.7. Statistical analysis of antibiotic challenge experiments at constant distances from sub-inlet	60
Figure 4.8. Statistical analysis of antibiotic challenge experiments at constant angles	61
Figure 4.9. Statistical analysis of phage challenge experiments at constant distances	62
Figure 4.10. Statistical analysis of phage challenge experiments at constant angles	63
Figure 5.1. Inlets and outlets of the device for simulation of fluid flow	67
Figure 5.2. Simulated velocity field in microchannels after 60 minutes	68
Figure 5.3. Simulation results of chemical gradient of repellent inside the device at different timesteps	73
Figure 5.4. Displacement of bacteria after 60 minutes assuming rigid micro channels and no chemotactic response	75
Figure 5.5. Change in total error at first region with respect to different values of F_{squeeze} at this region	79
Figure 5.6. Change in total error at first region with respect to different values of F_{squeeze} at this region	80
Figure 5.7 Change in total error at the third region with respect to different values of F_{squeeze} at this region	80

Figure 5.8. Total error in bacteria response to antibiotic in experiments compared to simulations for different values of x_0 in the simulation	82
Figure 5.9. Total error in bacteria response to phage in experiments compared to simulations for different values of x_0 in the simulation	84
Figure 5.10. Velocity difference on the walls and in the midpoint of 2 adjacent pillars along the device	87

List of Tables

Table 2.1. Advantages and disadvantage of soft lithography	16
Table 3.1. Naming code of the experiments	34
Table 3.2. Optimized parameters for microscopy of the device	36
Table 5.1. Composition of total error for identification of x_0 for <i>E. coli</i> -Ampicillin system	80
Table 5.2. Composition of total error for identification of x_0 for <i>E. coli</i> -T4 system	82

List of Symbols and Abbreviations

2D	2-Dimensional
3D	3-Dimensional
Amp	Ampicillin
atm	Atmosphere
BSA	Bovine Serum Albumin
CW	Clockwise
CCW	Counter-clockwise
DI	De-ionized
DNA	Deoxyribonucleic Acid
<i>E. coli</i>	<i>Escherichia coli</i>
Eq.	Equation
HGT	Horizontal Gene Transfer
IPA	Isopropyl Alcohol
LB	Lysogeny Broth
MCP	Methyl Accepting Proteins
OD	Optical Density
PBS	Phosphate-buffered Saline
PDMS	Polydimethylsiloxane
PFU	Plaque Forming Unit
Phage	Bacteriophage

PPM	Parts Per Million
PR	Photo Resist
RNA	Ribonucleic Acid
Sh	Sherwood Number
Tet	Tetracycline
UV	Ultraviolet
WWII	World War Two

Chapter 1. Motivation and Organization

1.1. Motivation and Objectives

Combating pathogenic bacteria to cure bacterial infections has been of a high importance to save many lives during history. According to the 2016 Canadian Antimicrobial Resistance surveillance report [8] 5% to 80% of *Escherichia coli*, *Staphylococcus aureus* and *Klebsiella* tested strains have developed resistance to antimicrobial treatments worldwide. Although this number is stabilized or in some cases reducing in Canada [8], tackling this issue demands a deep understanding of bacteria defense mechanisms to antimicrobial treatments and will consequently, decrease the imposed costs to health care systems.

Investigating the relationship between bacteria and its predators, bacteriophages (or for short “phage”) and antibiotics, can help us to understand and control many of natural processes affected by these microorganisms. Thereupon, we can conclude that investigating of bacteria response to its killers, is vital for us to combat the great problem of bacteria resistance to antibacterials and win this war between human and bacteria.

The aim of my research is to investigate, quantify and predict the chemotactic response of bacteria to phage and antibiotics on the micron scale with the help of microfluidic platforms. Understanding bacteria response to antibacterials will help medical research community and pharma companies to better understand the mechanism behind bacteria resistance to phage and eventually optimize the process of phage development as an

alternative antibacterial therapy. The knowledge generated as a result of my research will serve to elucidate the mechanism(s) of bacterial escape from phage predation and other types of stresses and will be critical to developing bacteriophage-based therapeutics to treat infectious disease caused by bacteria resistant to available treatments.

To reach this goal, I could successfully calculate the chemotactic sensitivity of bacteria in response to T4 phage and ampicillin using simulations and experimental results. This developed method can be generalized for studying and quantifying bacteria chemotactic response to any other chemo effector. According to the aim of this study mentioned before, identification of this parameter for different systems of bacteria-chemo effector is essential for understanding the chemotactic behavior of bacteria and to demonstrate a good understanding of how bacteria respond to chemical attractants or repellents.

1.2. Sequence of the Chapters

The 6 chapters of this thesis are presents in a standard style. The sequence of the chapters is as described below:

Chapter 2 provides a detailed literature review on available microfluidic platform for studying bacteria response to different stressors and environmental conditions. Conventional methods to study bacteria response to different stressors are compared to

novel methods in chapter 2. Subsequently, an introduction to bacteria, antibiotics and bacteriophages are given in this chapter.

Chapter 3 describes the materials and methods following detailed description of the experimental setup and procedure. In this chapter I present the design criteria of the proposed device and extended fabrication process and techniques used for fabrication of the device.

Chapter 4 discusses the results and their analysis for all three different experiments of bacteria encounter with DI water, ampicillin and T4 phage.

Chapter 5 focuses on the simulation of all experiments using COMSOL Multiphysics and discuss the results obtained from these simulations. Parameters setup for the simulations and comparison of results from experiments and simulations are discussed in this chapter.

Chapter 6 focuses on suggestions to extend this study for future work.

Chapter 2. Introduction

The human body hosts a great number of bacteria that are essential for our health and well-being and regulate many vital processes such as food digestion or immune response. However, not all bacteria are beneficial to us; bacteria are also able to cause infectious disease. Co-discovered by Frederick Twort (1915) and Felix d'Hérelle (1917), bacteriophages were used as the sole antimicrobial for treatment of infectious disease, before they were overshadowed by antibiotics in 1940 [3]. As bacteria's natural predators, bacteriophages (bacterial viruses) can target bacterial cells with high specificity and devitalize the bacteria cell during a replication lytic cycle [5]. After the discovery of the first antibiotic in 1928 by Alexander Fleming, and the first clinical success of antibiotics in 1930, broad-spectrum antibiotics rapidly replaced highly host-specific bacteriophages in the Western Hemisphere. The Soviet Union however, not having easy access to western antibiotics during WWII and the cold war, continued to develop phage therapeutics to cure bacterial infections and phage-therapy is still being practiced in the former Soviet domain.

The rising concern over antibiotic resistance in the past decade has resulted in a renewed interest in phage antimicrobials [4]. while bacterial communities can evolve resistance towards phage as well, the mechanisms of bacterial resistance to phage are entirely different to that towards antibiotics [5][6]. The unique superiority of phage compared to antibiotics is that unlike antibiotics, phages have their own genetic information as DNA or RNA strands. Random mutations in phage's gene structure can cause development of new sub-populations of phage able to infect resistant bacteria to phage. This mutation in the

phage gene can cause phage to be effective on the resistant bacteria. Hence, the genetic mutations can help both bacteria and viruses to evolve and adapt new mechanisms to interact with each other by entering this co-evolutionary cycle.

2.1. Introduction to Bacteria, Bacteriophages, Antibiotics and Their Interactions

Bacteria are single cell microorganisms able to grow, move, metabolize and reproduce independently. Lacking a nucleus, nucleoid of bacteria consists of DNA strands alongside with ribosomes and plasmids floating inside the cytoplasm, surrounded by cytoplasm membrane, cell wall and capsule membrane respectively from inside to outside (Figure 2.1. The structure of a bacterial cell. Adapted from [9]). On bacteria's surface we can find "Pili" which help bacteria to attach to a surface and exchange genetic information with other bacteria and "flagella" which help bacteria to move by rotating in clockwise and counter clockwise directions.

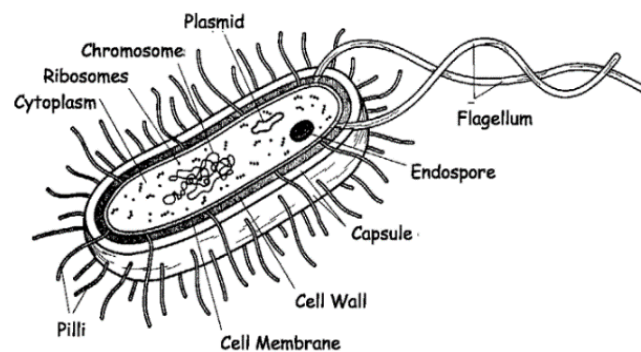


Figure 2.1. The structure of a bacterial cell. Adapted from [9] with permission granted from copyright clearance center.

Bacteriophages, phage, are described as bacteria's natural predators that can target bacterial cells with high specificity [10]. Bacteriophages were used as the sole antimicrobial for treatment of infectious disease, before they were overshadowed by antibiotics in 1940 [3]. Bacteriophage can regulate the population of its host, bacteria, and cause 2-10% of bacteria cell population to lyse per day [11]. The structures of phages are widely varied in different aspects. However, they all have a viral gene (single or double stranded DNA or RNA) and a symmetric protein encasement covering their gene called "Capsid". Viral capsids are formed of protein units called capsomers which are encoded by viral gene and their number and diversity are restricted by small size of viral gene. Compared to "Naked Viruses" which only have a capsid, in "Enveloped Viruses", the capsid itself is covered by a protein shell called envelope. As bacteria's natural predators, phage can attack its specific host bacteria by attaching to the receptors on bacterial membrane and injecting its genome into the bacteria using its tail. Since viruses are metabolically inert and dependent on their host to produce metabolic enzymes, they need to propagate new copies of their genome inside their specific host bacteria. Phage reproduction inside bacteria can go through two different cycles of "Lytic" and "Lysogenic". In a lytic cycle, phage will completely destruct and lyse the bacteria cell and new assembled viruses come out of the bacteria cell by bursting the cell membrane, while in a lysogenic cycle, phage continues to reproduce inside the bacteria and replicate their gene without killing the host cell (bacteria) [12].

Antibiotics are natural or synthetic chemicals that fight bacteria by either interfering with the formation of bacterial membrane or limit reproduction in bacterial cells. After

the discovery of the first antibiotic, penicillin, in 1928 by Alexander Fleming, and the first clinical success of antibiotics in 1930, broad-spectrum antibiotics rapidly replaced highly host-specific bacteriophages in the Western Hemisphere. The Soviet Union however, not having easy access to western antibiotics during WWII and the cold war, continued to develop phage therapeutics to cure bacterial infections and it is still being practiced in the former Soviet domain. More than discovery of antibiotic, Fleming also warned about developing resistant bacteria to penicillin by overusing this newly-discovered antimicrobial. However, growing success and popularity of antibiotics, prevented scientists to consider Fleming's concern about antibiotic resistance, important. No further than 1955, bacteria resistance to antibiotic was reported [13].

Among a population of bacteria challenged with an antibiotic or phage, several bacteria are resistant to the given treatments. Given that a population of bacteria with identical genetic information, some bacteria have different phenotypic information that enables them to develop defense mechanisms to different treatment, it is revealed that we need to study such bacteria in a single cell resolution to investigate their resistance development to treatments. The mechanisms by which bacteria develop resistant to a treatment can be either evolutionary which can be studied by investigating gene mutations in bacteria and the mechanisms to pass this genetic changes to other bacteria (such as horizontal gene transfer), or non-evolutionary such as spatial refuge, which is highly dependent on the geometrical landscape of the environment. In the evolutionary mechanism, random mutations of genes in some of the bacteria in a population may cause the bacteria to be resistant to antibiotic by mechanisms such as increasing drug

efflux [14]. When applied to antibiotics, these randomly mutated bacteria will survive, and all other bacteria will die. Having no competitor for food, these mutated resistant bacteria will grow widely and develop new generations of antibiotic resistant bacteria. The resistance genes can be passed thorough the bacteria populations by “Horizontal Gene Transfer” (HGT) process. Knowing that the bacteria owes its survival against antibiotics to its mutated genes, will specify the need to a smart antimicrobial such as bacteriophage to replace antibiotics. Although bacteria can also develop resistance mechanisms to phage predators by removing, changing or hiding the receptors on bacteria which help phage to bind to bacteria, independent viral gene of phages can help them to evolve as the bacteria do. The fact that both phage and bacteria have a genetic content as either DNA or RNA strands, makes them able to enter a co-evolutionary cycle to affect and regulate each other populations and change the defense mechanism of each entity in response to the other one as its predator [15]. In the co-evolutionary cycle of prey-predator, bacteria can evolve and develop new stratagem to defend phage infection. In the meantime, genetic content of phage can also allow it to co-evolve with bacteria and learn new ways to defeat evolved bacteria.

2.2. Microfluidics for Studying Bacteria

We can divide available methods for investigation of bacteria interactions with antibacterial into two groups of conventional and non-conventional methods. Conventional methods suggest co-culture of bacteria and antibacterials from either a clinical or an environmental strain in a biological laboratory, in corresponding media

and investigate any changes in the behavior of bacteria and the overall mortality rate confronting with these stressors. These conventional methods enhanced our knowledge of bacterial infections, possible treatment and different mechanisms leading to bacteria resistance to these treatments. The invention of first antibiotics, characterization of bacteria and basics of phage-bacteria interactions were only possible using the conventional batch culture of bacteria and it is beyond doubt that these methods offered valuable insight in all the mentioned areas and more. However, it is known that in each genetically identical population of bacteria there could exist multiple sub-populations which respond heterogeneously to a given treatment like antibiotic treatment or environmental stimulus[16] [17] [18] which cannot be studied in the batch culture of bacteria. Hence, it is revealed that accurate and comprehensive investigation of bacteria response to different stresses needs monitoring and studying of bacteria in a single cell resolution before, during and after exposure to different stresses such as antibiotic treatment or phage treatment. Figure 2.2 can better reveal the importance of single cell resolution in microbiology studies. Figure 2.2 shows a 10 by 10 array of squares are randomly colored using 5 different colors in the spectrum of yellow to red. Each of these colors can be described using 3 numbers of RGB color coding. However, if one is asked to describe the RGB color codes of the main square formed by 100 smaller squares, she is not able to provide an accurate answer. Although average RGB codes of all small squares may be able to give us an approximate understanding of the colors used in this array of squares such as tone of the used colors, but this understanding is neither accurate nor a discriminator of colors used in each different square.

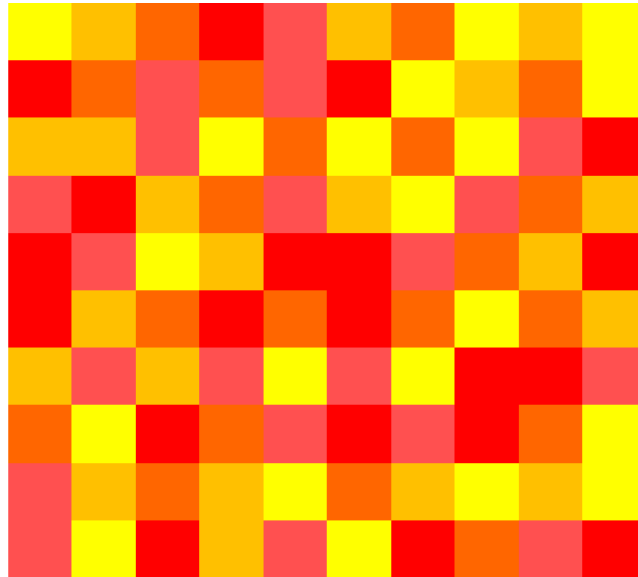


Figure 2.2. An array of multi-colored squares

A bacterial population formed by numerous cells of bacteria is similar to this multi-colored array of squares. Although the conventional methods for studying bacteria provided us with worthy information and for many years, was the only and most important available method for studying these population, developing antimicrobials and saving millions of lives, there is yet much valuable information shadowed by the effects of population study. While a population can show a drastic decrease in growth rate after exposure to an antibacterial, phenotypic differences of single cells in that very population, can cause single cells to be resistant to that antibacterial, or in general show a different behavior than the average behavior of the population. While these differences provide us with valuable information about antibacterial resistance, they can easily stay out of sight if we only rely on population level studies of bacteria.

Altogether, single cell studies of bacteria-phage communities can enhance our knowledge on the mechanisms and conditions governing bacteria behaviour and response to stresses and treatments which cannot be studied in the batch culture of bacteria due to its unspecific averaged characterization of results [19].

One of the available methods to study cells, including bacteria cells, in single cell resolution is microfluidic devices. Tunable perfusion of fluids and feasibility of manufacturing complex spatial geometries are particular advantages of microfluidic devices which help us to analyze bacteria-antibacterial interactions. In addition, microfluidic devices let us control micro scale transportation of bacteria, viruses and nutrients [20]. Therefore, utilizing all these facilities, we can mimic in-vivo microenvironment of the body or any other environment suitable for bacteria to grow on.

During the past few decades, Microfluidics application in biology is growing gradually [2]. The studies available on bacteria response to different stressors can be classified to the following groups: 1) investigation of bacteria response stimulated by attractant and repellent chemicals and biological agents. 2) investigation of bacteria response manipulated by geometry.

Salman *et al.* [21] used a one-dimensional temperature gradient generator to study the chemotaxis behavior of bacteria in response to heat stresses. The bacteria culture in this study tend to accumulate in the region of natural temperature at the beginning and move to lower temperatures later. Cell-cell communication of bacteria in critical concentration of cells appear to initiate a sharp pulse traveling wave that move faster

than the remaining of the population. Zhu *et al.* [22] concluded that the bacteria start to lose their ability to synchronize their chemotaxis response in high change frequency of spatial and temporal properties of attractant. Long *et al.* [23] studied bacteria chemotaxis response to high concentration of nutrient and chemical attractants in 2 different levels. 1) accumulation of bacteria in the region with high concentration of nutrient (or chemical attractant) and 2) secretion of signaling chemicals to inform the distant bacteria. Van Vilet *et al.* [24] co-cultured two different competing population of bacteria from opposite sides of a rectangular microfluidic channel. Each bacteria population formed a traveling wave moving toward the other population. They observed that once these 2 traveling waves meet each other, one population will take over most of the habitat. However, if these 2 populations are co-cultured together before entering the device, they tend to stay together and do not compete for space.

Mannik *et al.* [25] investigated motility and growth of *E. coli* and *B. subtilis* in micro channels with different diameters relative to bacteria diameter. The bacteria retained their motility in channels with width of 1.3 times of bacteria diameter. However, in channels narrower than 1.2 μm , *E. coli* showed a decrease in swimming speed and in channels as narrow as 0.4 μm , *E. coli* could only penetrate (not swim inside) the channel. After leaving these channels cells were misshapen in a wide variety of forms and sizes.

As another example of studying bacteria motility manipulated by geometry, Park *et al.* [26] launched a population wave of wild-type *E. coli* cells in a background environment

and observed escape and accumulation of the population into confining chambers through microchannels connecting the chambers to the background environment.

Using PDMS-based soft-lithography, microfluidics facilitates the single cell studies of bacteria populations due to its possibility for tunable perfusion of fluids, complex topographies, control of micro scale transportation of bacteria, phage and nutrients, as well as application of different chemical, thermal or pH gradients and get us closer to simulation of *in-vitro* environment in lab [27] [28].

It worth mentioning that microfluidics introduces several challenges to bacterial study too. The design and fabrication of a microfluidic chip for bacteria culture requires a high-level knowledge of fluid mechanic, biology and material science. In addition, the time and cost linked to design and fabrication process of such devices are not ignorable.

2.3. Introduction to Photolithography and Soft Lithography

Photolithography is the process of projecting a designated pattern onto a substrate coated by a photosensitive material called photoresist. This method is widely used to fabricate mold for microfluidic devices. In this method, a silicon wafer is used as a substrate and using spin coating method, a layer of negative or positive photoresist with designated thickness is coated on the wafer. The thickness of the photoresist layer is affected by parameters such as spin coating speed, volume of photoresist loaded on the wafer, and photoresist viscosity [29]. The photoresist is then covered with the designed mask and exposed to UV light. The designed pattern which is created on the mask is

usually a few times bigger than the desired dimensions and then will be rescaled to the final dimensions using a reduction optical lens [30]. This mask is not permeable to UV light, hence the areas covered by the mask will not be exposed to UV and the mask-less areas project the designed pattern onto the photoresist. In case of using a negative photoresist, unexposed regions (exposed regions for positive photoresist) can be washed away using proper developers. Finally, the designed pattern on the mask is projected on the silicon wafer and extruded with height of coated photoresist thickness and form the "master mold" (figure 2.3).

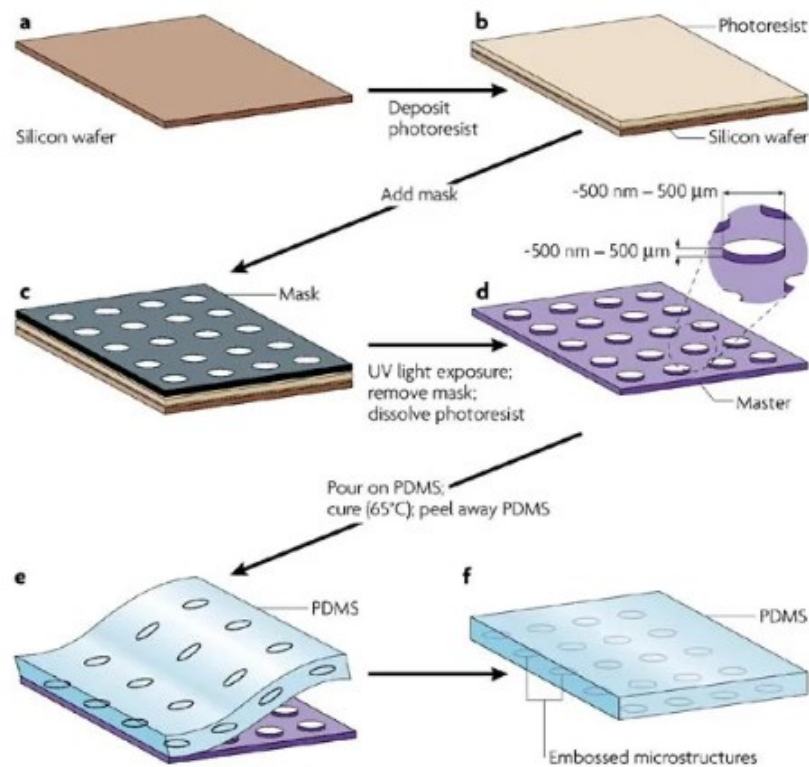


Figure 2.3. Schematic of photolithography and soft lithography steps. Adapted from [7] with permission granted from copyright clearance center.

In soft lithography, an uncured elastomeric polymer, usually polydimethylsiloxane or PDMS, will be poured on the master mold. Then the polymer will be cured and heated in the oven to solidify and form a block with the master mold pattern, hollow in it. The thin block of PDMS is then peeled off the master mold and attached to a glass substrate to form the final microfluidic device with designed channels and patterns on the master mold (figure 2.3).

While 3D printing is expensive and not easily accessible for fabricating microstructures smaller than 10 μm , several polymer-based microfabrication methods are employed for fabricating of microfluidic devices. Among all these methods such as 3D printing, etching, machining, deposition and wire bonding, soft lithography suggests the greatest advantages for fabrication of microfluidic devices. The advantages of soft lithography using PDMS polymer are listed in table 2.1 [31], [32]. As mentioned in table 2.1, cured polydimethylsiloxane (PDMS), as the base material in soft lithography, is transparent, which facilitate microscopy and real time imaging and monitoring of these devices. PDMS is also permeable to oxygen which makes PDMS-based microfluidic devices a suitable option for culturing cell and bacteria [27]. In addition, PDMS is biocompatible, chemically inert and the most important of all allows for perfect replication of micro and nano structures designed on mold [33]. Hence, PDMS is known as one of the best polymers for fabrication of microfluidic devices [34].

Table 2.1. advantages and disadvantage of soft lithography

Advantages	Disadvantages
Ability to create complex geometries	Not efficient for batch production
High resolution (features in nanoscale)	Low commercial availability
Cost effective	Not able to create grayscale geometries
Possibility of microscopy imaging due to PDMS transparency	Needs complicated and time-consuming preparing steps
Reusability of master mold	
Permeability to gas (oxygen)	

As discussed here, conventional photolithography process needs fabrication of mask for each different design. Any trivial change in the design of the device, need a new mask designed and fabricated. This step makes the photolithography process expensive and sometimes cumbersome. A set of masks needed to fabricate a chip can be the most expensive material in the fabrication step and may in some cases cost even more than \$2 million [35]. However, usually there won't be more than a few chips fabricated using those masks [30]. The great amount of time and cost needed to be spent on fabrication of masks, decreases the efficiency of photolithography for non-batch production applications such as research projects [36].

To confront these problems and reduce the cost and time of microfabrication process, different mask-less methods are developed. In this project, a direct writing machine is used to fabricate the master mold. The “ μ PG 101” direct writing system is developed

by “Heidelberg Instruments” company and is capable of create patterns on substrates using UV laser with a high writing speed (up to $90 \frac{mm^2}{min}$) and ability to create small features resolution (up to 600 nm) [37].

2.4. Introduction to Chemotaxis in Bacteria

Each motile bacterial cell can rotate its flagella to swim and move toward (or away) attractants (from repellents). Bacteria movement process in a neutral environment consists of two different steps: periods of moving in a random direction with an average speed of 20 [38] to 28 $\mu\text{m/s}$ [39] [40] (last about 1 second) called “free run” and periods of random reorientation (approximately 0.1 second) [38] called “tumble”. Frequency of these two steps causes bacteria random walk in absence of attractant or repellent factors. In non-neutral environments, bacterial cells cannot feel gradient of attractant (or repellent) along their length due to their small size and hence cannot promptly choose the best direction to move. Favorable moving direction in bacteria in these environments is decided through a series of complicated reactions inside the cell that cause the flagella to rotate clockwise (to randomly reorient the cell) or counter-clockwise to move the bacterium toward the chosen direction and create bacteria “biased random walk” [41]. Figure 2.4 [43] shows signal transduction pathways in an *E. coli* cell. 4 (Tsr, Tar, Trg and Tap) out of 5 receptors inside a bacterial cell are able to regulate bacteria chemotaxis by changing the rate of autophosphorylates in CheA. The protein CheW connects these receptors to a histidine kinase called CheA.

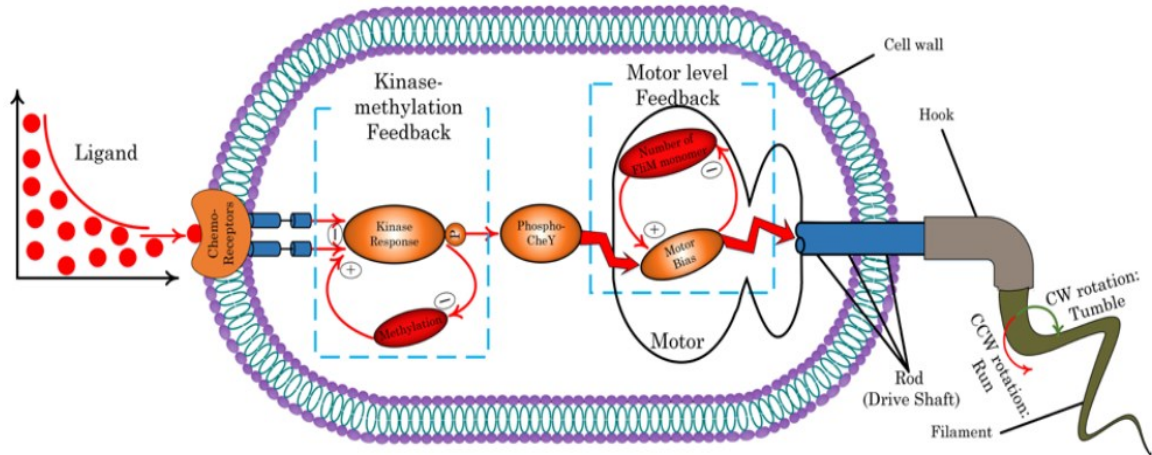


Figure 2.4. Signal transduction pathways in an *E. coli* cell. adapted from reference [43] with permission granted from copyright clearance center.

In case of bacteria interaction with a chemoattractant, the rate of phosphorylation will decrease in CheA and CheY, a protein responsible to control the frequency of tumbles in flagellar motor. This will decrease the frequency of tumbles and bacterium will continue its run cycle for a longer time without reorientation. In case of interaction with repellents, tumble frequency will increase due to higher rate of phosphorylation in CheY and CheA [42] [43] [44]. Bacterium will then compare the time derivative of attractant (or repellent) concentration in current direction and previous directions and increase (or decrease) the “run” period length toward the more suitable direction.

2.5. Experimental Studies on Bacteria Chemotaxis

Motile cells (including bacteria) play important roles in many aspects of life. Contamination of soil and water sources, biological decontamination and water source treatment, growing patterns in plants roots, biofilm formation process, propagation of cancer cells inside body and their response to drugs are a few examples of many that are affected by motility in different cells. Chemotaxis, the ability of cells to relocate in response to a chemical gradient, is one of the methods adopted by motile cells to move and displace in their habitat. While some studies use mathematical models to characterize chemotaxis, there are experimental methods developed to quantify this movement in cells. As an example of mathematical methods, Ford *et al.* (1990) [45] used a mathematical model of a stopped-flow diffusion chamber to measure bacteria motility in response to a chemical gradient inside the chamber and they characterized bacteria chemotaxis in terms of chemotactic sensitivity, X_0 (a parameter that proportionally relates the velocity of chemotactic cell to the gradient of chemical in which the cell is swimming), and random motility coefficient, μ (can be interpreted as a diffusion coefficient of the cell particles in the population). As for experimental analysis, there are different conventional and new methods to quantify and analyze chemotaxis in bacteria and other cells. In conventional methods, cells were usually spread on soft agar containing a nutrient gradient. The ring formed by population of the cells following the gradient was quantified in order to analyze chemo taxis behavior [44]. In this section I focus on experimental methods to study chemotaxis in cells.

As discussed in the review paper of Xiao-Qian *et al.* [46] many different methods are available to study chemotaxis of bacteria. Some of these methods can only provide us with qualitative analysis of bacterial chemotaxis, among them capillary assays, stopped-flow diffusion chambers, and swarm plate assays [47]. Meanwhile, methods such as tethering assays and automated tracking of swimming cells can study and quantify chemotaxis in single cell resolution. However, shortcomings of these conventional methods such as poor reproducibility and complication of experimental equipment can affect the precision of these studies. Among new methods developed to overcome these obstacles, microfluidics provides valuable features to study chemotaxis in bacteria and other cells. This leads us to another point of view for classification of studies on chemotaxis: “microfluidic and non-microfluidic methods”. In the following section, I first briefly mention a few non-microfluidic studies and then follow this chapter by presenting some examples of microfluidic methods to study chemotaxis in cells and specifically bacteria.

Bacteria quantification inside a specified area in microfluidic platforms is one of the most prevalent methods to quantify bacteria chemotaxis [48] [49]. Kojima *et al.* [50] related the number of bacteria in a micro-sensor to the capacitance of two embedded electrodes inside the chip. Their fabricated micro-sensor can eliminate the need to manually count the bacteria under microscope or using computer software and can be used to study chemotaxis in bacteria toward or away from unknown chemo effectors in large scale. Among other common methods to characterize chemotaxis in cells, I can

mention fluorescence measurement [51][52] and OD measurement in a sample of bacteria exposed to chemo effectors.

Tena-Garitaonaindia *et al.* [53] used a modified capillary assay (described in [54], is a method developed by Adler to quantify bacteria chemotaxis using the number of bacteria attracted to an attractant inside a capillary) to study halophilic bacteria chemotaxis in response to environmental pollutants (phenol and naphthalene) that react as chemoattractants for these bacteria. To measure bacteria chemotaxis in this study, bacteria were incubated in direct contact with a capillary tube filled the desired chemoattractant for one hour. Then the bacteria suspension was plated on agar plates and the number of colonies formed on the plate were counted after 24 hours of incubation at 32° C. The CFU count of bacteria was considered as a parameter to quantify bacterial chemotaxis. The results from this study indicates that a concentration of 100–1000 ppm of phenol and 100–500 ppm of naphthalene acts as chemoattractants for halophilic bacteria.

Virgile *et al.* [55] developed a control system to guide engineered *E. coli* cells toward a region of interest using the chemotactic behavior of cells in response to hydrogen peroxide. To characterize this guidance system, Virgile *et al.* plated *E. coli* in the middle of agar plates and then they poured hydrogen peroxide mixed with warm motility agar on the plates to create a gradient of hydrogen peroxide. The plates were incubated at 30° C for 18 hours. The diameter of the bacteria ring grown on the plate in different concentrations of hydrogen peroxide was an indicator of chemotaxis response for that concentration.

Abe *et al.* [49] measured chemotaxis of *Salmonella enterica* cells toward a capillary with internal diameter of 5-10 μm containing 1000 mM serine solution by counting the number of cells overtime inside a square area of $80\times 80 \mu\text{m}$ around the tip of the capillary. They also observed convective flow around the capillary caused by motile cells after the number of cells reach a threshold which can be related to different chemotaxis rates in response to different initial concentrations of chemoattractant.

Tunchai *et al* [56] characterized negative chemotactic response of *R. pseudosolanacearum* to maleate using computer-assisted capillary assays. Based on their observations, normalized cell number (ratio of number of cells accumulated close to the tip of a capillary containing chemorepellent at each given time to the initial number of accumulated cells) decreases as the concentration of maleate increase in the capillary from 0 to 5 mM. They validated the toxicity of maleate to *R. pseudosolanacearum* using experimental results showing a decrease in growth of *R. pseudosolanacearum* culture by 30% at maleate concentration of 5 mM. They studied 22 different strains of mutant *R. pseudosolanacearum*, each of them distinguished from the others by elimination of one of the methyl accepting proteins (MCP). Hence, they could successfully identify the MCP responsible for negative chemotactic response of *R. pseudosolanacearum* to maleate.

The mentioned studies are focused on bacteria chemotaxis quantification using non-microfluidic methods. The following paragraphs reviews a few studies on chemotaxis of bacteria using microfluidic methods. Figure 2.5 shows a schematic of these

microfluidic experiments and the chemotaxis quantification method for each experiment.

Murugesan *et al.* [57] studied *E. coli* response to different concentrations of sorbitol (as a chemoattractant) and NiSO₄ solution (as a chemorepellent) inside a diffusion based microchannel. They quantified rate of migration of bacteria in terms of the change in ratio of N to N_{avg} over time, where N is the number of cells at a specific time step and N_{avg} is the number of cells before the initiation of the chemical gradient. While bacteria showed no chemotactic response in low concentration of sorbitol (0.01 mM), initial sorbitol concentration of 1 mM caused accumulation of bacteria to the sorbitol side of the device and concentration of 100 mM caused negative chemotaxis in *E. coli* cells. NiSO₄ acted as a chemorepellent at both initial concentrations of 1 and 10 mM but did not activate bacteria chemotactic response at concentration of 0.1 mM.

Brumley *et al.* [58] designed a microfluidic device to mimic the nutrient gradient conditions that bacteria face in the oceans to measure bacteria motility response to nutrient pulses in such environments. They recorded trajectories of over one million cells in response to nutrient gradient inside the device. Based on their observations cells can only move toward an unsteady nutrient source when the gradient signal of the source is not affected by the noise in bacteria sensory system for chemical gradient. The results obtained from this study were validated using numerical simulation of chemotaxis in cells.

Jin *et al.* [59] modeled the chemotaxis of microorganism using oil-in-water droplets. They observed chemotaxis of these droplet swimmers inside a maze. High concentration of the chemoattractant (surfactant) in the outlet of the maze creates a chemical gradient along the shortest path from inlet to outlet. The droplet swimmers solve the maze by climbing up the chemical gradient and moving toward the higher concentration of chemoattractant.

Gu *et al.* [60] study the effects of fluid flow velocity, concentration of chemicals, chemical solution viscosity and dimensions of the microchannel on the gradient formed by different gradient generators which are used to study motility in cells. They design a microfluidic gradient generator to measure and minimize the effect of convective flow on cells. The chitosan membranes used to separate 3 different channels (source channel, gradient channel and sink channel) prevent convection from one channel to the other, however, allows the sink and source channel to create a chemical gradient inside the gradient channel through diffusion.

Studies on chemotaxis in bacteria cover many chemoeffectors and classify them as chemoattractant or chemorepellent at different concentrations, spatial conditions and different scales from single cell studies to population level studies. However, they are more frequently focused on bacteria response to attractants and favorable agents for bacteria to characterize bacteria response to attractants and study the pathways that regulate bacteria flagellar motion in positive gradients (towards attractants), hence there are yet more areas to be covered to have a full understanding of bacteria and other cell's response to negative chemoeffectors. Since the receptors and their effective

pathways linked with negative chemotaxis are different from the ones of positive chemotaxis response, we need studies that are focused specifically on cell's response to chemorepellents to completely comprehend the biological phenomena behind this response. Moreover, despite of attractant response, bacteria response to bacteriophages (as a biological stressor) or other repellents is less commonly studied using microfluidic platforms. We need to characterize biological (bacteriophage) repellents for each system of bacteria-repellent to move towards a full understanding of their interaction, how they affect one another and how bacteria can be threatened by these agents. Although characterization of bacteria response to bacteriophages is a crucial step towards development and optimization of new therapeutic methods to cure bacterial infections, they are not well-studied using robust and innovative platforms like microfluidic devices. Invaluable features suggested by microfluidics allow us to study bacteria interactions with different biological and chemical repellents in a single cell resolution, quantify their response and extend the results of this quantification to different conditions. The aim of this study is to use microfluidic platforms to focus on studying bacteria interaction with bacteriophage (as a biological repellent) which is less frequently covered in the available literature. The interaction between *E. coli* and T4 bacteriophage has not been studied inside microfluidic devices in single cell resolution before. In this study, I treat T4 phage as a repellent chemical (and not a biological repellent) because I am not looking into the biological phenomena behind bacteria response to phage.

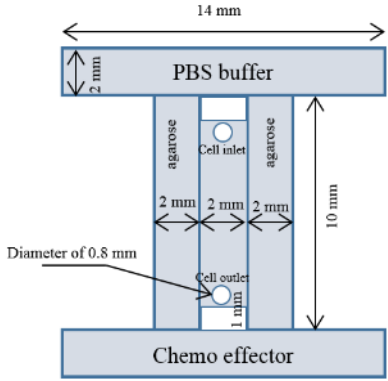
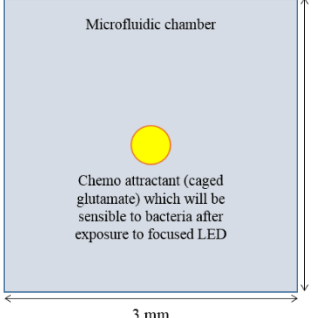
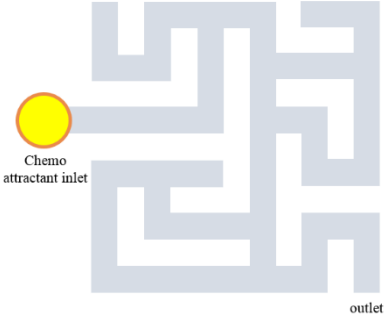
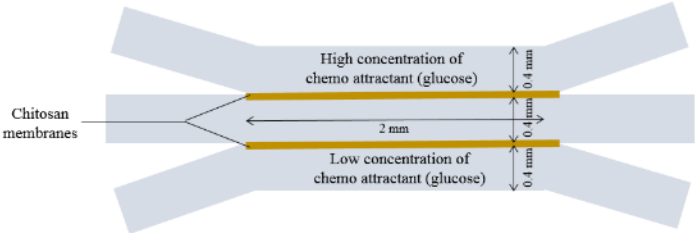
	Geometry	Quantification of Chemotactic agent
a)		<p>Change in number of bacteria cells inside the middle chamber during time after initiation of chemotactic gradient (measured for different concentrations)</p>
b)		<p>a) Measurement of the angle between cell's position vector (connecting cell to the center of chemical gradient) and cell velocity vector b) ratio of cell's concentration to background concentration of cells in a specified area</p>
c)		<p>Plotting the change in trajectory length of droplets that solved the maze against the time they entered the maze (the later cells enter, the stronger the chemical gradient)</p>
d)		<p>Measurement of tracer particles velocity (to quantify the flow forming the chemical gradient). Chemotaxis can be quantified as the ratio of cells present at a specified area close to top membrane to bottom membrane for future possible studies.</p>

Figure 2.5. Schematic of microfluidic experiment geometries and their methods for quantification of chemotaxis

Bacteria are known to have negative and positive autochemotaxis in response to chemoeffectors secreted by the cells [61]. This means even in response to a biological repellent (such as bacteriophage), bacteria will secrete chemorepellents (cell-cell communication) to enhance negative chemotactic response in the population (in addition to direct effect of phage on bacteria). Hence, I can define and quantify chemotactic response of bacteria to T4 phage although using the term “chemotaxis” for bacteria response to phage is not accurate. I also study bacteria interaction with antibiotic to quantify the response of bacteria to a gradient of these 2 repellents. The study of bacteria in response to repellents (and specifically ampicillin and T4 bacteriophage) and identification of bacteria chemotactic sensitivity coefficient (a parameter to quantify chemotaxis response) in these systems using experimental and simulation results have not been conducted in the previous researches. This method can be extended to any other system of bacteria-repellent/attractant reaction in order to identify chemotactic sensitivity and measure bacteria response to that specific agent or chemoeffector.

Chapter 3. Materials and Methods

3.1. Source of Chemicals and Reagents

In this section, all the materials and biological agents used for device fabrication, sample preparation, and other steps are introduced.

3.1.1 Silicon Wafers

I used 4-inch diameter silicon wafers supplied from University wafer, MA, USA as substrate for fabrication of the mold.

3.1.2 Photoresist

Positive and negative photoresists are two different groups of available photoresists for photolithography. Positive photoresists will be more soluble to their developer after UV exposure due to change in their chemical structure. In positive photoresists, the pattern exposed to UV light (not covered by UV blocking mask) will be removed after washing the substrate by photoresist developer. On the other hand, UV exposure crosslinks the building block of negative photoresists and this type of photoresist will be insoluble in photoresist developer unlike the non-exposed areas. In this thesis, I used SU-8 5 photoresist which is a negative photoresist and suitable for creating the PR thickness of 10 μm desired for this design. This photoresist was kindly donated from Dr. selvaganapathy's lab in McMaster university, department of mechanical engineering.

3.1.3 PDMS

I used Sylgard 184 silicon elastomer kit for fabrication of microfluidic devices using the fabricated master mold. Polydimethylsiloxane or PDMS is a transparent polymer with chemical formula $\text{CH}_3[\text{Si}(\text{CH}_3)_2]_n\text{Si}(\text{CH}_3)_3$ and the most common material used for micro fabrication. I supplied the PDMS used in this project from Sigma Aldrich in form of SYLGARD® 184. Also, some of the PDMS I used in this project was generously donated from Didar Lab, McMaster university, department of mechanical engineering.

3.1.4 LB media, BSA and PBS

LB media, BSA and PBS stocks were purchased from Sigma Aldrich. I used standard protocol to prepare LB liquid media and LB agar plates for culture of bacteria. I prepared PBS at 1X concentration and for loading bacteria inside the device, I suspended bacteria in BSA 5% in PBS.

3.1.5 Tetracycline and Ampicillin

I sourced both antibiotics used in this study from Biohybrids Lab stock. I used Tet for culturing *E. coli* ER2738 strain and Amp (10 µg/mL) as one of the stressors introduced to bacteria. The ampicillin was diluted in DI water from amp stock at concentration of 100 mg/mL.

3.1.6 *E. coli* Strain

I used *E. coli* ER2738 strain for this study. This strain of *E. coli* (genotype: F'proA+B+ lacIq Δ(lacZ)M15 zzzf::Tn10(TetR)/ fhuA2 glnV Δ(lac-proAB) thi-1 Δ(hsdS-mcrB)5) is resistant to Tetracycline and fluorescent tagged on mRuby protein. This strain was gained from Biohybrids Lab stock.

For each experiment I picked a single colony of *E. coli* ER2738 cultured on a Tetracycline LB agar plate. Then I grow bacteria inside culture tubes containing LB and incubate to OD=1. I use fresh culture from the tubes for filling each device for all the experiments

3.1.7 T4 Phage Strain

I used T4 bacteriophage in this study which infects *E. coli* bacteria. The T4 strain used in this project was sourced from Biohybrids Lab stock. The concentration of phage suspension used in this study is at concentration of 10^8 PFU/mL.

3.2 Device Design and Fabrication

Figure 3.1 shows the designed geometry and the notation and naming system used in this report. This design has 2 main channels connected to inlets and outlets, one square lattice with pillars designed inside to maintain the structure of square lattice and prevent buckling and two sub-inlets which connects the main channels to the square lattice. The

main channels are both 1 cm long and 400 μm wide. I designed the main channels long enough to ensure that fluid is fully developed after leaving the inlets and before reaching the sub-inlet and entering lattice. The square lattice is 2 mm by 2 mm and the 20 by 20 array of pillars inside it are 50 μm by 50 μm squares. The sub-inlet is 40 μm long and 5 μm wide. The designed sub-inlet has the optimum dimensions (compared to a single bacterium cell diameter of 200 to 400 nm and length of 2 μm) to ensure that bacteria cells swimming inside the fluid can easily enter the square lattice one by one following the fluid flow and won't be able to leave the lattice through the sub-inlet as easy. The sides of the square lattice are rotated 45 degree relative to the main inlets to help filling the device better, since the velocity of fluid inside the connecting channel has components in the direction of both sides of the square lattice. In each experiment, after washing the device with PBS, I seed the device with bacteria using one of the main channels and introduce water or stressors (antibiotic or phage) to the bacteria population through the other main channel. The designed device is 10 μm in height uniformly and controlled by the thickness of the photoresist coated on the silicon wafer substrate. This height for channels is proved to provide a single layer of bacteria inside the geometry in similar studies [23] which is crucial for microscopy and high quality of imaging and further analysis of images. As the bacteria movement is neglected along the height of the channels, all the simulations in this study are considered in 2D.

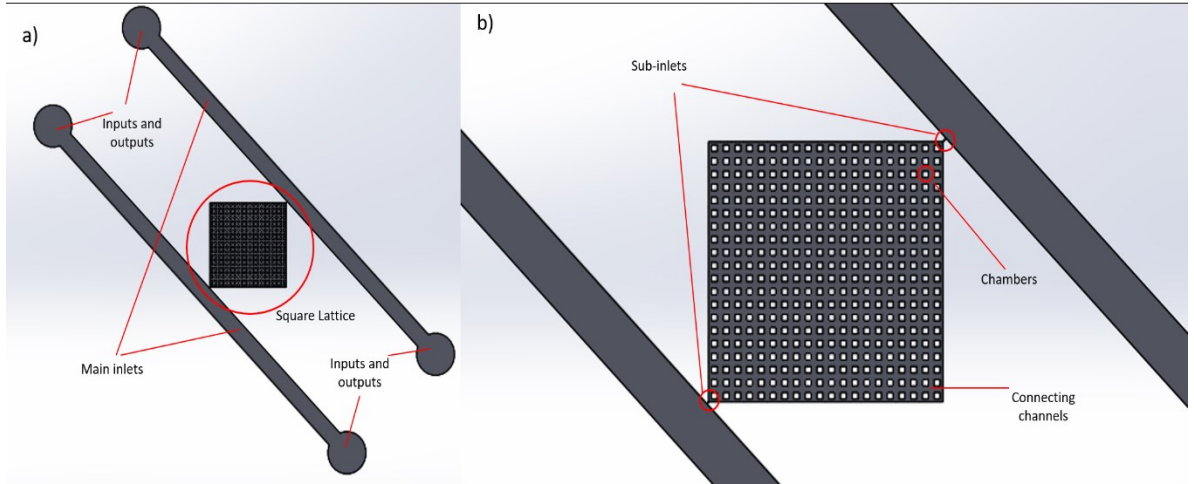


Figure 3.1. Designed geometry of the device

In this section, I explain the fabrication process of the designed device in details. I first fabricated a master mold relative to the design and I used this mold for fabrication of multiple devices. Mold fabrication steps are as followed:

I first soaked a silicon wafer in acetone for 2 minutes and then in methanol for 2 minutes and finally in DI water for 5 minutes. I then dried the wafer with a nitrogen gun and baked at 200° C for 5 minutes to assure evaporation of all cleaning substances. In the next step, I treated the substrate using plasma oxidization at 50 W for 2 minutes. To coat the silicon wafer with a 10 μm thick film of photoresist, I dispensed 1 mL of PR SU-8 5 per 1 inch of wafer of and spread it using the spin coater (from 0 rpm to 500 rpm with a rate of 100 rpm/sec and then to 3000 rpm with a rate of 300 rpm/sec and hold for 30 seconds). Then I baked the coated wafer on a hot plate at 65 ° C for 2

minutes and afterward at 95 ° C for 5 minutes (soft bake). To crosslink the photoresist and harden the designated area using UV light, I exposed the substrate “μPG 101 Direct Writing System”¹ [settings used for 10um thickness: 50 mW at 100% intensity; filter OFF; write head mode III; overlap x1; focus 0 or 1; energy mode x1]. It is worth mentioning that I found the optimum intensity of UV laser emitted by μPG 101 direct writing machine with series of trials and errors. Low UV intensity results in detachment of the whole photoresist from the wafer in developing step and high intensity will increase the exposure time. Hence the best UV intensity is the minimum intensity (to decrease fabrication time and cost) that has enough exposure energy to crosslink photoresist polymer and guarantee full attachment of photoresist to the substrate at desirable areas. Subsequently, I baked the wafer on a hot plate at 65 ° C for 1 minute and afterward at 95 ° C for 5 minutes (post exposure bake). To develop and stabilize the photoresist, I soaked the wafer in SU 8 developer for 2 minutes. Rinse with isopropyl alcohol (IPA) and then dry with gentle stream of nitrogen and baked the wafer on a hotplate at 200° C for 2 minutes (hard bake). I then treated the mold using oxygen plasma treatment at 50 W for 5 minutes to increase surface hydrophilicity and ease detachment of cured PDMS from mold in the next steps. Since removing of poured PDMS from the silicon wafer in fabricated prototypes was challenging, in the next step I placed the wafer inside a vacuum chamber with 200 μL of Trichloro(1H,1H,2H,2H-perfluorooctyl)silane under vacuum for 3 hours and keep in oven at 60 °C overnight.

¹ <https://www.himt.de/index.php/upg-101.html>

After this step the master mold is stabilized and can be used for a long time to fabricate multiple devices.

To make devices using the master mold I followed standard soft lithography steps described here. First I poured PDMS and curing agent (PDMS Kit-Sylgard 184) in a dish with a ratio of 10:1 and mixed vigorously and then placed the mold substrate in a petri dish, poured the mixture on the mold and left the dish inside a vacuum chamber for 30 minutes to remove any bubbles created during the mixing process. Then I cured PDMS on a hot plate at 180 °C for 10 minutes before cutting the edges of PDMS block and peel of PDMS from the silicon substrate. To allow introduction of fluid to the device, I punch inlets and outlets using a PDMS puncher with the appropriate size. To enclose the fabricated device, I first placed the PDMS block and a glass slide inside a centrifuge tube filled with ethanol and sonicate for 2 minutes. After full evaporation of liquids from the glass and PDMS surface, I plasma oxidized the PDMS block (the surface that has channels on it) and the glass slide at 50 W for 5 minutes. Following this step, the oxidized surfaces of glass slide and PDMS block easily attach to each other and form a bond in between by slightly pushing them together. Inlets were then connected to a syringe pump using syringe needles and Tygon tubing and all inlets and outlets were sealed using epoxy glue. Since the epoxy glue is fluorescent and can interfere with fluorescence microscopy imaging of the bacteria, the imaging area should be clear of epoxy glue.

3.3. Device Preparation and Filling

Before starting each experiment and treat bacteria with water or different stressors (antibiotic or phage), I prepared and seeded bacteria into each device using the following protocol:

First, I wash the device with PBS for 10 minutes with a flow rate of 0.5 mL/h to wash away all the dust and particles and any possible contamination inside the channels. Then I load bacteria culture (*E. coli* ER2738) suspended in 5% BSA in PBS and OD=1 inside the device using flow rate of 0.01 mL/h for 30 minutes and then leave the device on bench for 1 hour with sealed inlets and outlets before introduction of phage, antibiotic or water to the seeded bacteria.

Table 3.1 shows a list of experiments with their name coding used in this report. This table shows the naming system for easier referring to the experiments. Experiments for control and both stressors (antibiotic or phage) are categorized and named in this table. As shown in table 3.1, the experiments in this study are categorized into 3 groups. In the first group, control experiments, after seeding the device with bacteria, I treat the bacteria with DI water and measure bacteria response to DI. For this purpose, I run DI water into the device through one of the main channels at a flow rate of 0.01 mL/h for 1 hour. For the next groups of experiments, antibiotic treatment and phage treatment, I run antibiotic solution and phage suspension respectively through one of the main channels at a flow rate of 0.01 mL/h for 1 hour.

Table 3.1. Naming code of the experiments

	Water	Antibiotic Treatment	Phage	BSA	NO BSA
	Control	(Ampicillin)	Treatment (T4)	Control	Control
Experiment 1 (E1)	C_E1	AT_E1	PT_E1	BSA_C	NBSA_C
Experiment 2 (E2)	C_E2	AT_E2	PT_E2		

3.4. Imaging and Sampling Method

As shown in figure 3.2, for analyzing each image, I defined 3 different radial distances using quarter circles with their center on the square lattice vertex and radii of 5, 10 and 15 chambers. In each distance, I chose 3 different bacteria at angles of 15°, 45° and 75° to measure their displacement in each of the C_E, AT_E and PT_E, with vertical side of the square lattice defined as the reference 0° angle. Positive values for X and Y displacement are also shown in figure 3.2 All the analysis on the images are done using “ImageJ”¹ software. For each analyzed cell, I first measure displacement of bacteria in X and Y directions separately. Then, I use these measured numbers to calculate total displacement of bacteria using equation (1):

$$R = \sqrt{d_x^2 + d_y^2} \quad (1)$$

¹ <https://imagej.nih.gov/ij/>

Where R is total displacement of bacteria, d_x is bacteria displacement in x direction and d_y is bacteria displacement in y direction. I determine the sign of R based on the sign of component (d_x or d_y) with larger absolute value.

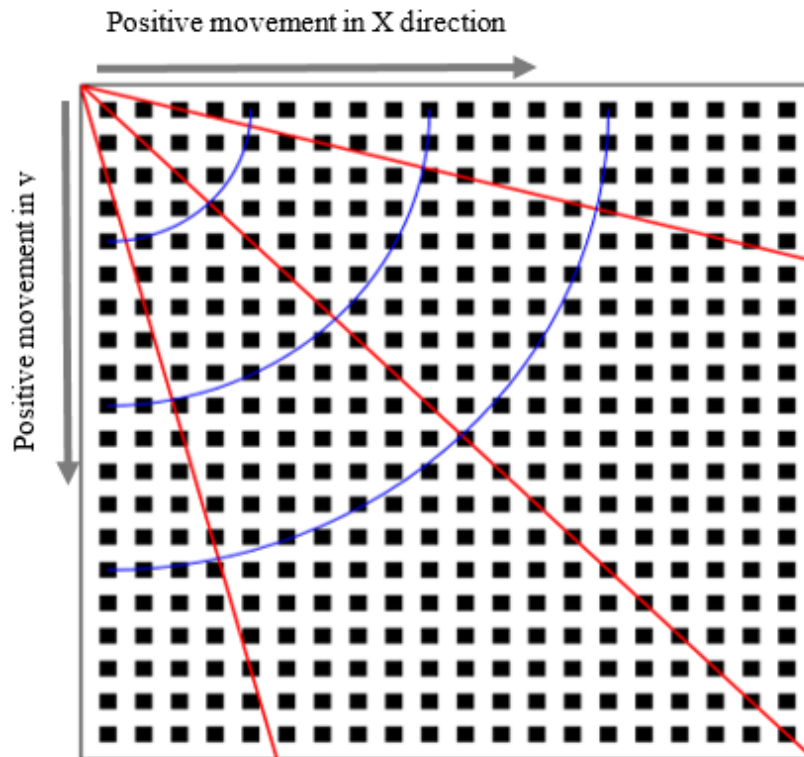


Figure 3.2. Sampling spots for bacteria movement analysis

For each experiment, I imaged the chip at 5 different sections (figure 3.3, sections 1-1 to 3-1) once with the initial distribution of bacteria and then during the treatment of bacteria the same 6 areas are imaged at the time steps of 10 minutes for the whole 60 minutes duration of the experiments. The contrast of bacteria with the background

decreases overtime in most of the experiments, due to photo bleaching of the bacterial cells. The device was imaged using Olympus IX51 inverted microscope¹ and proper filter (Texas Red). I used settings mentioned in table 3.2 to image the device.

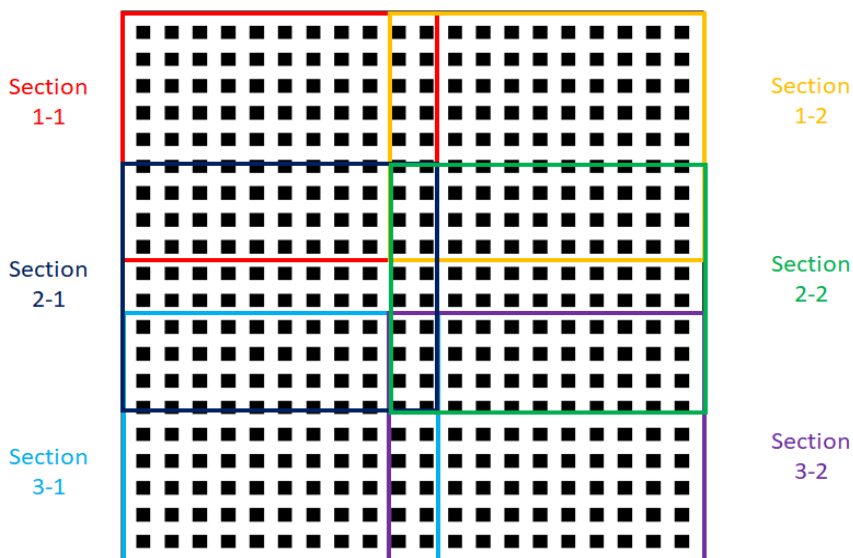


Figure 3.3. Different imaging areas

Table 3.2. Optimized parameters for microscopy of the device

Parameter	Optimized Value
Fluorescent Lamp Intensity	Maximum Setting
Exposure Time	100 ms
Gain	20

¹ <https://www.biocompare.com/19419-Inverted-Microscopes/396657-IX51-Inverted-Microscope>

3.5. Image Processing

For finding bacteria displacement using the microscopy images, I first compare two consecutive images taken at timesteps of 10 minutes starting from $t=0$ min and randomly choose a cell in the radius of $100\ \mu\text{m}$ of favorable position and orientation of study. Comparing the image taken at $t=10$ min to the image taken at $t=0$ min, I can transfer the initial position of the chosen cell at $t=0$ min to latter image at $t=10$ min. The cells are visually identifiable due to relatively small displacements at timescale of 10 minutes and minor differences in cell shapes. Following the same process for images at $t=10$ min and $t=20$ minutes, I find bacteria position at each of these times and so on to image taken at $t=60$ min. To find the displacement of cells at each timestep using the identified initial and final positions of the cells, I first load the image in the ImageJ software and modify it for further analysis using the following path (figure 3.4.a)):

File > Open > (Browse picture and click) open

Image > Type > 8-bit

Using the “line” option, I connected the identified position of cell at beginning and end of each timestep. To measure the length of this line (and hence displacement of cell during this timestep) I used “Measure” tool in the “Analyze” menu which reports the length and angle of the line (figure 3.4.b). Following the same procedure for all the timesteps, I recorded bacteria displacement every 10 minutes for the whole duration of each experiment (60 minutes). Finally, I compared the microscopy images at $t=0$ min to image at $t=60$ min to measure bacteria total displacement for each experiment. I

could also measure total displacement of bacteria by making a vector sum of measured displacement for each timestep from $t=0$ to $t=60$ min, however, accumulation of measurement errors in this method can result in a bigger error compared to a direct measurement of total displacement. Hence, I measured the total displacement of each cell directly using images at $t=0$ and 60 min to minimize the error.

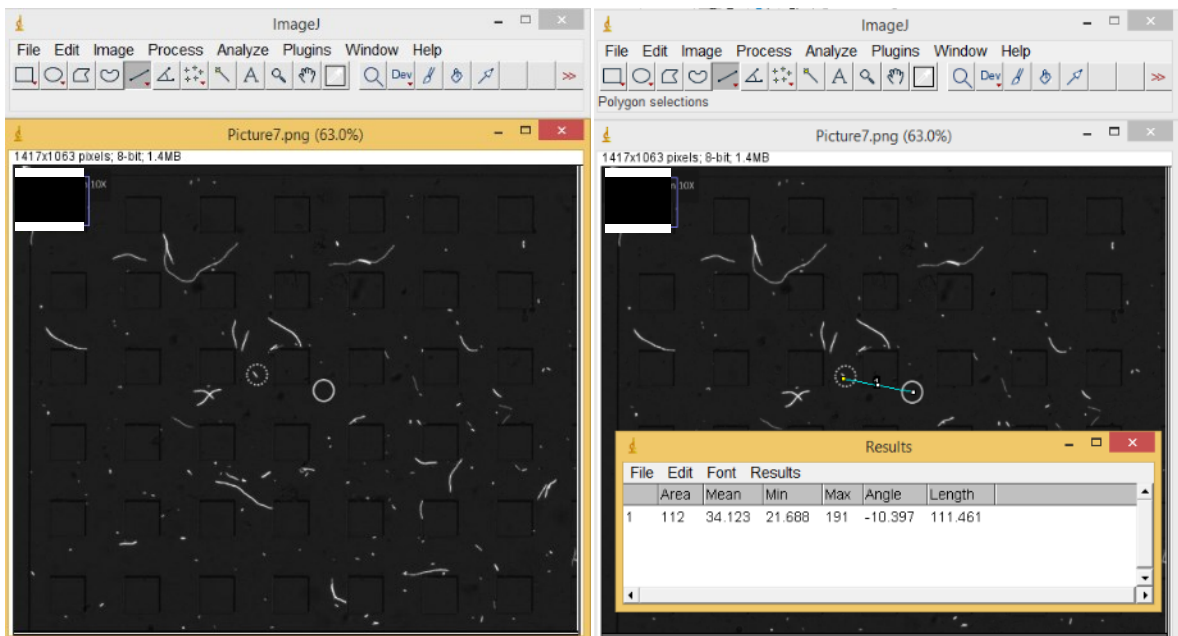


Figure 3.4. Modification of microscopy images and measurement of bacteria displacement using ImageJ. Figure a) shows the initial (dashed) and final (solid) position of the cell in one image. The final position was obtained from comparing this image with

3.6. Challenges

In this section I will mention and discuss all the challenges I faced during design, fabrication and experimental setup.

As discussed in the literature review, there are many previous researches studied bacteria in single cell resolution using microfluidic platforms. In this study I was aiming for a robust design which does not require complicated or expensive fabrication steps but at the same time is easy to setup, collect data (imaging) and minimize the error in results. I first designed a few prototypes of the microfluidic device which were revised as discussed below according to simulations, required fabrication steps, and the feasibility of design for studying different chemicals and biological agents in reaction with bacteria inside the device:

- 45° rotation of square lattice sides relative to inlet and outlet channels for facilitating flow of running fluid inside the device and filling the device symmetrically (fluid velocity has equivalent components in directions of both sides of the square lattice)
- Enlarging the square lattice for ensuring a demonstrated and varying chemical gradient from sub-inlet to the other corner of the lattice
- Choosing a channel height that allows bacteria to spread in a single layer (for imaging purposes) while is easy to fabricate using common photoresists

- Choosing sub-inlet dimensions that allows transfer of bacteria to the square lattice with minimum mechanical stress on cells while preventing bacteria that are already in from leaving

To fabricate a mold for the finalized design, I chose to use a mask less method using the direct writer device (mentioned in chapter 3.2). The challenge here was the limited use of this device in McMaster University, among colleagues and in literature and rare experience on microfabrication using this device. Hence, I had to run many trial and errors to optimize fabrication parameters such as exposure time, exposure intensity, time and temperature of post exposure bake which are thoroughly discussed in chapter 3.2.

After fabrication of the master mold, the soft lithography process for fabrication of devices introduced new challenges. Due to the stickiness and high viscosity of photoresist, peeling of the poured PDMS on the master mold was problematic regardless of any tested post exposure baking temperature and time, ratio of PDMS and curing agent and PDMS curing time and temperature. Hence, I decide to silanize the mold to increase hydrophobicity and ease the detachment of PDMS from silicon.

For the next step, I punched inlets and outlets in the fabricated device and connected it to the pump and sealed the inlets and outlets with epoxy glue. However, these connections were not stable enough and the epoxy glue started to leak frequently before completion of experiments. Epoxy glue is also fluorescent and interfered with fluorescence microscopy of the cells. To solve these problems, I eliminated the punching and assembling steps by placing Tygon tubing (cut into pieces a few millimeters longer than the PDMS block thickness) in intended places for inlets and outlets before curing the PDMS. After PDMS was cured, these tubing are fixed and sealed and can connect the device to syringe needles and longer tubing accordingly.

The next challenge during the experiments was cell adhesion to the walls of the channels. Bacteria cells tend to attach to the PDMS walls and become immobile even after confronting repellents such as antibiotic and phage. To prevent cell adhesion to the walls, I added a prewash step of the device with PBS and also considered adding BSA to the bacteria medium. BSA prevents cell adhesion to the walls and hence cells can freely move after they are loaded inside the device and threatened by stressors.

Any other minor or major challenges I faced in this study is discussed throughout this document in the related section.

Chapter 4. Results and Discussion

4.1. Effect of Bovine Serum Albumin on Cell Adhesion to PDMS

Walls

BSA control experiment (BSA_C) shows that bacteria suspended in BSA 5% in PBS have larger displacements after treating them with PBS (60 minutes, 0.01 mL/h), compared to bacteria suspended in only PBS (figure 4.1). BSA_C results (figure A.1.2) show bacteria are motile at all 9 considered positions while in the control experiment with no BSA (NBSA_C), bacteria were immobile in 6 positions out of 9 (figure A.1.1).

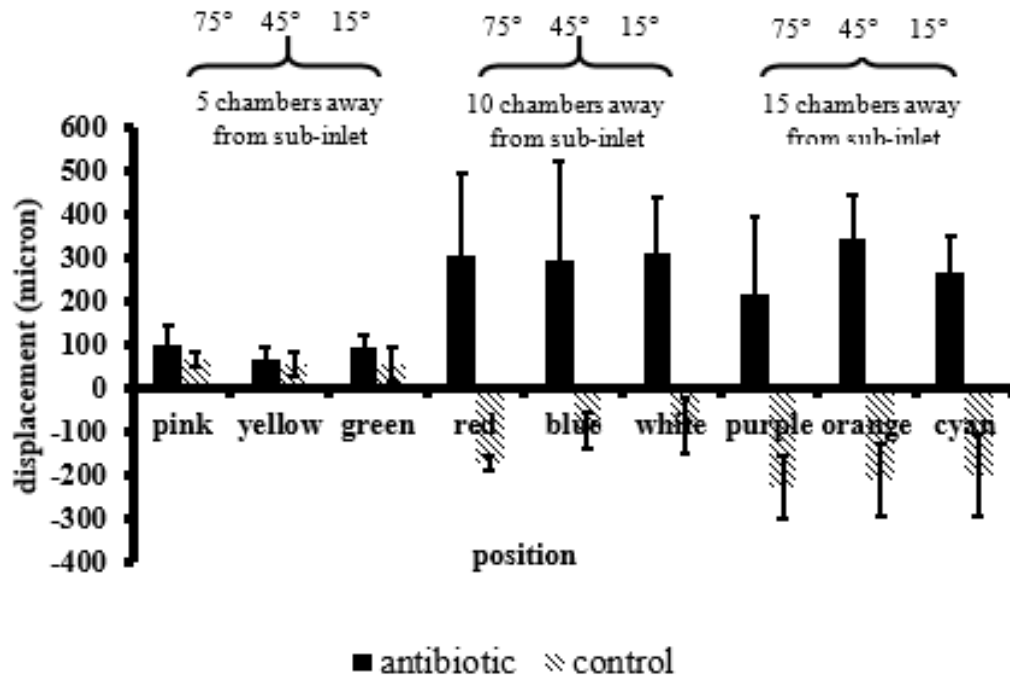


Figure 4.1. Total displacement of bacteria suspended in PBS (NBSA_C) and BSA 5% in PBS (BSA_C) after 60 minutes

BSA helps to prevent cell adhesion to the PDMS walls of the device. Bacteria suspended in PBS will enter and remain inside the sub-inlet and channels and reach a high concentration, while bacteria suspended in BSA 5% in PBS does not stay inside the device and most cells escape the channels through the sub-inlet which prevent the bacteria to reach a concentration as high as the control experiment with no BSA (NBSA_C) inside the connecting channels.

Comparing the images of bacteria initial distribution for the NBSA_C (figure A.1.1) to BSA_C (figure A.1.2) experiments shows that, loading bacteria suspended in BSA 5% in PBS is harder than bacteria suspended in only PBS. Bacteria suspended in PBS will attach to the walls and do not exit while bacteria suspended in BSA 5% in PBS does not stay inside the device during the filling process. However, attachment of cells to the walls interfere with the bacteria response to antimicrobials and affect the results of our experiments. Therefore, for all the following experiments, i.e. treatment of bacteria with water in the control experiment (C_E), antibiotic treatment experiment (AT_E) and phage treatment experiment (PT_E), I suspended bacteria in BSA 5% in PBS to prevent cell adhesion to the walls and allow bacteria to move freely in response to the applied stresses. In this chapter, I use the same naming code explained in table 3.1 to refer to different types of experiments.

4.2. Bacteria Response to Antibiotic Challenge

In this section, I am studying bacteria movement after 60 minutes of exposure to antibiotic challenge to see accumulative response of bacteria during this period. As discussed in the introduction chapter, length of a single bacterium cell (1-2 μm) is not long enough for the cell to be able to sense the desirable or undesirable gradient along its length and bacteria is not equipped with tools which sense immediate presence of attractants or repellents. However, the complicated chain reactions in bacteria result in biased random walk of bacteria population. Therefore, we need to study bacteria during time steps which are long enough to reveal the effect of the chain reactions and bacteria accumulative behavior during this time. Thereupon, I focus on the long-term effect of bacteria exposure to repellants (antibiotic or phage). The microscopy images of control experiments (C_E1 and C_E2) and antibiotic experiments (AT_E1 and AT_E2) are given in appendix (figures A.2.1 to A.2.9 and A.3.1 to A.3.9). Figure 4.2 compares bacteria total displacement after 60 minutes in two cases of control experiment, treating with water (C_E), and antibiotic experiment, ampicillin (AT_E). These results show that bacteria cells treated by DI water in C_E (control) generally respond by moving in negative direction (swimming toward the sub-inlet) in different positions at the end of experiment duration (after 60 minutes treatment). However, in response to antibiotic treatment, bacteria generally show large positive movement (swimming against antibiotic gradient) at different positions after 60 minutes. Statistical analysis of these result is available in chapter 4.5.

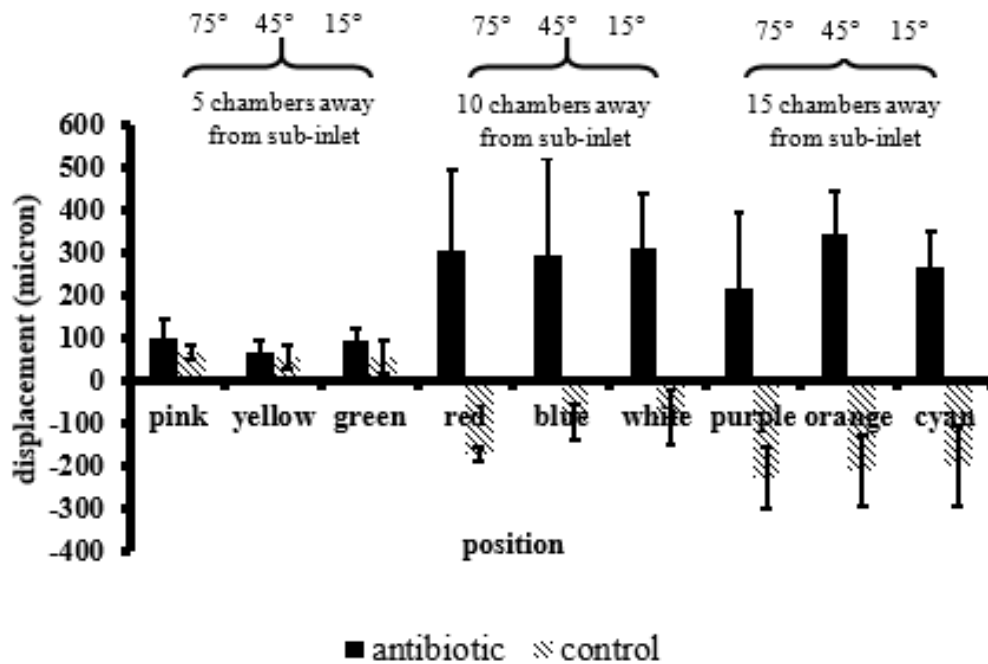


Figure 4.2. Bacteria total displacement after 60 minutes in response to antibiotic and DI water at different positions

Figure 4.2 shows the vector summation of cell displacement in each step (intervals of 10 minutes) throughout the 60 minutes duration of the experiments. As we can see, bacteria can show a relatively stronger reaction (larger movements) to antibiotic treatment compared to water treatment. In figure 4.2, we can see in both cases of C_E and AT_E, bacteria show relatively smaller movements closer to the sub-inlet (5 chambers away from the sub-inlet) compared to further bacteria (10 or 15 chambers away from the sub-inlet). Considering the fluid flow simulations (next chapter) which show maximum fluid velocity close to the sub-inlet, we can conclude that bacteria movement is caused by other factors in addition to convective displacement (such as response to repellents). Considering the fact that the antibiotic concentration is

inversely related to the distance from the sub-inlet which means it has higher concentrations closer to the sub-inlet and lower concentrations in further distances from the sub-inlet. Hence, one may expect larger displacements closer to the sub-inlet as a result of higher concentration of repellent. In contrast, we see that the bacteria displacement closer to the sub-inlet is 2-10 times smaller than further bacteria which is exposed to lower concentration of ampicillin antibiotic. This fact tells us that these forces (drag and chemotactic response) are not the only forces affecting bacteria displacement. We already know that bacteria are moving due to their chemotactic sensitivity and also drag force applied to them from the convective flow they are suspended in. I name these forces, $F_{\text{Chemotaxis}}$ and F_{Drag} respectively. Considering control experiments, we expect positive direction of $F_{\text{Chemotaxis}}$ and F_{Drag} sum because of higher concentration of media in positive direction and positive direction of convective flow. However, experimental results show bacteria have positive displacement in the first region (figure 4.3) and negative displacement in middle and last region. Hence, we can conclude there is a third force in negative direction affecting bacteria displacement and changing the total displacement direction from positive in first region to negative in middle and last region.

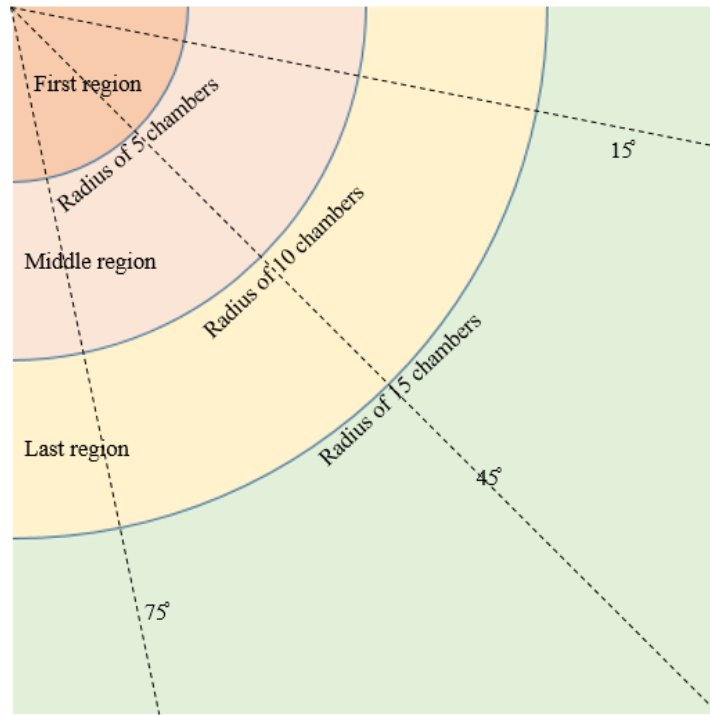


Figure 4.3. Different regions of bacteria movement analysis

Searching for the source of this force, I suggest hydrodynamic forces related to pressurized fluid entering the device through inlet. The effect of PDMS deformation on fluid velocity in microfluidic devices has been studied in many previous researches ([62], [63], [64], [65] and [66]). As mentioned in [61] and shown in figure 4.4, a pressurized inlet flow inside a PDMS channel with low aspect ration, will deform the PDMS and cause pressure drop (related to deformation by a factor of 4) inside the channel due an increase in cross sectional area (figure 4.4). This pressure drop will lower the hydraulic resistance of channel disturbing the fluid flow inside the channel (figure 4.4). As discussed in [66], upon reaching a steady state condition, the elasticity of PDMS brings it back to a relaxed position and change back part or whole (if flow

stops) of the deformation in PDMS. This change in geometry will create a “squeeze flow” which eject the excess flow through inlets and outlets. Since the deformation of PDMS is not symmetric in the cross section parallel to inlet flow (figure 4.4.b), and is larger closer to the inlet where there is larger fluid pressure, the squeeze flow caused by returning to initial geometry is not symmetric either, and tend to drive more excess fluid out through the inlet rather than the outlet. This flow again changes the convective transfer of bacteria and as discussed, this change can be in the opposite direction of expected flow (and direction of bacteria response to antibiotic) close to inlet and make the vector sum of bacteria displacement smaller in positive direction.

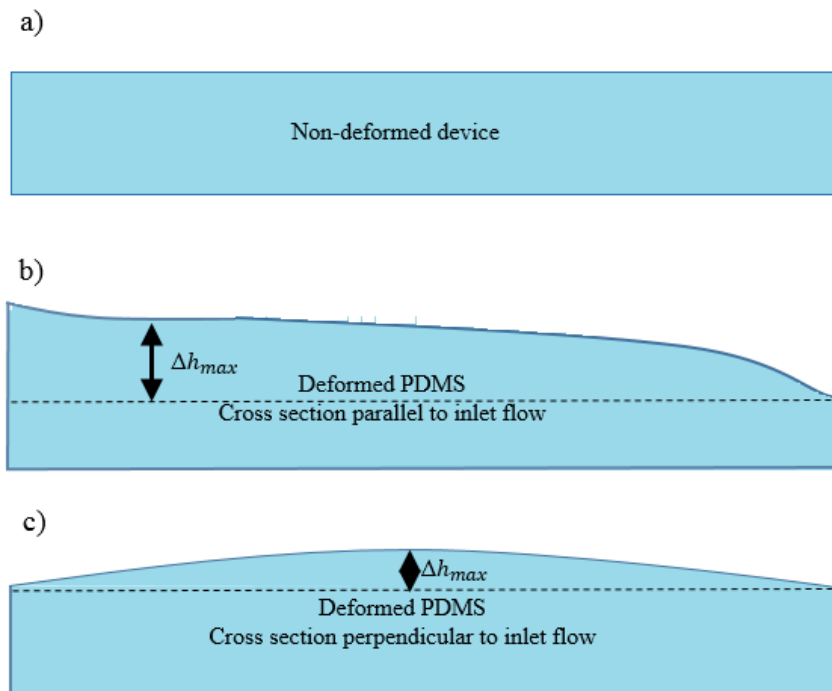


Figure 4.4. a) Device before filling with pressurized flow. B) Exaggerated deformation pattern of the device due to pressurized inlet flow

Comparing bacteria displacement during different 10-minute steps, can confirm that this force is applied to bacteria as a result of device expansion caused by pressurized flow. As expected bacteria negative movement in experiment results is comparably larger during the first 10 minutes of experiments compared to the remaining 50 minutes (Appendix, section A.6 figures A.6.1 to A.6.9), since the pressure difference inside the device will be equilibrated as time passes by 5% BSA in PBS solution flow from high pressure to low pressure and the device will reach a steady state condition as mentioned in [66]. Calling the drag force caused by the squeeze flow, F_{squeeze} . The vector sum of these 3 forces, $F_{\text{Chemotaxis}}$ and F_{Drag} and F_{squeeze} is a function of time and relative distance from the sub-inlet and can change bacteria moving direction at different positions during the experiment (equation 2):

$$\sum F = F_{\text{Chemotaxis}} + F_{\text{Drag}} + F_{\text{squeeze}} \quad (2)$$

Since the first 2 forces in Eq.2 are always in positive direction and F_{squeeze} has negative values in the first region, $\sum F$ can take either positive or negative values according to relative magnitude of $F_{\text{Chemotaxis}} + F_{\text{Drag}}$ and F_{squeeze} .

Considering AT_E, bacteria total displacement is in positive direction in all 3 regions, however, have a very smaller magnitude in the first region compared to the other 2 regions. knowing that both $F_{\text{Chemotaxis}}$ and F_{Drag} are always moving bacteria in positive direction, I can write:

$$\text{First region: } F_{\text{Chemotaxis}} + F_{\text{Drag}} > F_{\text{squeeze}} \quad (3-1)$$

$$\text{Middle region: } F_{\text{Chemotaxis}} + F_{\text{Drag}} \gg F_{\text{squeeze}} \quad (3-2)$$

$$\text{Last region: } F_{\text{Chemotaxis}} + F_{\text{Drag}} \gg F_{\text{squeeze}} \quad (3-3)$$

Which is expected since as I discussed before, the squeeze force is expected to be smaller further from inlet and even in the opposite direction close to outlet. According to simulation results (next chapter) in all 3 experiments the gradient of repellent factor (water, antibiotic, and phage) decreases as we increase the distance from the sub-inlet. Hence $F_{\text{Chemotaxis}}$ in first region is greater than $F_{\text{Chemotaxis}}$ in middle and last region. Convective force of the fluid flow is also directly related to fluid velocity which is lower in middle and last region compared to first region and decreases F_{Drag} in middle and last region compared to first region. Comparing equations 3-2 and 3-3 to 3-1, and noting decrease of $F_{\text{Chemotaxis}}$ and F_{Drag} in middle and last region compared to the first region we can conclude that F_{squeeze} also decreases in middle and last region compared to first region and this decrease is higher in order compared to the decrease in $F_{\text{Chemotaxis}} + F_{\text{Drag}}$:

$$F_{\text{Chemotaxis}} \downarrow \text{ and } F_{\text{Drag}} \downarrow \longrightarrow F_{\text{squeeze}} \downarrow\downarrow$$

Accordingly, I can explain smaller movements of bacteria in the first region compared to middle and the last region in the antibiotic experiment and also the change in bacteria displacement direction in different regions in the control experiment.

4.3. Bacteria Response to Phage Challenge

Figure 4.5 compares bacteria response to DI water, control experiment (C_E), and T4 phage, phage treatment experiment (PT_E). After 60 minutes bacteria show stronger responses to phage treatment compared to water treatment. In response to T4 phage treatment, bacteria show positive displacements (swimming against phage gradient) at different positions during the 60 minutes of the treatment. The microscopy images of PT_E1 and PT_E2 are given in appendix (figures A.4.1 to A.4.9). As I expected, bacteria total displacement in response to phage (figure 4.5) is considerably smaller compared to antibiotic (figure 4.2). This is due to the fact that χ_0 , chemotactic sensitivity coefficient, and K_D , receptor/ligand dissociation constant, are smaller in case of *E. coli* interaction with T4 phage compared to ampicillin (discussed in details in next chapter and equation 4).

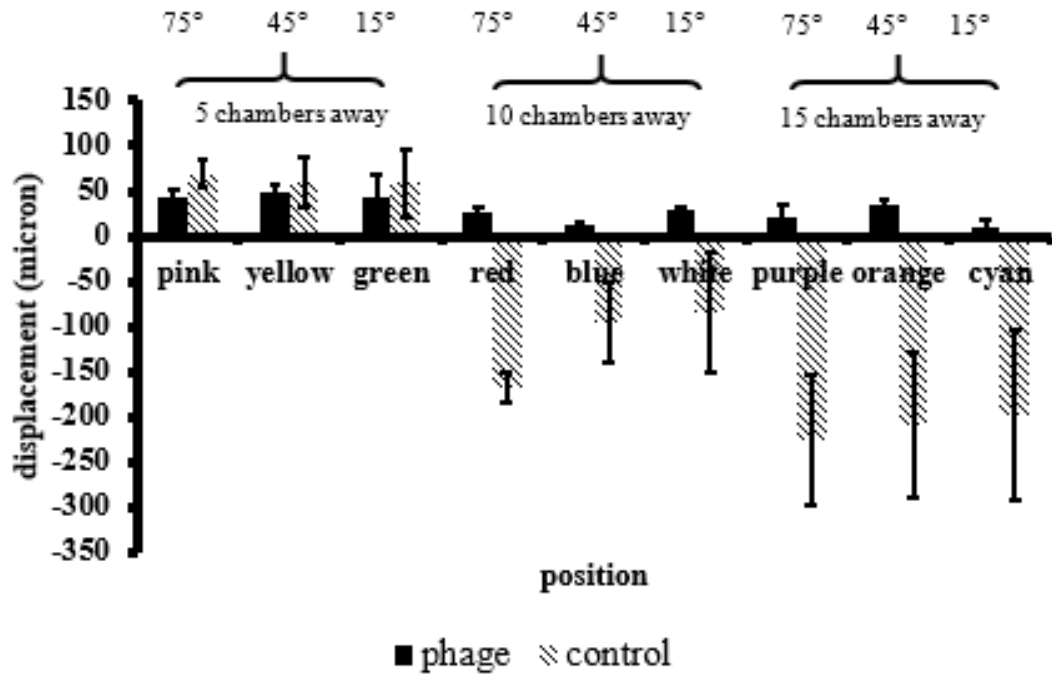


Figure 4.5. Bacteria total displacement after 60 minutes in PT_E compared to C_E at different positions

Like antibiotic experiment, bacteria response to phage is also smaller in middle and last region compared to bacteria closer to the inlet. Again this is affected by relative magnitude of 3 forces exerted on bacteria, $F_{\text{Chemotaxis}}$, F_{Drag} and F_{squeeze} , which I discussed thoroughly in the previous section. Statistical analysis of these result is available in chapter 4.5.

4.4. Effect of Orientation on Bacteria Total Displacement

Figure 4.6 shows the effect of change in angle and position on bacteria total displacement after 60 minutes in both cases of AT_E (antibiotic) and PT_E (phage) and compare them to C_E (control). In control experiments, in same distance from the sub-inlet, bacteria displacement is approximately constant at all different angles (except 45° at last region) and change in orientation does not affect bacteria displacement. Hence, I can conclude that the change in total force exerted on bacteria, $\sum F$, is constant at all different regions for the C_E (control). For antibiotic experiment, at 5 chambers away the minimum displacement happens at 45° while at 15° and 75° bacteria have almost the same displacement. At middle region, we see equal displacement at all 3 different angles and at the last region we see maximum displacement of bacteria at 45° and at 15° and 75° bacteria have almost the same displacement.

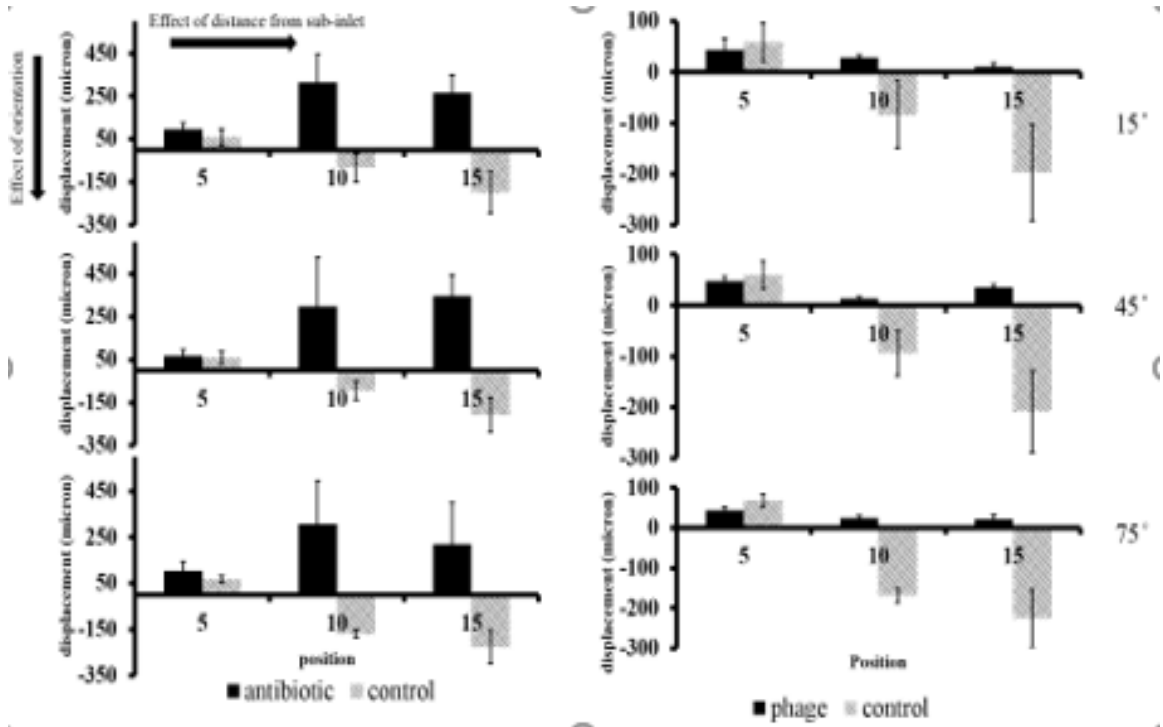


Figure 4.6. Bacteria total displacement at different positions and orientations, antibiotic and phage treatment experiments

We can say bacteria displacement in antibiotic experiments is symmetric around the diagonal of square lattice. Since both $F_{\text{Chemotaxis}}$ and F_{Drag} are symmetric around this axis (symmetric chemorepellent gradient and velocity field), I can claim that F_{squeeze} is also symmetric around the square lattice diagonal. Changes in these forces along with change in orientation and positions are different at different angles when moving from the first region to the middle and last region. This fact causes bacteria to show different response and behavior at different regions with change of orientation.

In the phage experiments, bacteria total displacement is nearly constant at all 3 different angles at the first region, take a minimum in the middle region at 45° and a maximum in the last region at 45° as well. Again, we can see symmetrical behavior of bacteria at the first and middle region, however, at the last region, bacteria have relatively smaller response to phage at 15° compared to 75°. Again, as same as AT_E, we can relate bacteria scattered behavior at different regions as we go from one region to another, to variable dependency of different forces on orientation at these regions.

Looking at all experiments, we can see the ratio of error bar sizes to the total displacement at most positions decrease as we move away from the sub-inlet (from the first region to middle and last regions). It should be noted that for measuring the movement of the 6 randomly chosen bacteria at a specific position and orientation, it is not possible to choose all 6 cells at the exact same coordinates since they are not attached to each other or aggregated at a fixed spot of our interest. Instead the cells are chosen as closest as possible to the desirable position. Knowing that the gradient of chemorepellent concentration and hence $F_{\text{Chemotaxis}}$ is higher close to the sub-inlet one can conclude that with a constant difference at 6 cells position, the difference in the $F_{\text{Chemotaxis}}$ is larger closer to sub-inlet compared to middle and last region. The same explanation is valid for velocity field close to sub-inlet compared to middle region. Hence, bacteria have more scattered response close to sub-inlet because they are exerted to more scattered forces at this area.

All in all, meticulously analyzing these 3 sets of experiments, I conclude that in each experiment, bacteria movement inside the device is affected by 3 different forces. I

thoroughly discussed F_{Drag} and F_{squeeze} here, where are they sourced from and how they affect bacteria movement and I also talked briefly about $F_{\text{Chemotaxis}}$. I discussed how these forces change as we change bacteria position and orientations inside the device, their effect on total displacement of bacteria and how the ratio of these changes in these forces are different in each experiment. I identified these differences as the main reason of bacteria varied behavior at different angles and regions for 3 experiments. Other studies on *E. coli* chemotaxis in single cell resolution also show in a population of bacteria cells can show a very wide range of X_0 , chemotactic sensitivity coefficient, even in populations cultured from the same colony [67]. The difference in the X_0 , parameter results in difference in chemotactic response and then large error bars on quantified response of bacteria to chemoattractants and chemorepellents.

In the next chapter, I give a detailed description about simulation of these 2 forces and I also talk about $F_{\text{Chemotaxis}}$, how it is formulated in the literature and how I simulated all these forces in order to simulate bacteria response to DI water, ampicillin antibiotic and T4 phage.

4.5. Statistical Analysis of the Results

In this section, I discuss the significance of experimental results using a T-test and probability value (p-value). Figure 4.7 compares the results of antibiotic experiments to control experiments while maintaining a constant distance from the sub-inlet and figure 4.8 compares control and antibiotic results at a constant angle. Figure 4.7 shows

an average of bacteria total displacement in the specified distance (at all 3 angles) while figure 4.8 shows the average of bacteria total displacement in the specified angles. The p-value in these figures, distinguishes the significance of data is calculated using “t.test” function in “Excel Microsoft Office” and data is considered to be significant when p-value is below 5%. In all statistical analysis of the results, 4 asterisks indicate a P-values lower than 0.0001 and 3, 2 and 1 asterisks indicate P-values lower than 0.001, 0.01 and 0.05 respectively. Figure 4.7 shows at all 3 regions, bacteria total displacement is significantly different for antibiotic experiments compared to control. This significance indicates that the only changing variable in control and antibiotic experiment (treatment of bacteria with water and antibiotic) affects bacteria behavior.

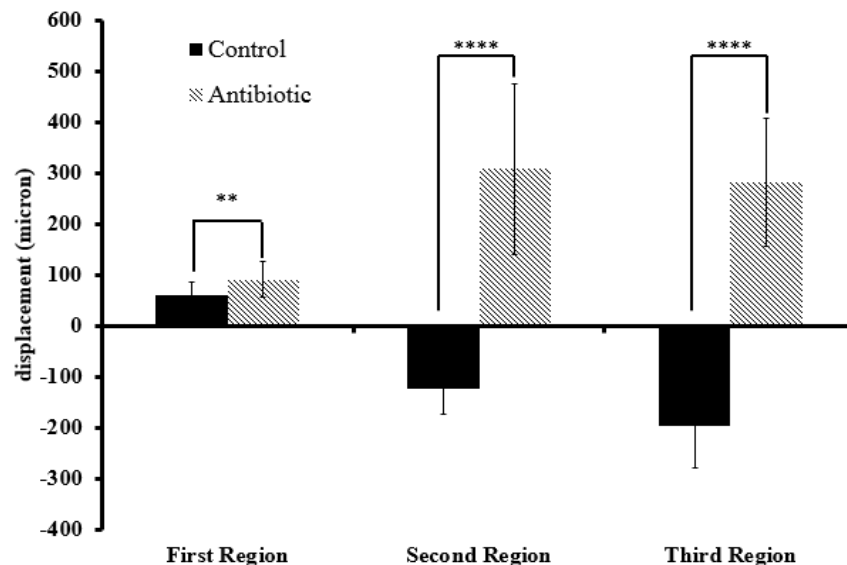


Figure 4.7. Statistical analysis of antibiotic challenge experiments at constant distances from sub-inlet

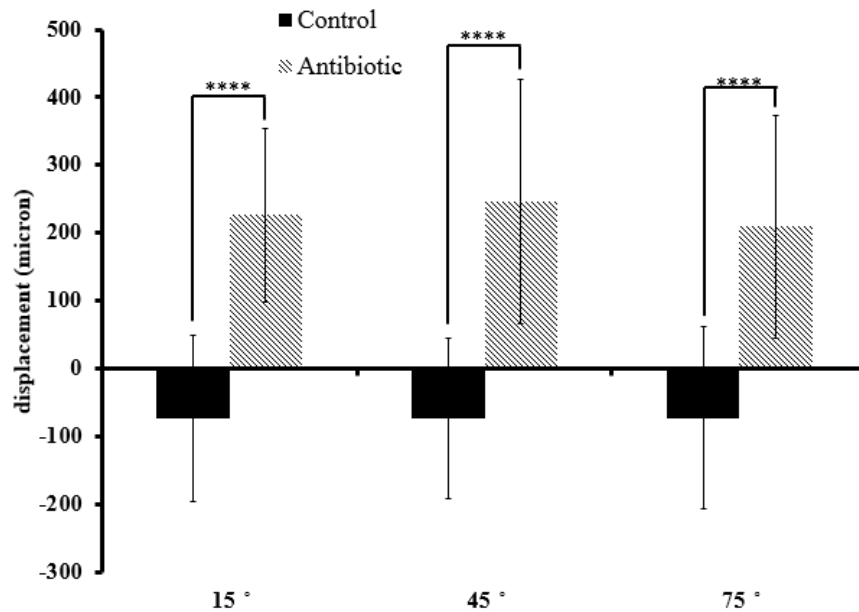


Figure 4.8. Statistical analysis of antibiotic challenge experiments at constant angles

As shown in figure 4.9, the average displacement of cells in each angle is also significantly different for control and antibiotic experiments. According to these results, cells are sensitive to the given dose of treatment (antibiotic) and their response to this chemo-repellent is activated in the duration of experiment.

The same as figures 4.7 and 4.8, figures 4.9 and 4.10 compares bacteria total displacement for phage and control experiments at constant distances and constant angles respectively. Figure 4.9 shows that in the first region, bacteria do not show a significantly different behavior while challenged with phage compared to control experiment. This is mainly because bacteria generally have lower sensitivity to phage compared to antibiotic as reported in literature (and discussed here before). Also, as

discussed in previous sections, in the first region the convective velocity of cells is the largest and can dominate other forces moving cells. Hence, the effect of chemotactic response, which is the only different variable in the phage and control experiment, can be overshadowed by convective force in this region. In figure 4.7, we can observe the same effect where the significance level in the first region is smaller compared to the second and third regions. Although antibiotic is a stronger chemo-repellent for bacteria, statistical analysis in figures 4.9 and 4.10 shows bacteria is still responsive to the given dose of phage in less than 60 minutes.

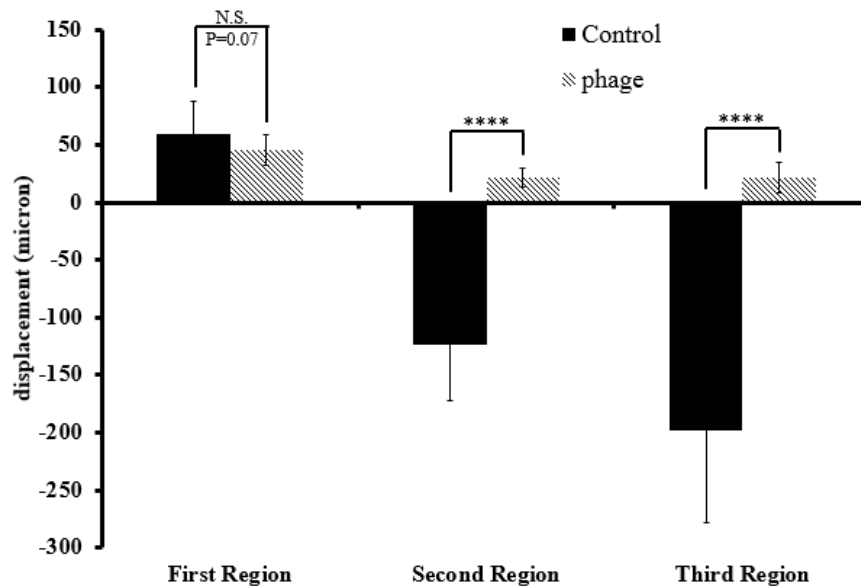


Figure 4.9. Statistical analysis of phage challenge experiments at constant distances from sub-inlet

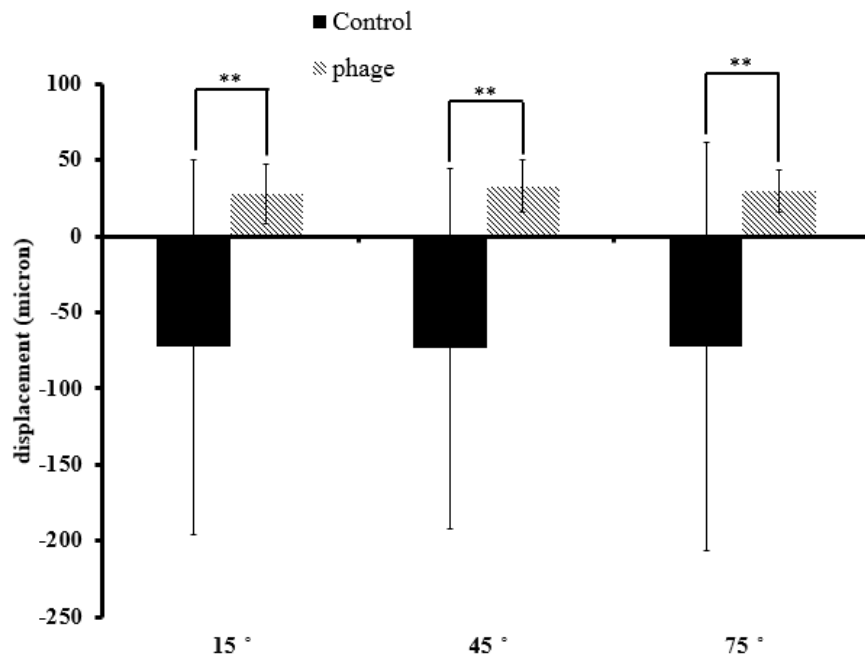


Figure 4.10. Statistical analysis of antibiotic challenge experiments at constant angles

5.1. Modeling of Chemotaxis

There are different approaches in previous studies to model cell (and bacteria) distribution in response to attractants and repellents. At first, I briefly discuss these approaches and then focus on the approach used in this study. Most of available studies discuss response of motile cells to attractants in more details compared to repellents.

The first mathematical model to describe cell movement was presented by Keller and Segel [68]. This model relates collective behavior of bacteria, in terms of amoeba density, to gradient of two chemicals. This model could successfully present some collective behavior of bacteria like aggregation of cells due to a sufficient increase in their sensitivity and acrasin production rate, however, the simplifying assumptions were not precise enough to explain cell behavior in many other conditions.

After Keller-Segel model, Alt et al. developed a more precise stochastic model [69], [70] for chemotaxis of cells focusing on “run” and “tumble” frequency. This model assigns velocities and directions to cells and predicts a distribution of cell position possibilities due to different environmental factors. This study related the direction and magnitude of bacteria population biased random walk to frequency of switches between run and tumble periods. They presented a hypothesis to describe tumbling frequency and angle in cells using a biomechanical control mechanism inside the cells. They also improved previous differential equations which related bacteria behavior in cell resolution to population behavior of bacteria. Their work improved the previous models to better predict and understand collective behavior of motile cells but still incapable

of explaining cell behavior in many cases. There are many other studies following aforementioned studies modeled chemotaxis response of motile cells in different conditions using different approaches [71], [72], [73], [74], [75].

Another model developed to predict chemotaxis is presented by Chen and Ford [76] .

In this model bacteria chemotaxis velocity is given by equation (6) [77]:

$$V_c = \frac{2V}{3} \tanh\left(\frac{x_0}{2V} \frac{K_D}{(K_D + C)^2} \frac{dC}{dS}\right) \quad (6)$$

Where V is individual bacterium swimming speed, X_0 is chemotactic sensitivity coefficient, K_D is receptor/ligand dissociation constant, C is the concentration of chemoattractant and S is the direction in which V_c is measured. Although this equation was developed assuming a small chemical gradient, experiments showed that it is still functional with an acceptable error range for a vast range of chemical gradients. Hence, I can say this equation is valid for our study since there is a shallow chemical gradient and isotropic environment. Using COMSOL Multiphysics, I first simulate the concentration and velocity field created inside the microfluidic device of our experiments and then I solve equation (6) for each single cell to find the cell chemotactic velocity at each time step. Putting together the effect of convective velocity and chemotactic velocity, simulations predict bacteria position (and hence displacement from the initial position) at each time step. The simulation of chemical

gradient is coupled with velocity field and hence the effect of convection is considered in the simulations. After solving the system for fluid velocity and chemical gradient, simulation of bacteria trajectories is coupled with these simulations to study the effect of convection and chemical concentration on cells' trajectory.

5.2. Geometry, Particle Properties and Initial Conditions

In the design sectioned, I mentioned that the device design has a height of 10 μm which is considerably smaller compared to length and width of the channels and bacteria are studied in a single 2D layer (x and y directions) inside the device and bacteria movement in z direction is neglected. Hence, I considered only 2 dimensions for all the simulations as well. Simulation of each experiment is composed of 3 part: 1) modeling of laminar flow inside the device, 2) modeling of transport of agent reacting with bacteria (water, antibiotic solution or phage suspension) considering convective flow from part 1 and 3) modeling of bacteria reacting with water or stressor and moving inside the device using equation (6).

Figure 5.1 shows the inlet (with input rate of 0.01 mL/h) and outlets (atmosphere pressure) for fluid flow simulation. I defined the inlet and outlets as boundary conditions of the designed geometry. I cropped the main inlet length to reduce the geometry size, number of mesh elements and calculation time. Hence, I set entrance length to 1 cm (same as length of main channels in fabricated device) to ensure the flow is fully developed when entering the device from the inlet boundary defined in the geometry. I simulated fluid flow considering slip of the flow on the walls. Initial

geometry. I simulated fluid flow considering slip of the flow on the walls. Initial amounts of velocity field inside the device and pressure were set to 0 and 1 atm respectively. Figure 5.2 shows the simulated velocity inside the microfluidic device using the mentioned settings here. I use this simulation in the next step to find the chemical gradient of repellents (figure 5.3).

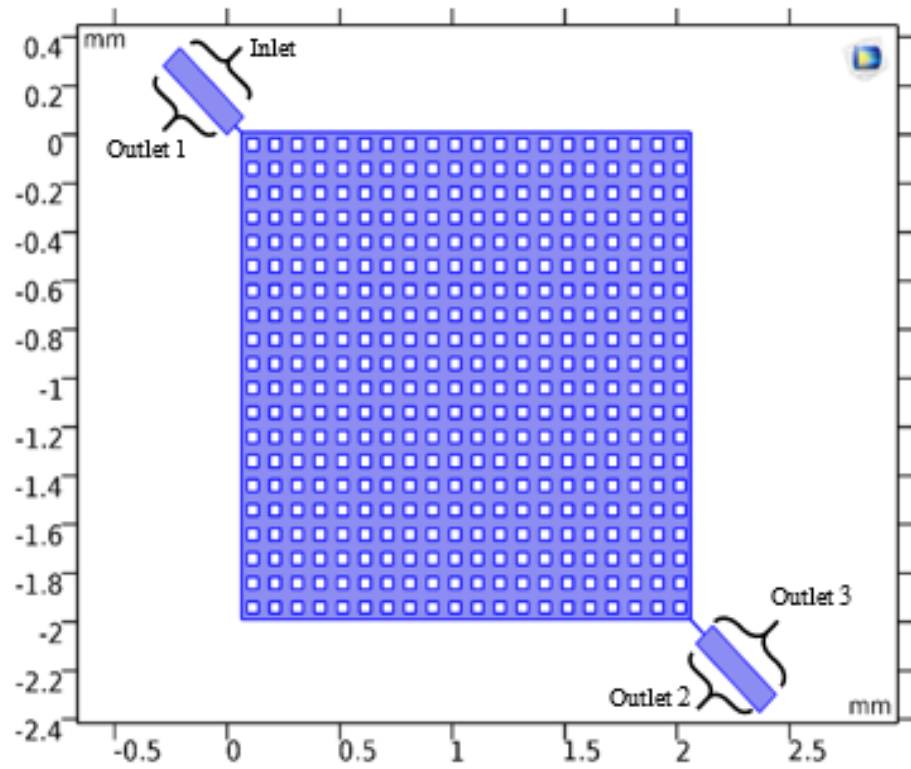


Figure 5.1. Inlets and outlets of the device for simulation of fluid flow

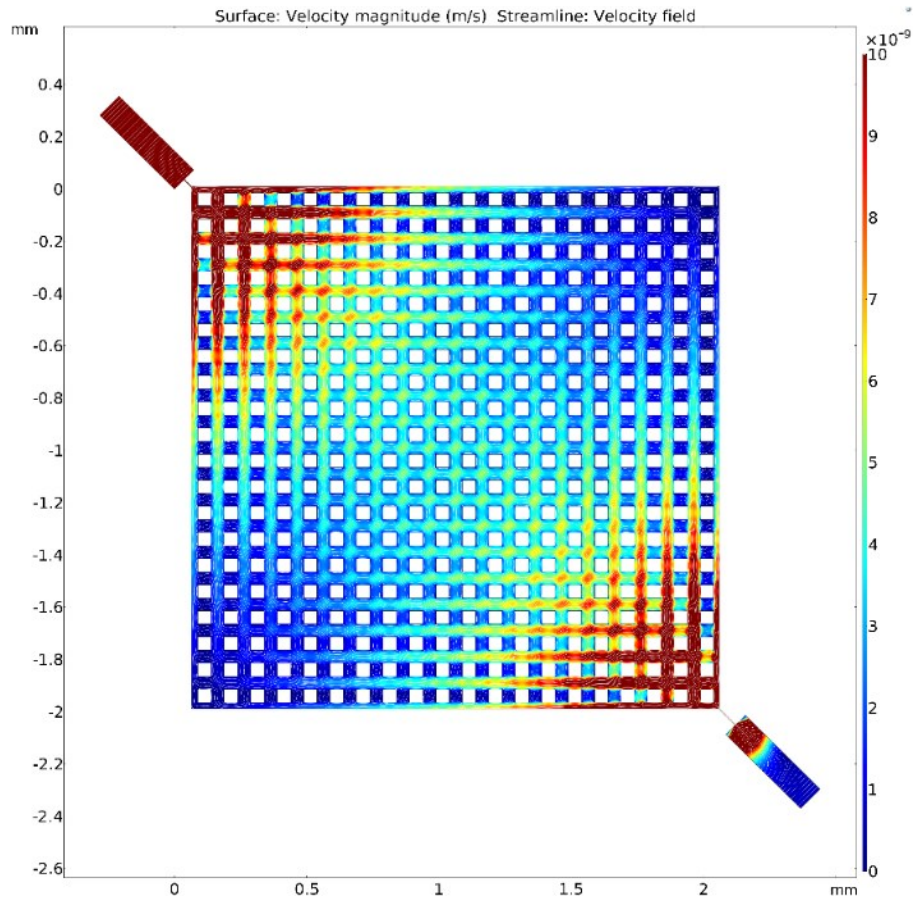


Figure 5.2. Simulated velocity field in microchannels after 60 minutes

I modeled bacteria as spherical particles with radius of $0.72 \mu\text{m}$. This geometry for the bacteria results in the same volume (and hence the same mass) to a rod shape bacterium with length of $2 \mu\text{m}$ and diameter of $1 \mu\text{m}$:

$$\frac{4}{3}\pi \times r^3 = \pi \times 0.5^2 \times 2$$

$$r \approx 0.72 \mu\text{m}$$

Applying approximate density of 1.1166 *g/ml* for bacterial cells [78] results in mass of $\approx 1.75 \times 10^{-15}$ *kg* for each bacterium.

For “control” experiment, literature report values of K_D ranging from 25–30 μM to 0.125 *mM* for *E. coli* in different conditions [40] [79] and x_0 in the range of 0.4-12.4 $\times 10^{-4} \frac{\text{cm}^2}{\text{s}}$ [80][40]. For C_E (bacteria response to water) I select $X_0 = 5 \times 10^{-4} \frac{\text{cm}^2}{\text{s}}$ and based on literature and previous studies K_D for *E. coli* is 0.125 *mM*. V is set to 28 $\mu\text{m/s}$ in all simulations [40].

After simulating the fluid flow velocity inside the device (figure 5.2), I found the concentration of secondary agent (water, antibiotic solution, phage suspension) at different times and positions inside the device. In these simulations, I neglected mass transfer through diffusion since the flow velocity is high at the sub-inlet making convection the main driving force for mass transfer. To show that diffusion is negligible, I calculated Sherwood number for the worst-case scenario.

Sherwood number or Sh indicates the ratio of convective mass transfer to mass transfer due to diffusion. The larger the Sherwood number is, the greater the role of convection and the smaller the role of diffusion will be in mass transfer. Here I showed that for the experiment with highest diffusion rate, Sh is still large enough to neglect mass transfer due to diffusion. To compare the diffusivity in 3 experiments, for water [81] and antibiotic solution [82], [83] I can say:

$$\text{For control experiment: } D_{\text{water}} = 2.3 \times 10^{-9} \frac{\text{m}^2}{\text{s}}$$

For antibiotic experiment: $D_{amp} = 4.58 \times 10^{-10} \frac{m^2}{s}$

And for T4 phage suspension I can calculate the diffusivity using Stokes-Einstein equation for diffusion of particles through a low Reynolds number liquid:

$$D_{T4} = \frac{K_B T}{6\pi\eta r}$$

Where K_B is Boltzmann constant, T is the absolute temperature, η is dynamic viscosity and r is the diameter of particles. K_B is $1.380649 \times 10^{-23} \frac{J}{k}$ and η for water is known to be 8.9×10^{-4} Pa.s. I substitute r with the radius of a sphere that has the same volume as a T4 phage particle (length of 200 nm and width of 90 nm):

$$\pi (45 \times 10^{-9})^2 \times 200 \times 10^{-9} = \frac{4}{3} \pi r^3$$

$$r = 67.22 \text{ nm}$$

Using Stokes-Einstein equation I can write:

$$\text{For phage experiment: } D_{T4} = \frac{1.380649 \times 10^{-23} \times 298}{6\pi \times 8.9 \times 10^{-4} \times 67.22 \times 10^{-9}} = 3.247 \times 10^{-11}$$

I can also calculate diffusivity of ampicillin to verify this formula. From literature, the density of the ampicillin is $1.5 \frac{g}{mL}$ and the molecular weight is $349.406 \frac{g}{mol}$. I can calculate the volume of a molecule (N_A = Avogadro number = 6.022×10^{23}):

$$\frac{349.406 \frac{g}{mol}}{1.5 \frac{g}{mL} \times N_A \times 1000000 \frac{mL}{m^3}} = 3.8681 \times 10^{-28} m^3$$

Assuming a spherical shape, the radius of the molecule is 0.452 nm. Using Stokes-Einstein equation, the diffusivity for ampicillin is:

$$D_{amp} = \frac{1.380649 \times 10^{-23} \times 298}{6\pi \times 8.9 \times 10^{-4} \times 4.52 \times 10^{-10}} = 5.426 \frac{m^2}{s}$$

Which shows an error of 18% for diffusivity of ampicillin compared to reported diffusivity in the literature.

Hence, the biggest diffusivity coefficient is for water and if Sherwood number for the experiment with water is large enough to neglect the diffusion, it is negligible in antibiotic and phage experiments too. Sherwood number for control experiment is calculated as followed:

$$Sh = \frac{\text{Convective mass transfer}}{\text{mass diffusion rate}} = \frac{h}{D/L}$$

Where h is convective mass transfer coefficient, D is diffusivity coefficient and L is characteristic length:

$$Sh_{control} = \frac{h}{D/L} = \frac{0.01 \frac{mL}{h} \div (5 \mu m \times 10 \mu m)}{2.3 \times 10^{-9} \frac{m^2}{s} / 5 \mu m} = 120.77$$

In the worst case, convective mass transfer is almost 121 times bigger than mass diffusion and hence I can safely neglect mass transfer through diffusion in all 3 experiments without introducing a big error to the simulations.

For simulation of all 3 experiments, I used water properties (room temperature and atmosphere pressure) for media containing bacteria, since the media is mainly water. Figure 5.3 shows the simulated gradient of chemical repellent inside 5% BSA in PBS solution.

For initial positions of the bacteria cells, I created a random distribution of 5000 particles (bacteria) inside the device. Then I applied convective force created by velocity field and chemotaxis force (equation 6) on bacteria simultaneously. Among 8 different types of wall interaction with bacteria, I chose “general reflection” which means in case of collision of bacteria to the walls, bacteria will be reflect from the wall maintaining the defined velocity. Other options (stick, freeze, bounce, disappear, pass through, diffuse scattering, mixed diffuse and specular reflection) are clearly not a good representative of the realistic experiments. Under realistic conditions, bacteria interactions with each other (attaching together) or with particle surface can stop bacteria from moving [71]. However, in this study, coating PDMS device walls with BSA, decreases the probability of bacteria sticking to the walls and the bacteria will follow the streamlines even after streaking a wall. This issue cause differences between simulation results and experimental results. Eliminating this effect is only possible through complicated modeling of bacteria and wall interactions [39], [75] and can be covered in subsequent studies.

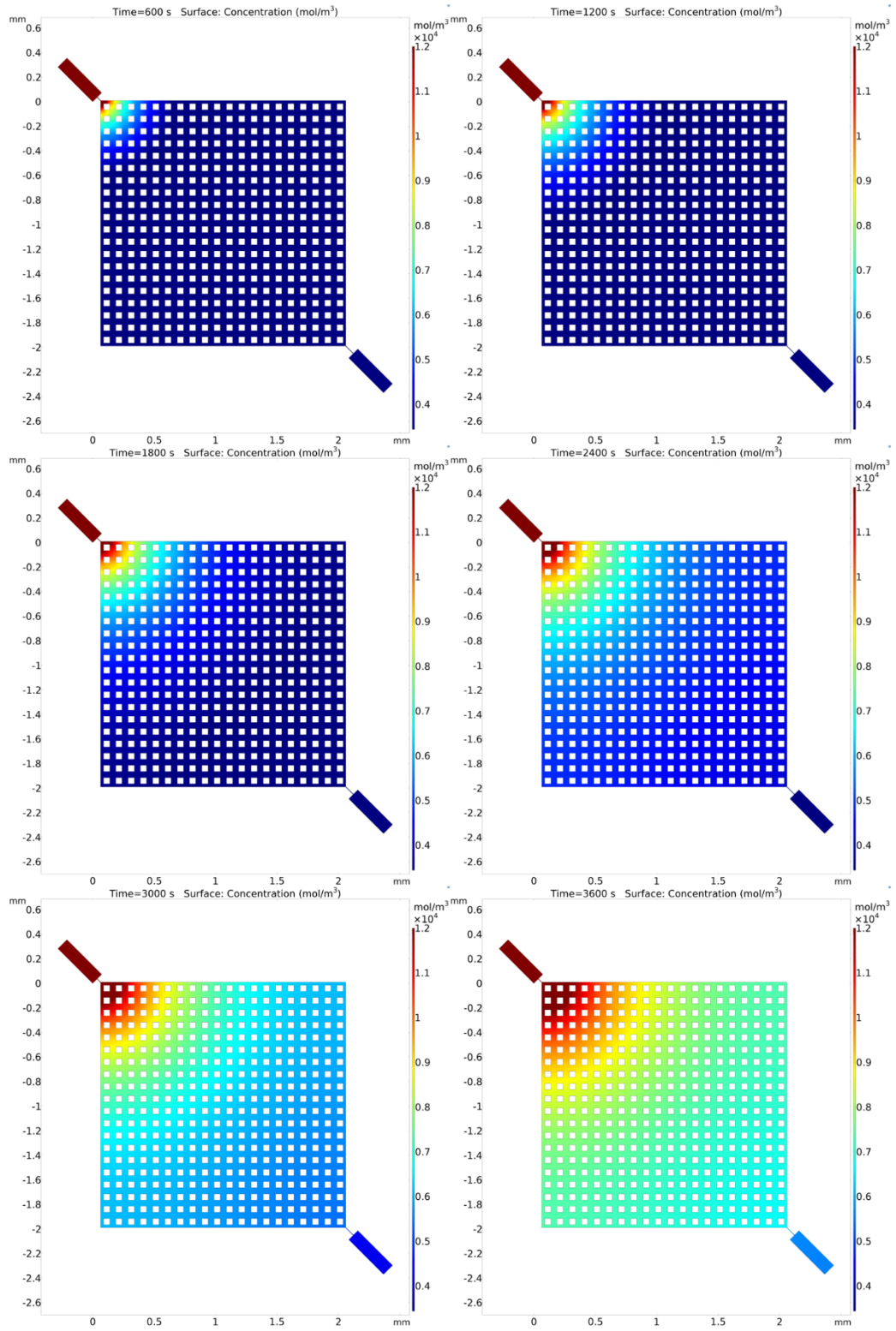


Figure 5.3. Simulation results of chemical gradient of repellent inside the device at different timesteps

5.3. Effect of Convection on Bacteria Displacement

As discussed in chapters 4 and 5, bacterial cells displacement is affected by different forces. In this section I elaborate on effect of convection on bacteria displacement. Since, the bacterial cells are scattered inside the fluid flowing inside the device, the velocity field of the fluid applies a drag force to the cells swimming inside the fluid. This drag force is proportional to the velocity magnitude of the flow. I solved the velocity field of flow for the duration of experiment (60 minutes) using COMSOL laminar flow module assuming of rigid microchannels that do not deform under pressure driven flow. Knowing the velocity field at each position and time, the geometry of the cells and the properties of the fluid, I can calculate the drag force exerted on the cells at each position during the 60 minute duration of the experiment. In all three sets of experiments (with water, antibiotic and phage), the bacteria are suspended in 5% BSA in PBS and then treated with water or a water-based solution or suspension. Hence, the physical properties of the secondary agent for all three experiments is close to water and I can substitute them with water for simulation purposes. Figure 5.4 shows bacteria displacement due to convection (assuming rigid micro channels) after 60 minutes. I eliminated the effect of chemotaxis of bacteria for this simulation and the only force effective on bacteria for this simulation is the drag force originated from the fluid velocity field in a rigid channel.

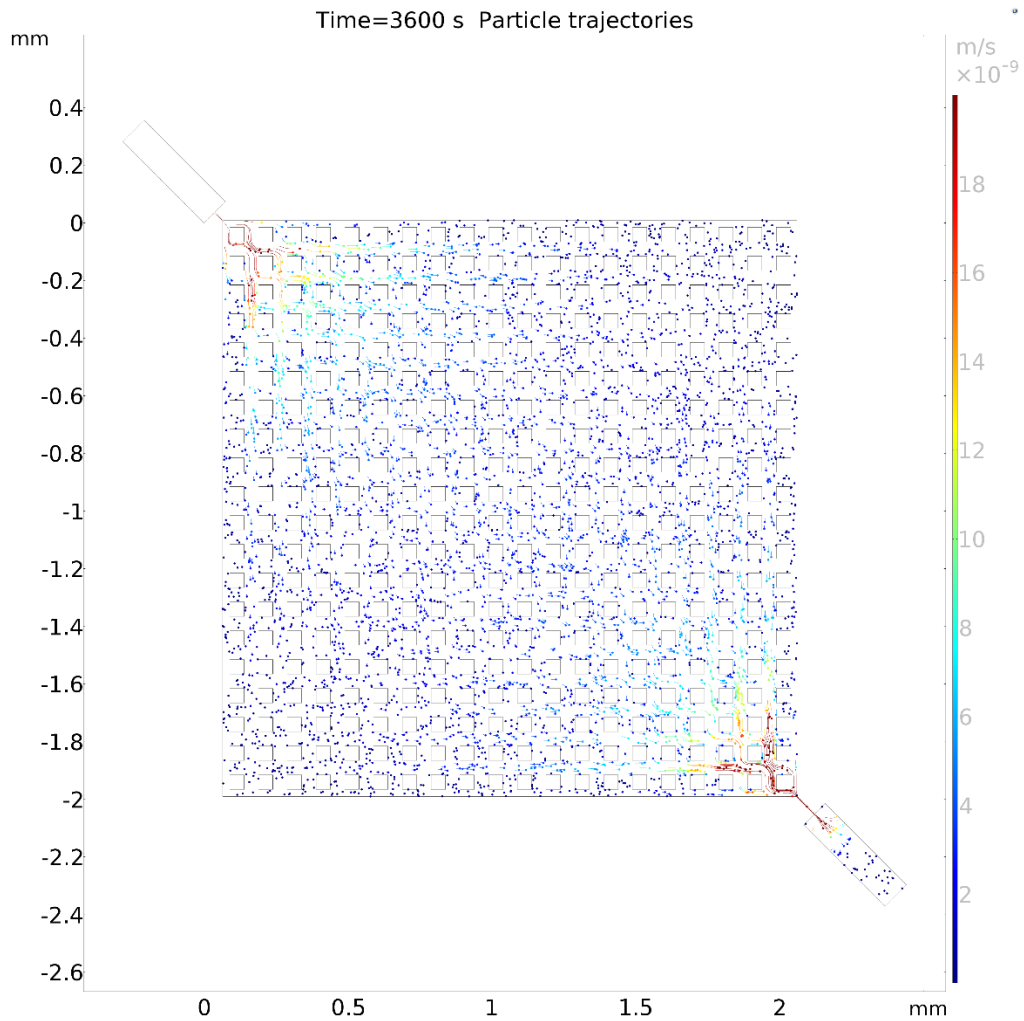


Figure 5.4. Displacement of bacteria after 60 minutes assuming rigid micro channels and no chemotactic response

Figure 5.4 shows that the maximum convective displacement of cells happens close to the corners of the square lattice connected to the main inlet and outlet channels. At 5 chambers away from the sub-inlet (the closest position to sub-inlet where I measure cell's displacement at), the total convective displacements of cells are smaller than $30 \mu\text{m}$ in positive direction and this number drops to $15 \mu\text{m}$ and $10 \mu\text{m}$ in the same direction for second and last region respectively.

Investigating results of all 3 experiments and comparing to convective displacement of cells in the simulations, we can see that in the first region (5 chambers away from the sub-inlet) convective displacement of cells can form a major part of total displacement (up to 50% for treatment with water and antibiotic and up to 66% for phage treatment). However, since the total displacement of cells for control and antibiotic experiments are relatively larger in second and third region compared to the first region, and the convective displacement is smaller in those regions due to smaller velocity field, the ratio of convective displacement to the total displacement reduces drastically when we move away from the sub-inlet. For control experiment, this ratio is approximately $-\frac{1}{5.6}$ and $-\frac{1}{20}$ for second and third regions respectively. The minus sign is just to indicate that the convective displacement and total displacement are in opposite directions. Also, for antibiotic experiment, the maximum ratio of convective displacement to total displacement is approximately $\frac{1}{20}$ for the second region and $\frac{1}{22}$ for the third region. So here we can see as we move away from the sub-inlet, convective displacement forms a smaller portion of the total displacement in cells. However, the case is different for phage experiments. Not having an increase in bacteria response to phage in second and third region, the ratio of convective to total displacement does not decrease for phage experiments in these regions. The maximum ratio is approximately $\frac{1}{1}$ in both second and third region.

The simulations of the fluid flow are conducted assuming rigid channels with no deformation. However, as I discussed before the deformation in PDMS will change the

flow pattern and hence the fluid velocity field and the drag force on bacteria. Since the other 2 forces (drag in rigid channels and chemotactic) moving bacteria are known from the simulations, and the total displacement in experiments is a result of superposition of chemotactic force, drag force in a rigid channel and the squeeze force, I can calculate the squeeze force having the experimental results of total displacement of cells due to sum of these forces. In the next sections, I will discuss and elaborate on the exact method for calculation of squeeze force and hence total force effective on bacteria. It should be mentioned that since the drag in case of rigid channels is simulated using COMSOL and the total drag can be calculated from other parameters of the system, a big ratio of convective displacement to total displacement (like in phage experiment) is not a concern for the calculations since its effect on cell's displacement is known and measurable using fluid flow simulations for rigid channels.

5.4. Calculation of Total Force Effective on Cells in *E. coli*-water

System

In previous chapter, I discussed the experimental results and 3 different forces effective on bacteria during treatment with secondary agents. In addition to $F_{\text{Chemotaxis}}$ and F_{Drag} , I also talked about F_{squeeze} , and the process lead to formation of this force. Water entering the device through inlets causes the device ceiling made of flexible PDMS to buckle and expands the volume of the device. As a result of this expansion, media (containing bacteria) flows from high pressure regions (inside the square lattice)

to low pressure regions (inside the main inlet) and drags bacteria in negative direction. As expected, bacteria negative movement in experiment results is comparably larger during the first 10 minutes of experiments compared to the remaining 50 minutes, since the pressure difference inside the device will be equilibrated as time passes by PBS flow from high pressure to low pressure. Hence, I could explain negative movement of bacteria from the square lattice area to the main channel in the control experiment.

I simulated all this effect by applying an assumptive drag force to bacteria that makes simulation results adapted with experimental results. This assumptive force, like drag force, is a function of bacteria position (and hence velocity) and also has a larger magnitude close to the sub-inlet because of the great pressure difference close to the sub-inlet. Hence, I considered a different force for each of the regions, since they have different distance from the sub-inlet and F_{squeeze} is expected to get smaller as we move away from the sub-inlet. If F_{squeeze} effective on bacteria in the first region is shown as $F_{\text{squeeze}, R1}$ and use the same notation for other regions I can say:

$$F_{\text{squeeze}, R3} < F_{\text{squeeze}, R2} < F_{\text{squeeze}, R1}$$

I found any of these 3 forces by a series of trials and errors in the simulations. Finally, for each region, I chose the F_{squeeze} which results in minimum difference between simulation results and experimental results (minimum error). For each region, then add up the absolute value of average error calculated at all different orientations (15°, 45° and 75°) to have the total error for that region. I name this total error for first, middle and last region, $E_{\text{control},R1}$, $E_{\text{control},R2}$ and $E_{\text{control},R3}$ respectively. Figures 5.5 to 5.7 show the

change in total error of each region by the change in F_{squeeze} in that region. According to these figures:

$$F_{\text{squeeze}, R1} = 2.22 \times 10^{-10} N, \quad E_{\text{control}, R1} = 9.72$$

$$F_{\text{squeeze}, R2} = -7.26 \times 10^{-10} N, \quad E_{\text{control}, R2} = 4.05$$

$$F_{\text{squeeze}, R3} = -73.27 \times 10^{-10} N, \quad E_{\text{control}, R3} = 2.66$$

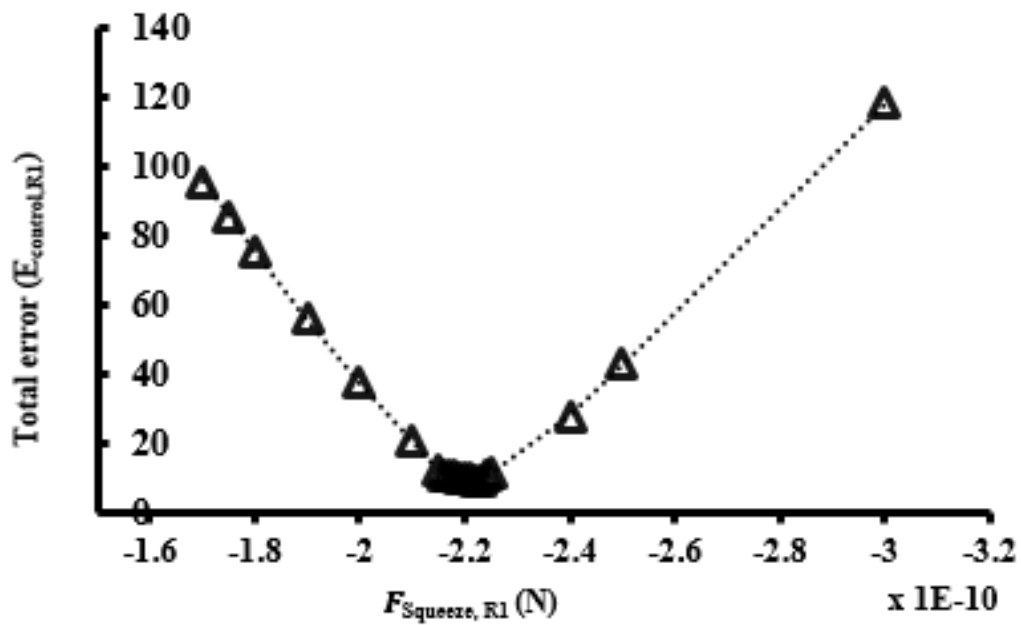


Figure 5.5. Change in total error at first region with respect to different values of F_{squeeze} at this region

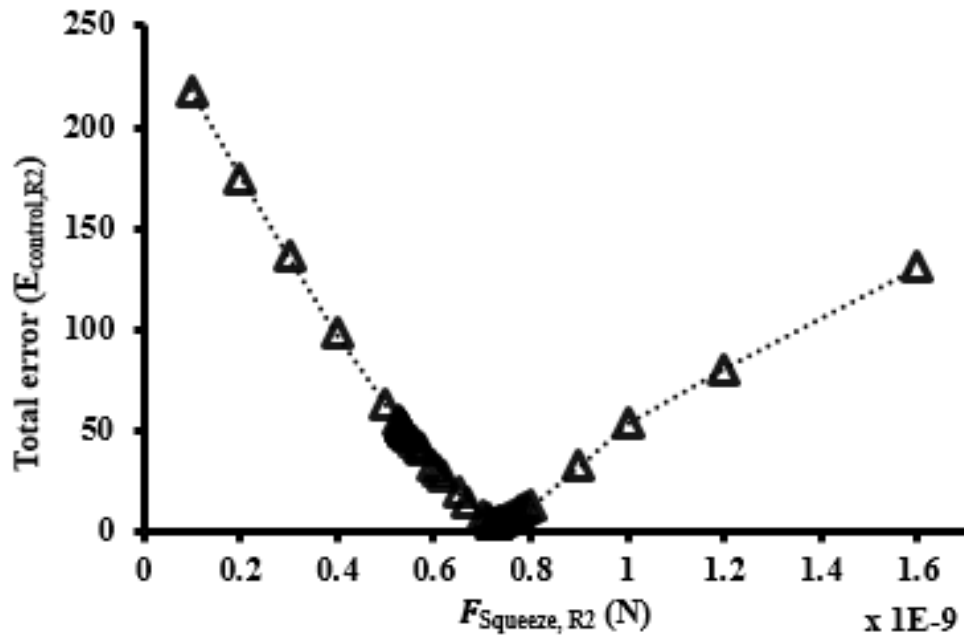


Figure 5.6. Change in total error at first region with respect to different values of F_{squeeze} at this region

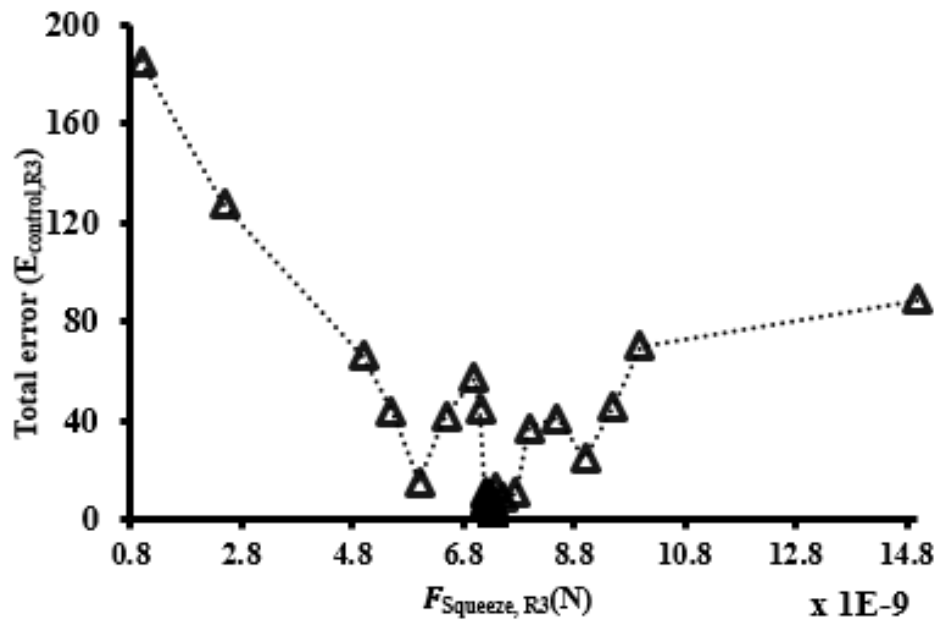


Figure 5.7. Change in total error at the third region with respect to different values of F_{squeeze} at this region

Accordingly, I will be using the respective force for each region is added to all other simulations (antibiotic and phage) to compensate for the effect of PDMS deformation.

5.5. Identification of X_0 for *E. coli*-Ampicillin System

K_D values are reported as 82 μM for ampicillin binding (an antibiotic in penicillin group) [84]. Unlike K_D , X_0 values for bacteria response to repellents are not available in literature. Available studies estimate X_0 by comparing results from modeling bacteria behavior with experimental results [52] [53] or through complicated mathematical models [62], [65] and [70]. Using the same approach, considering the simulation results and comparing them with experimental results, I can find X_0 values for *E. coli* interaction with ampicillin and T4 phage without going through the trouble of developing complicated mathematical models. The next two following sections cover identification of X_0 , chemotactic sensitivity coefficient, for cases of *E. coli* interaction with ampicillin and phage respectively.

As I discussed in previous section, bacteria chemotactic sensitivity in response to antibiotic can be identified by comparing simulation results to experimental results. According to previous section, all the parameters in equation 6 are known from literature for *E. coli*-ampicillin system except for the X_0 , chemotactic sensitivity. In this section, I simulated bacteria response to antibiotic for different values of X_0 . Bacteria displacement in response to antibiotic in these simulations is then compared to experimental results of bacteria response to antibiotic. I measure average bacteria

experimental results of bacteria response to antibiotic. I measure average bacteria displacement in the simulation at 9 different positions of study (5, 10 and 15 chambers away from the sub-inlet at 15, 45 and 75 degrees). Then I add up the absolute value of average error calculated for each of the 9 positions to have the total error ($E_{\text{Ampicillin}}$). Figure 5.8 shows the total error for different values of X_0 in the antibiotic experiment using the F_{squeeze} I calculated for each region at previous section. I identify the X_0 value which results in the smallest difference between experimental and simulation results (and hence minimum total error) as the actual value of X_0 measured by these simulations.

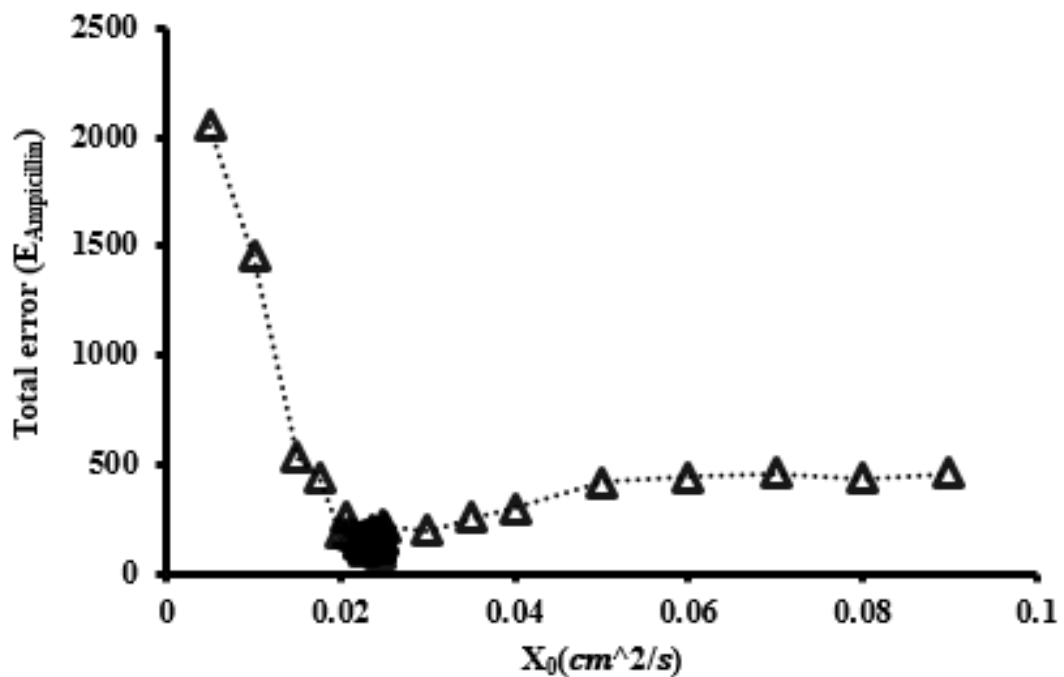


Figure 5.8. Total error in bacteria response to antibiotic in experiments compared to simulations for different values of x_0 in the simulation

As shown in figure 5.8, at $X_0=0.0246 \frac{cm^2}{s}$ the total error is minimum ($E_{Ampicillin}=92.88$) compared to other values of X_0 , hence I identify value of $0.0246 \frac{cm^2}{s}$ for X_0 in *E. coli*-ampicillin system. Table 5.1 shows the composition of $E_{Ampicillin}$. According to this table, there is an unexpectedly large error in the last region at 45° ($E_{Ampicillin, R3-45} = -46.76$) while the average error in the 8 other positions is 5.77.

Table 5.1. Composition of total error for identification of X_0 for *E. coli*-ampicillin system

	First region			Middle region			Last region		
	15°	45°	75°	15°	45°	75°	15°	45°	75°
Error	-11.58	5.58	-3.29	-2.1	1.32	-8.01	-13.25	-46.76	-0.99

5.6. Identification of X_0 for *E. coli*-T4 Phage System

K_D values are reported as 0.2 μM for T4 phage binding with *E. coli* [88]. The same as *E. coli*-ampicillin system, I identify X_0 , chemotactic sensitivity in *E. coli*-T4 system by comparing bacteria response to this repellent in simulation results and experimental results. In this section, I simulated bacteria response to T4 phage for different values of X_0 . Bacteria displacement in response to T4 phage in these simulations is then compared to experimental results of bacteria response. Accordingly, I calculate total error, sum of the absolute value of errors at all 9 different positions (E_{T4}). Figure 5.9 shows the total error for different values of X_0 for *E. coli*-T4 system. Same as *E. coli*-

ampicillin System, I introduce the X_0 value which results in the minimum total error as the actual value of X_0 identified by these simulations.

As shown in figure 5.9 , at $X_0 = 5.15 \times 10^{-5} \frac{cm^2}{s}$ the total error is minimum $E_{T4} = 142.33$ compared to other values of X_0 , hence I identify value of $5.15 \times 10^{-5} \frac{cm^2}{s}$ for X_0 in *E. coli*-T4 system.

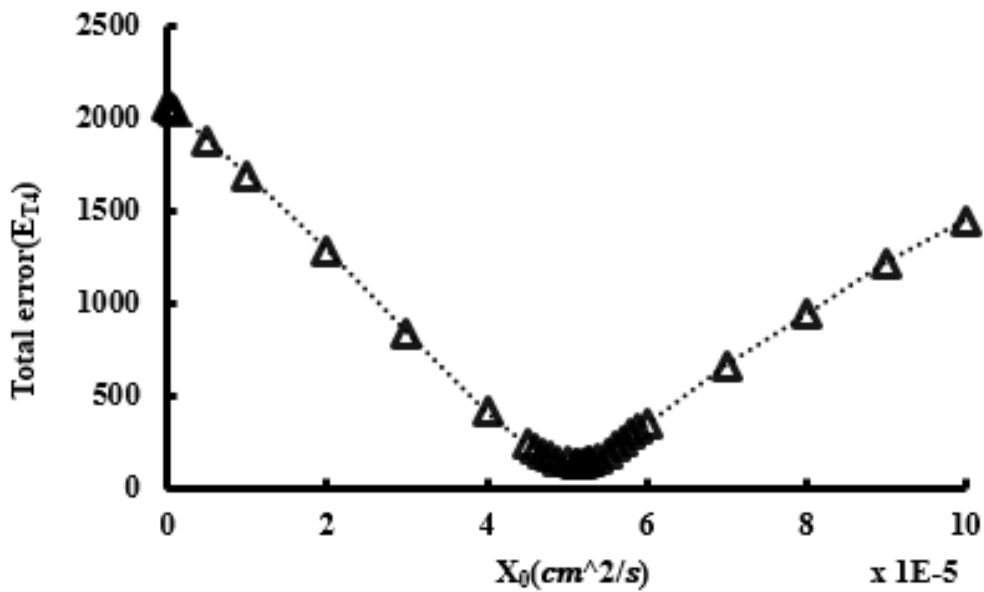


Figure 5.9. Total error in bacteria response to phage in experiments compared to simulations for different values of x_0 in the simulation

Table 5.2 shows the composition of E_{T4} . According to this table, there is an unexpectedly large error in the middle region at 15° ($E_{T4, R2-15} = -43.78$) while the average error in the 8 other positions is 10.95.

The nonhomogeneous and unexpected behavior of bacteria at 2 different positions in antibiotic and phage experiments can be a question of interest. A possible reason for

this behavior is that there are randomly mutated bacteria cells accumulated in the relative position and these bacteria are showing different behavior compared to the rest of the population. Different factors can cause these randomly mutated bacteria to choose that specific area as their desirable place to accumulate. Nonhomogeneous concentration of repellent (due to imperfection and contamination inside the device), different extracellular signals among the mutated cells compared to the rest of the population and different sensed chemotaxis force are a few possibilities that can result in this behavior which are not evaluated in this study. Understanding the reason explaining this behavior can reveal valuable information about the mutated cells and their mechanism of response to threat (e.g. antibiotic, phage). I discuss future possible works in this area and the impact it can make in the next chapter. However, it is important to make sure the F_{squeeze} I simulated for 3 different regions of the device is not affected by the randomly mutated cells. Hence, I suggest increasing the number of replicates of the control experiment in order to reduce the effect of nonhomogeneous behavior of cells.

Table 5.2. Composition of total error for identification of X_0 for *E. coli-T4* system

	First region			Middle region			Last region		
	15°	45°	75°	15°	45°	75°	15°	45°	75°
Error	24.53	-6.8	-0.04	-43.78	20.89	-2.17	25.94	-11.48	-6.71

5.7. Error Sources in Identification of X_0 , Chemotactic Sensitivity

Studying chemotaxis inside microfluidic devices can be distorted by fluid flow and other physical parameters [89]. Hence, we need to note that the movement of cells in a chemical gradient inside a microfluidic device is not only a result of chemotaxis response but also can be affected by flow velocity, drag force, Brownian motion force and changes in geometry (for flexible materials like PDMS) caused by shear forces and many other factors, which I discussed thoroughly in previous sections. The velocity field simulation results, Figure 5.10 shows that in addition to position and orientation of the bacteria, their relative distance from the pillars inside the square lattice affects their behavior and displacement too. A cell in close proximity of a wall is exposed to different F_{Drag} as it is when further from the walls. This difference is a result of different streamline velocities inside the device (as shown in figure 5.10). While the fluid velocity is smaller close the walls, the velocity profile is maximum in the middle of 2 pillars and this maximum velocity ranges approximately from 0.5 nm/s to 10 nm/s throughout different regions of the device. This rapid change in velocity in a small distance (25 μm) can apply widely different drag forces on 2 adjacent bacteria and cause different convective displacement of cells.

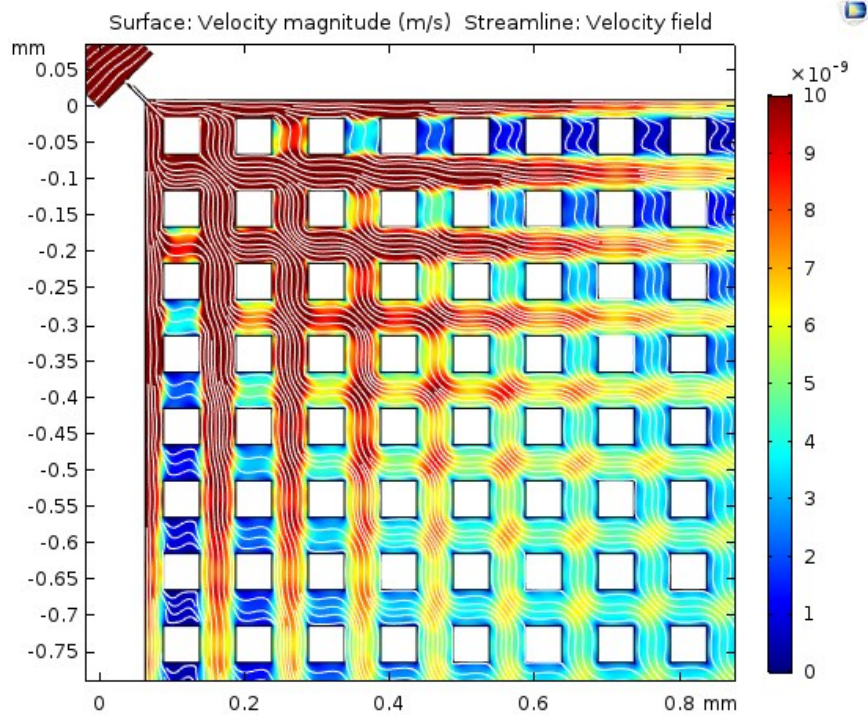


Figure 5.10. Velocity difference on the walls and in the midpoint of 2 adjacent pillars along the device

In addition to the forces I discussed in this chapter and previous chapter, there are other non-significant forces affecting bacteria movement inside the device, such as cell-cell interactions (which becomes significant in high concentration of bacteria or bacteria interaction with the walls (which is minimized by coating the PDMS walls by BSA) and etc. Taking these forces into account can increase the accuracy of the analysis and predicted X_0 .

Chapter 6. Summary and Future Work

The main contribution of this study is the identification of X_0 , chemotactic sensitivity, for 2 different systems of *E. coli* interaction with ampicillin, and T4 bacteriophage. X_0 shows bacteria sensitivity to a chemical which can attract or repel bacteria. We can interpret X_0 as a factor which relate bacteria chemotactic velocity to chemotactic gradient concentration proportionally. Hence, the importance of X_0 identification and its role in understanding and predicting bacteria chemotaxis is clear. X_0 is measured for case of interaction with different types of bacteria and chemicals. However, X_0 is still unknown for many bacteria-chemical interaction systems. In the previous chapters I discussed different experimental or computational methods developed to calculate and measure this parameter. In this study, in the first step used an experimental setting with known X_0 (*E. coli*-DI water) system to identify the unknown factors and parameters introduced by the experimental setup and physics. Then I employed the measured parameters to identify X_0 in *E. coli*-ampicillin and *E. coli*-T4 system with unknown chemotactic sensitivity. In addition to importance of chemotactic sensitivity for understanding chemotaxis, such method for identification of X_0 can be employed in design and development of methods for bacteria cell sorting and separation of heterogeneous bacteria in a sample. The main and most important reason causing this heterogeneity is bacteria resistance to the reagent interacting with it. The random mutations in bacteria gene, can change or hide chemical receptors on the surface of the cell. These receptors are responsible for bacteria chemotaxis in presence of repellent by changing the frequency of run and tumbles periods. The random mutations change

chemotactic sensitivity by physically hiding or removing these receptors from the surface of bacteria and hence develop resistance of the bacteria to the repellent. This fact reveals the importance of detecting any bacterium which shows a heterogeneous response compared to the average response of the population. Knowing the average X_0 and chemotactic velocity, we can design a microchannel that collect bacteria with chemotactic velocity of $V_{ch} = V_{avg,ch} \pm R$ where $V_{avg,ch}$, is the average chemotactic velocity of the population and R is certainty factor. The drift force applied to each cell is directly related with the cell velocity. Hence, we can use the V_{ch} range to find the range for drift force and accordingly design a microfluidic channel to accumulate all the cell exposed to drift force in this range. Any bacteria that escape this trap and leave the microchannel through a designated outlet channel are the bacteria with different chemotactic behavior compared to the bacteria population. The output flow can be collected and tested to verify presence of bacteria in the sample. With an appropriate design of microchannel, we can detect resistant bacteria to a specific treating agent in each sample.

As mentioned in previous chapters, I suggest importing other minor forces affecting bacteria chemotaxis (such as cell-cell interactions, cell-wall interactions, effect of bacteria aggregation and etc. in the simulation of bacteria displacement to increase the accuracy of predicted X_0 . Such a device can be a critical step in the pharmacological development of phage therapy and designing new phage antimicrobials.

As another extension of this work, I suggest adding more biological, chemical and geometrical features to the designed device to make the bacteria culture environment more similar to the environment of human's body. This can help us to model *in-vivo*

environments such as stomach tissue (involved with PH gradient) and *Helicobacter pylori* refuge in stomach microgrooves which can be simulated by micro features inside the device, or biofilm formation in tongue tissue and dental surfaces to study oral infections.

Using these studies, the effect of geometrical, chemical, and biological parameters on antibacterial resistance can be investigated to eventually optimize the process of phage development as an alternative antibacterial therapy and enhance the efficacy of phage therapy to defeat the epidemic problem of bacterial resistance to antibiotic.

References

- [1] D. Freitak, C. W. Wheat, D. G. Heckel, and H. Vogel, “Immune system responses and fitness costs associated with consumption of bacteria in larvae of *Trichoplusia ni*,” *BMC Biol.*, vol. 5, no. 1, p. 56, 2007.
- [2] R. Rusconi, M. Garren, and R. Stocker, “Microfluidics expanding the frontiers of microbial ecology,” *Annu. Rev. Biophys.*, vol. 43, pp. 65–91, 2014.
- [3] D. H. Duckworth, ““ Who Discovered Bacteriophage? ”,” *Bacteriol. Rev.*, vol. 40, no. 4, pp. 739–802, 1976.
- [4] C. L. Ventola, “The antibiotic resistance crisis: part 1: causes and threats,” *P T*, vol. 40, no. 4, pp. 277–283, Apr. 2015.
- [5] Z. Drulis-Kawa, G. Majkowska-Skrobek, B. Maciejewska, A.-S. Delattre, and R. Lavigne, “Learning from bacteriophages - advantages and limitations of phage and phage-encoded protein applications,” *Curr. Protein Pept. Sci.*, vol. 13, no. 8, pp. 699–722, Dec. 2012.
- [6] Z. Hosseini, N. Tufenkji, and T. G. M. van de Ven, “Formation of biofilms under phage predation: considerations concerning a biofilm increase,” *Biofouling*, vol. 29, no. 4, pp. 457–468, 2013.
- [7] D. B. Weibel, W. R. Diluzio, and G. M. Whitesides, “Microfabrication meets microbiology,” vol. 5, no. March, pp. 209–218, 2007.
- [8] Government of Canada, “Canadian Antimicrobial Resistance Surveillance System Report,” 2016. [Online]. Available: <https://www.canada.ca/en/public-health/services/publications/drugs-health-products/canadian-antimicrobial-resistance->

surveillance-system-report-2016.html.

- [9] P. S. Hiremath, "Identification of Flagellated or Fimbriated Bacterial Cells using Digital Image Identification of Flagellated or Fimbriated Bacterial Cells using Digital Image Processing Techniques," no. December, 2012.
- [10] P. Reference and P. Vol, "Brock biology of microorganisms , 13th ed . (online access included)," vol. 27, no. Jun, pp. 1–2, 2012.
- [11] J. A. Fuhrman, "Marine viruses and their biogeochemical and ecological effects.," *Nature*, vol. 399, no. 6736, pp. 541–8, 1999.
- [12] M. R. J. Clokie, A. D. Millard, A. V Letarov, and S. Heaphy, "Phages in nature," no. February, pp. 31–45, 2011.
- [13] L. Bushak, "A Brief History Of Antibiotic Resistance: How A Medical Miracle Turned Into The Biggest Public Health Danger Of Our Time," *Medical Daily*, 2016. [Online]. Available: <https://www.medicaldaily.com/antibiotic-resistance-history-373773>.
- [14] D. I. Andersson and D. Hughes, "Antibiotic resistance and its cost : is it possible to reverse resistance ?," vol. 8, no. apRil, p. 2010, 2010.
- [15] S. B. Santos, C. Carvalho, J. Azeredo, and E. C. Ferreira, "Population dynamics of a Salmonella lytic phage and its host: Implications of the host bacterial growth rate in modelling," *PLoS One*, vol. 9, no. 7, 2014.
- [16] O. Gefen and N. Q. Balaban, "The importance of being persistent: Heterogeneity of bacterial populations under antibiotic stress: Review article," *FEMS Microbiol. Rev.*, vol. 33, no. 4, pp. 704–717, 2009.

- [17] P. D. Pérez and S. J. Hagen, “Heterogeneous response to a quorum-sensing signal in the luminescence of individual vibrio fischeri,” *PLoS One*, vol. 5, no. 11, 2010.
- [18] U. P. Cronin and M. G. Wilkinson, “Bacillus cereus endospores exhibit a heterogeneous response to heat treatment and low-temperature storage,” *Food Microbiol.*, vol. 25, no. 2, pp. 235–243, 2008.
- [19] S. V. Avery, “Microbial cell individuality and the underlying sources of heterogeneity,” *Nat. Rev. Microbiol.*, vol. 4, no. 8, pp. 577–587, 2006.
- [20] K. Ziółkowska, R. Kwapiszewski, and Z. Brzózka, “Microfluidic devices as tools for mimicking the in vivo environment,” *New J. Chem.*, vol. 35, no. 5, p. 979, 2011.
- [21] H. Salman, A. Zilman, C. Loverdo, M. Jeffroy, and A. Libchaber, “Solitary modes of bacterial culture in a temperature gradient,” *Phys. Rev. Lett.*, vol. 97, no. 11, pp. 5–8, 2006.
- [22] X. Zhu *et al.*, “Frequency-dependent Escherichia coli chemotaxis behavior,” *Phys. Rev. Lett.*, vol. 108, no. 12, pp. 1–5, 2012.
- [23] Z. Long, B. Quaipe, H. Salman, and Z. N. Oltvai, “Cell-cell communication enhances bacterial chemotaxis toward external attractants,” *Sci. Rep.*, vol. 7, no. 1, pp. 1–12, 2017.
- [24] S. Van Vliet, F. J. H. Hol, T. Weenink, P. Galajda, and J. E. Keymer, “The effects of chemical interactions and culture history on the colonization of structured habitats by competing bacterial populations,” *BMC Microbiol.*, vol. 14, no. 1, pp. 1–16, 2014.
- [25] J. Mannik, R. Driessen, P. Galajda, J. E. Keymer, and C. Dekker, “Bacterial growth and motility in sub-micron constrictions,” *Proc. Natl. Acad. Sci.*, vol. 106, no. 35, pp. 14861–14866, 2009.

- [26] S. Park *et al.*, “Influence of topology on bacterial social interaction,” *Proc. Natl. Acad. Sci.*, vol. 100, no. 24, pp. 13910–13915, 2003.
- [27] S. Halldorsson, E. Lucumi, R. Gómez-Sjöberg, and R. M. T. Fleming, “Advantages and challenges of microfluidic cell culture in polydimethylsiloxane devices,” *Biosens. Bioelectron.*, vol. 63, pp. 218–231, 2015.
- [28] D. J. Beebe, G. A. Mensing, and G. M. Walker, “Physics and Applications of Microfluidics in Biology,” *Annu. Rev. Biomed. Eng.*, vol. 4, no. 1, pp. 261–286, 2002.
- [29] D. B. Hall, P. Underhill, and J. M. Torkelson, “Spin Coating of Thin and Ultrathin Polymer Films,” *Polym. Eng. Sci.*, vol. 38, no. 12, pp. 2039–2045, 1998.
- [30] R. F. Pease, “Maskless lithography,” *Microelectron. Eng.*, vol. 78–79, no. 1–4, pp. 381–392, 2005.
- [31] H. Becker and C. Gärtner, “Polymer microfabrication technologies for microfluidic systems,” *Anal. Bioanal. Chem.*, vol. 390, no. 1, pp. 89–111, 2008.
- [32] Y. Xia and G. M. Whitesides, “Soft lithography,” *Annu. Rev. Mater. Sci.*, vol. 28, no. 12, pp. 153–184, 1998.
- [33] A. Mata, A. J. Fleischman, and S. Roy, “Characterization of Polydimethylsiloxane (PDMS) Properties for Biomedical Micro/Nanosystems,” *Biomed. Microdevices*, vol. 7, no. 4, pp. 281–293, 2005.
- [34] B. H. Jo, L. M. Van Lerberghe, K. M. Motsegood, and D. J. Beebe, “Three-dimensional micro-channel fabrication in polydimethylsiloxane (PDMS) elastomer,” *J. Microelectromechanical Syst.*, vol. 9, no. 1, pp. 76–81, 2000.

- [35] C. M. Weber, C. N. Berglund, and P. Gabella, “Mask Cost and Profitability in Photomask Manufacturing : An Empirical Analysis,” vol. 19, no. 4, pp. 465–474, 2006.
- [36] K. F. Chan, “High-resolution maskless lithography,” *J. Micro/Nanolithography, MEMS, MOEMS*, vol. 2, no. 4, p. 331, 2003.
- [37] “Heidelberg Instruments uPG 101.” [Online]. Available: <https://himt.de/index.php/upg-101.html>.
- [38] M. E. Cates, “Diffusive transport without detailed balance in motile bacteria: Does microbiology need statistical physics?,” *Reports Prog. Phys.*, vol. 75, no. 4, 2012.
- [39] K. Drescher, J. Dunkel, L. H. Cisneros, S. Ganguly, and R. E. Goldstein, “Fluid dynamics and noise in bacterial cell-cell and cell-surface scattering,” *Proc. Natl. Acad. Sci.*, vol. 108, no. 27, pp. 10940–10945, 2011.
- [40] R. M. Ford and R. W. Harvey, “Role of chemotaxis in the transport of bacteria through saturated porous media,” vol. 30, pp. 1608–1617, 2007.
- [41] Y. S. Dufour, X. Fu, L. Hernandez-nunez, and T. Emonet, “Limits of Feedback Control in Bacterial Chemotaxis,” pp. 1–14, 2019.
- [42] C. J. Wolfram, “ANALYSIS OF FLOW-BASED MICROFLUIDIC GRADIENT GENERATORS FOR THE STUDY OF BACTERIAL CHEMOTAXIS,” 2015.
- [43] S. Samanta, R. Layek, S. Kar, and S. Mukhopadhyay, “Transient drift of Escherichia coli under diffusing Step nutrient profile.”
- [44] A. J. Waite, N. W. Frankel, and T. Emonet, “Behavioral Variability and Phenotypic Diversity in Bacterial Chemotaxis,” pp. 595–616, 2018.

- [45] R. M. Ford and D. A. Lauffenburger, "Measurement of Bacterial Random Motility and Chemotaxis Coefficients : II . Application of Single-Cell-Based Mathematical Model," 1990.
- [46] Z. Xiao-qian, L. I. Zhe-yu, Z. Xiao-yan, J. Lei, R. E. N. Nan-qi, and S. U. N. Kai, "Advance in Bacteria Chemotaxis on Microfluidic Devices," vol. 45, no. 11, 2017.
- [47] R. E. Parales and J. L. Ditty, "Chemotaxis to Hydrocarbons," pp. 221–239.
- [48] B. Borer, R. Tecon, and D. Or, "Spatial organization of bacterial populations in response to oxygen and carbon counter-gradients in pore networks," no. 2018.
- [49] T. Abe, S. Nakamura, and S. Kudo, "Biochemical and Biophysical Research Communications Bioconvection induced by bacterial chemotaxis in a capillary assay," vol. 483, pp. 277–282, 2017.
- [50] M. Kojima, Z. Wang, M. Nakajima, T. Arai, and T. Fukuda, "Sensors and Actuators B : Chemical Microchip device with parallel operation for bacterial chemotactic analysis," vol. 245, pp. 695–701, 2017.
- [51] L. Laganenka, R. Colin, and V. Sourjik, "Chemotaxis towards autoinducer 2 mediates autoaggregation in Escherichia coli," 2016.
- [52] B. Lee, H. Jeong, K. Kang, C. Lee, and S. Lee, "Improvement of a diffusion-based microfluidic chemotaxis assay through stable formation of a chemical gradient," vol. 202, pp. 130–137, 2019.
- [53] M. Tena-garitaonaindia, I. Llamas, L. Toral, and I. Sampedro, "Science of the Total Environment Chemotaxis of halophilic bacterium Halomonas anticariensis FP35 towards the environmental pollutants phenol and naphthalene," *Sci. Total Environ.*, vol. 669, pp.

631–636, 2019.

- [54] J. Adler, “A Method for Measuring Chemotaxis and Use of the Method to Determine Optimum Conditions for Chemotaxis by *Escherichia coli*,” pp. 77–91, 1972.
- [55] C. Virgile *et al.*, “Engineering bacterial motility towards hydrogen-peroxide,” pp. 1–20, 2018.
- [56] M. Tunchai *et al.*, “Negative chemotaxis of *Ralstonia pseudosolanacearum* to maleate and identification of the maleate chemosensory protein,” vol. 124, no. 6, pp. 647–652, 2017.
- [57] N. Murugesan, S. Singha, and T. Panda, “A diffusion based long-range and steady chemical gradient generator on a microfluidic device for studying bacterial chemotaxis,” vol. 26, 2016.
- [58] D. R. Brumley, F. Carrara, A. M. Hein, Y. Yawata, and S. A. Levin, “Bacteria push the limits of chemotactic precision to navigate dynamic chemical gradients,” pp. 2–7, 2019.
- [59] C. Jin, C. C. Maass, and S. D. Swimmers, “Chemotaxis and autochemotaxis of self-propelling droplet swimmers,” vol. 114, no. 20, pp. 5089–5094, 2017.
- [60] Y. Gu, V. Hegde, and K. J. M. Bishop, “Lab on a Chip Measurement and mitigation of free convection in microfluidic gradient generators †,” pp. 3371–3378, 2018.
- [61] A. Sengupta and S. Van Teeffelen, “Dynamics of a microorganism moving by chemotaxis in its own secretion,” 2018.
- [62] T. Gervais, J. El-ali, A. Gunther, and Jensen Klavs F., “Flow-induced deformation of shallow microfluidic channels,” pp. 500–507, 2006.
- [63] C. Roh, J. Lee, and C. Kang, “Physical Properties of PDMS (Polydimethylsiloxane)

Microfluidic Devices on Fluid Behaviors : Various Diameters and Shapes of.”

- [64] B. S. Hardy, K. Uechi, J. Zhen, and H. P. Kavehpour, “The deformation of flexible PDMS microchannels under a pressure driven flow,” pp. 935–938, 2009.
- [65] C. Kang, R. A. Overfelt, and C. Roh, “Deformation properties between fluid and periodic circular obstacles in polydimethylsiloxane microchannels : Experimental and numerical investigations under various conditions,” vol. 054102, pp. 1–15, 2013.
- [66] D. Dendukuri, S. S. Gu, D. C. Pregibon, T. A. Hatton, and P. S. Doyle, “Stop-flow lithography in a microfluidic device {,” no. May, pp. 818–828, 2007.
- [67] M. M. Salek, F. Carrara, V. Fernandez, J. S. Guasto, and R. Stocker, “Bacterial chemotaxis in a microfluidic T-maze reveals strong phenotypic heterogeneity in chemotactic sensitivity,” *Nat. Commun.*, no. 2019.
- [68] K. EF and S. LA, “Initiation of slime mold aggregation viewed as an instability,” *J. Theor. Biol.*, vol. 26, no. 3, pp. 399–415, 1970.
- [69] H. G. Othmer, S. R. Dunbar, and W. Alt, “Models of dispersal in biological systems H.,” pp. 263–264, 1988.
- [70] W. Alt, “Biased Random Walk Models for Chemotaxis and Related Diffusion Approximations,” vol. 177, pp. 147–148, 1980.
- [71] R. Dillon and L. Fauci, “A Microscale Model of Bacterial and Biofilm Dynamics in Porous Media,” 2000.
- [72] A. Mathematics, “MULTISCALE MODELS OF TAXIS-DRIVEN PATTERNING IN BACTERIAL POPULATIONS Author (s): CHUAN XUE and HANS G . OTHMER

Source : SIAM Journal on Applied Mathematics , Vol . 70 , No . 1 (2009), pp . 133-167

Published by : Society for Industrial and Applied Mat, ” vol. 70, no. 1, pp. 133–167, 2019.

- [73] D. Saintillan and M. J. Shelley, “Active suspensions and their nonlinear models,” *Comptes Rendus Phys.*, vol. 14, no. 6, pp. 497–517, 2013.
- [74] O. A. Igoshin, A. Mogilner, R. D. Welch, D. Kaiser, and G. Oster, “Pattern formation and traveling waves in myxobacteria : Theory and modeling,” vol. 98, no. 26, pp. 14913–14918, 2001.
- [75] S. Valverde and R. V Sole, “Before the Endless Forms : Embodied Model of Transition from Single Cells to Aggregates to Ecosystem Engineering,” vol. 8, no. 4, 2013.
- [76] K. C. Chen and P. T. Cummings, “Perturbation Expansion of Alt ’ s Cell Balance Equations Reduces to Segel ’ s One- Dimensional Equations for Shallow Chemoattractant Gradients EQUATIONS REDUCES TO SEGEL ’ S ONE-DIMENSIONAL,” no. September, 1998.
- [77] X. Wang, T. Long, and R. M. Ford, “Bacterial Chemotaxis Toward a NAPL Source Within a Pore-Scale Microfluidic Chamber,” vol. 109, no. 7, pp. 1622–1628, 2012.
- [78] C. L. Lewis, C. C. Craig, and A. G. Senecal, “Mass and Density Measurements of Live and Dead Gram-Negative and Gram-Positive Bacterial Populations,” vol. 80, no. 12, pp. 3622–3631, 2014.
- [79] C. Picioreanu, X. Richard, C. Mazza, H. Van Lintel, and J. R. Van Der Meer, “Quantitative chemical biosensing by bacterial chemotaxis in microfluidic chips,” vol. 20, pp. 241–258, 2018.
- [80] T. Ahmed, T. S. Shimizu, and R. Stocker, “Bacterial chemotaxis in linear and nonlinear

- steady microfluidic gradients,” vol. 10, no. 9, pp. 3379–3385, 2011.
- [81] J. C. Thermodynamics, J. Andanson, M. Traïkia, and P. Husson, “Ionic association and interactions in aqueous methylsulfate alkyl-imidazolium-based ionic liquids,” *J. Chem. Thermodyn.*, vol. 77, pp. 214–221, 2014.
- [82] S. Wa, “Laser interferometry analysis of ciprofloxacin and ampicillin diffusion from liposomal solutions to water phase,” pp. 549–558, 2013.
- [83] J. M. K. PADFIELD and I. W., “The diffusion of penicillin G and ampicillin through phospholipid sols,” pp. 348–352, 1975.
- [84] X. Wen, J. Hua, and Y. Hong, “Bioorganic & Medicinal Chemistry Letters Discovery of loperamide as an antagonist of angiotensin II and angiotensin II by virtual screening,” *Bioorg. Med. Chem. Lett.*, vol. 22, no. 7, pp. 2388–2392, 2012.
- [85] F. R. M., P. B. R., Q. J. A., and L. D. A., “Measurement of bacterial random motility and chemotaxis coefficients: I. Stopped-flow diffusion chamber assay,” *Biotechnol. Bioeng.*, vol. 37, no. 7, pp. 647–660, 2004.
- [86] M. S. Olson and E. J. Fernandez, “Quantification of Bacterial Chemotaxis in Porous Media Using Magnetic Resonance Imaging,” vol. 38, no. 14, pp. 3864–3870, 2004.
- [87] S. Samanta, R. Layek, S. Kar, M. K. Raj, S. Mukhopadhyay, and S. Chakraborty, “Predicting *Escherichia coli* ’s chemotactic drift under exponential gradient,” vol. 032409, pp. 1–9, 2017.
- [88] J. Gordon *et al.*, “Identification of the RNA Binding Domain of T4 RegA Protein by Structure-based Mutagenesis * two structural domains , as revealed by the crystal struc-,” vol. 274, no. 45, pp. 32265–32273, 1999.

- [89] G. M. Walker, J. Sai, A. Richmond, M. Stremler, C. Y. Chun, and J. P. Wikswo, “Effects of flow and diffusion on chemotaxis studies in a microfabricated gradient generator,” *Lab Chip*, vol. 5, no. 6, pp. 611–618, 2005.

Appendix

A.1. Microscopy Images Control Experiments with and without BSA

Figures A.1.1.a to A.1.1.e show the microscopy images of control experiment without Bovine Serum Albumin (BSA). In this experiment, abbreviated as NBSA_C in this text (table 3.1) the bacteria loaded inside the device were suspended in 1X phosphate - buffered saline (PBS) while for control experiment with BSA (BSA_C), the bacteria were suspended in BSA 5% in PBS solution. Figures A.1.2.a to A.1.2.e shows the microscopy images of BSA_C. In both experiments, I washed the device loaded with bacteria with PBS for 60 minutes at flow rate of 0.01 mL/h. As mentioned in the text, BSA helps to prevent cell adhesion to PDMS walls. While 6 out of 9 cells in NBSA_C have no displacement during the 60 minutes of experiment, in BSA_C bacteria in all 9 position are motile. In all images of figures A.1.1 and A.1.2, dashed circles show initial position of cell at $t=0$ min and solid circles show final position of cells at $t=60$ min.

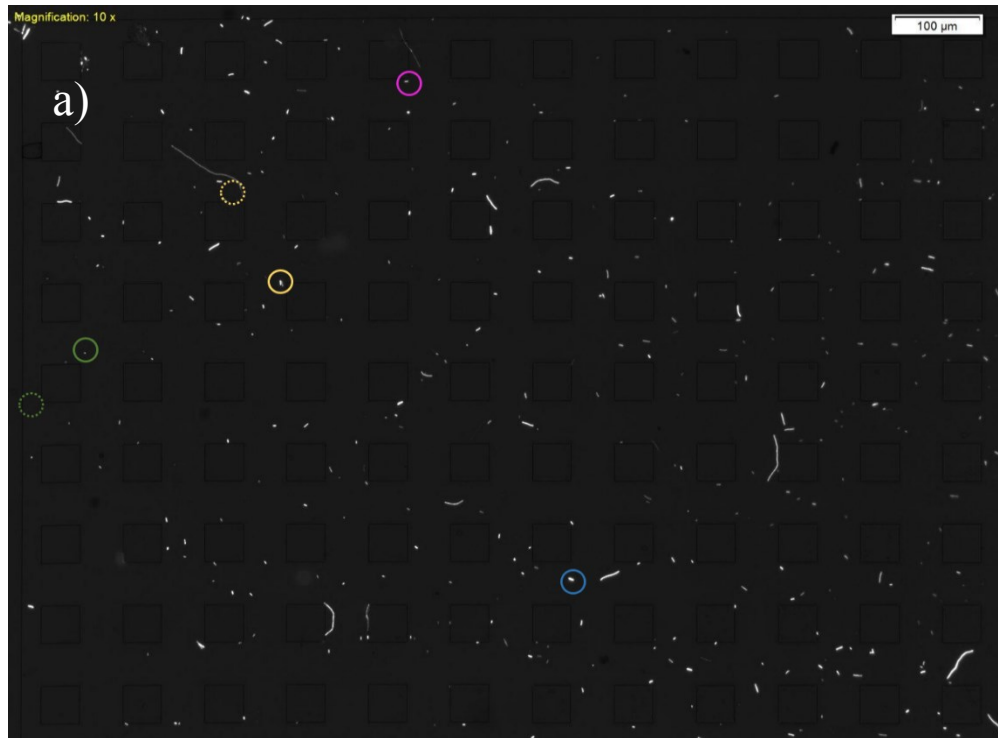


Figure A.1.1. a) Bacteria total displacement after 60 minutes for NBSA_C at first region at 15°, 45° and 75° and middle region at 45°

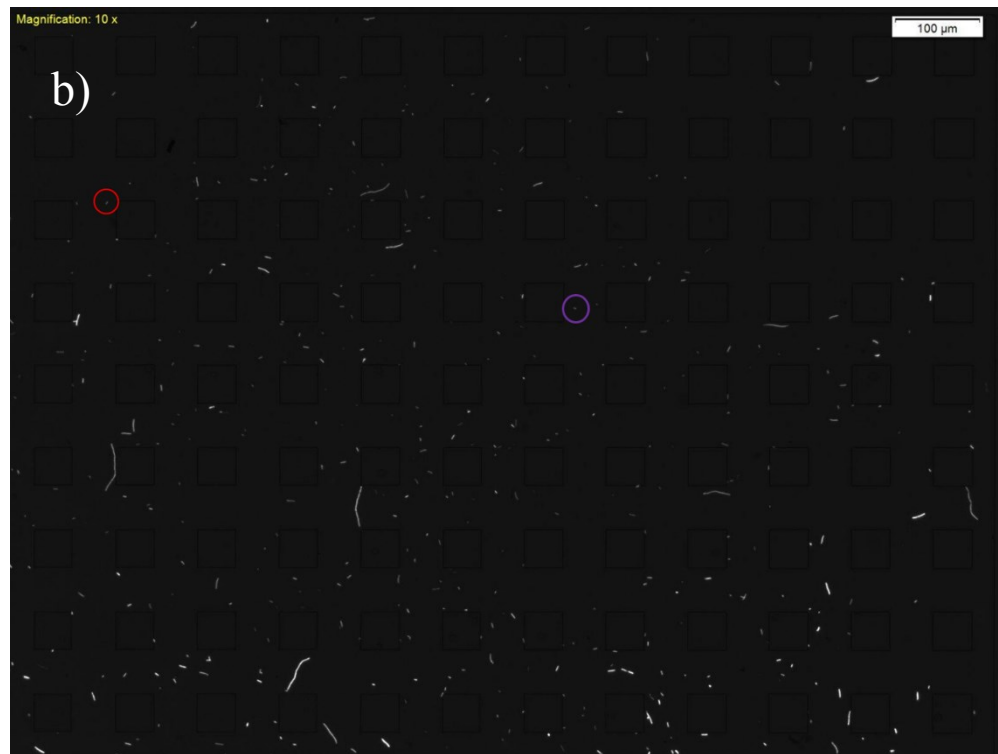


Figure A.1.1. b) Bacteria total displacement after 60 minutes for NBSA_C at middle and last at region 75°

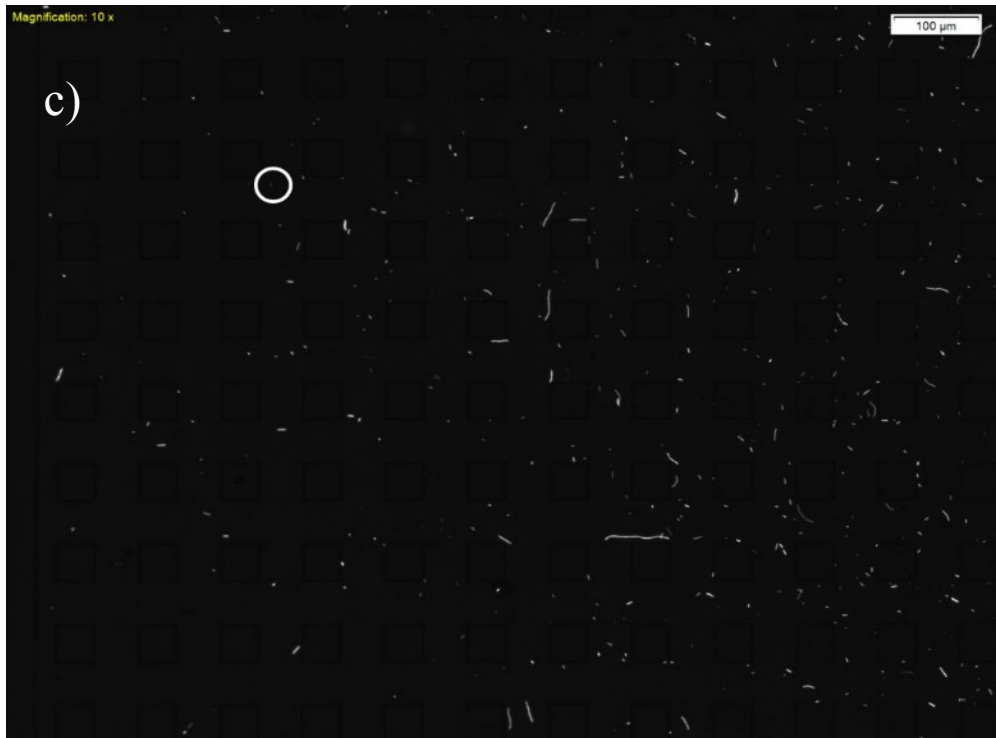


Figure A.1.1. c) Bacteria total displacement after 60 minutes for NBSA_C at middle region at 15°

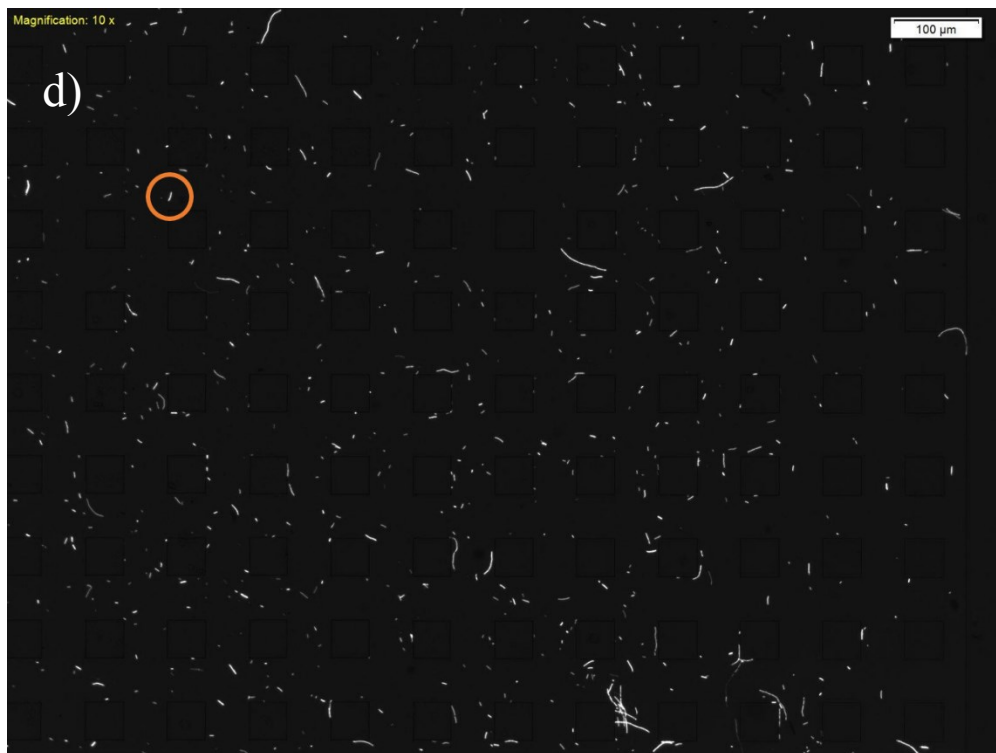


Figure A.1.1. d) Bacteria total displacement after 60 minutes for NBSA_C at last region at 45°

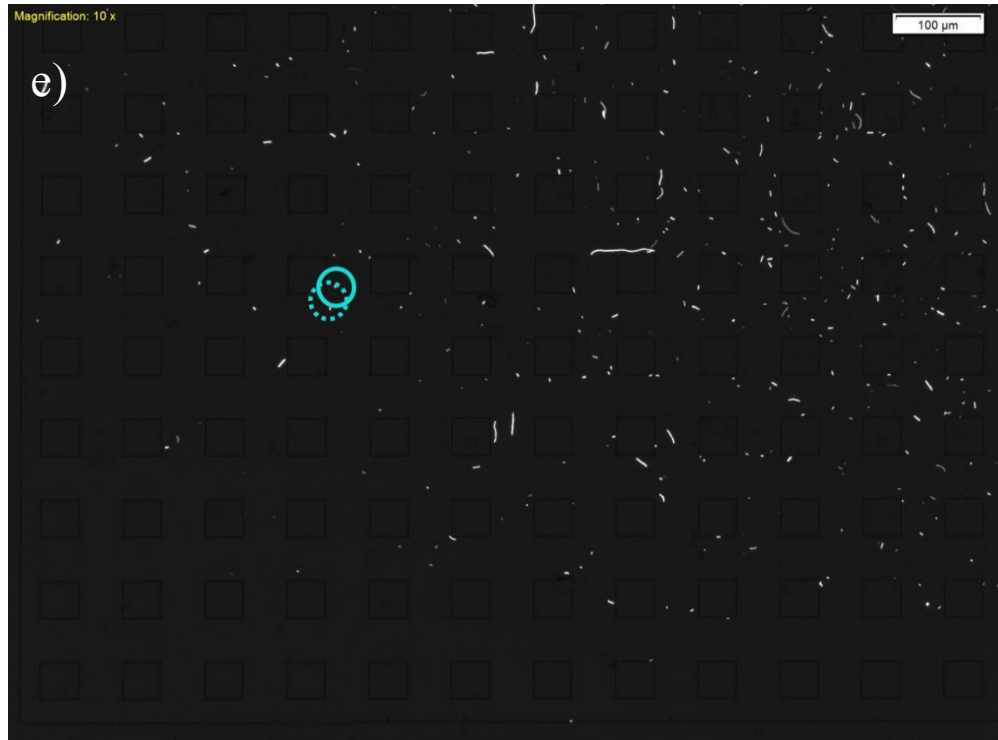
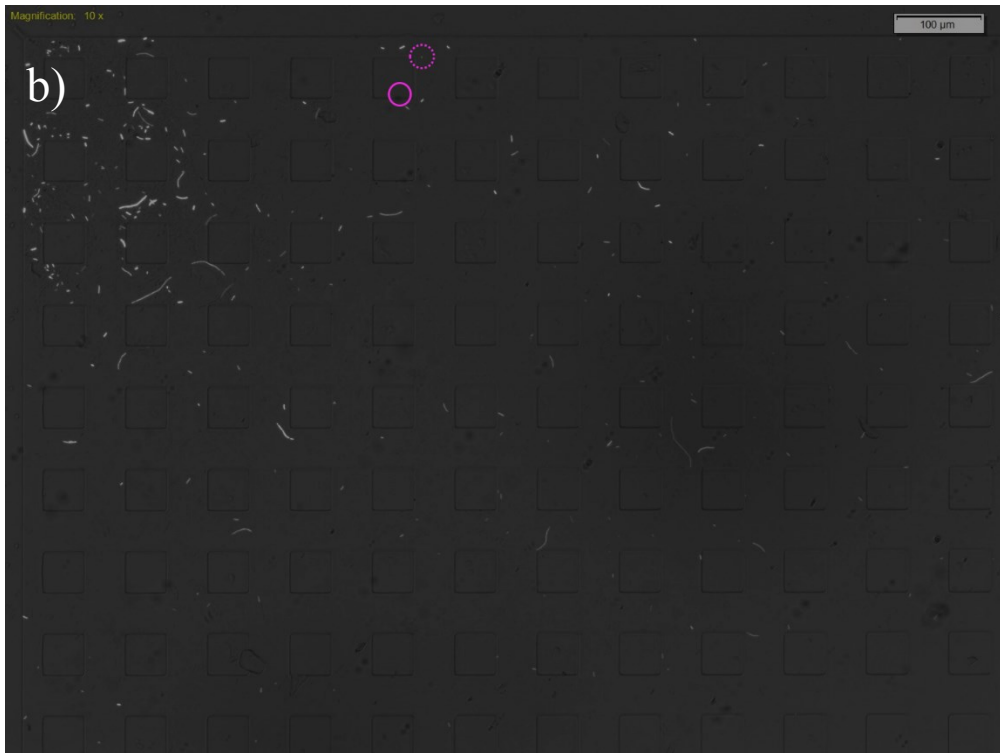
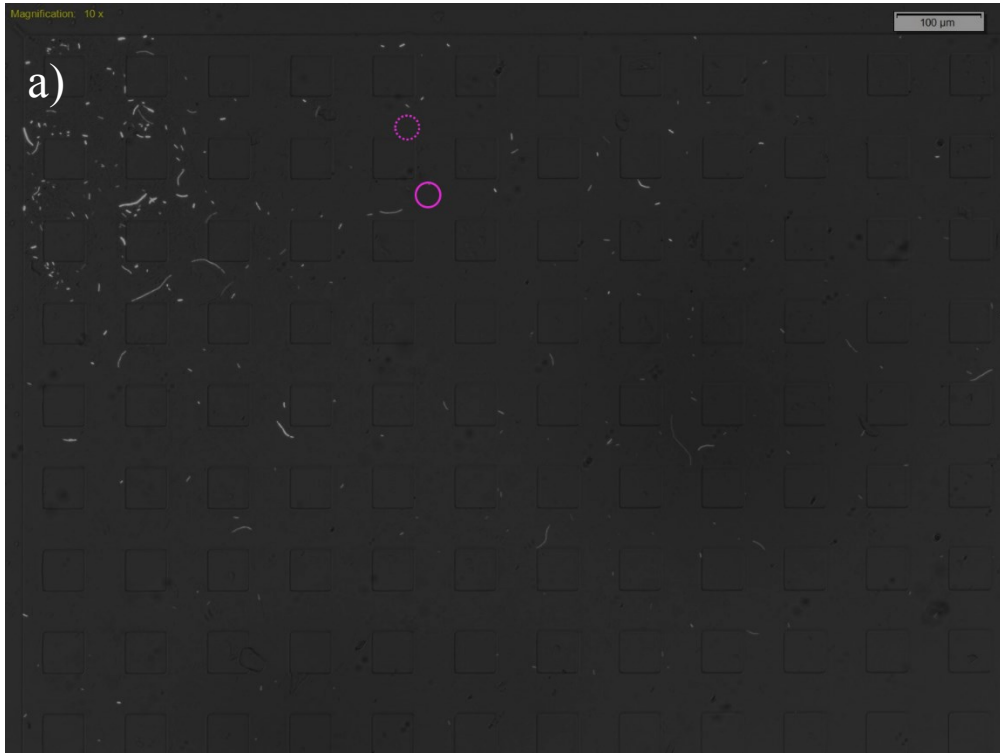


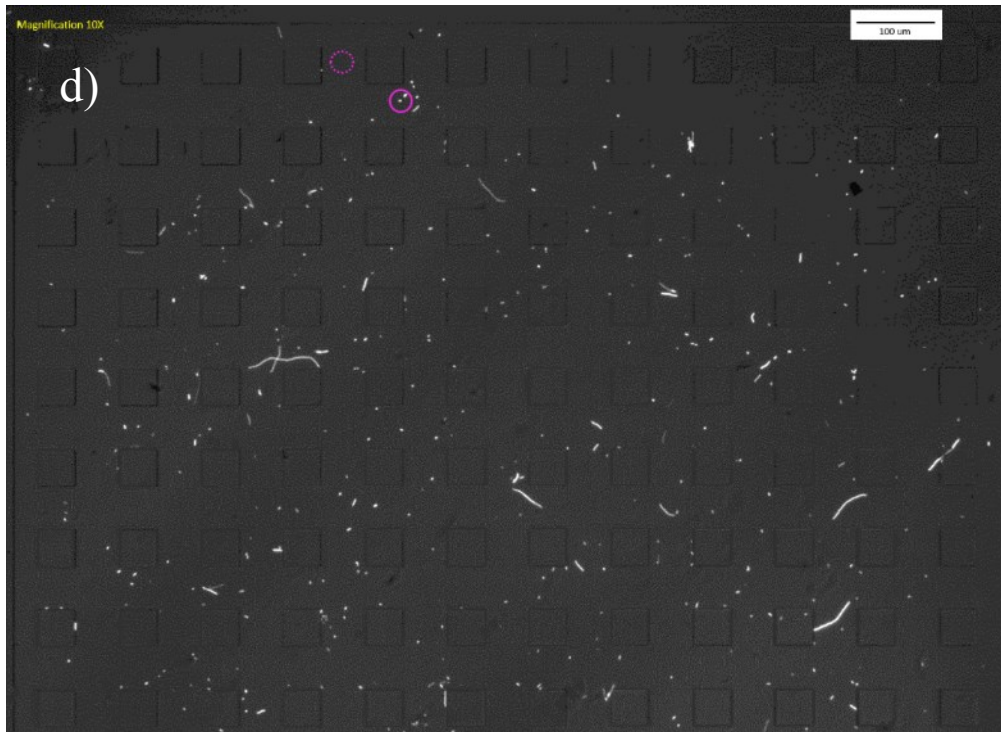
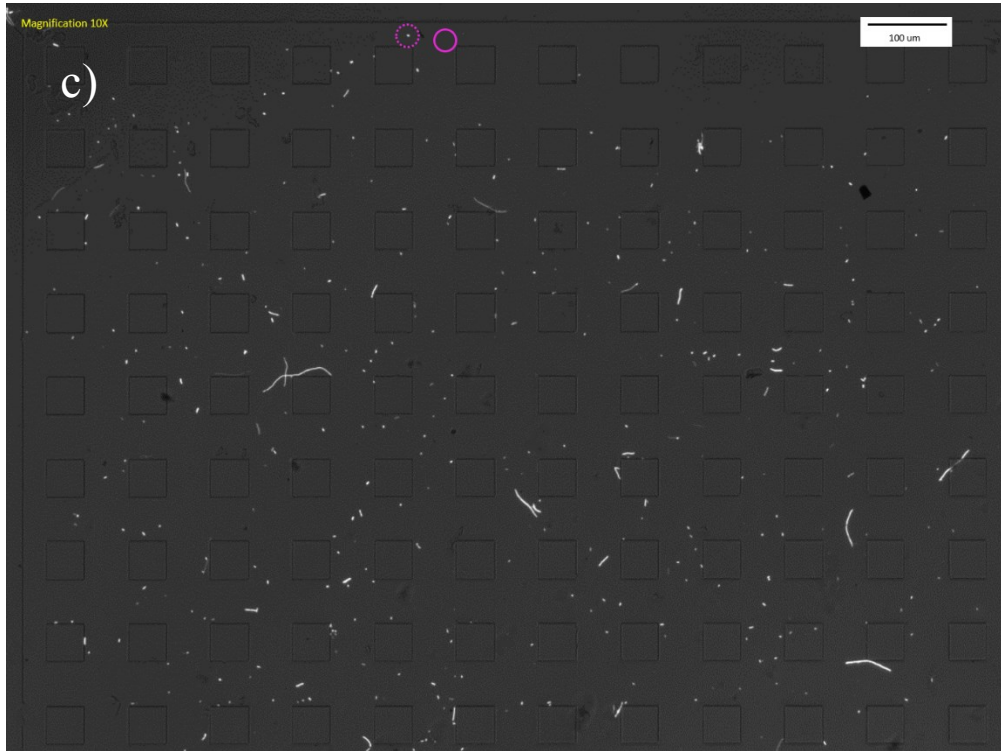
Figure A.1.1. e) Bacteria total displacement after 60 minutes for NBSA_C at last region at 15°

A.2. Microscopy Images of Control Experiments (Water Treatment)

Figure A.2.1 shows the microscopy images used to measure displacement of 6 bacteria (images a to f) during the 60 minutes of the control experiments. In control experiments, I introduce DI water to the loaded bacteria inside the device (flow rate of 0.01 mL/h) and I measured bacteria response to water during a period of 60 minutes. I repeated the experiment 2 times and the 2 practice of these experiments are abbreviated as C_E1 and C_E2 in this text (table 3.1). Figure A.2.1 shows the microscopy images used to measure bacteria displacement with initial position at the first region at 75° (section 1-1 of the imaging areas, see figure 3.4.2). In all images, dashed circles indicate the start position of bacteria and solid circle indicate the final position at that time step.

Figure A.2.2 shows the microscopy images used to measure displacement of 6 bacteria during the 60 minutes of the experiment for C_E1 and C_E2, first region at 45° (section 1-1 of the imaging areas, see figure 3.4.2). Figure A.2.3 is in regard to bacteria at first region at 15°, figure A.2.4 is in regard to bacteria at middle region at 75°, figure A.2.5 in regard to middle region at 45° and figure A.2.6 in regard to middle region at 15°. For the last region at 75°, 45° and 15° figures A.2.7, A.2.8 and A.2.9 show microscopy images respectively.





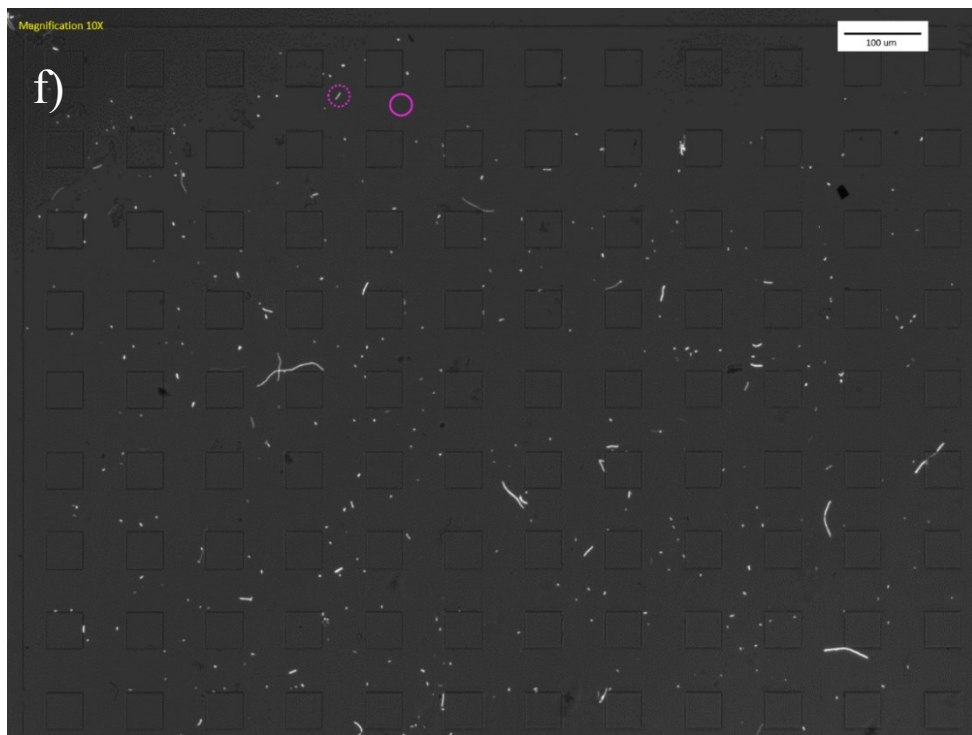
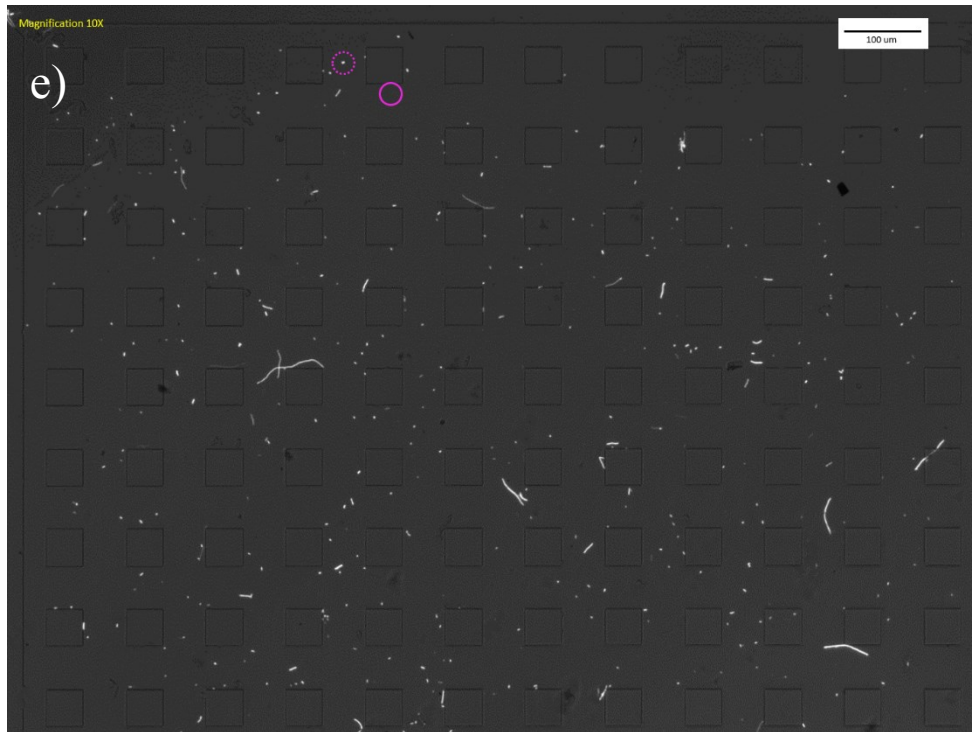
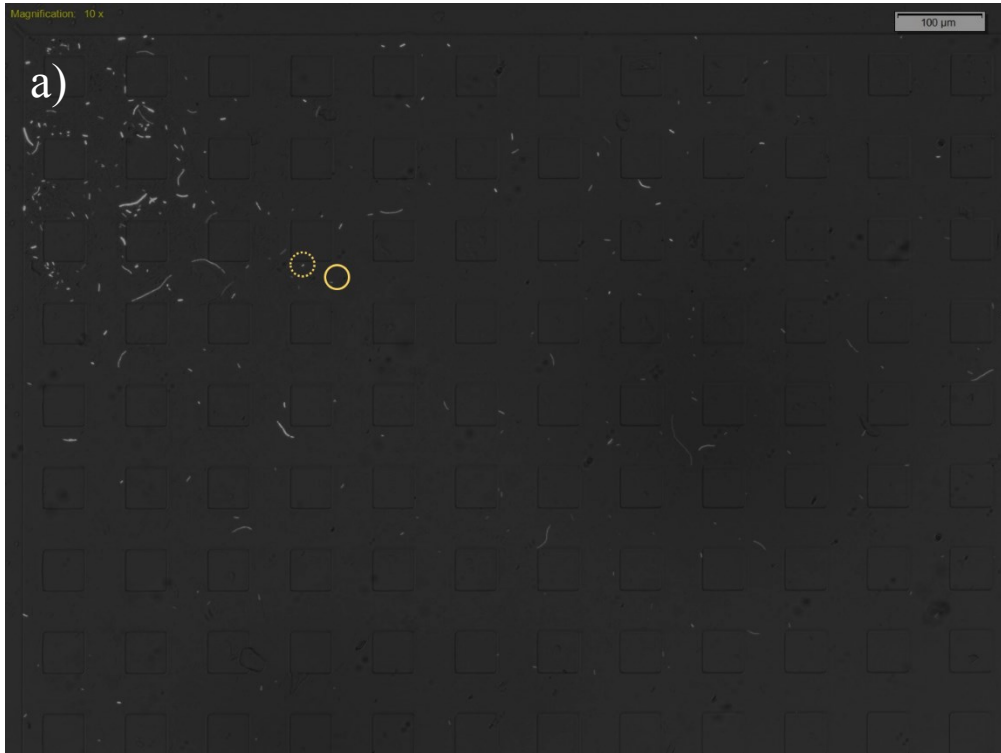
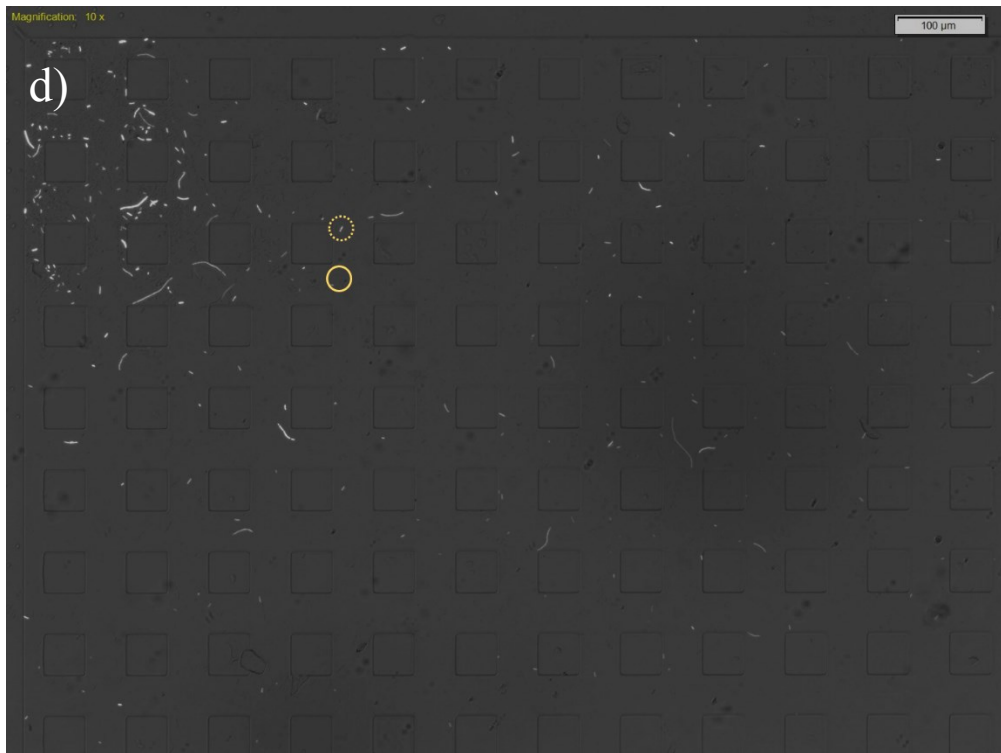


Figure A.2.1. Bacteria total displacement of 6 different analyzed bacteria (images a to f) at the end of 60 minutes for C_E1 (images a and b) and C_E2 (images c to f) at first region at 75°





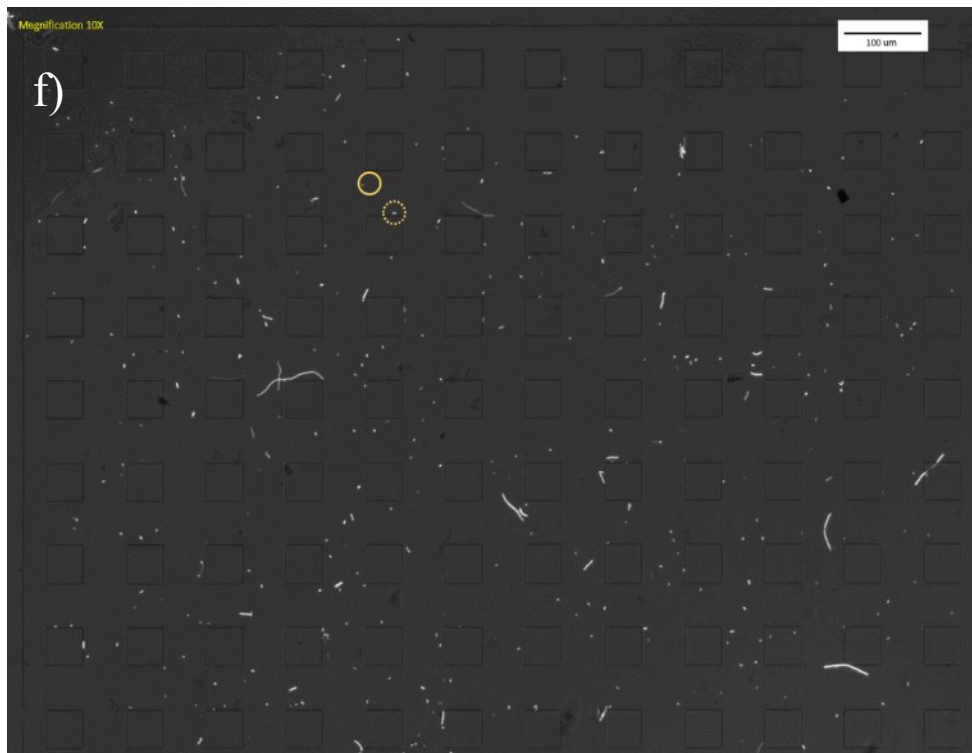
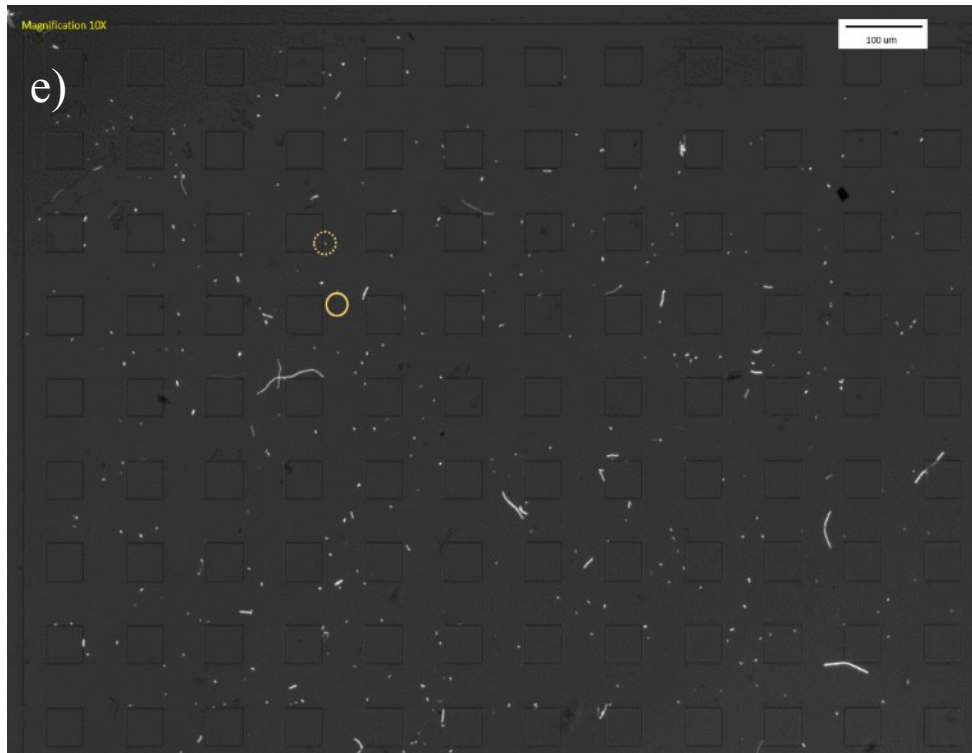
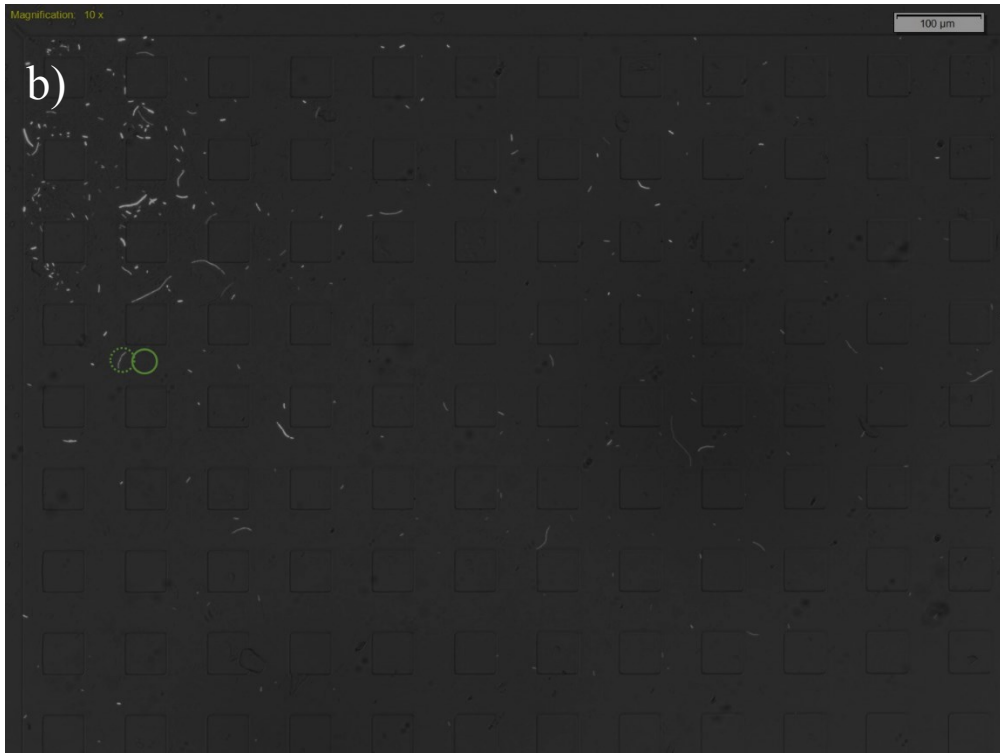
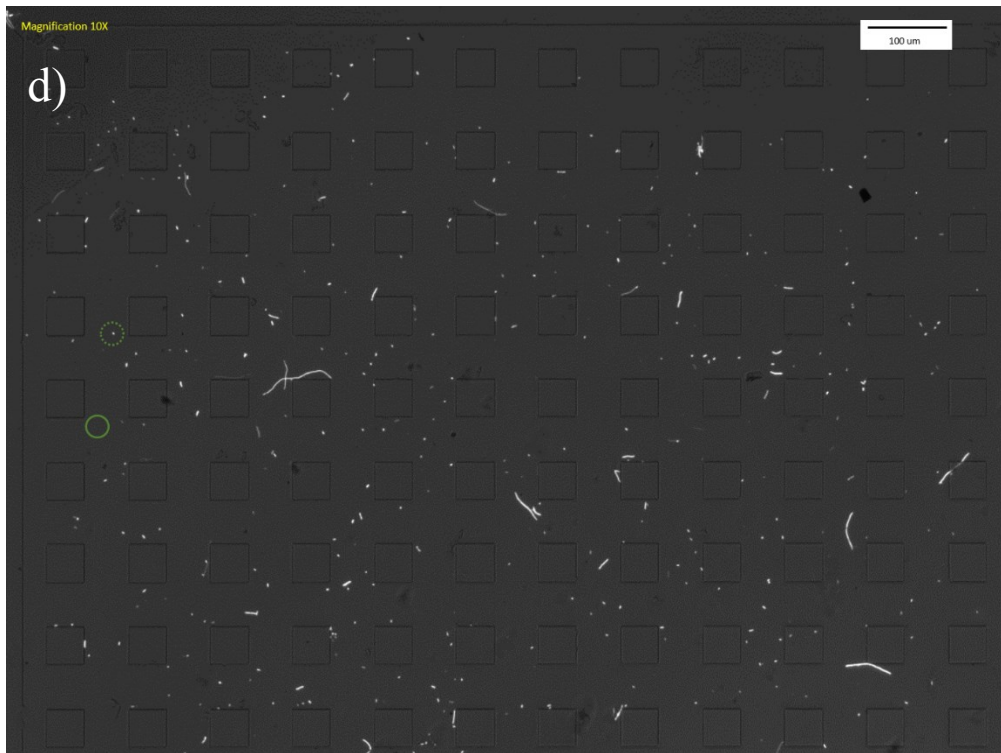


Figure A.2.2. Bacteria total displacement of 6 different analyzed (images a to f) at the end of 60 minutes for C_E1 (images a to d) and C_E2 (images e and f) at first region at 45°





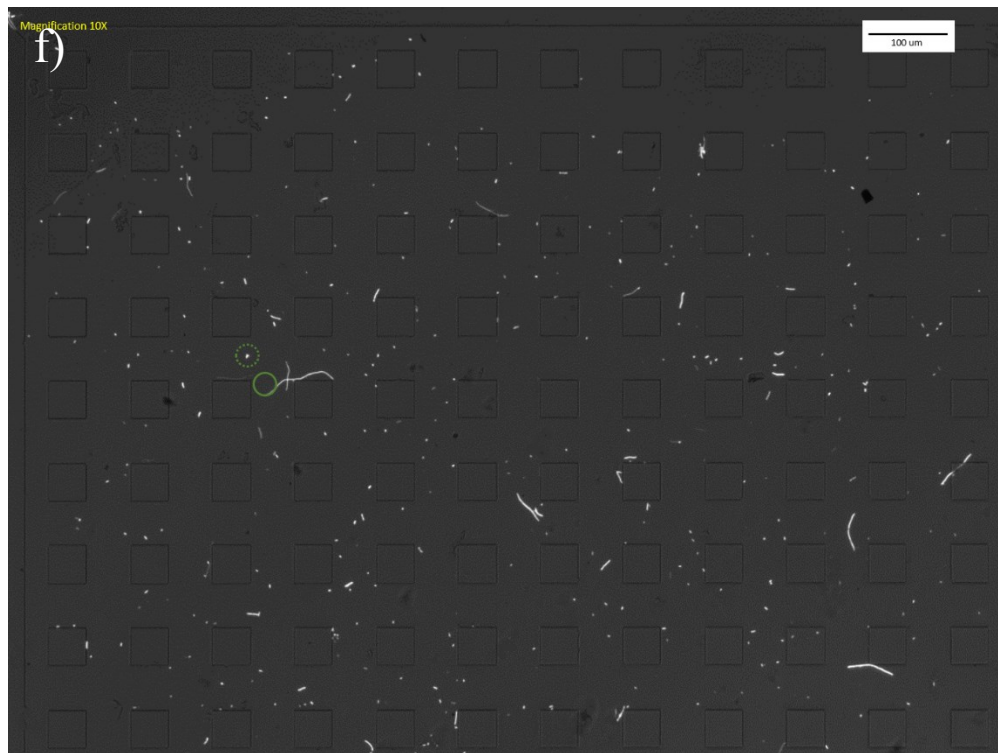
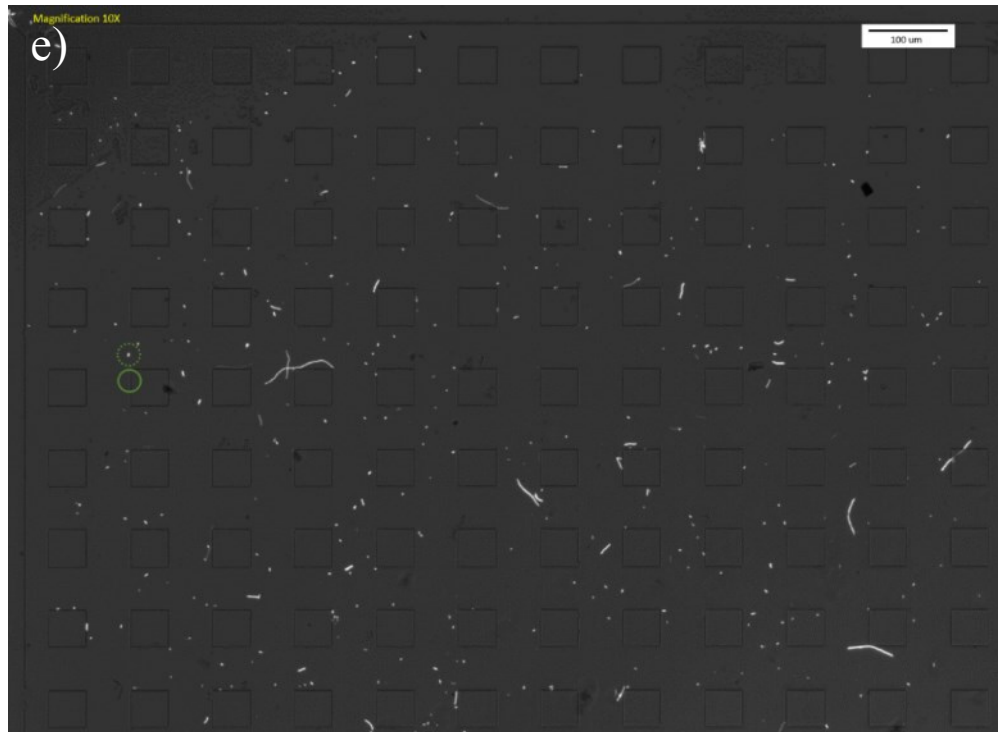
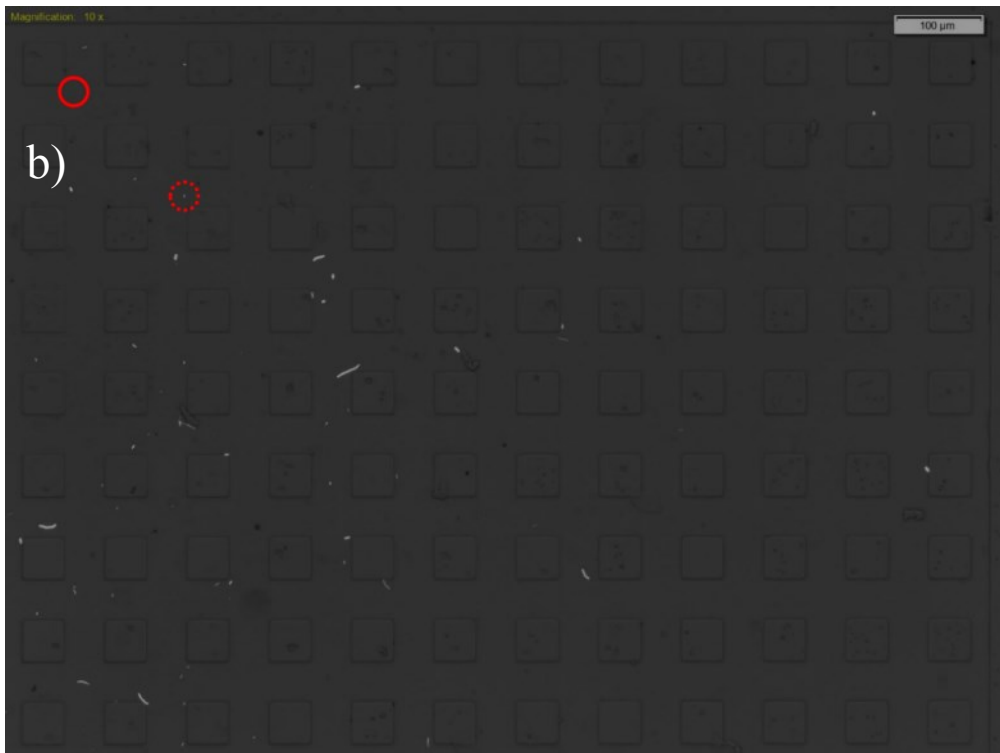
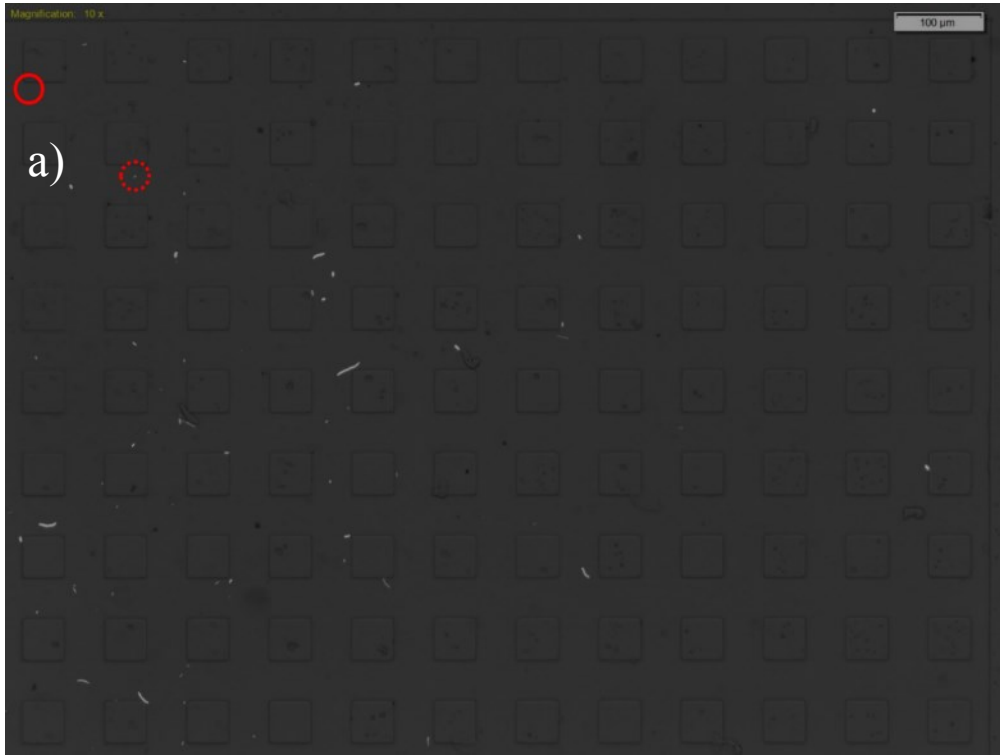
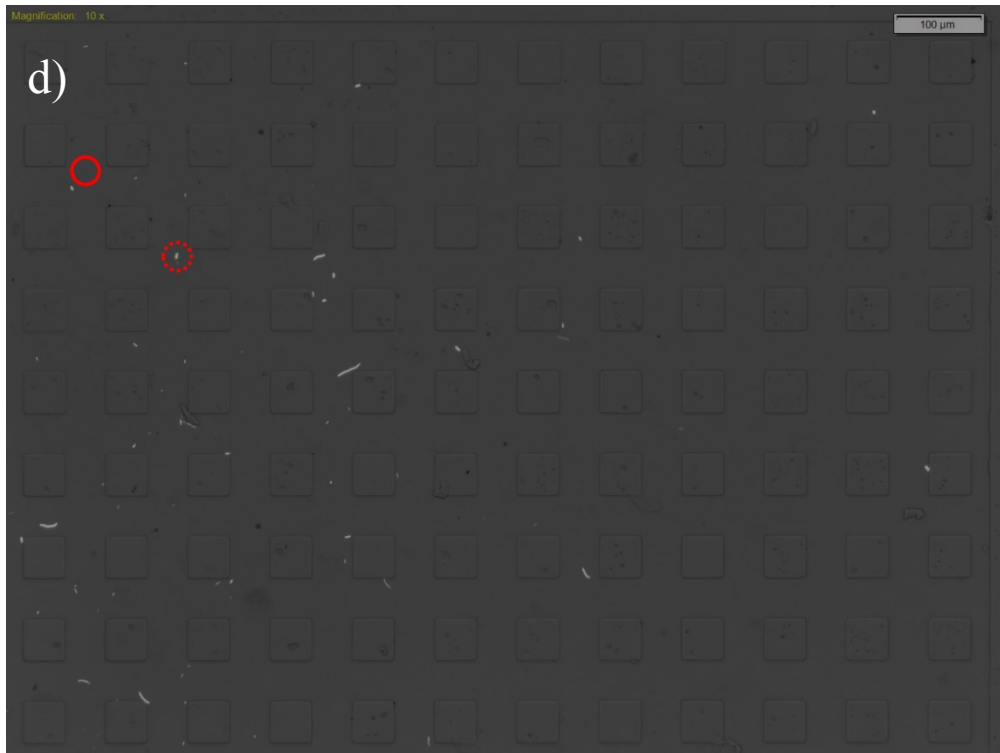


Figure A.2.3. Bacteria total displacement of 6 different analyzed bacteria (images a to f) at the end of 60 minutes for C_E1 (images a to c) and C_E2 (images d to f) at first region at 15°





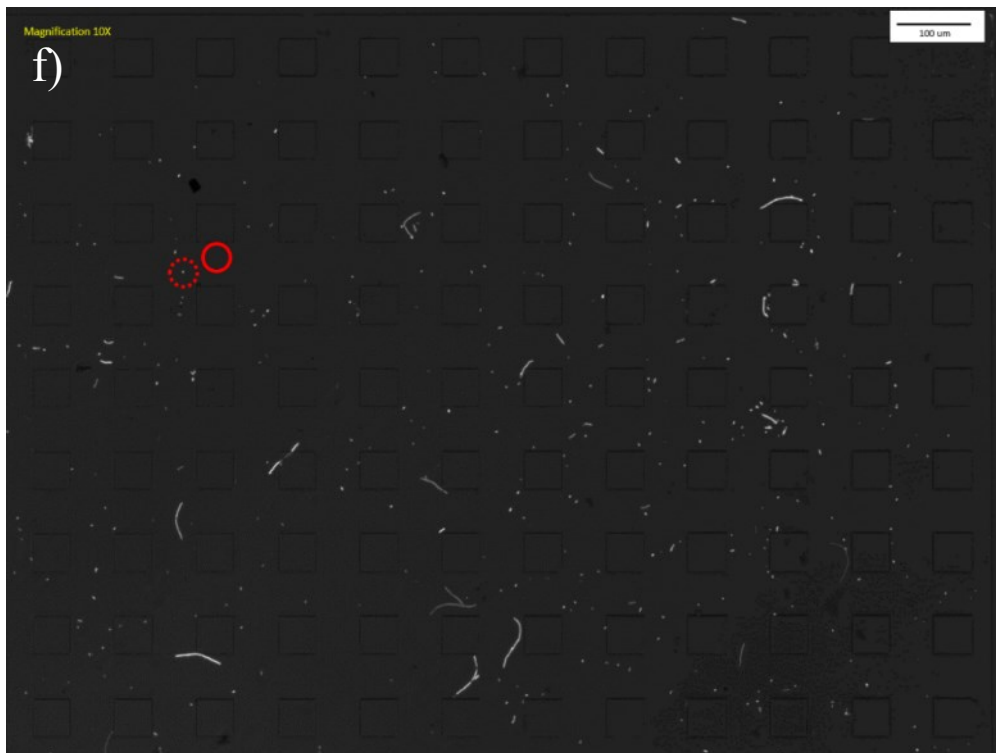
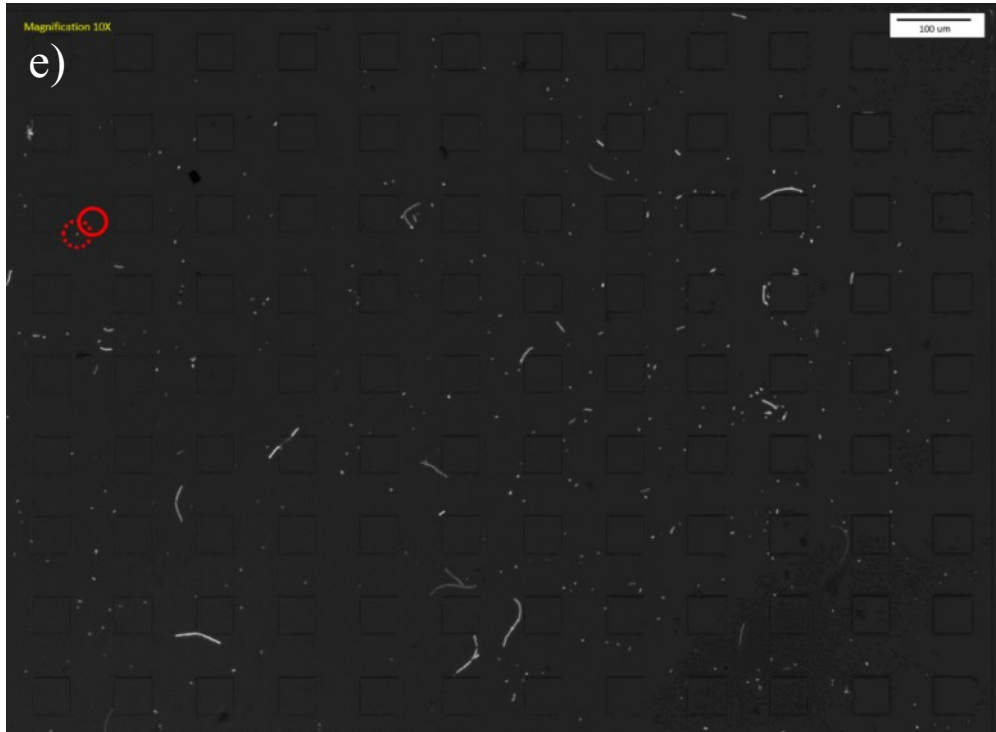
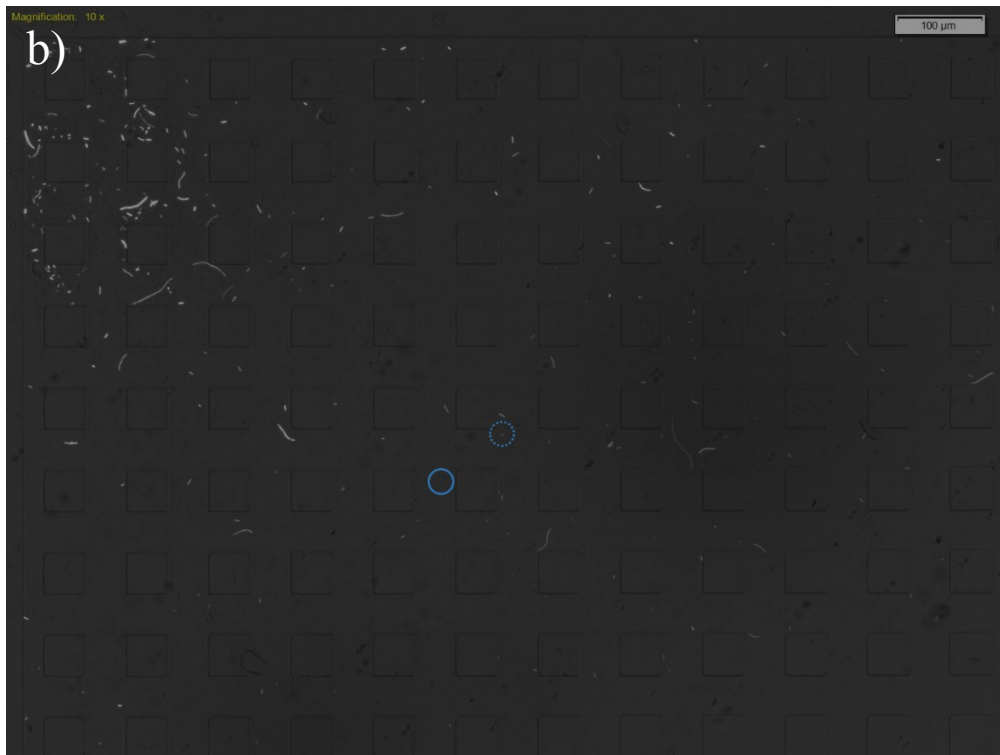
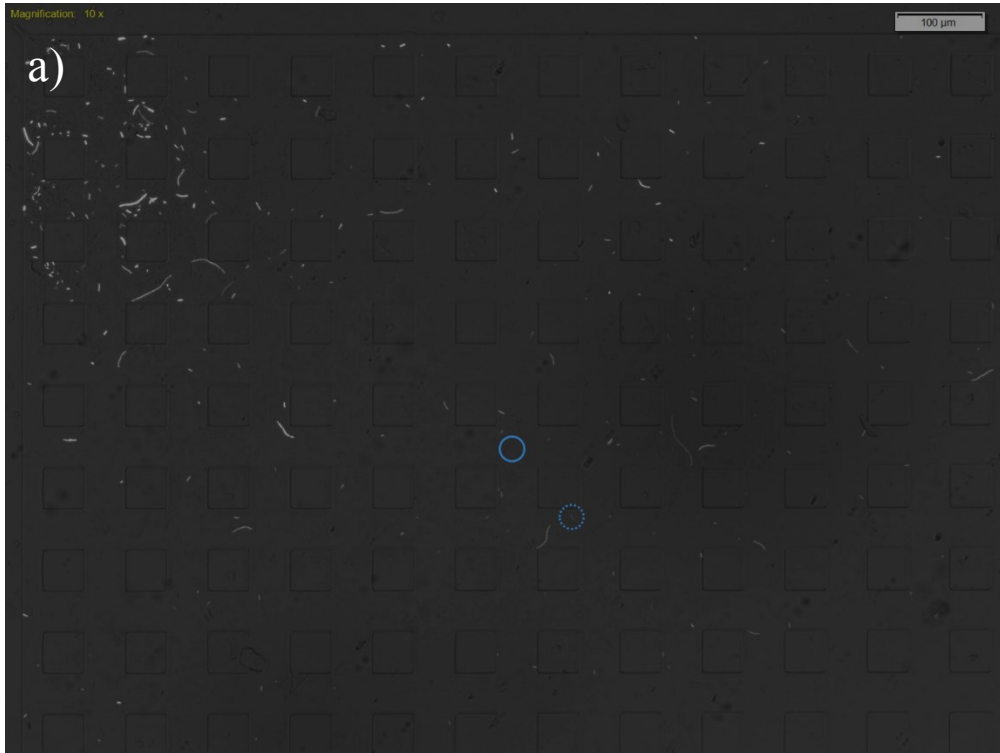
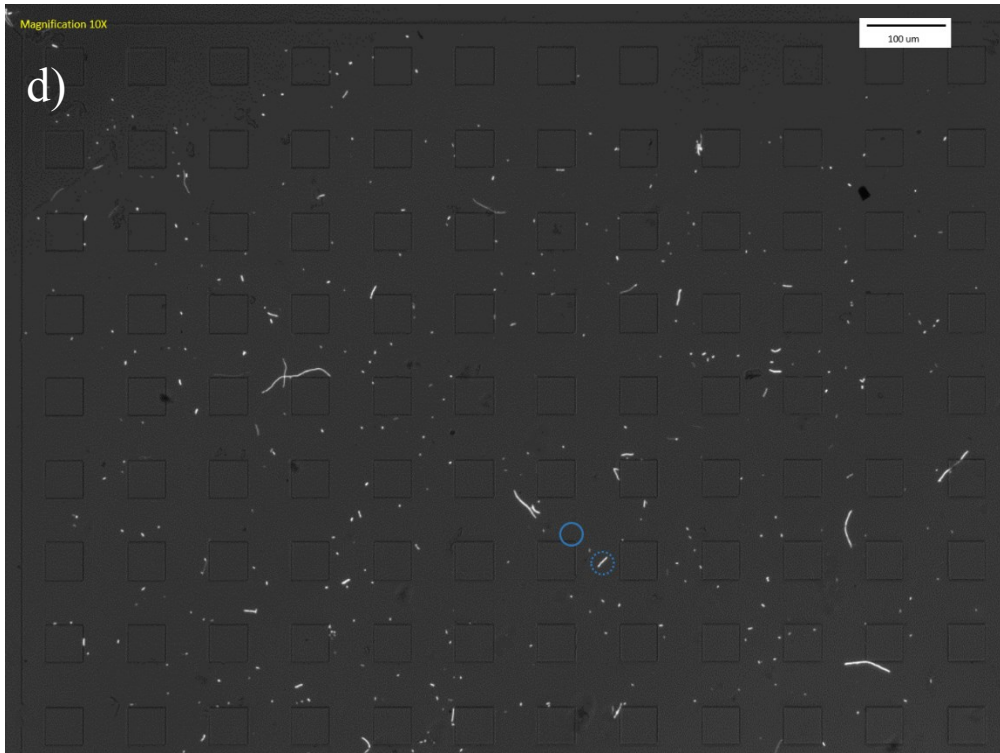
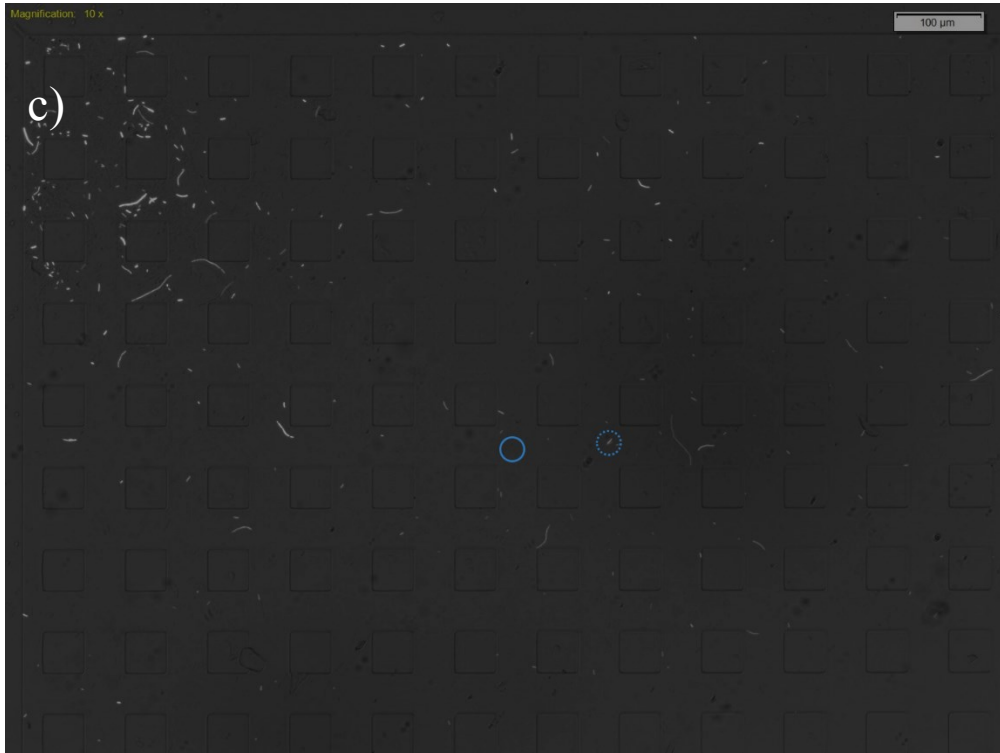


Figure A.2.4. Bacteria total displacement of 6 different analyzed (images a to f) at the end of 60 minutes for C_E1 (images a to d) and C_E2 (images e and f) at middle region at 75°





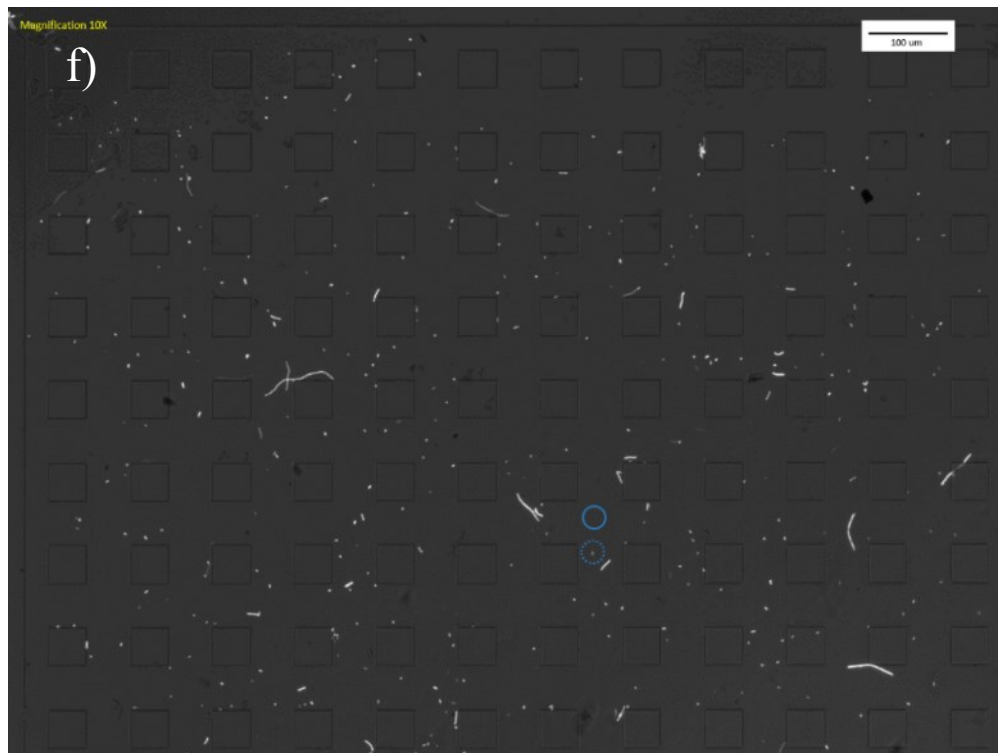
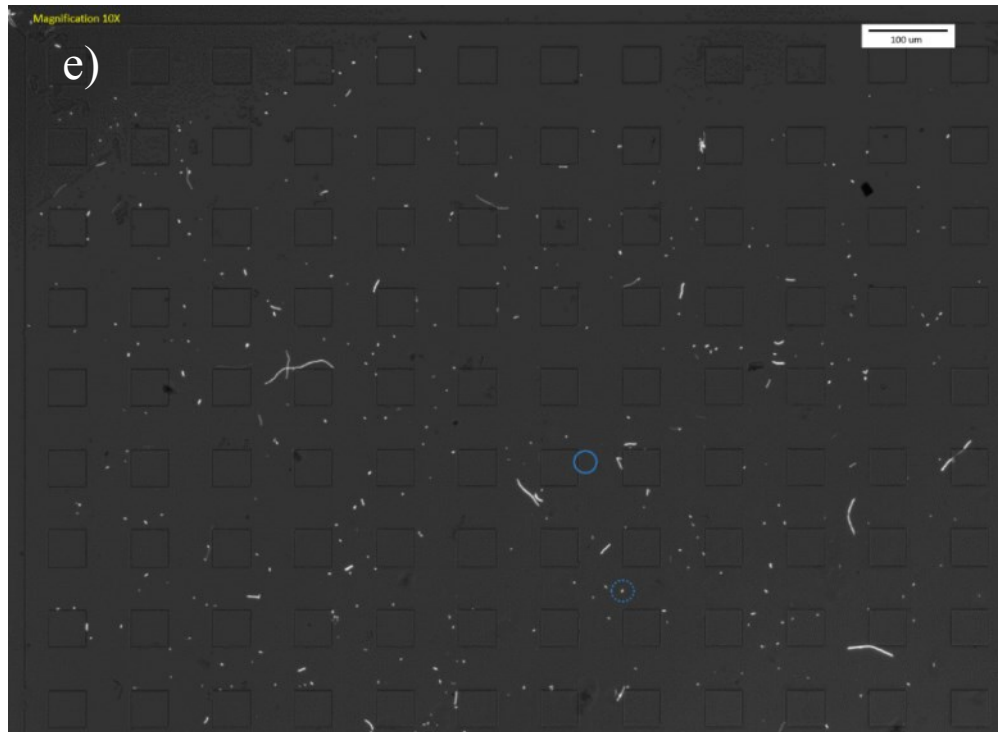
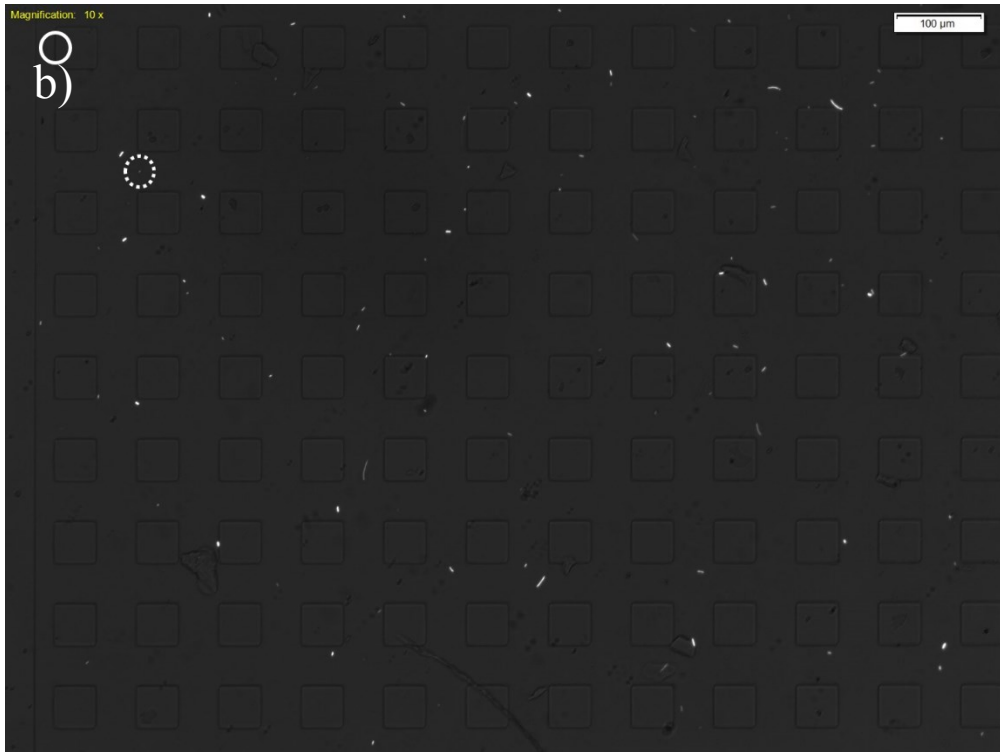
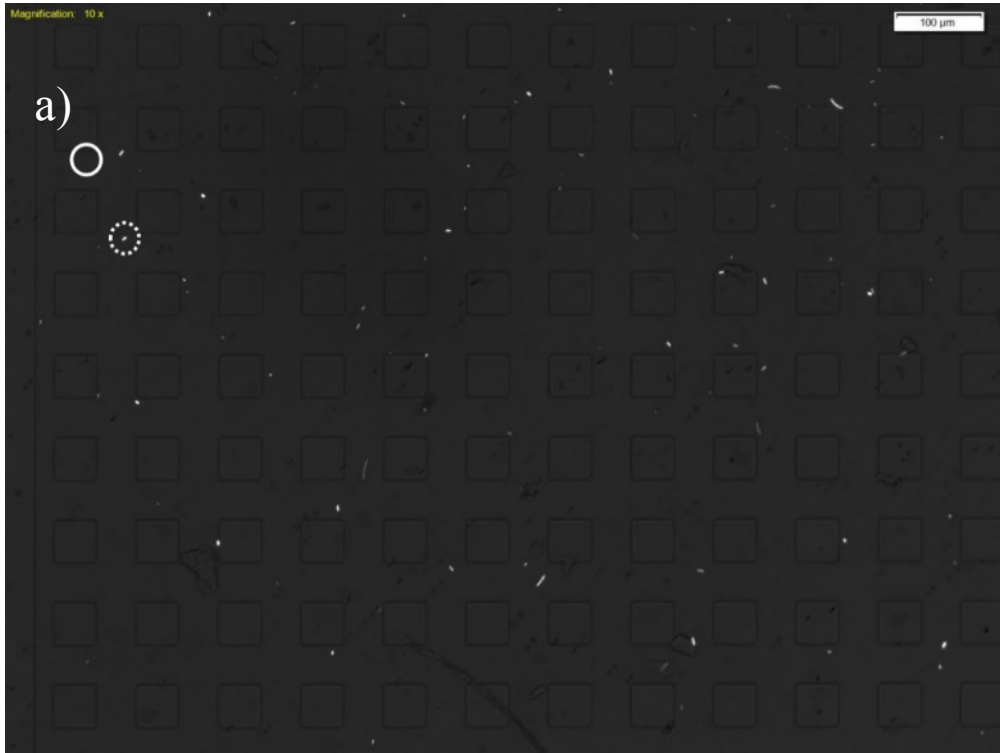
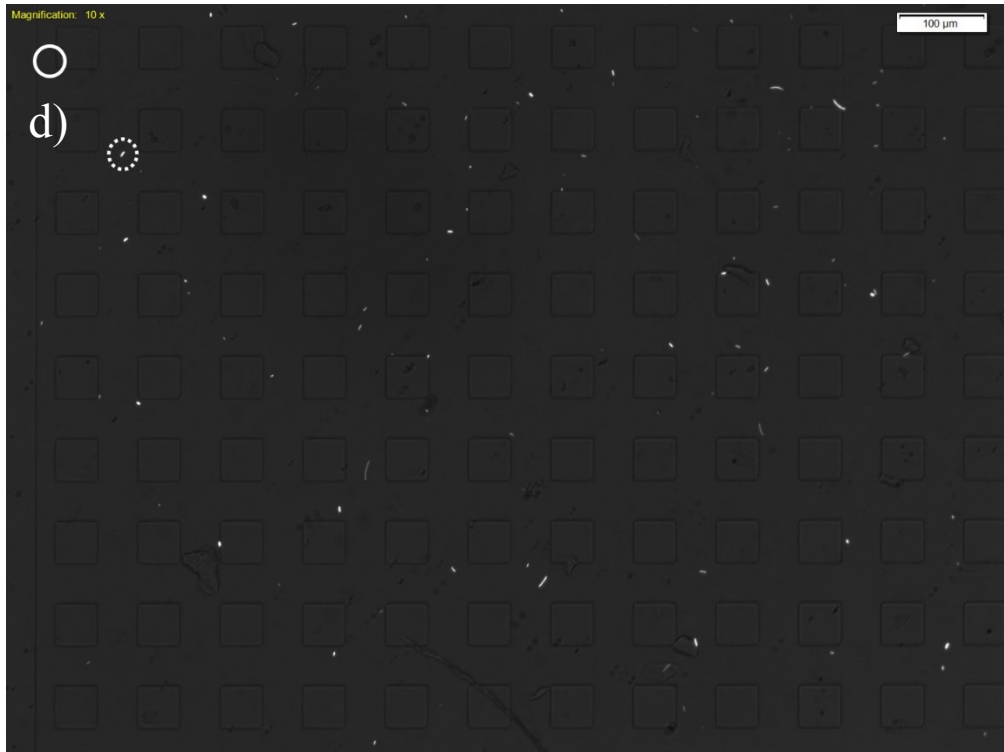
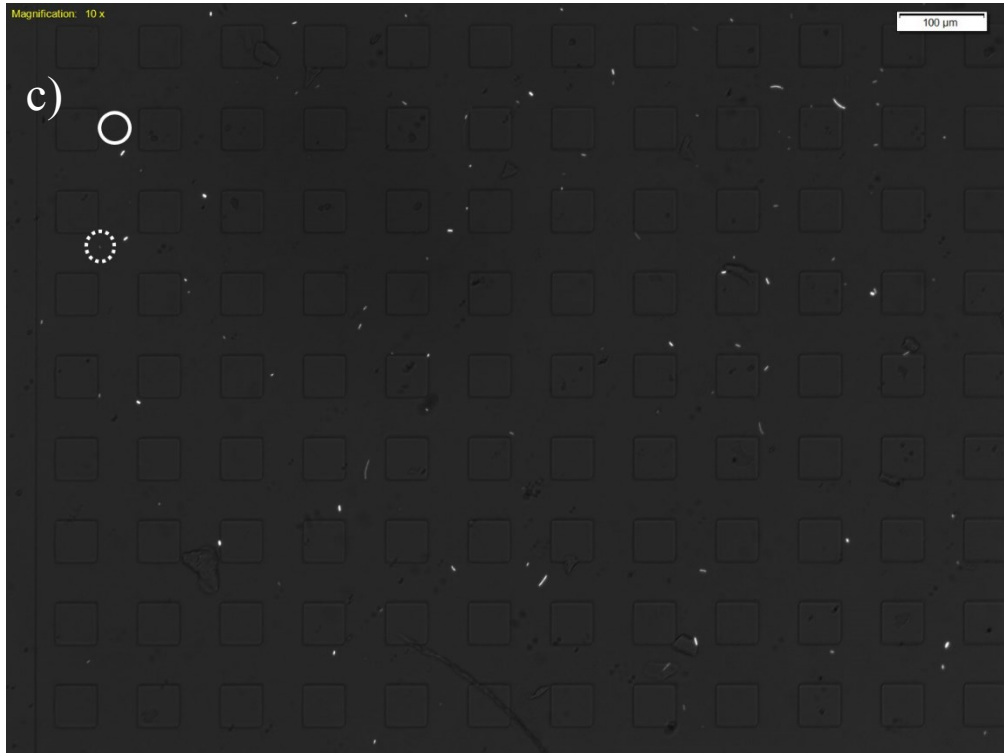


Figure A.2.5. Bacteria total displacement of 6 different analyzed bacteria (images a to f) at the end of 60 minutes for C_E1 (images a to c) and C_E2 (images d to f) at middle region at 45°





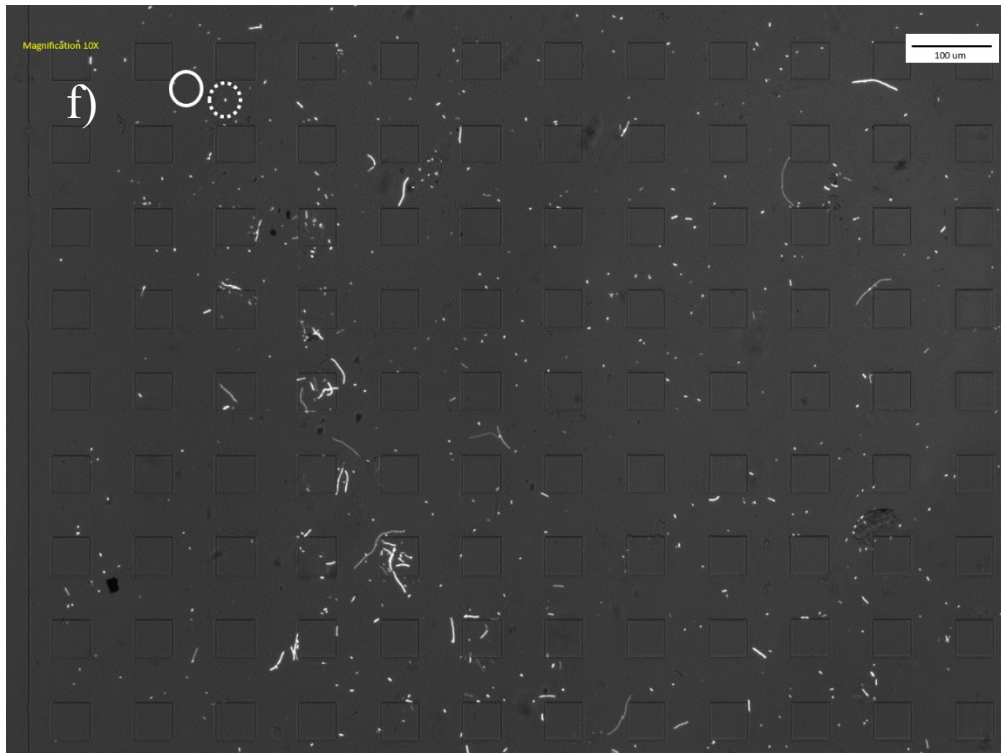
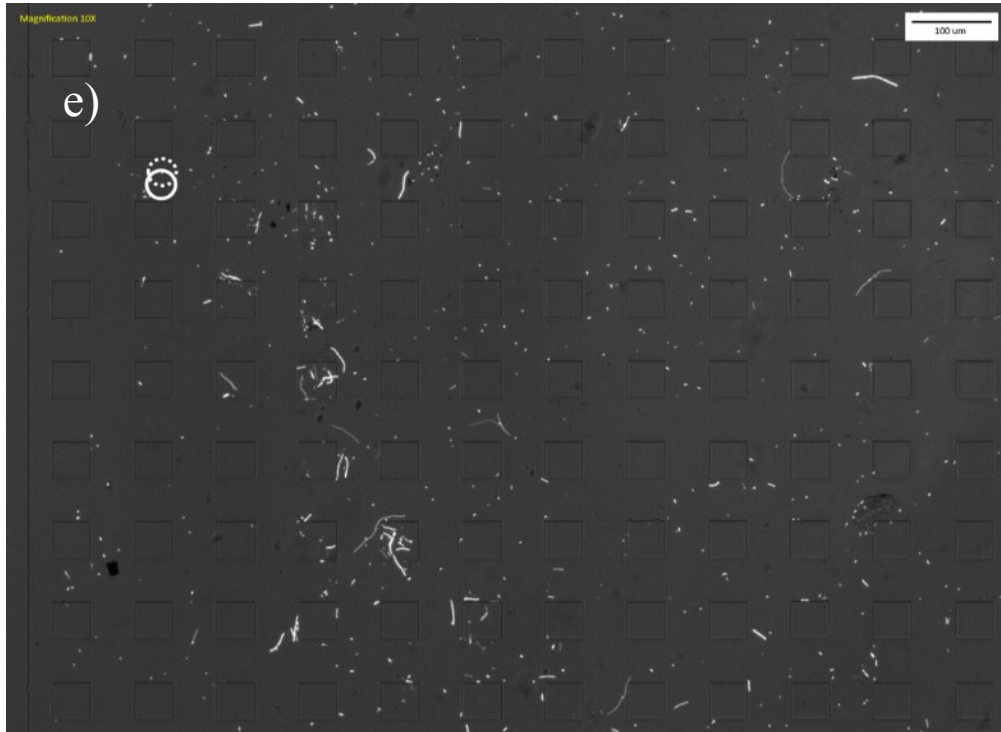
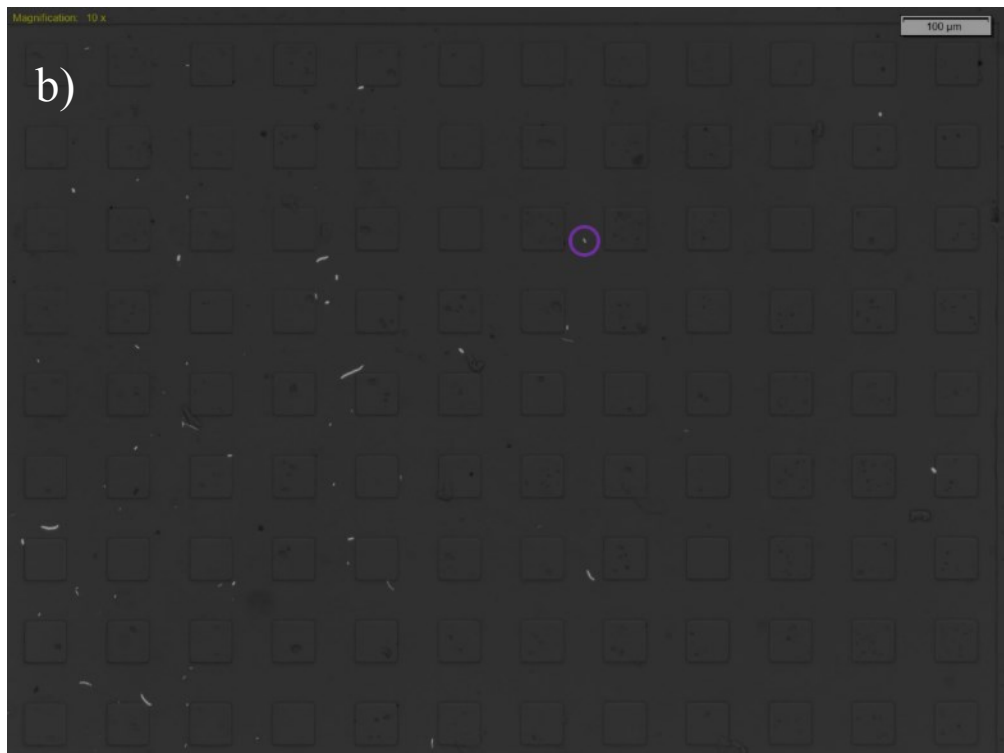
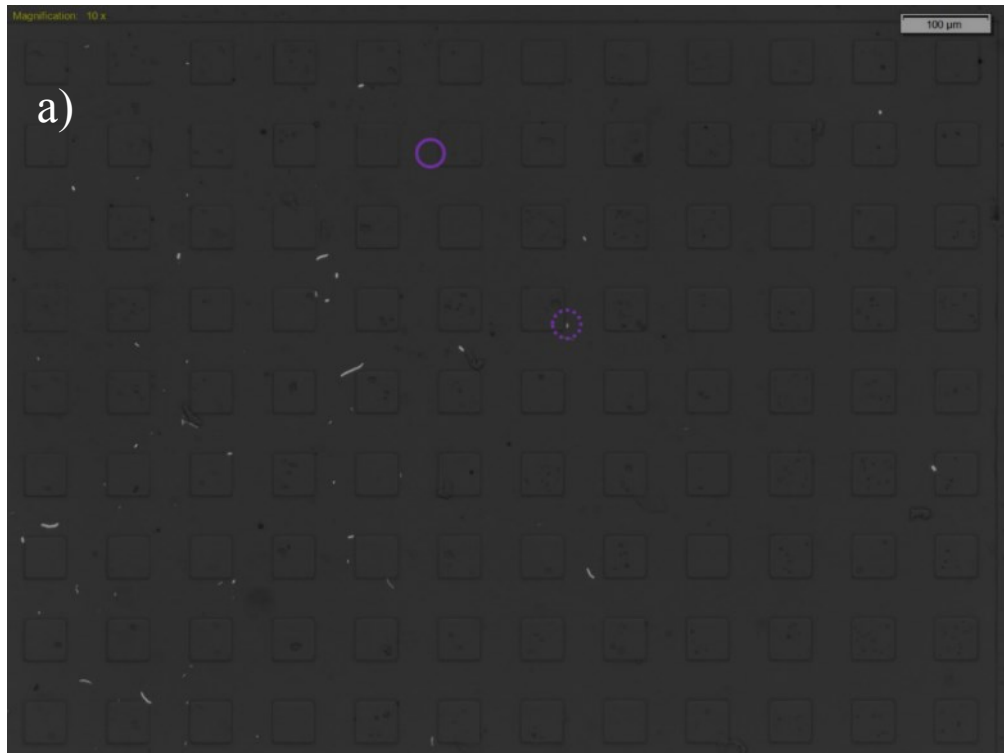
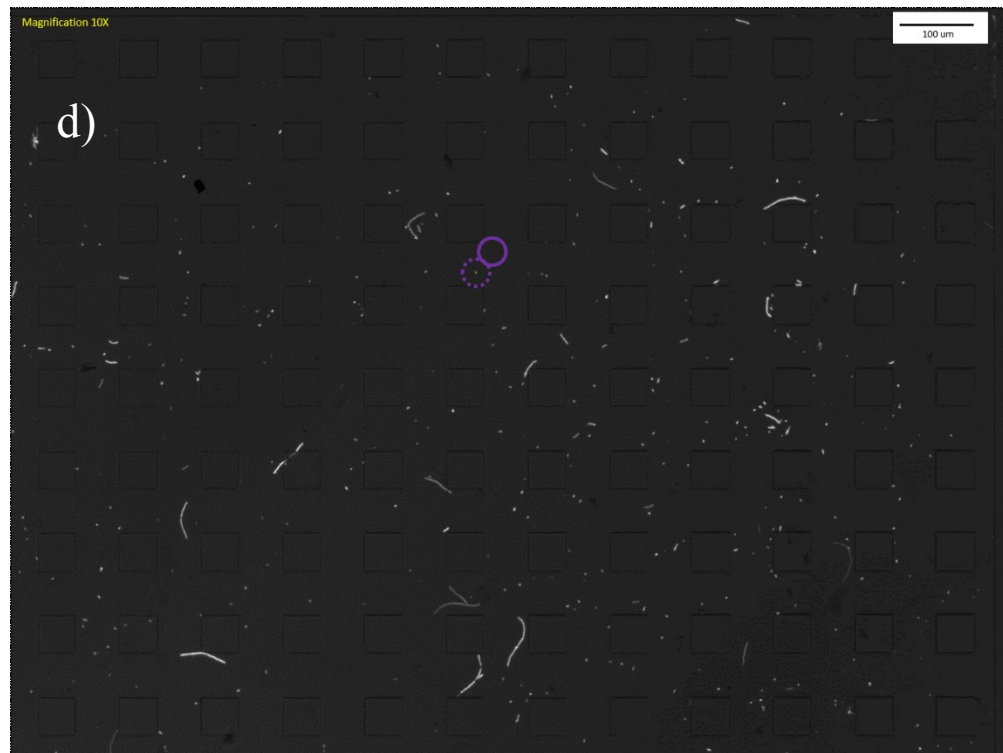
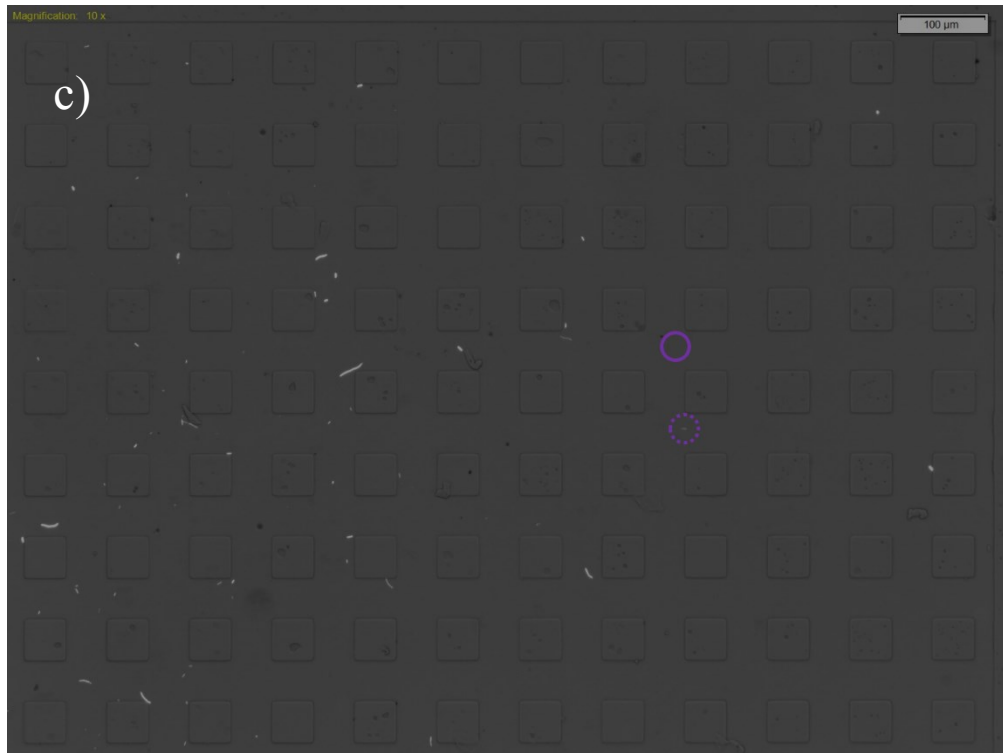


Figure A.2.6. Bacteria total displacement of 6 different analyzed bacteria (images a to f) at the end of 60 minutes for C_E1 (images a to d) and C_E2 (images e and f) at middle region at 15°





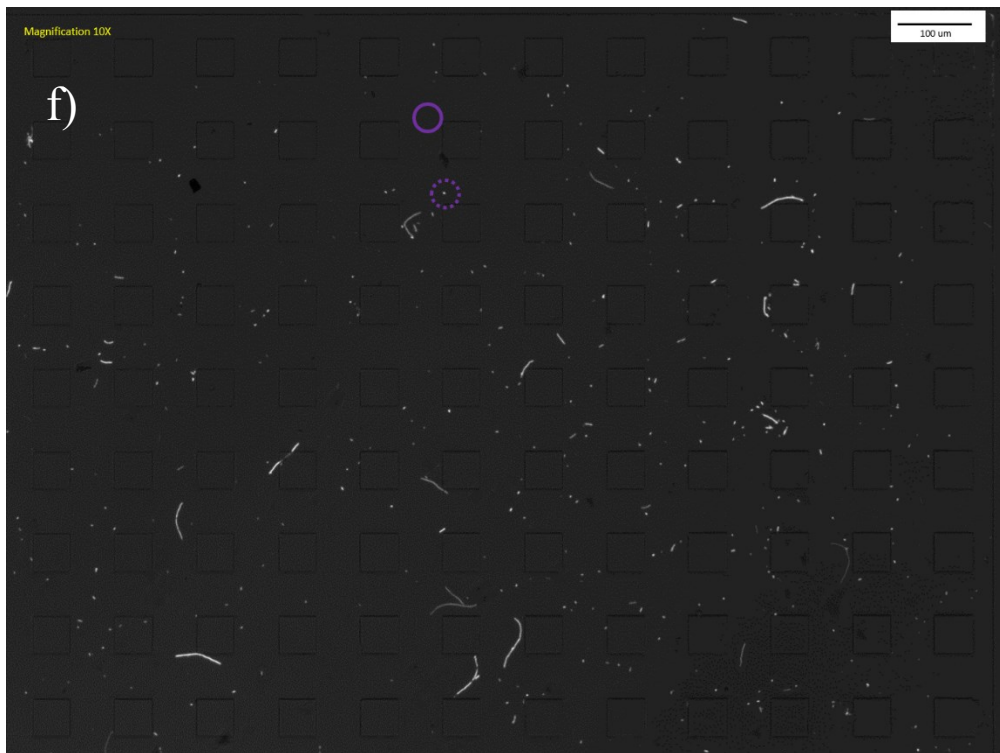
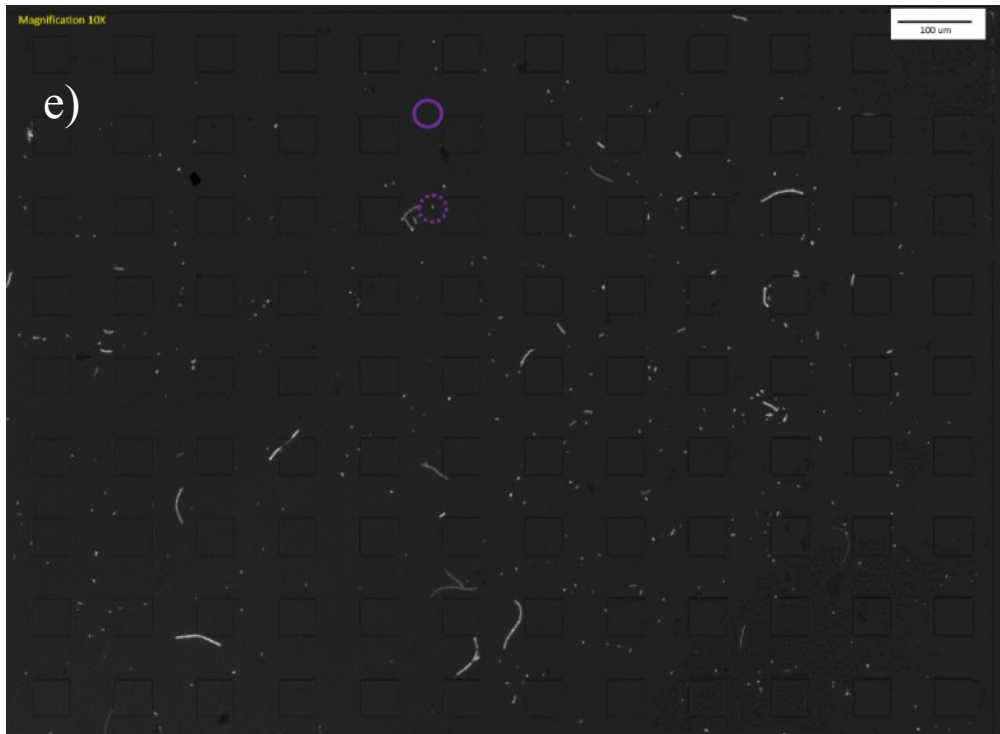
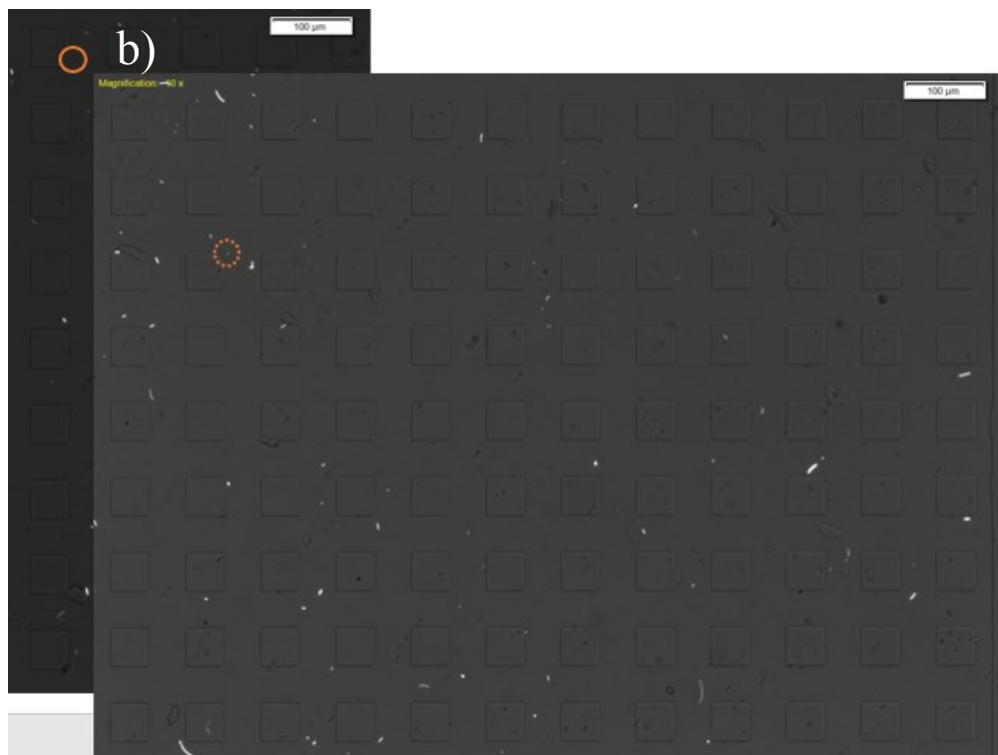
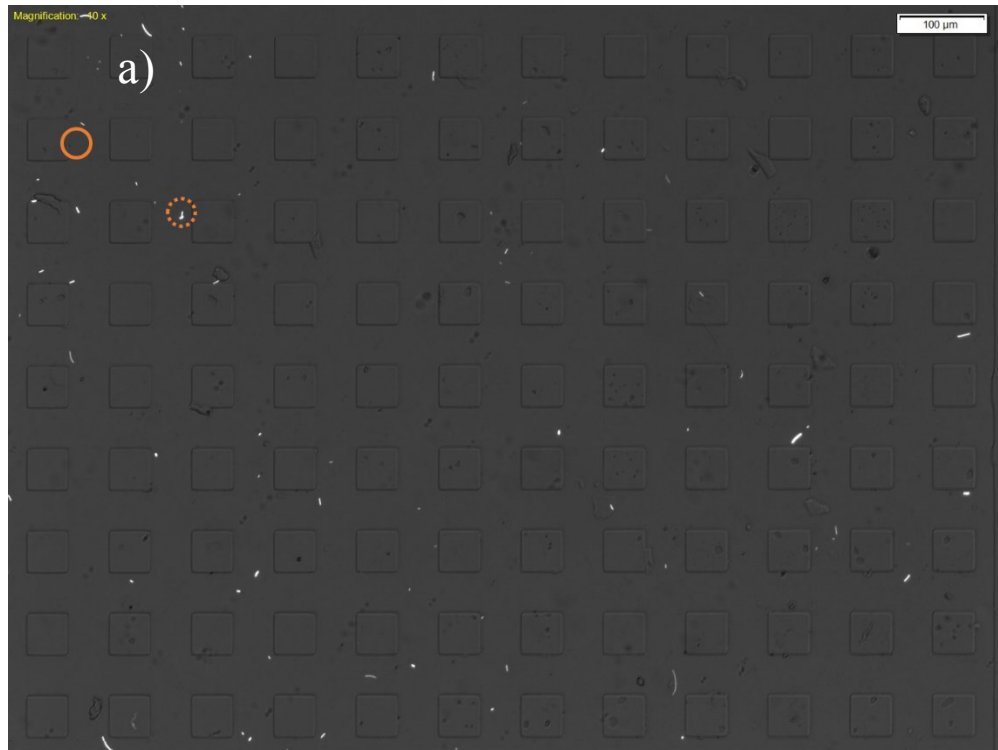
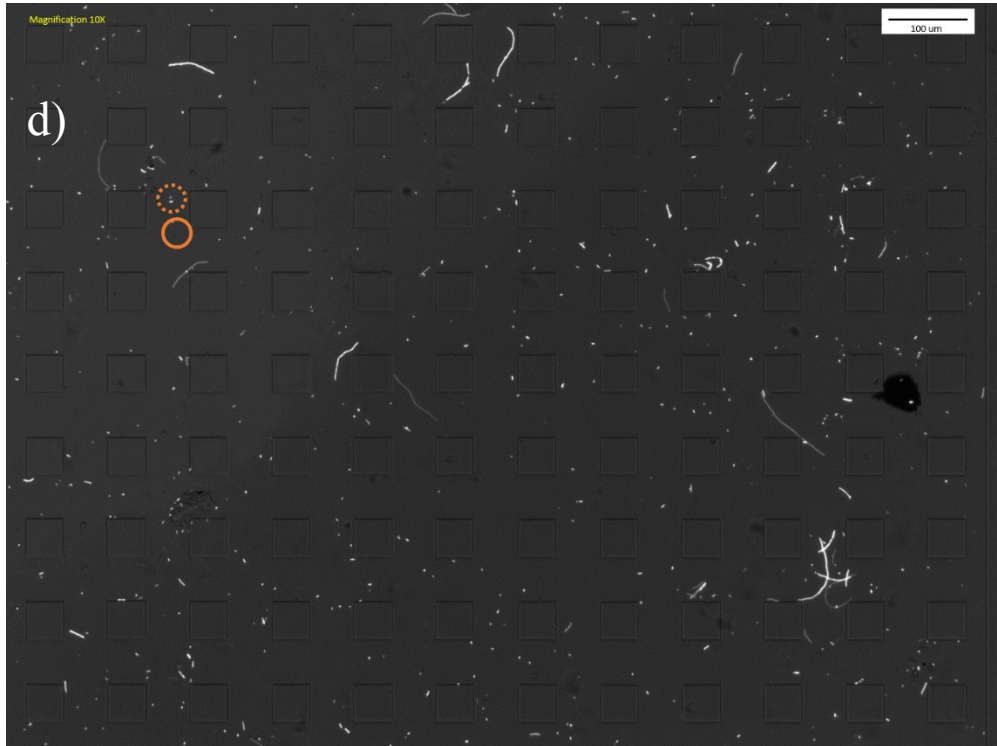
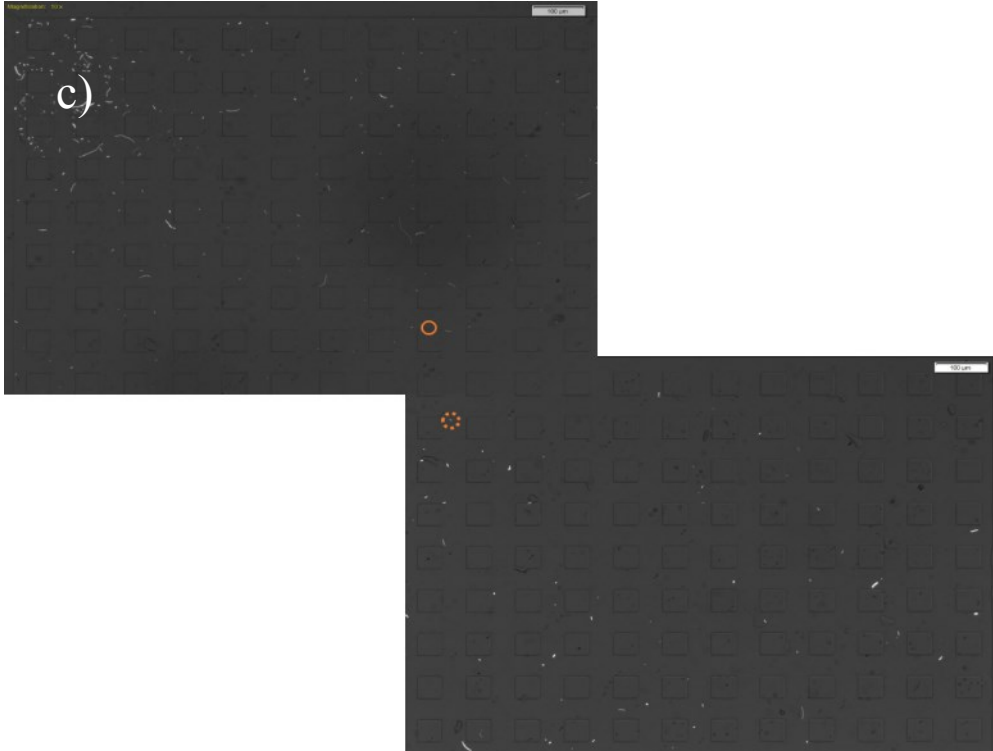


Figure A.2.7. *Bacteria total displacement of 6 different analyzed bacteria (images a to f) at the end of 60 minutes for C_E1 (images a to c) and C_E2 (images d to f) at last region at 75°*





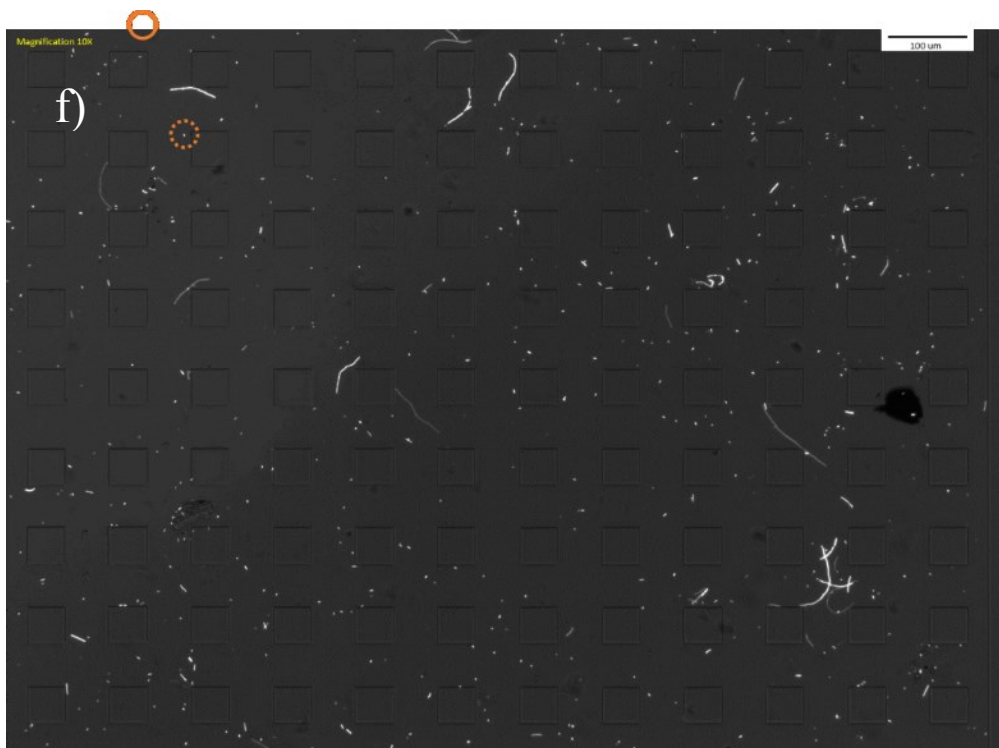
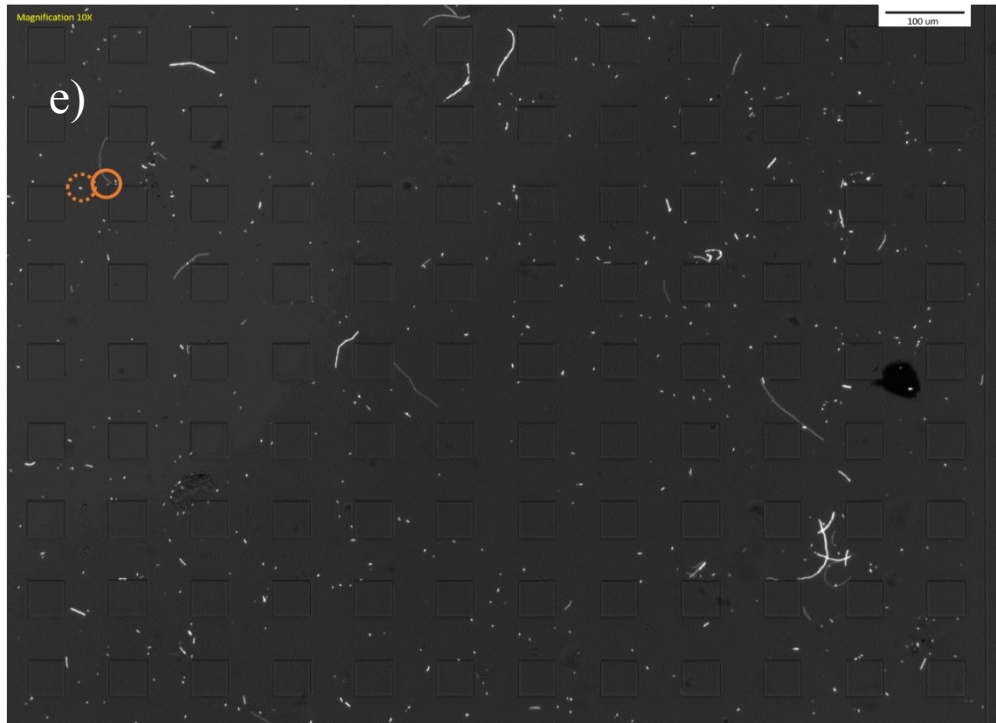
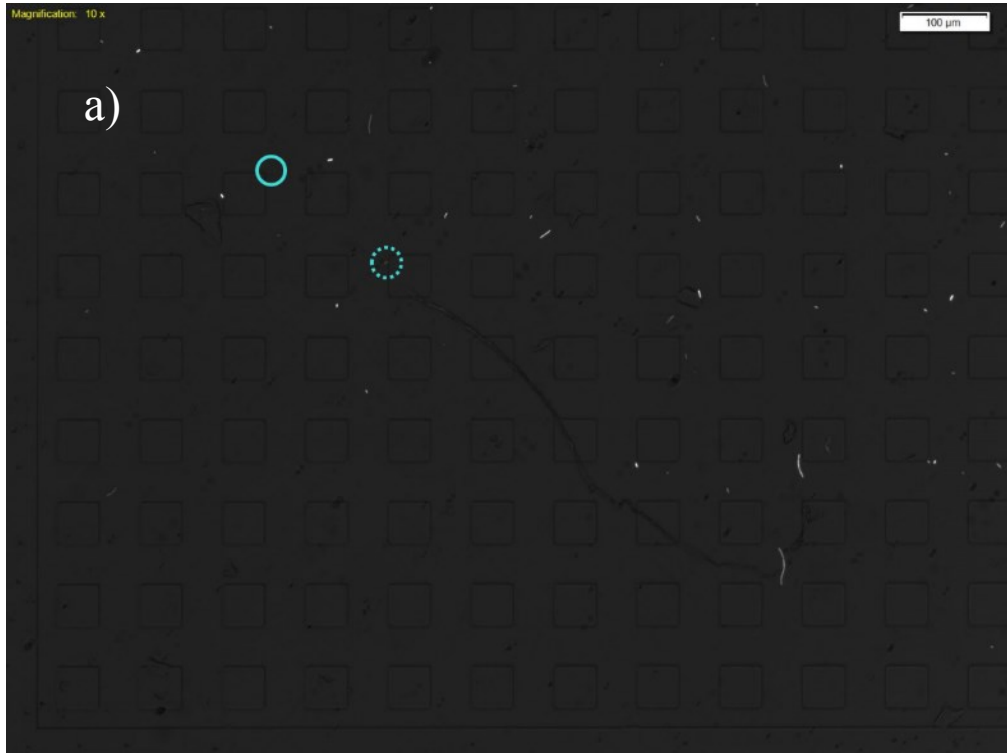
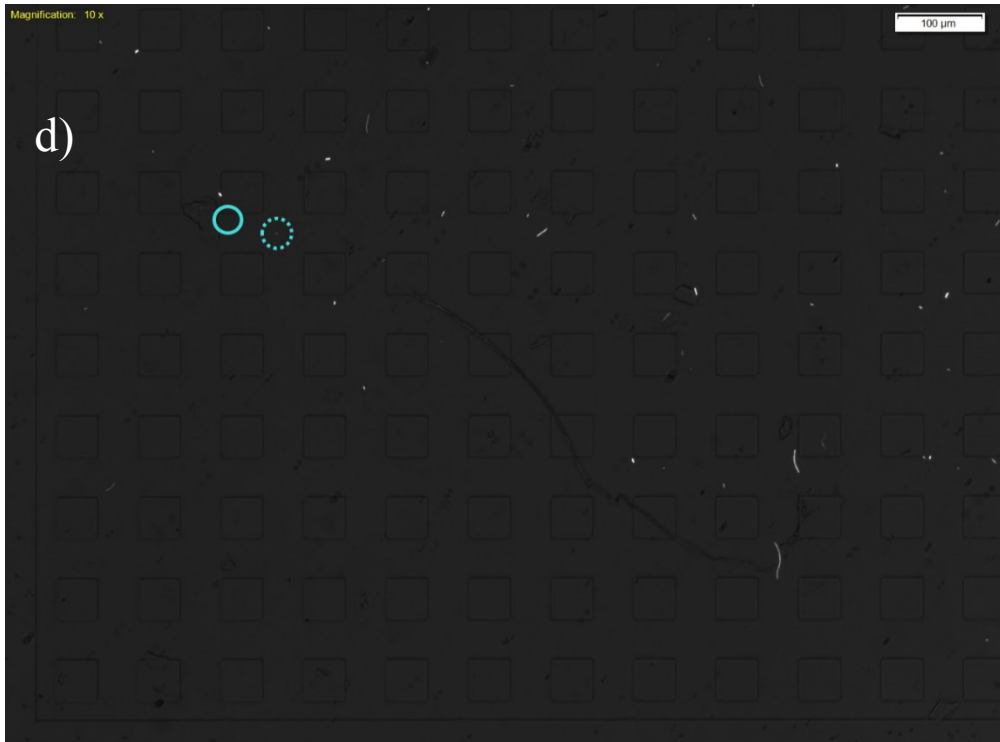
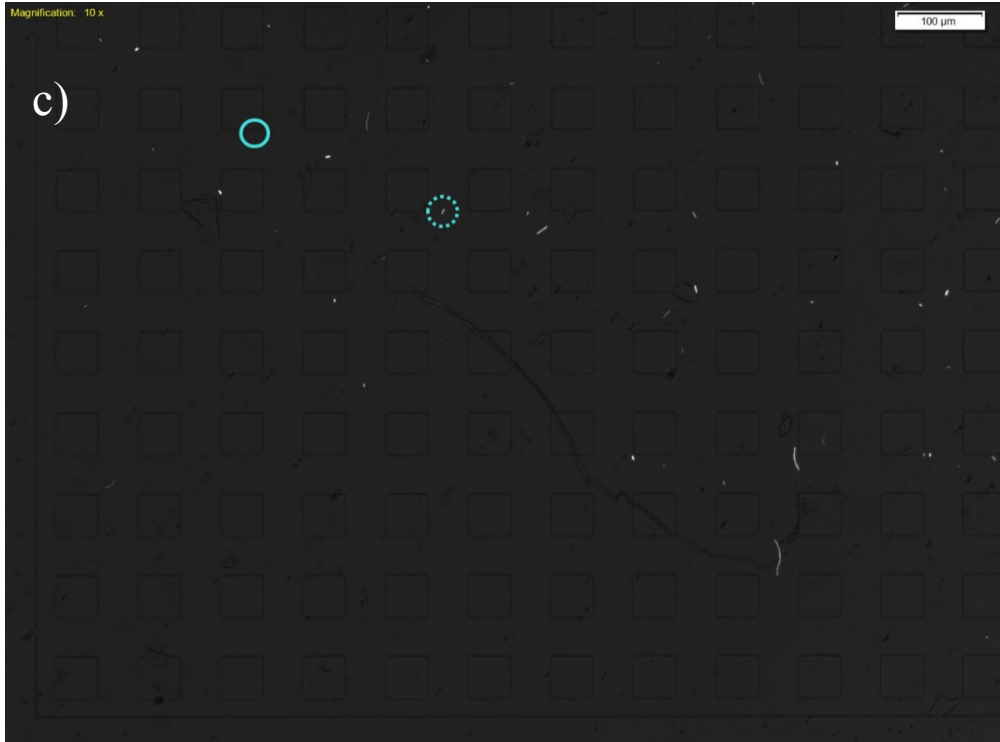


Figure A.2.8. Bacteria total displacement of 6 different analyzed bacteria (images a to f) at the end of 60 minutes for C_E1 (images a to c) and C_E2 (images d to f) at last region at 45°





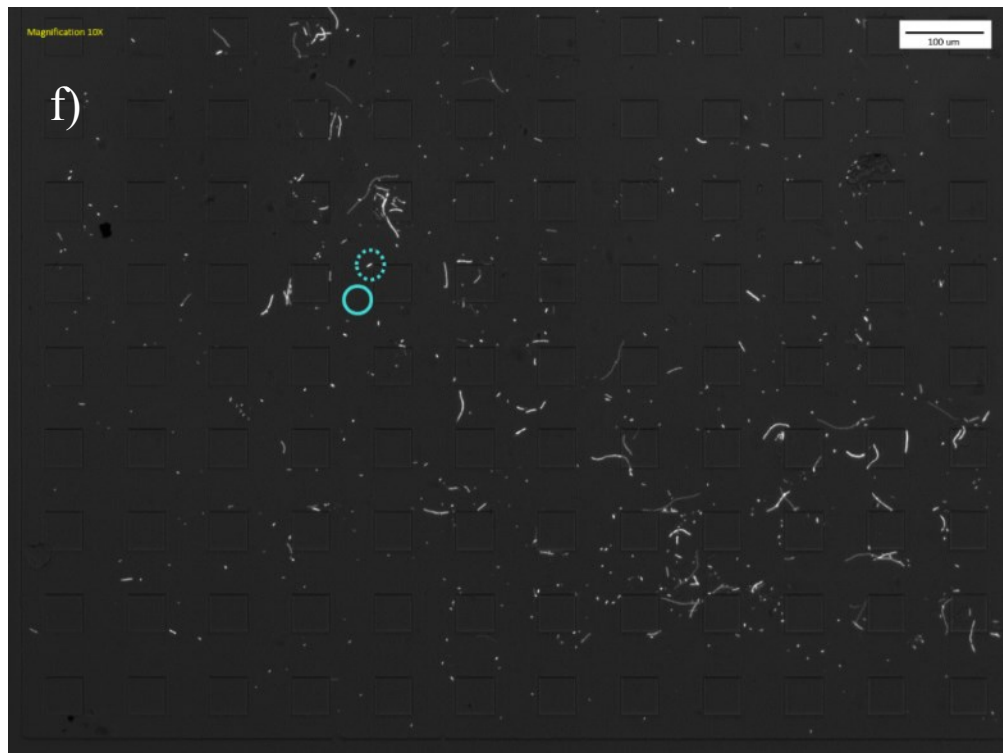
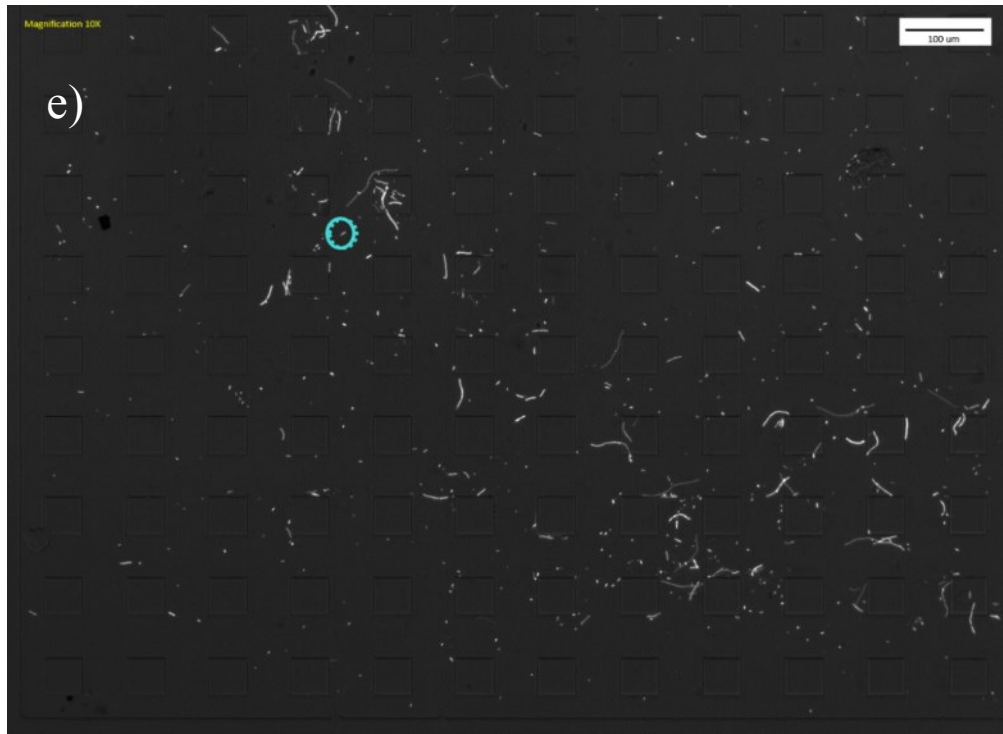
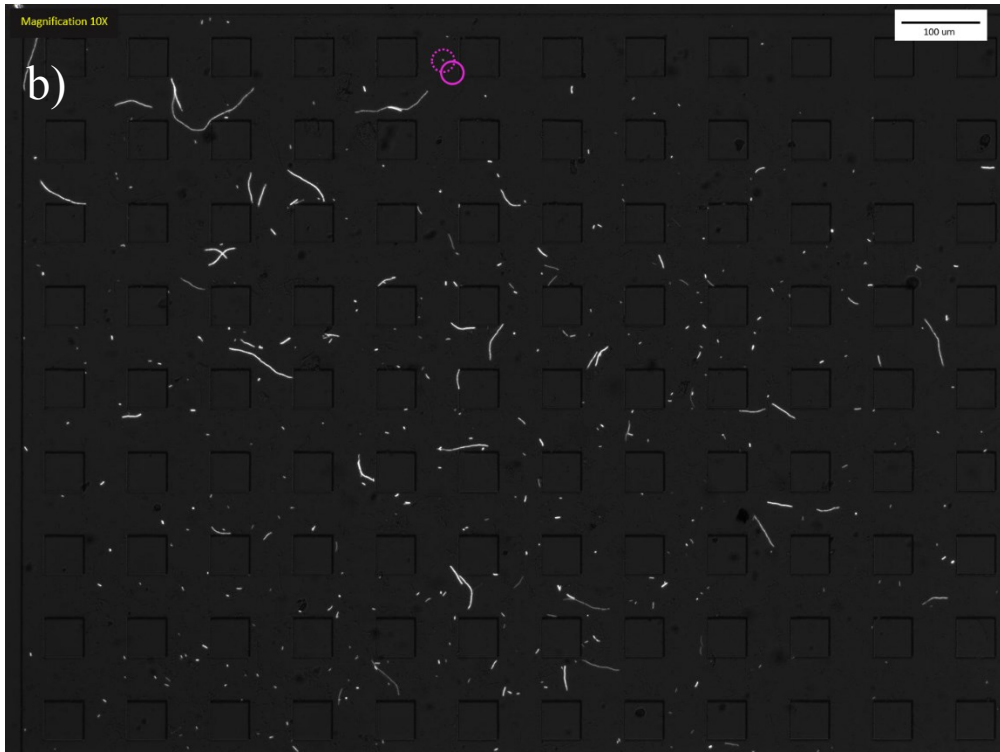
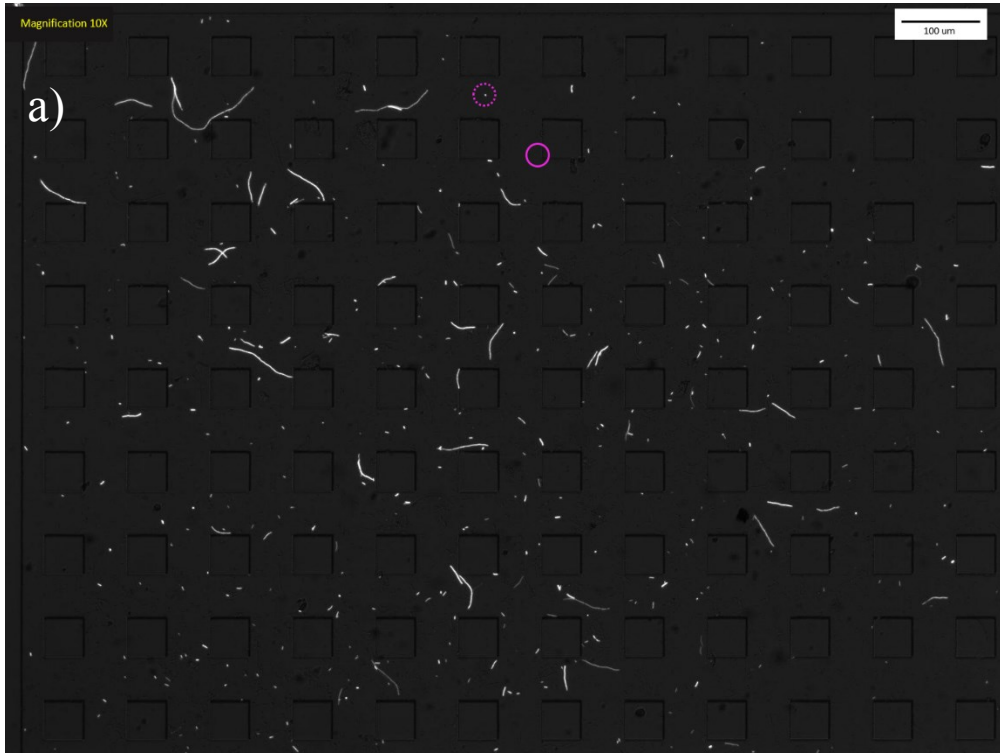


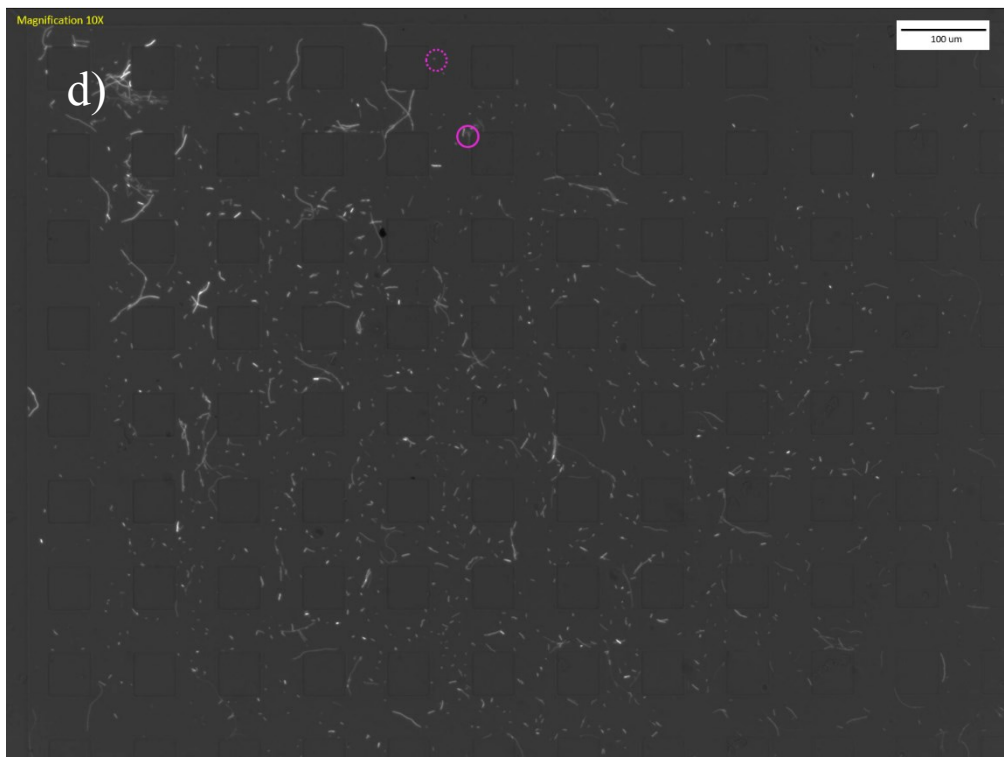
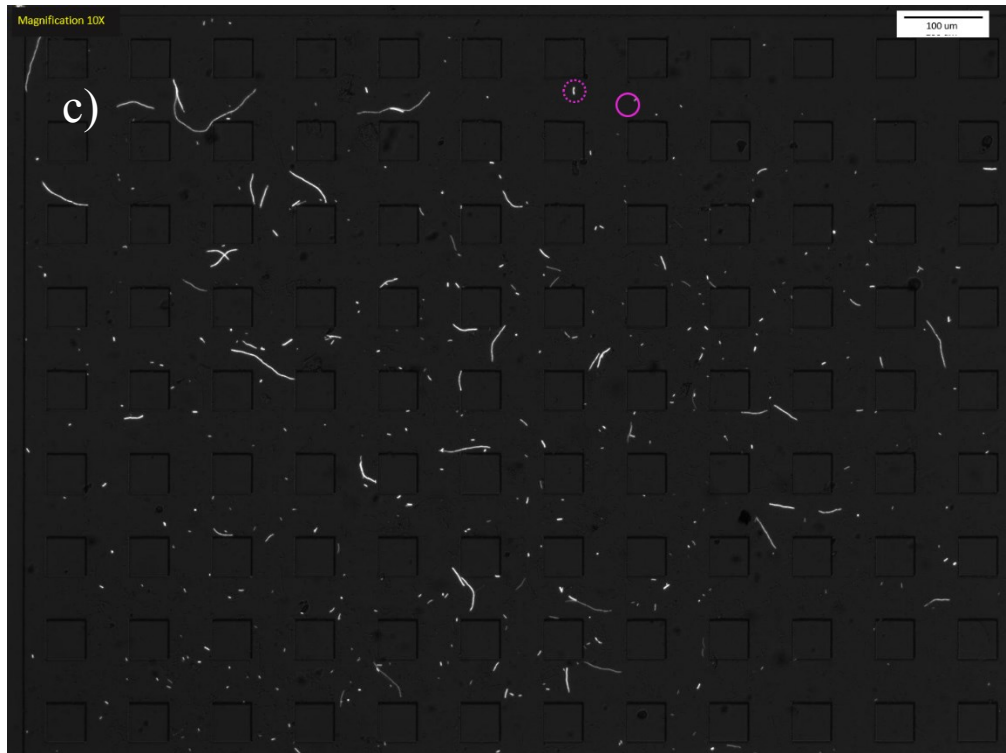
Figure A.2.9. Bacteria total displacement of 6 different analyzed bacteria (images a to f) at the end of 60 minutes for C_E1 (images a to c) and C_E2 (images d to f) at last region at 45°

A.3. Microscopy images of Antibiotic Treatment Experiments

Figure A.3.1 shows the microscopy images used to measure displacement of 6 bacteria (images a to f) during the 60 minutes of antibiotic treatment experiments. In antibiotic treatment experiments I introduce ampicillin (at concentration of 10 $\mu\text{g/mL}$) to the loaded bacteria inside the device (flow rate of 0.01 mL/h) and I measured bacteria response to ampicillin during a period of 60 minutes. I repeated the experiment 2 times and the 2 practice of these experiments are abbreviated as AT_E1 and AT_E2 in this text (table 3.1). Figure A.3.1 shows the microscopy images used to measure bacteria displacement with initial position at the first region at 75° (section 1-1 of the imaging areas, see figure 3.4.2). In all images, dashed circles indicate the start position of bacteria and solid circle indicate the final position at that time step.

Figure A.3.2 shows the microscopy images used to measure displacement of 6 bacteria during the 60 minutes of the experiment for AT_E1 and AT_E2, first region at 45° (section 1-1 of the imaging areas, see figure 3.4.2). Figure A.3.3 is in regard to bacteria at first region at 15°, figure A.3.4 is in regard to bacteria at middle region at 75°, figure A.3.5 in regard to middle region at 45° and figure A.3.6 in regard to middle region at 15°. For the last region at 75°, 45° and 15° figures A.3.7, A.3.8 and A.3.9 show microscopy images respectively.





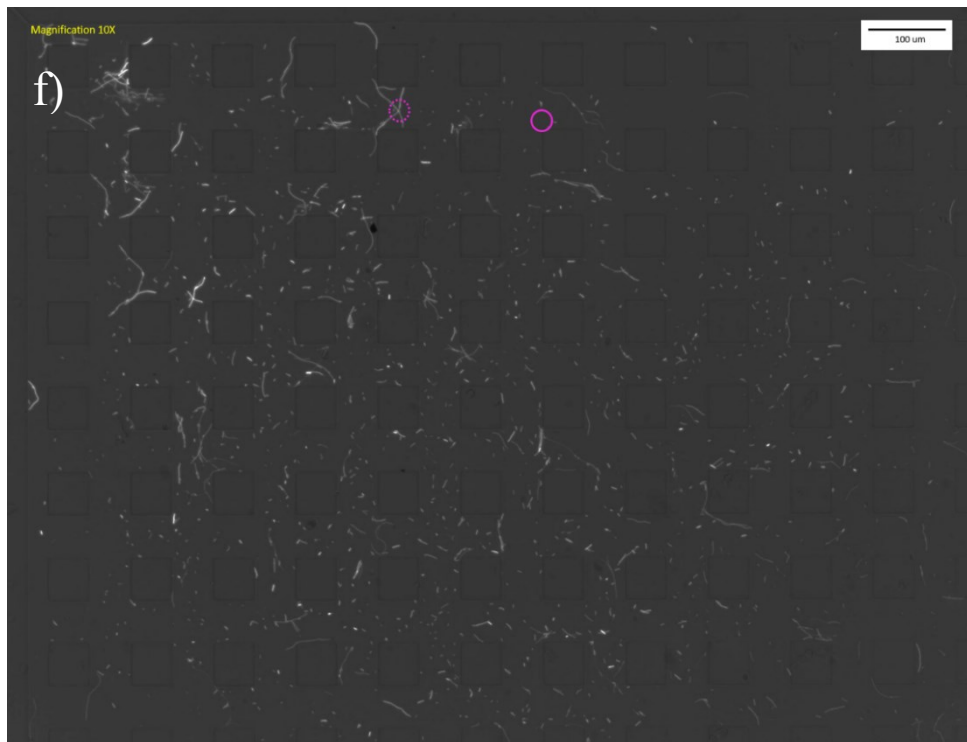
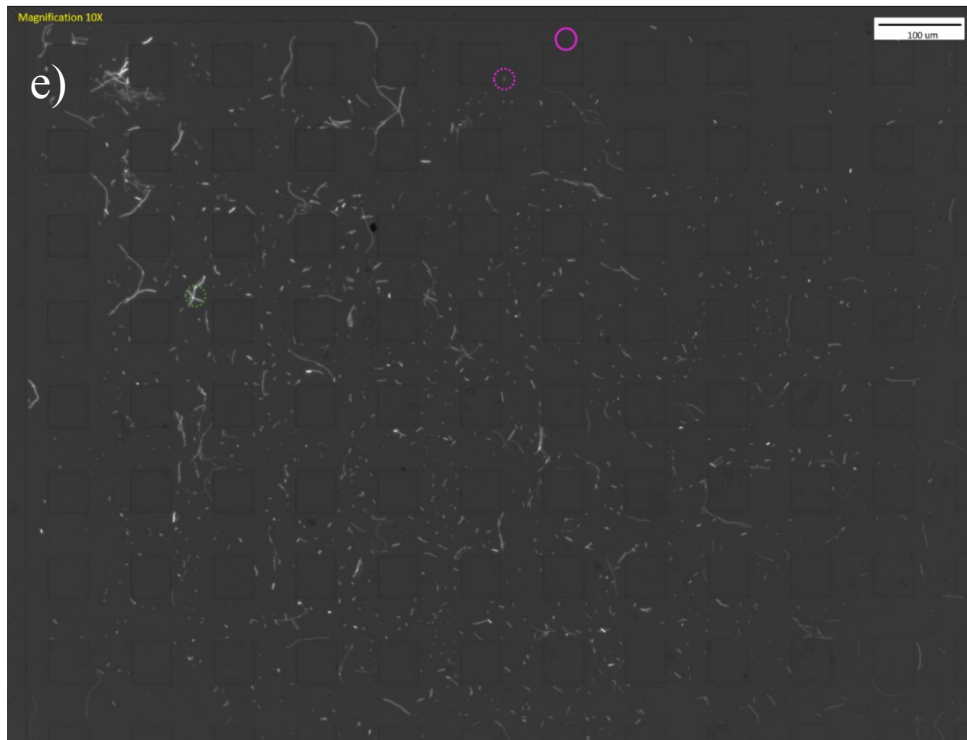
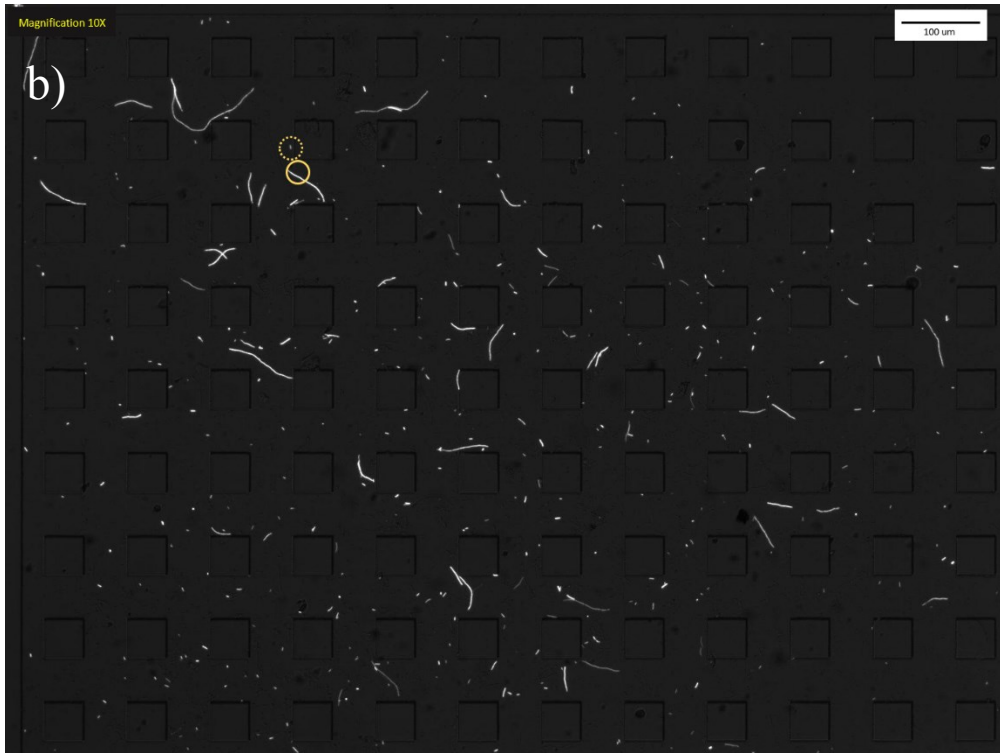
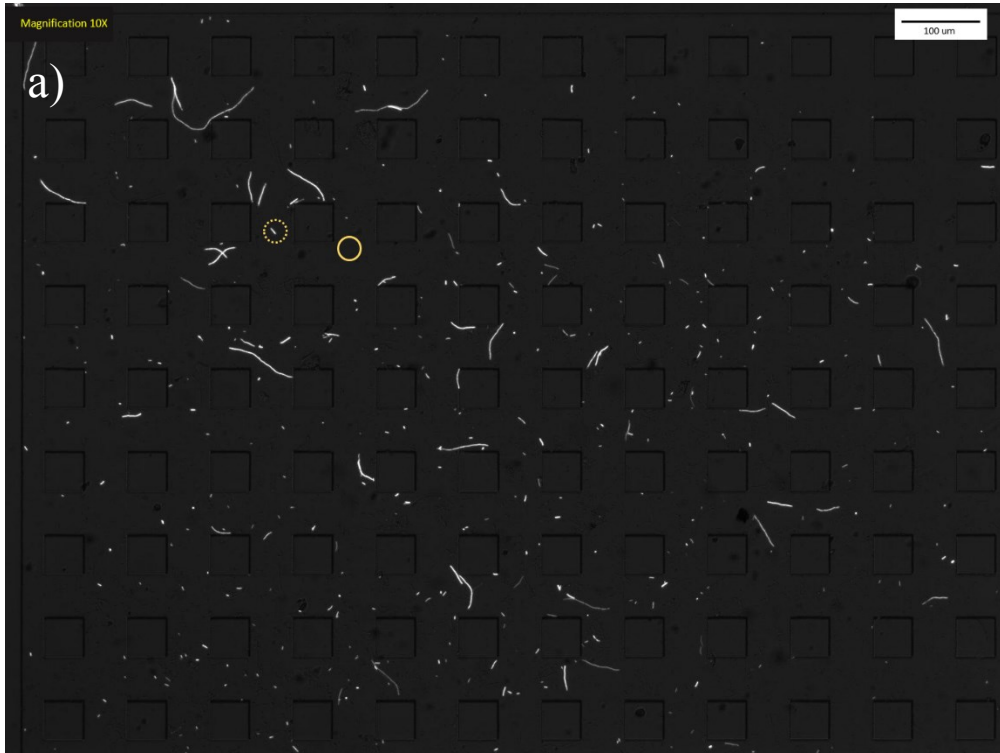
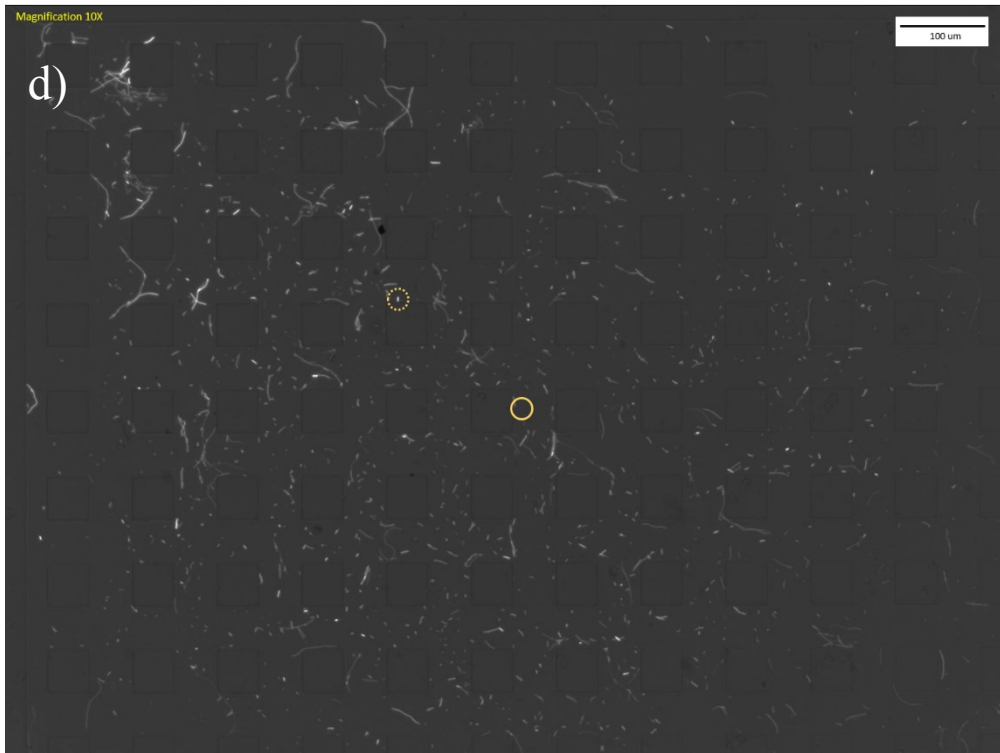
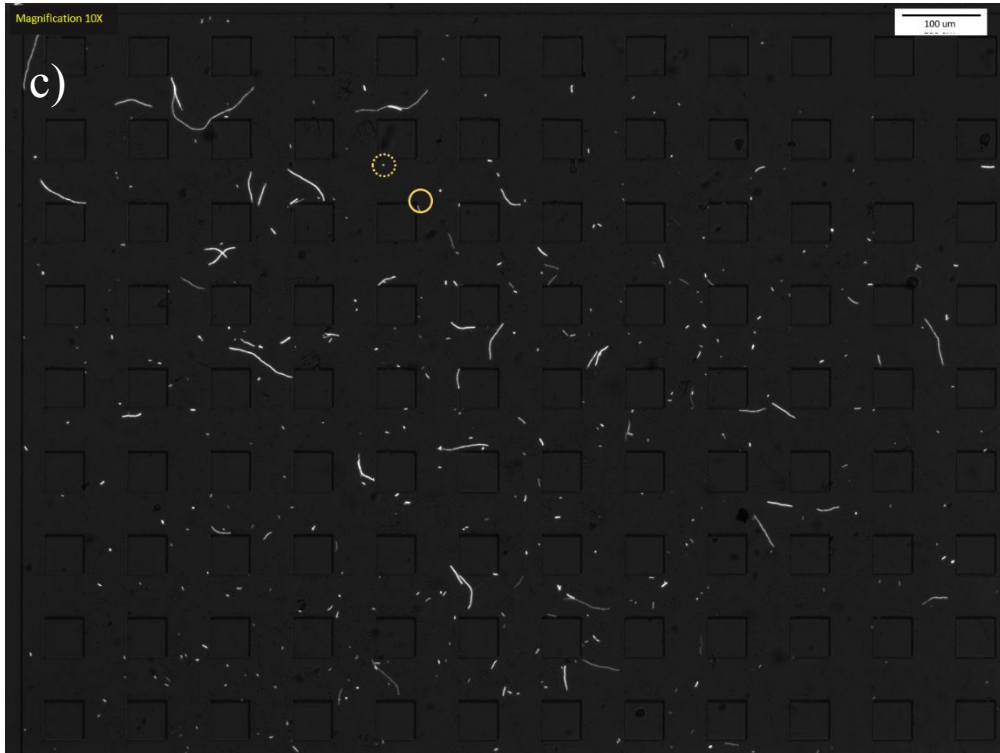


Figure A.3.1. Bacteria total displacement of 6 different analyzed bacteria (images a to f) at the end of 60 minutes for AT_E1 (images a to c) and AT_E2 (images d to f) at first region at 75°





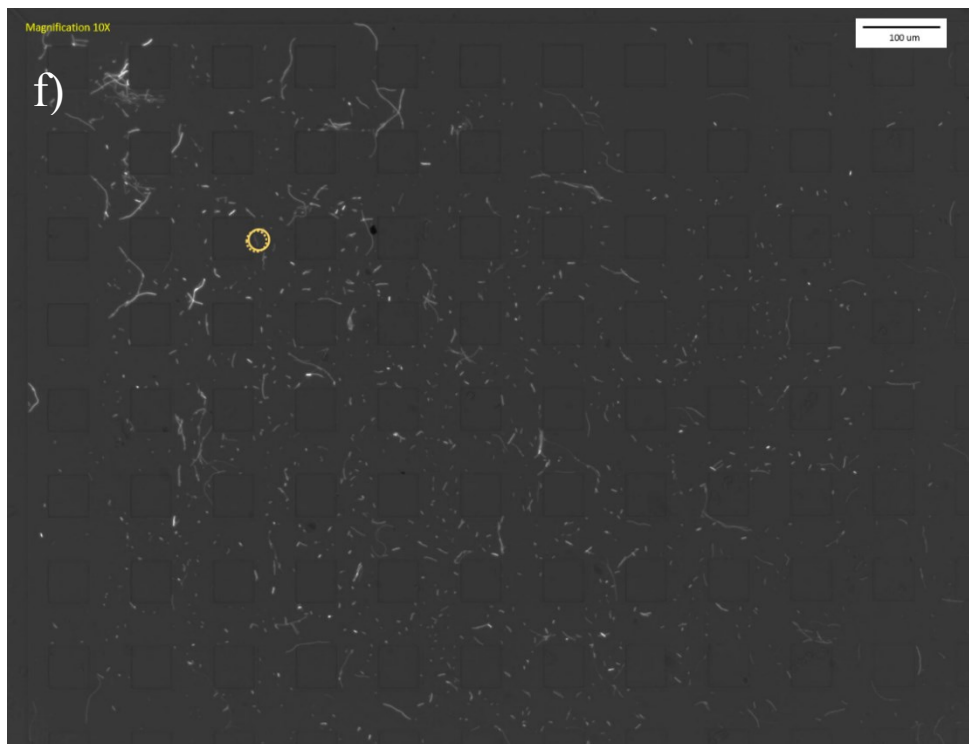
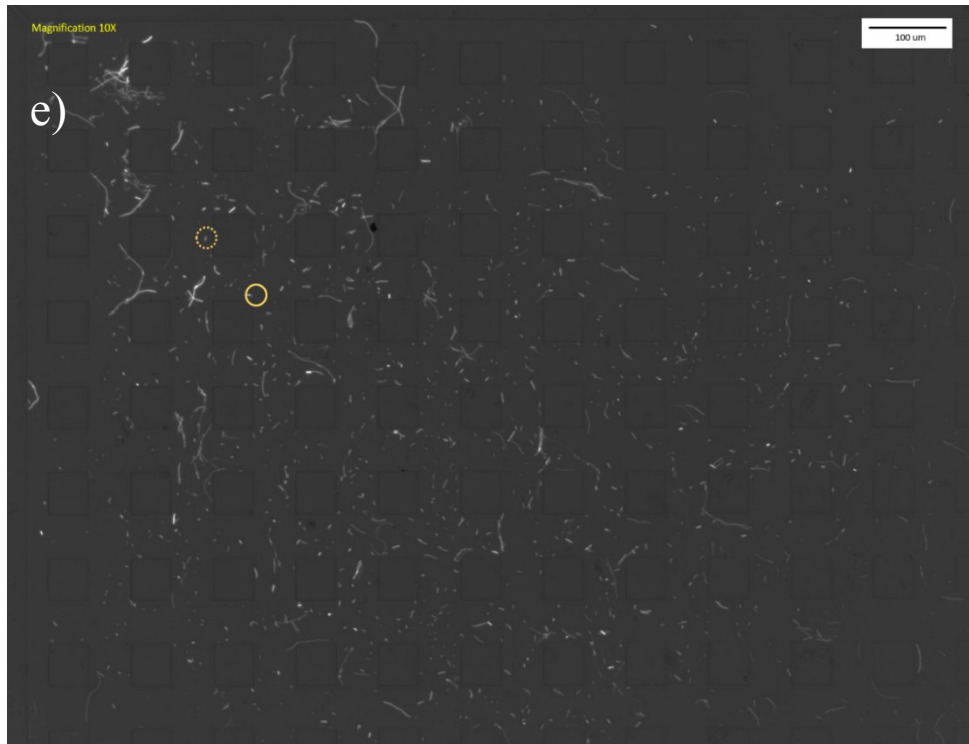
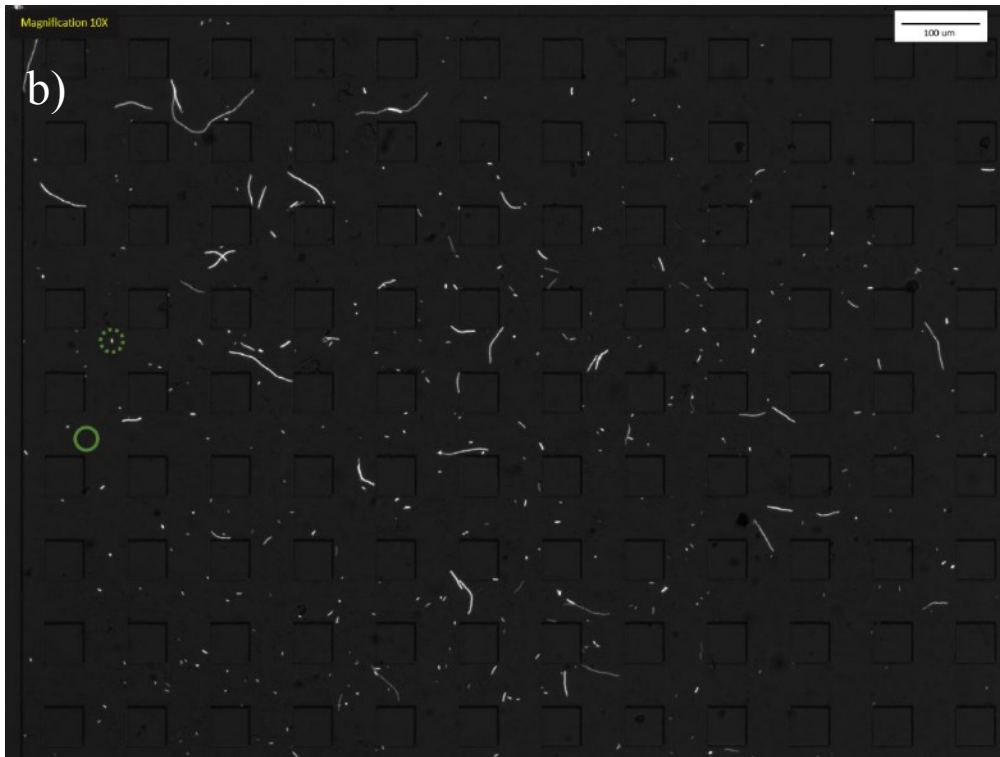
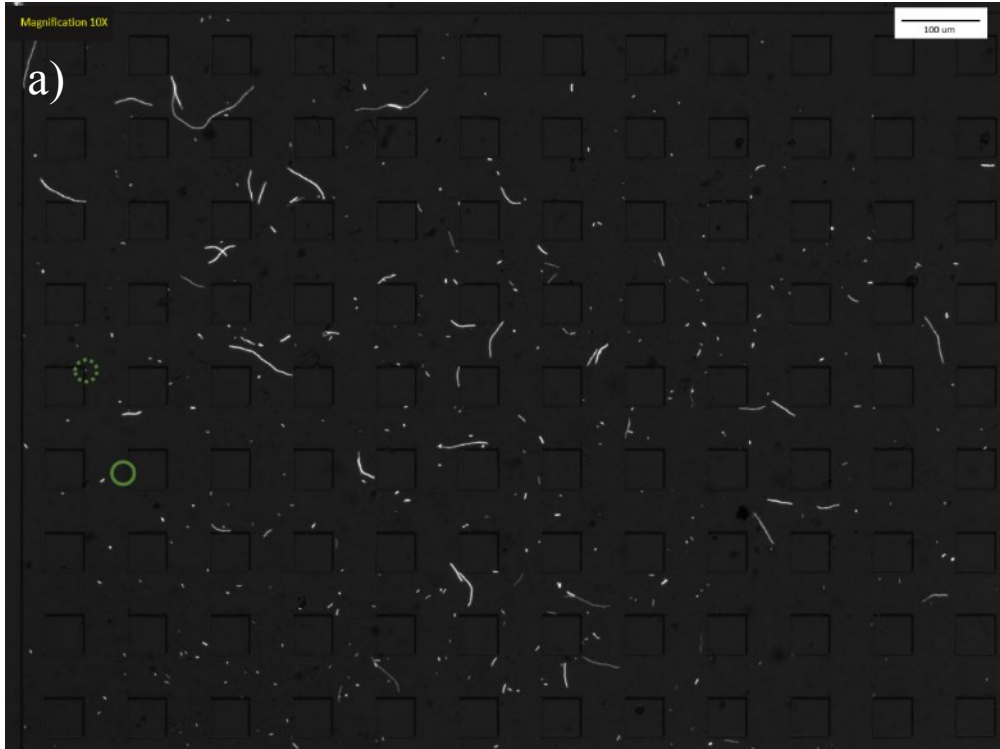
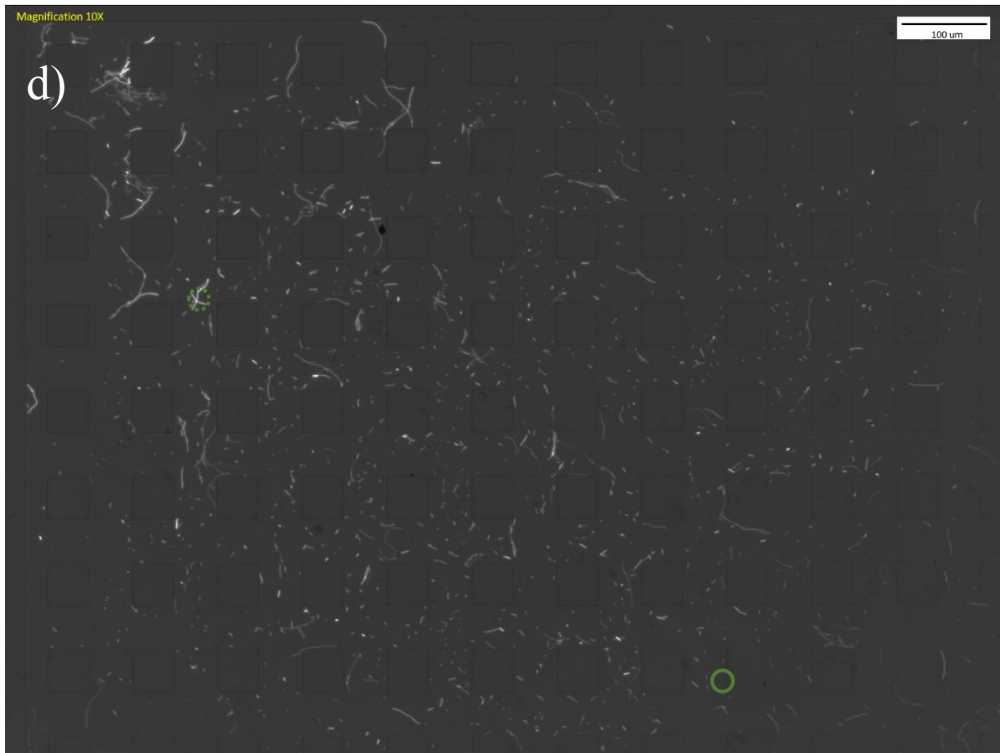
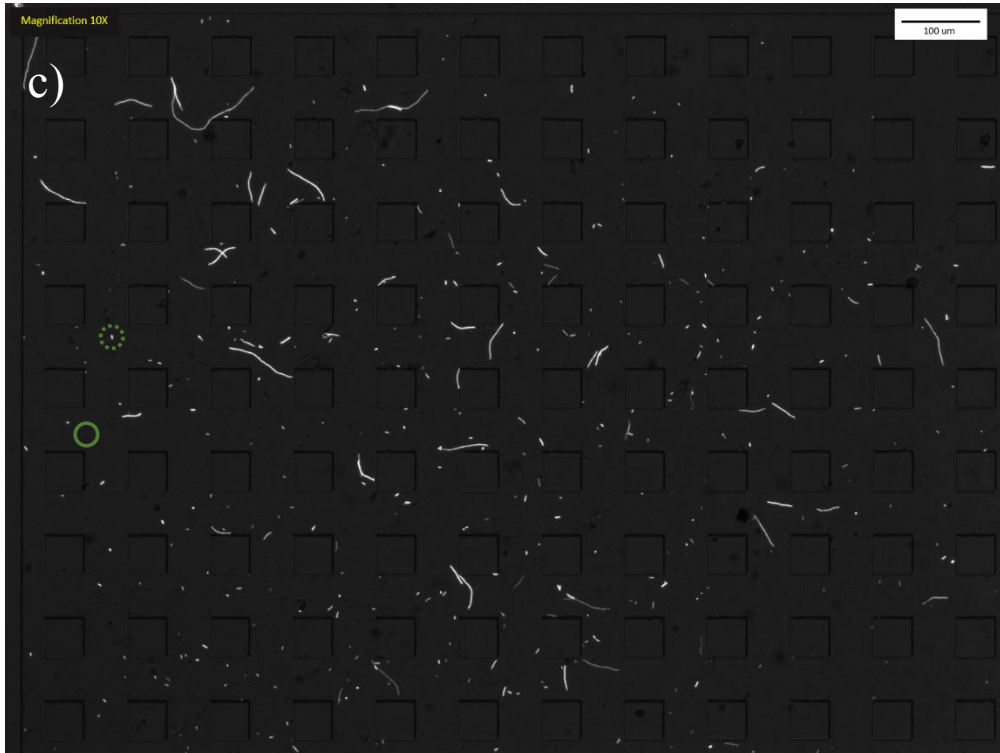


Figure A.3.2. Bacteria total displacement of 6 different analyzed bacteria (images a to f) at the end of 60 minutes for AT_E1 (images a to c) and AT_E2 (images d to f) at first region at 45°





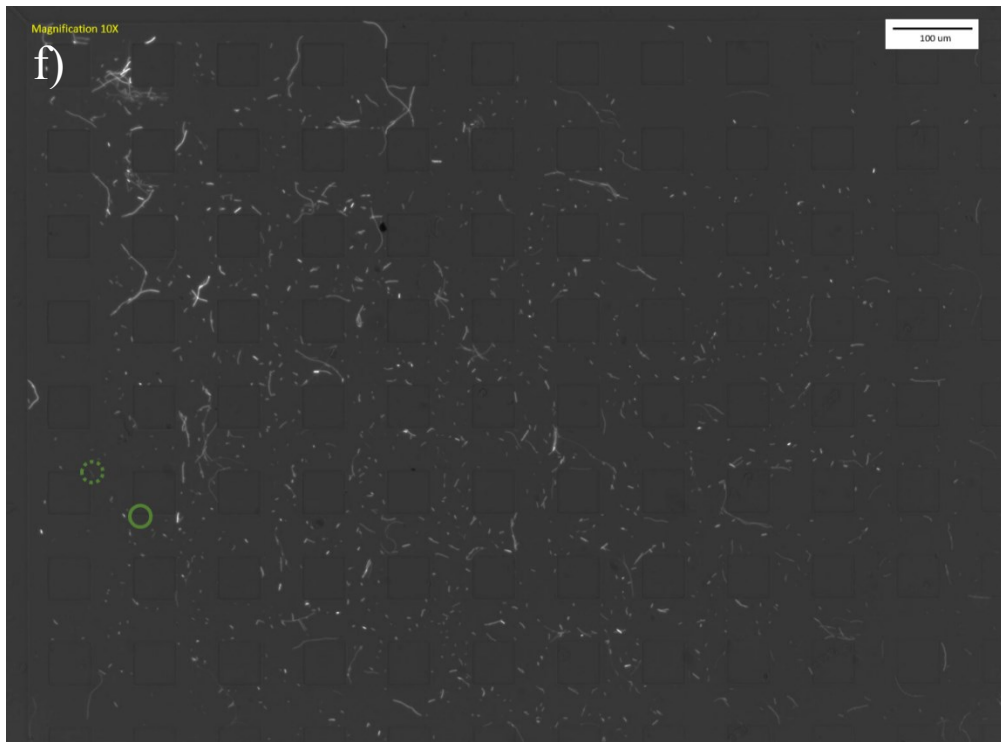
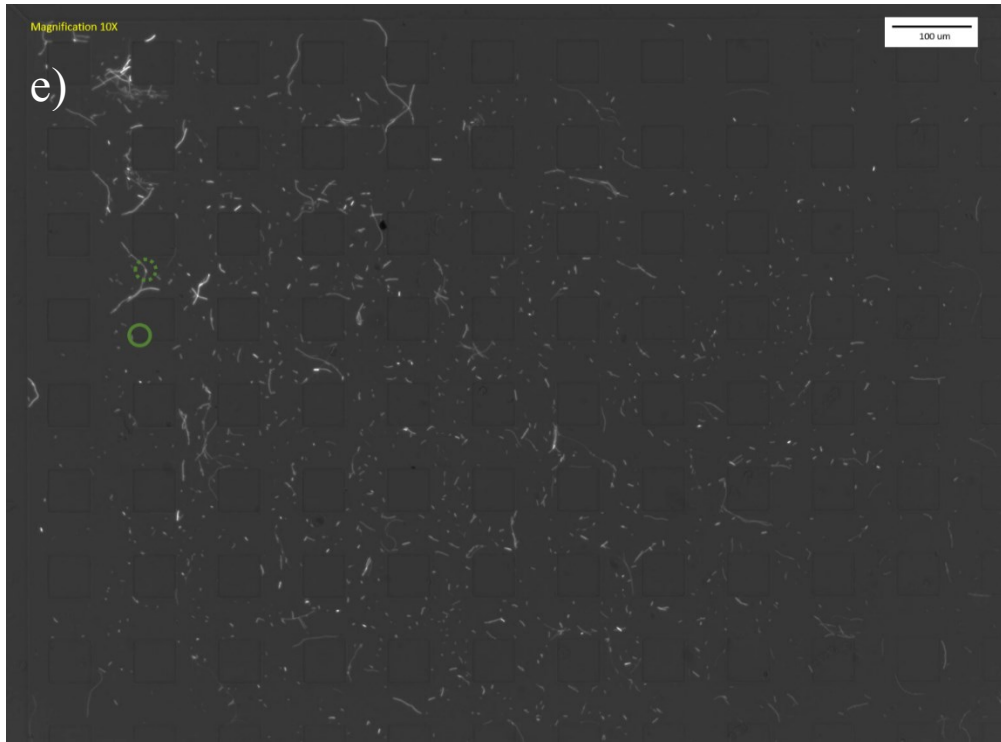
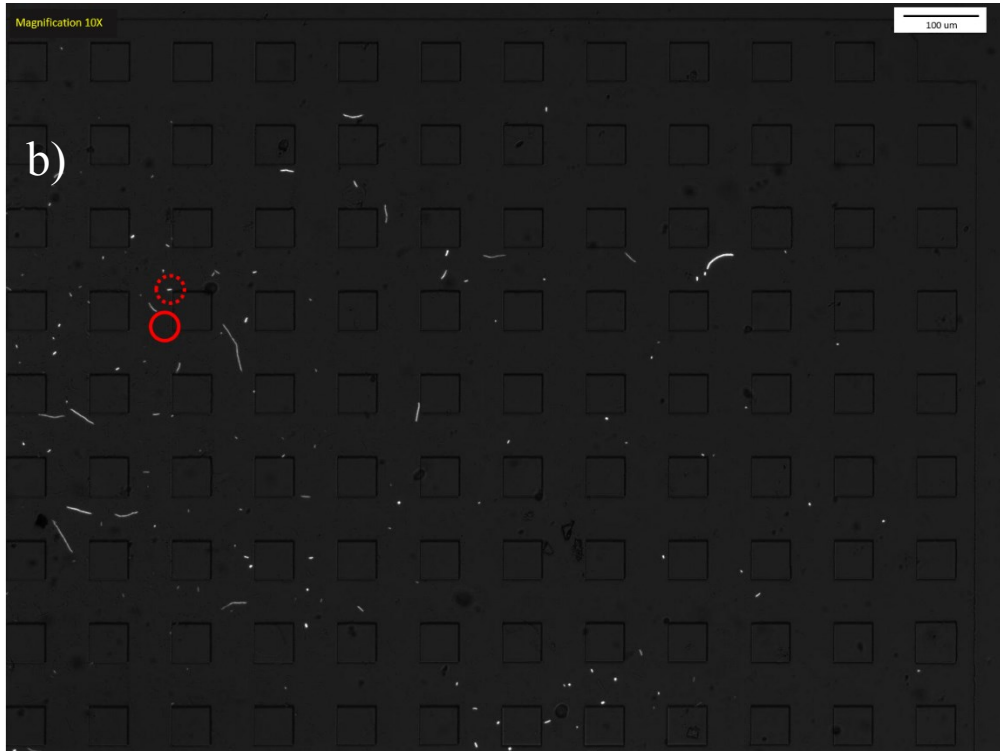
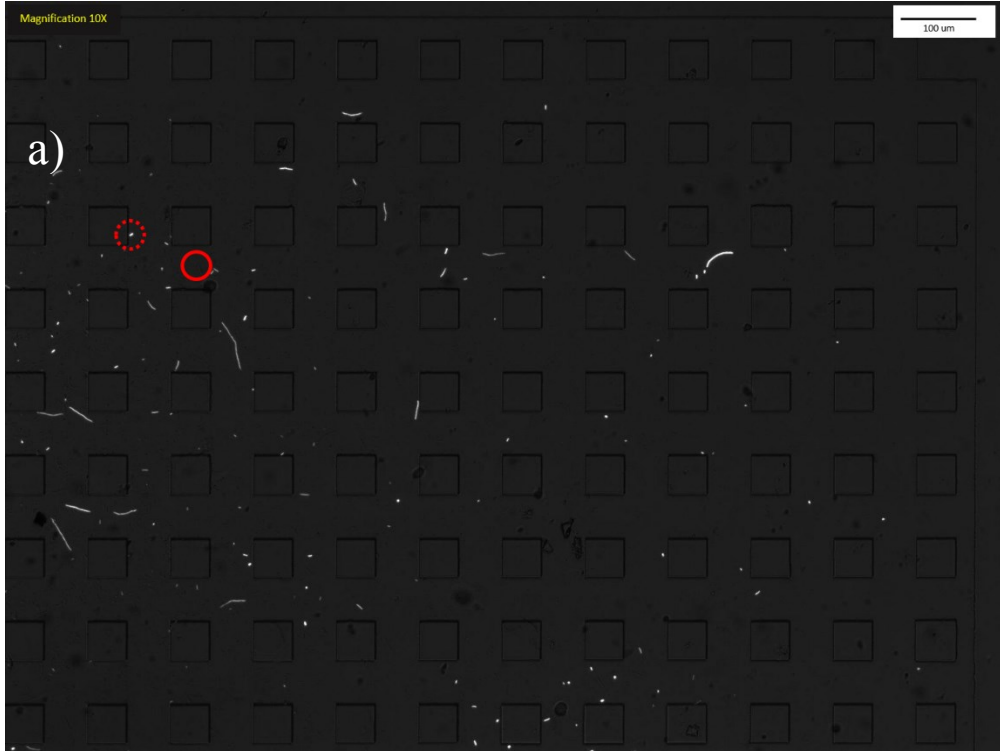
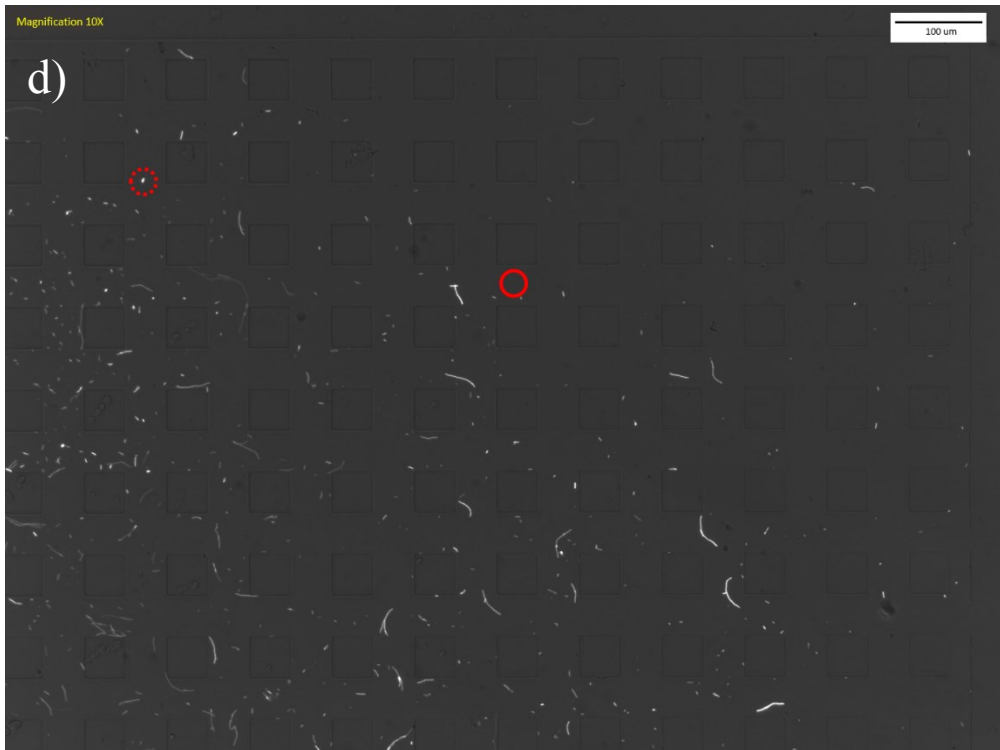
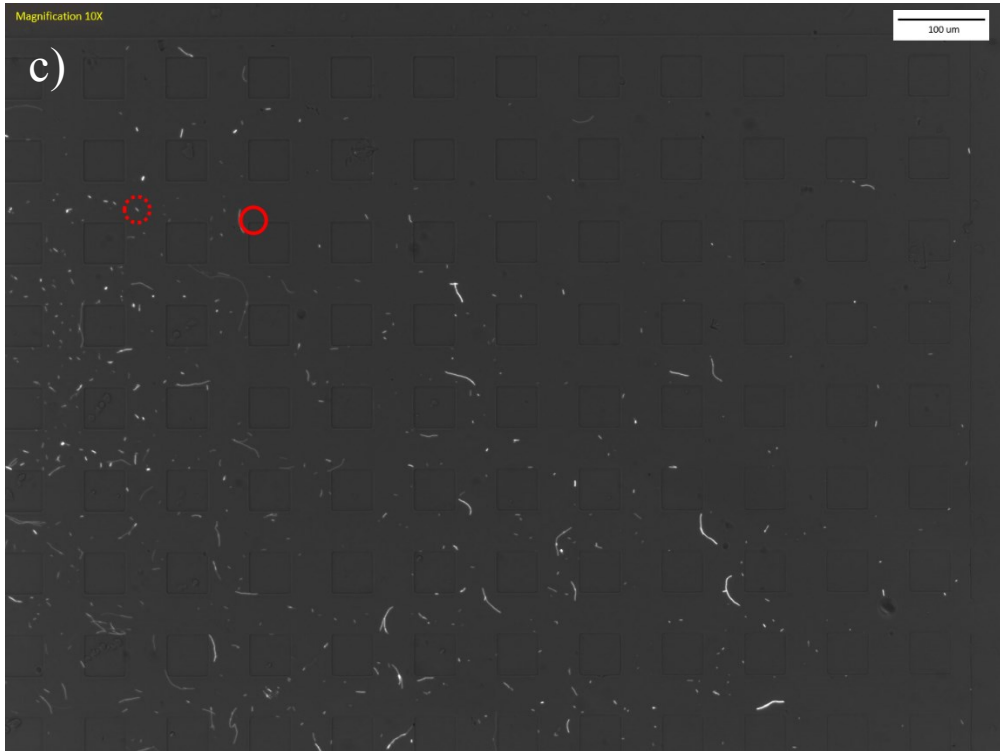


Figure A.3.3. Bacteria total displacement of 6 different analyzed (images a to f) at the end of 60 minutes for AT_E1 (images a to c) and AT_E2 (images d to f) at first region at 15°





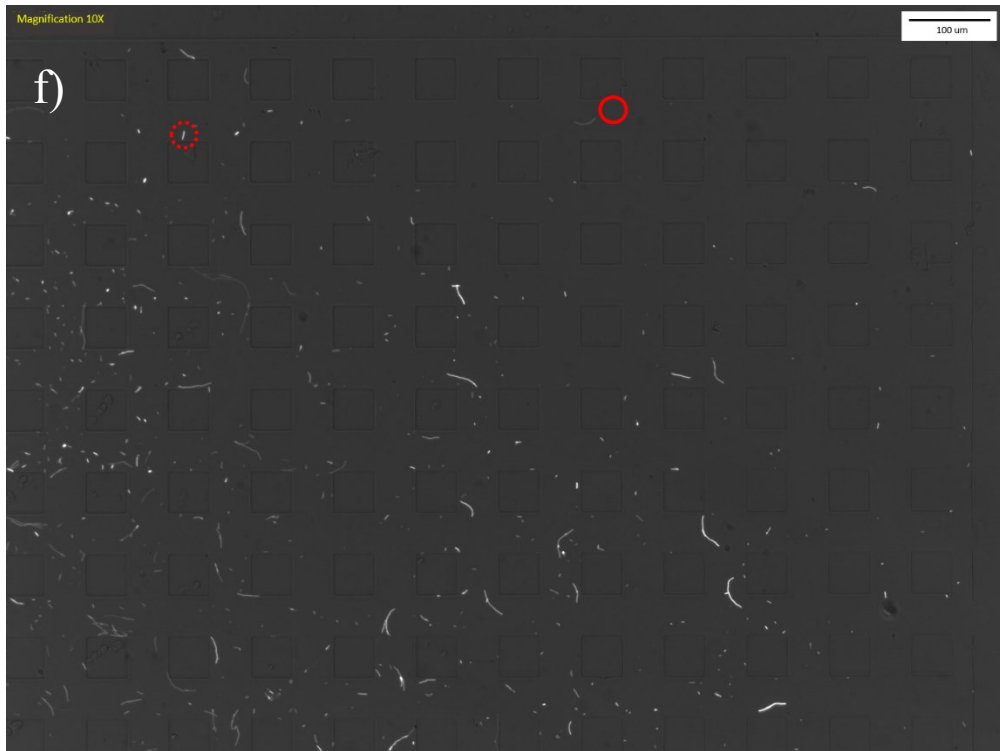
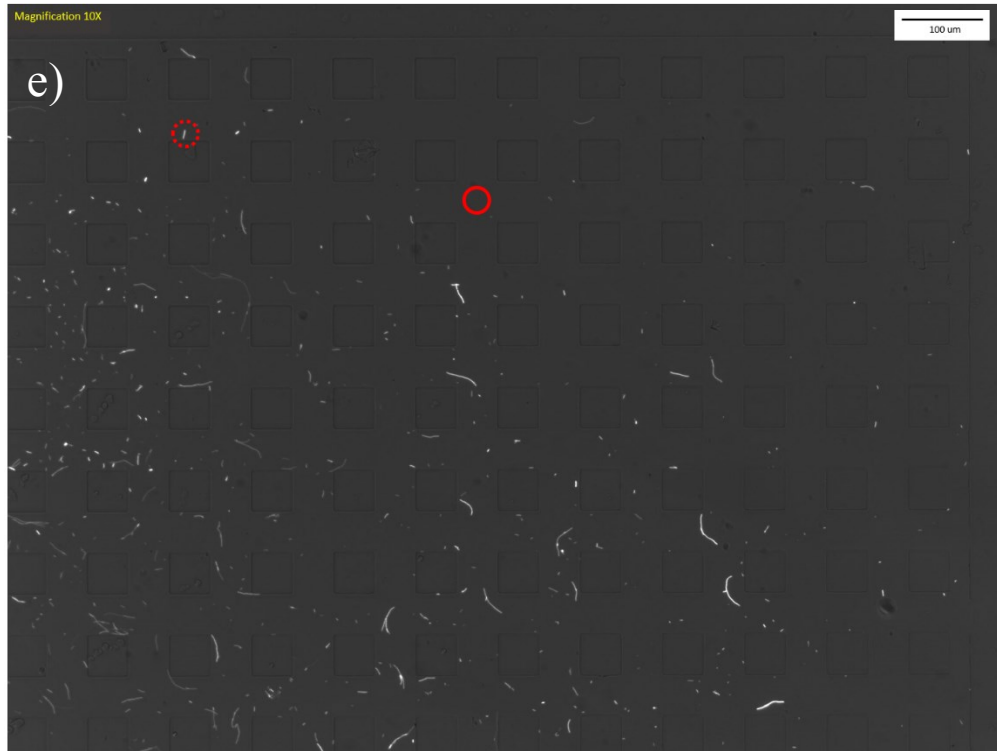
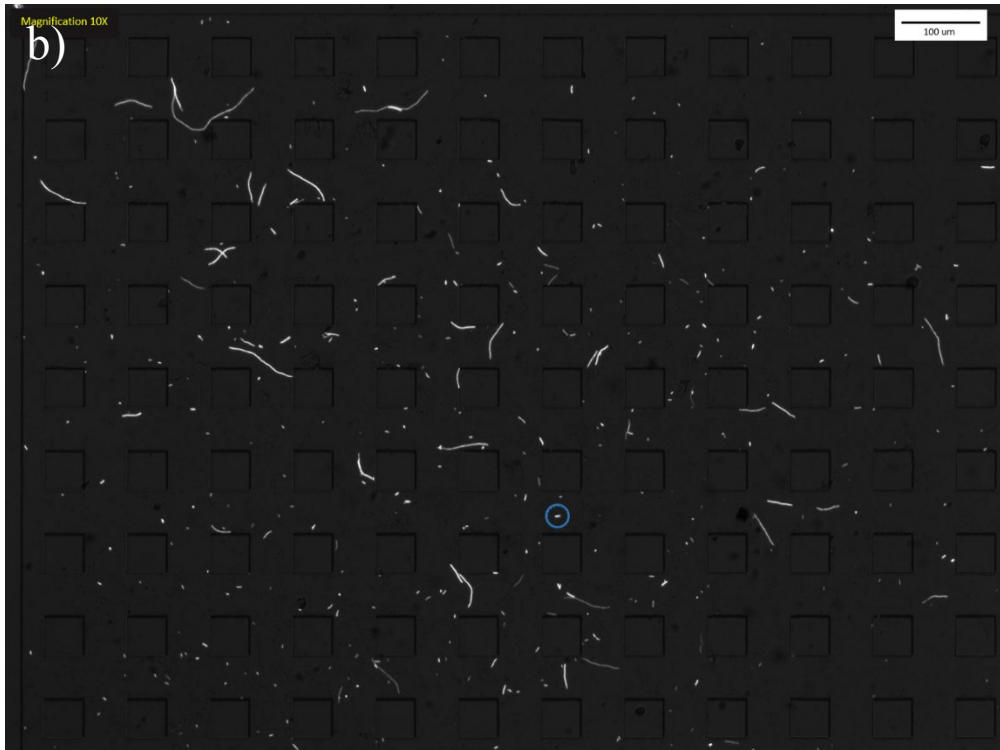
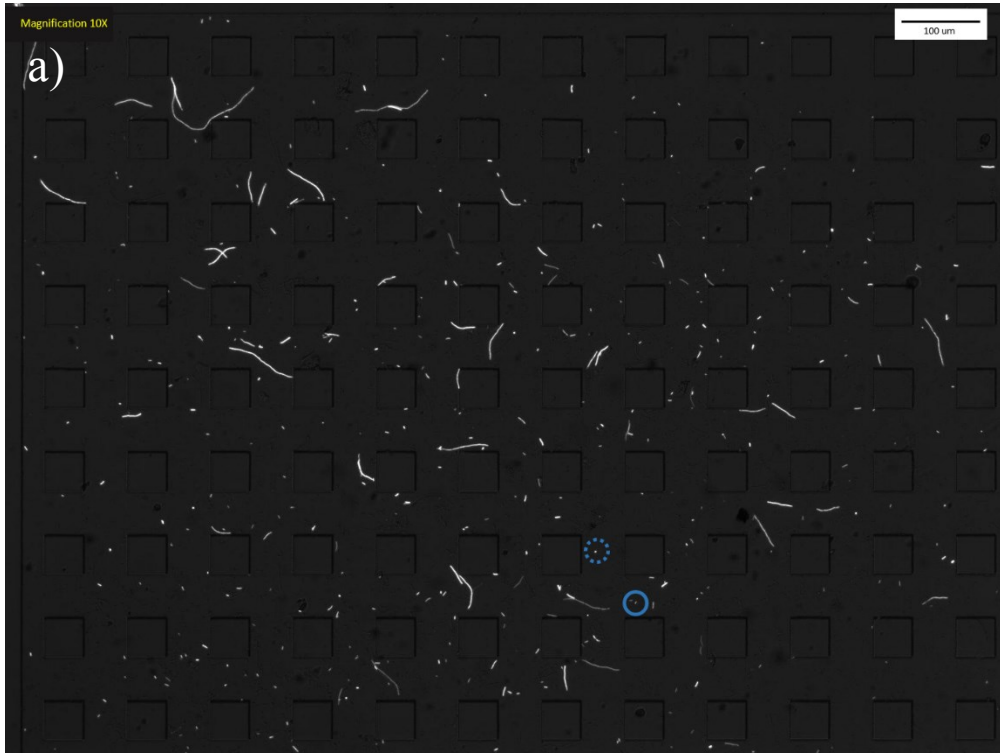
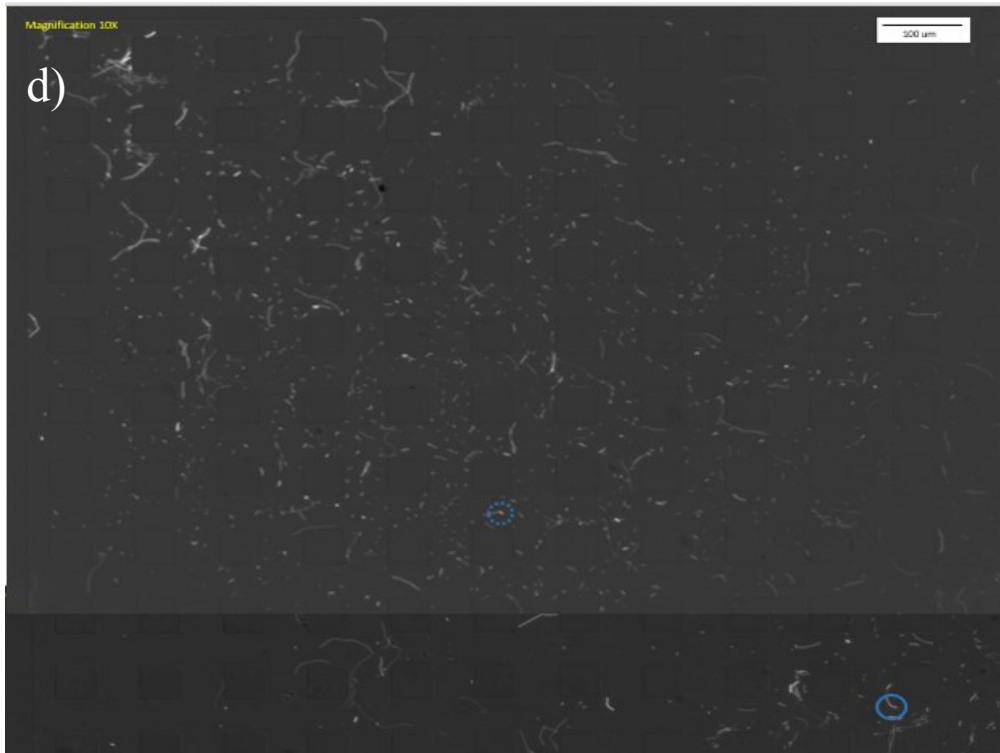
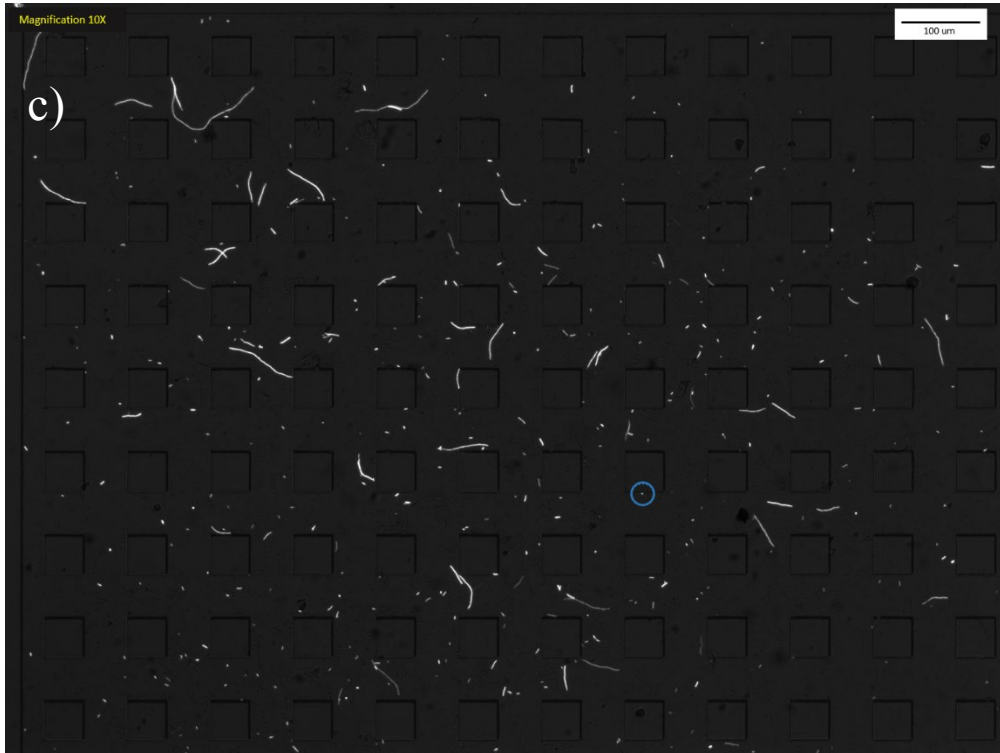


Figure A.3.4. Bacteria total displacement of 6 different analyzed bacteria (images a to f) at the end of 60 minutes for AT_E1 (images a and b) and AT_E2 (images c to f) at middle region at 75°





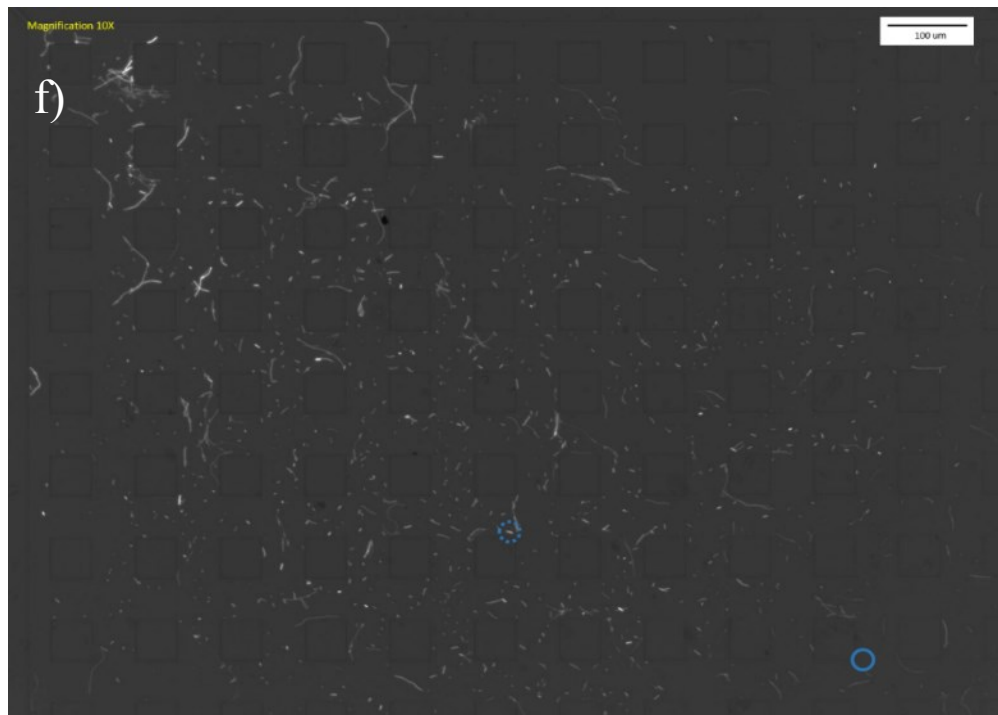
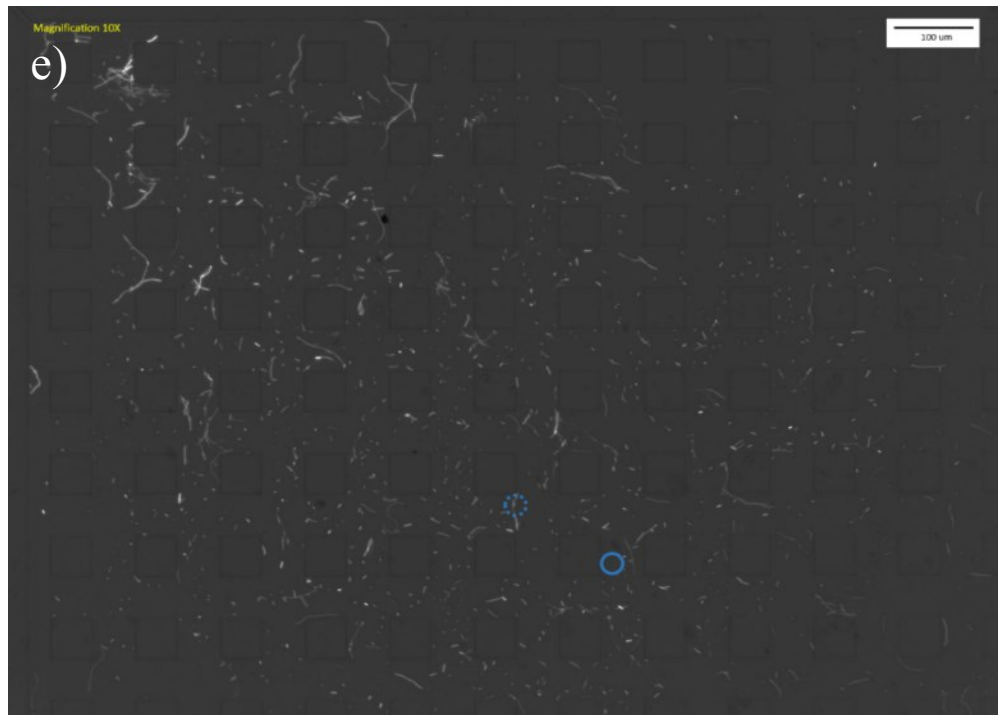
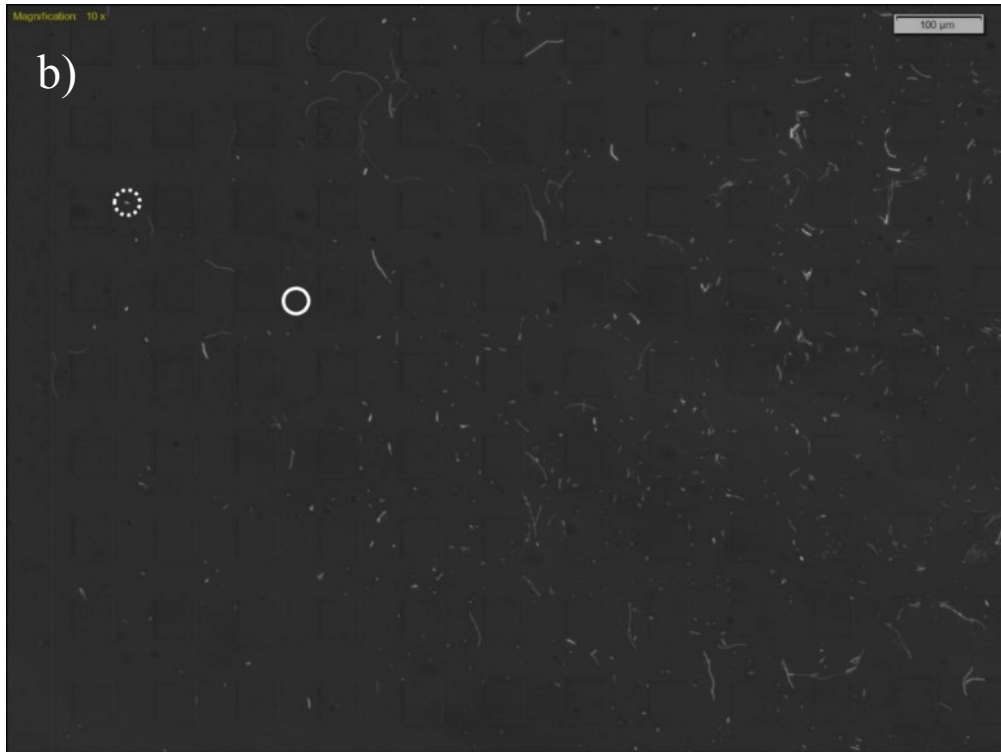
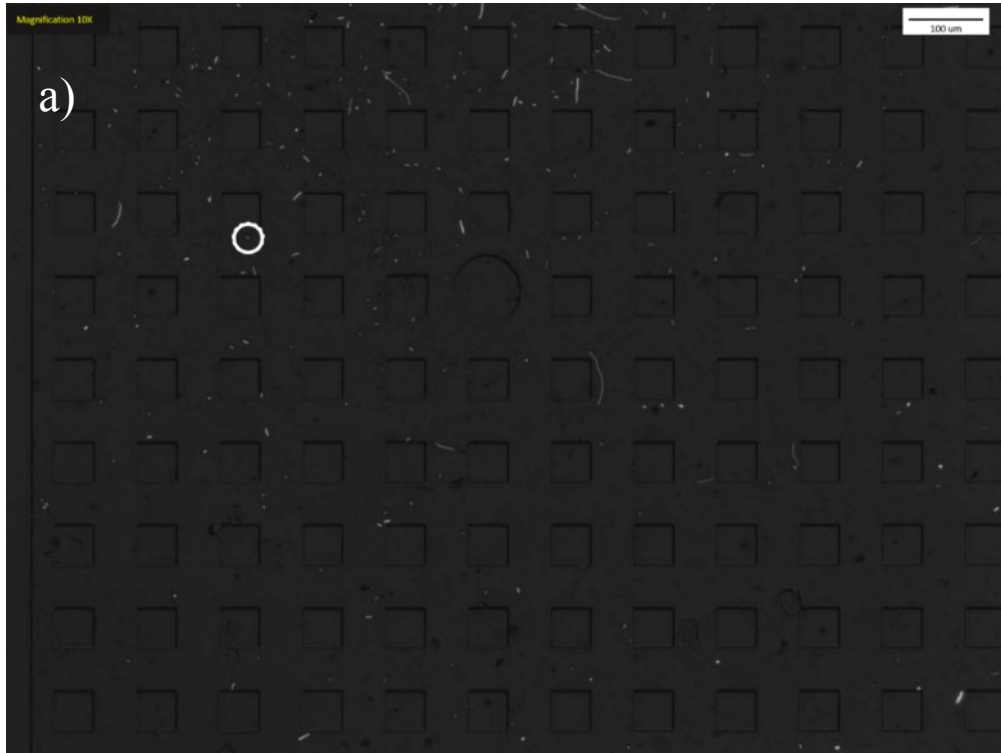
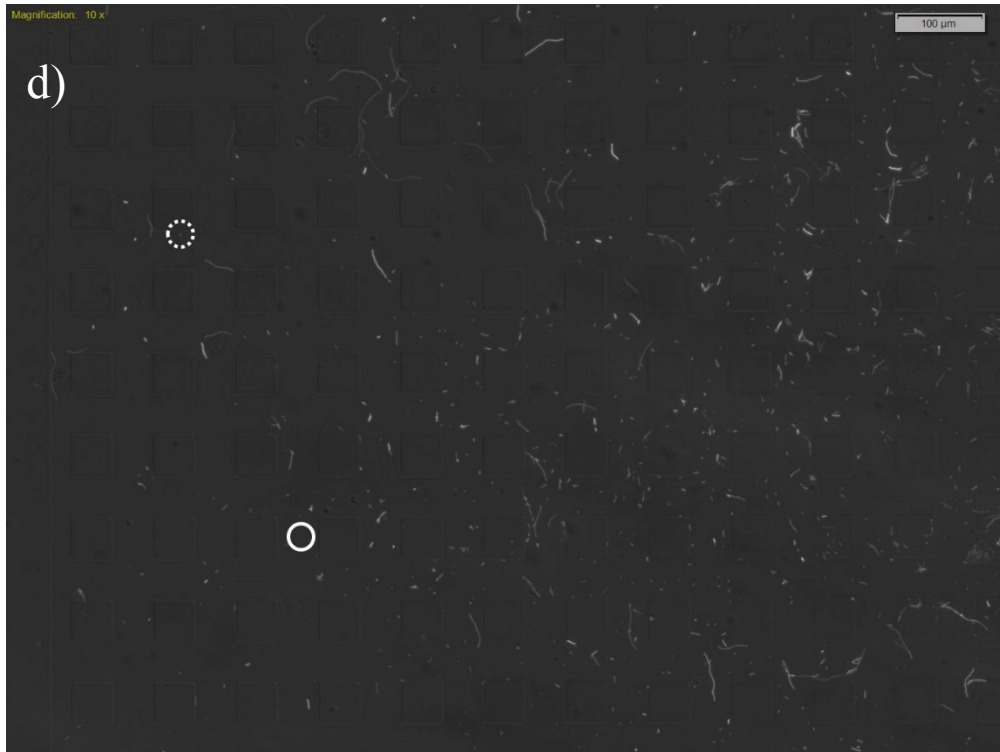
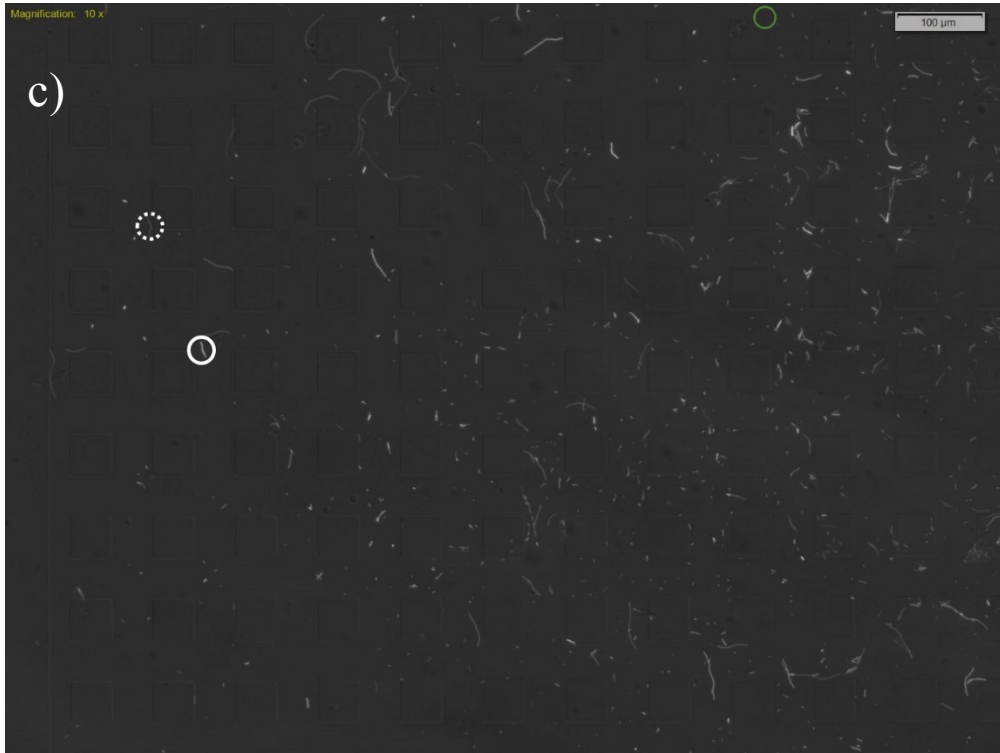


Figure A.3.5. Bacteria total displacement of 6 different analyzed bacteria (images a to f) at the end of 60 minutes for AT_E1 (images a to c) and AT_E2 (images d to f) at middle region at 45°





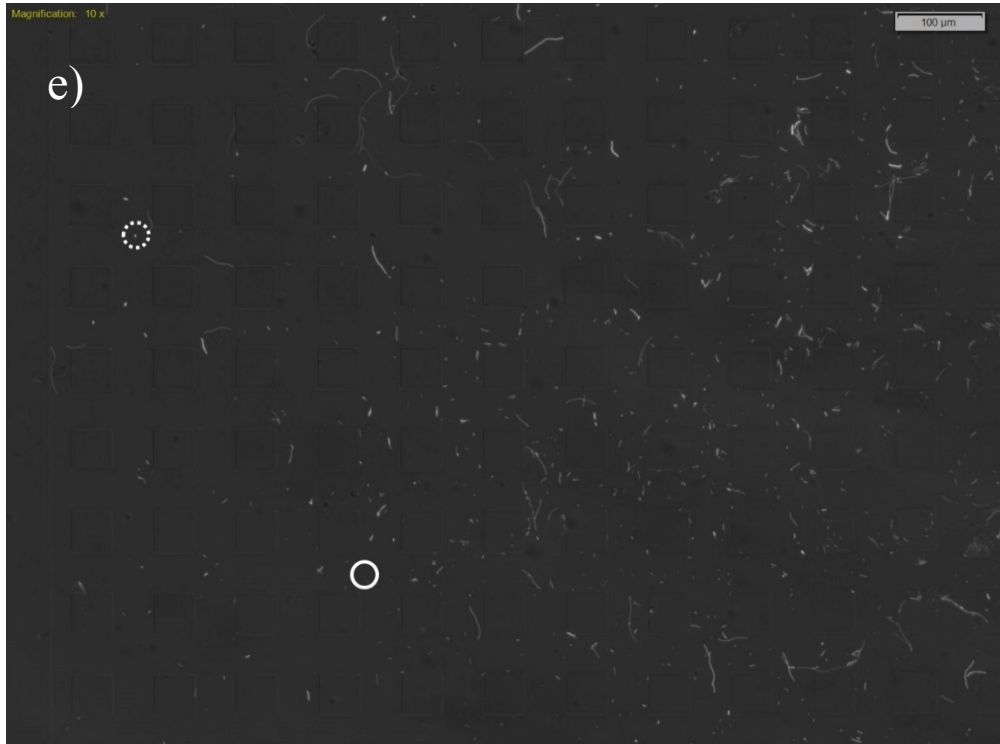
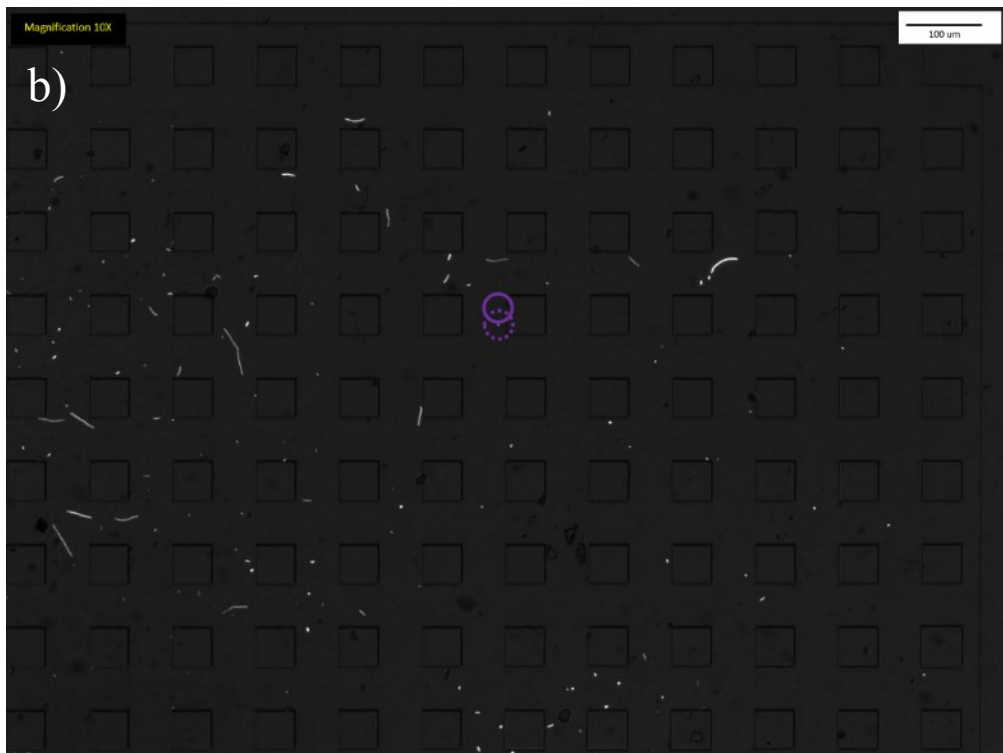
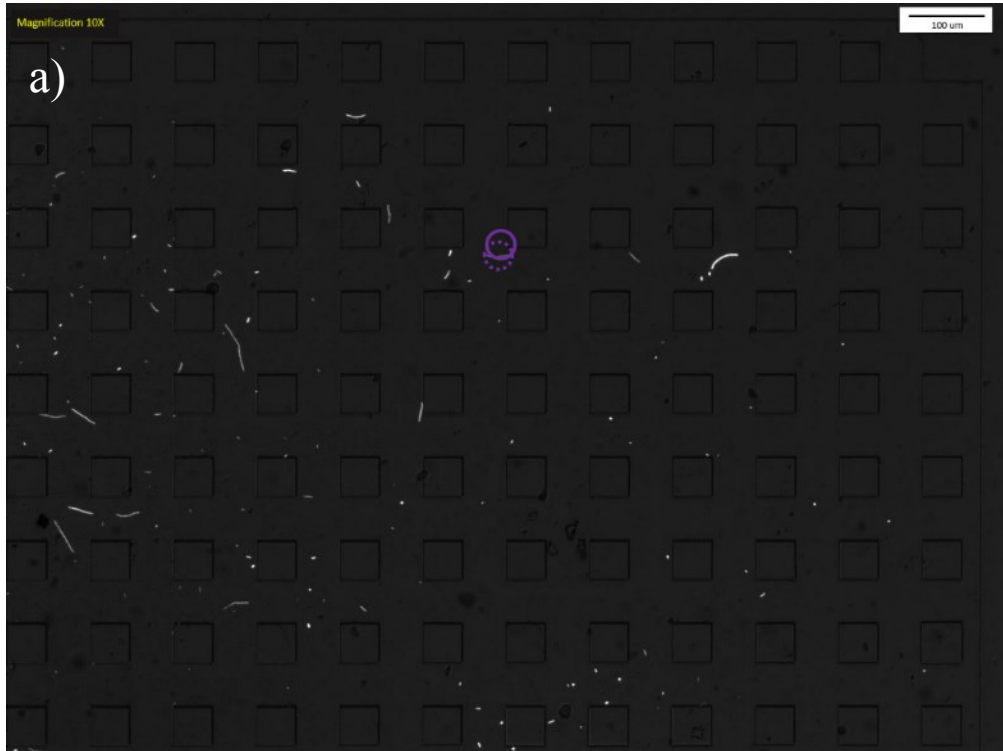
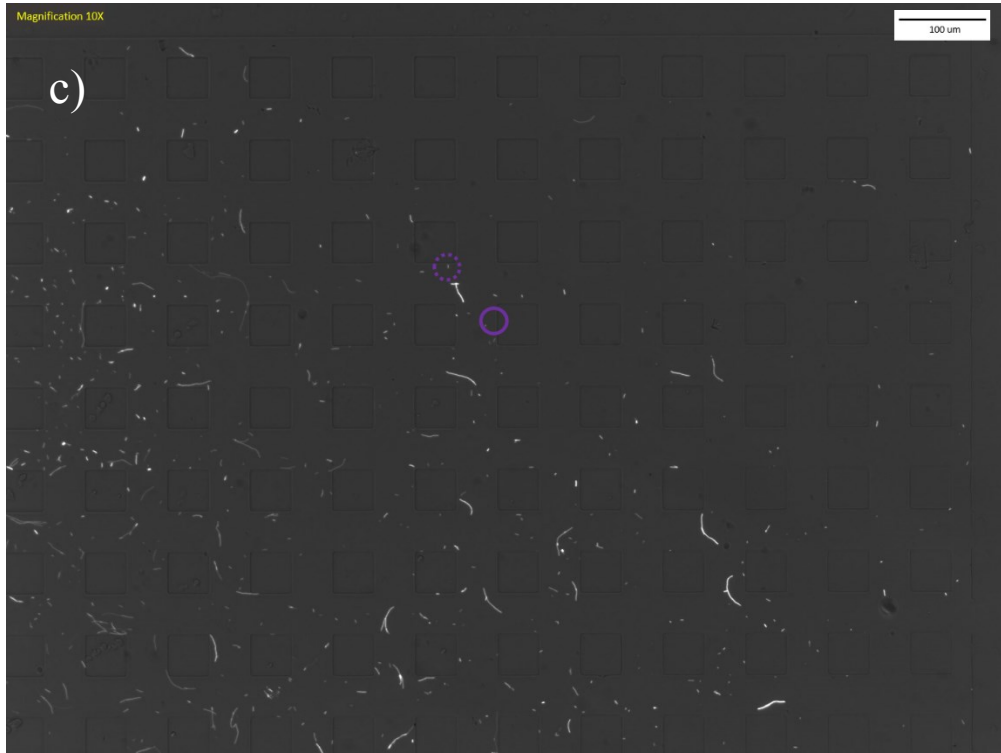


Figure A.3.6. Bacteria total displacement of 6 different analyzed (images a to f) at the end of 60 minutes for AT_E1 (image a) and AT_E2 (images b to f) at middle region at 15°





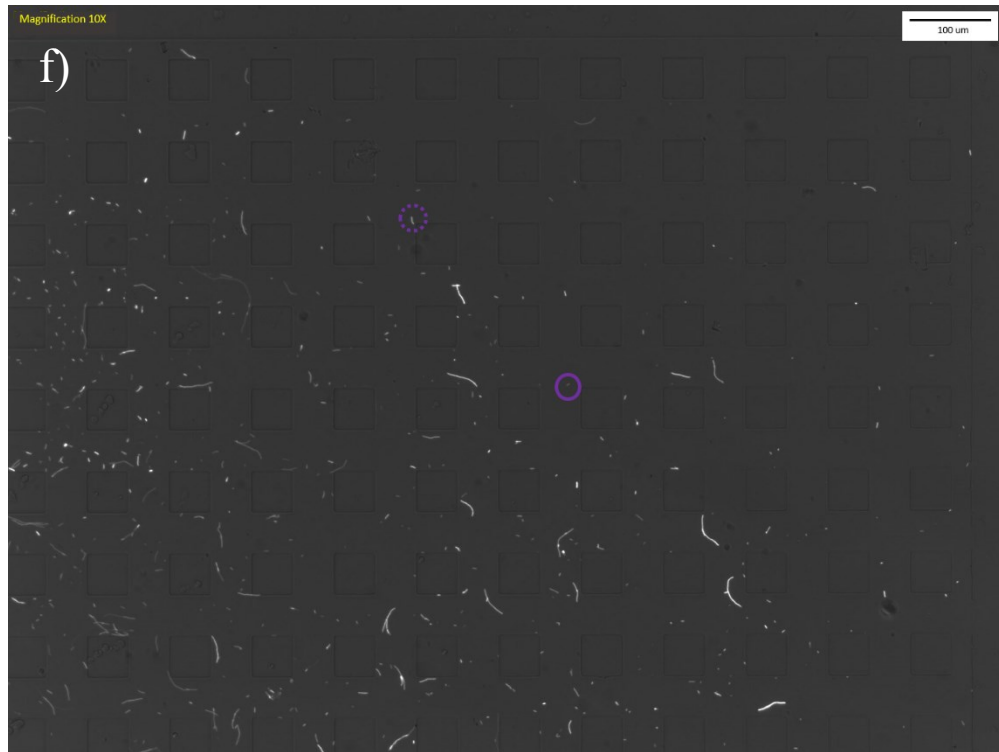
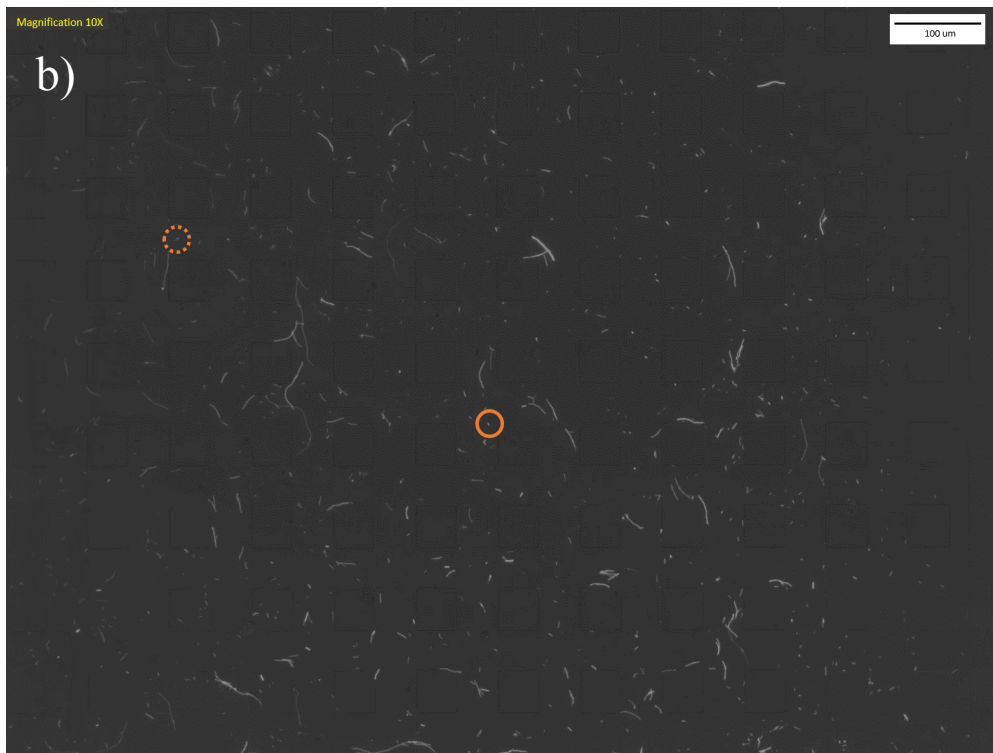
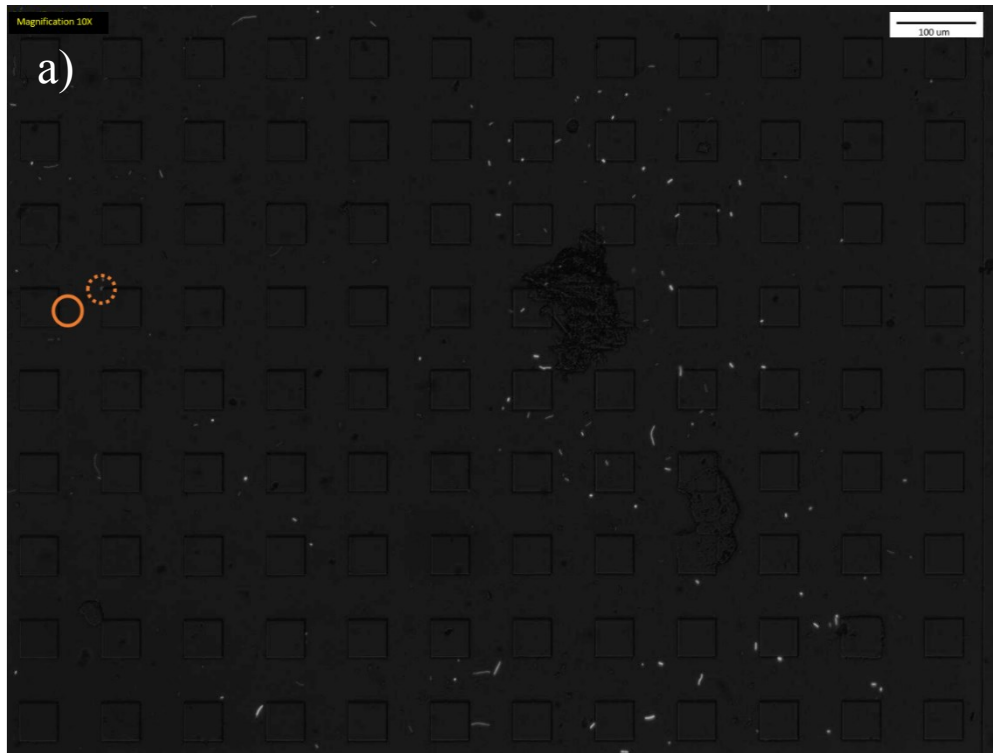
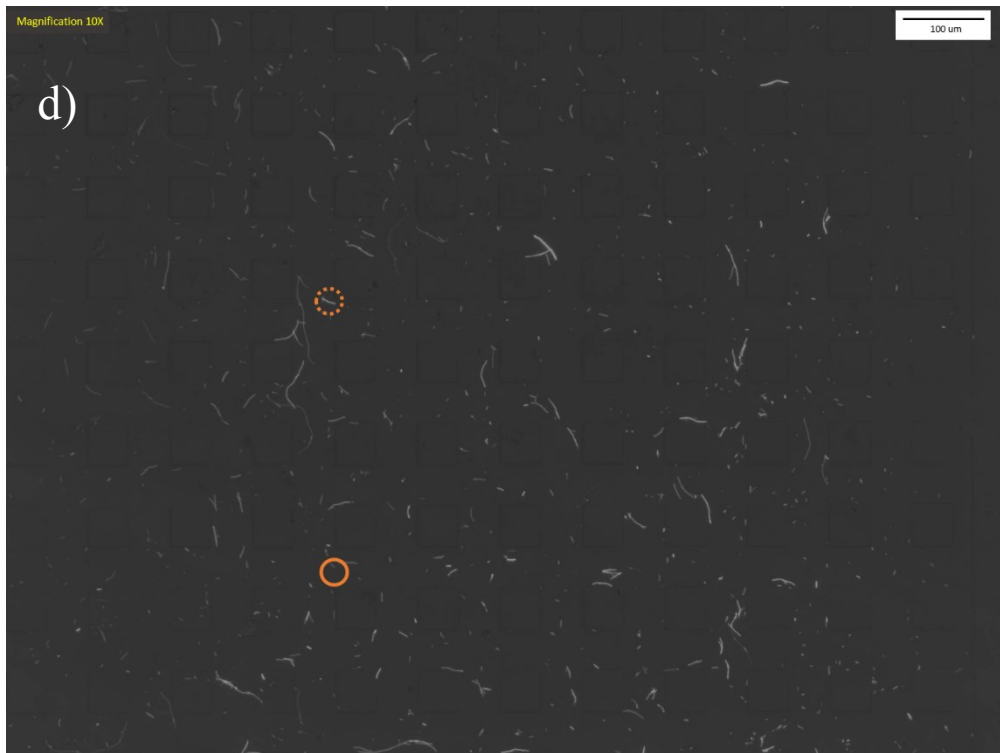
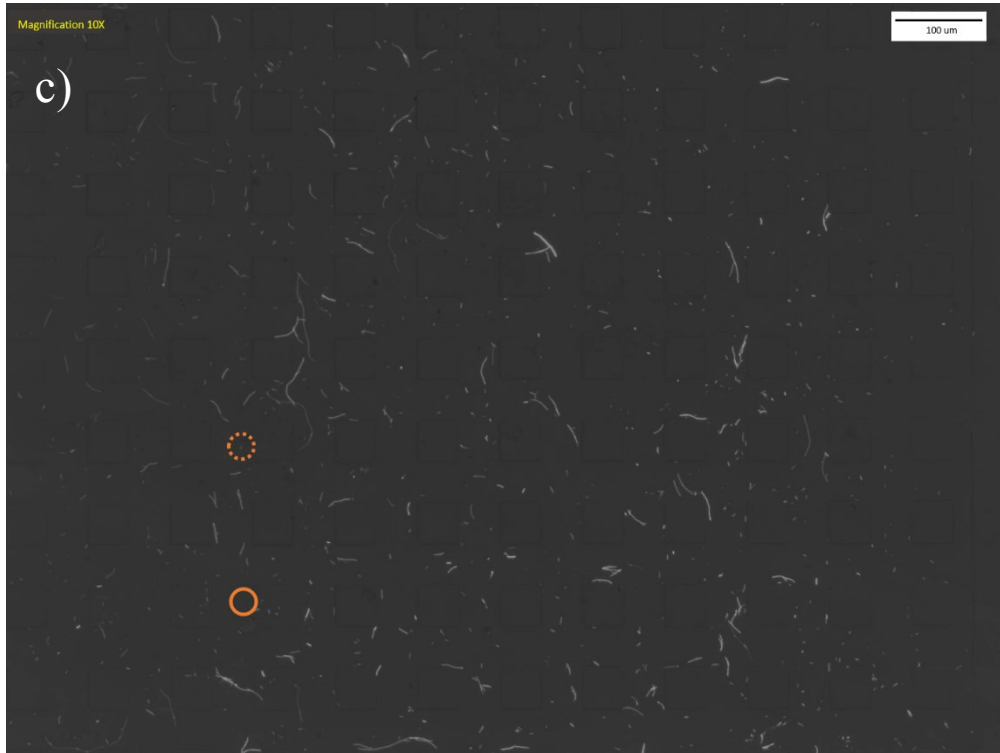


Figure A.3.7. Bacteria total displacement of 6 different analyzed bacteria (images a to f) at the end of 60 minutes for AT_E1 (images a and b) and AT_E2 (images c to f) at last region at 75°





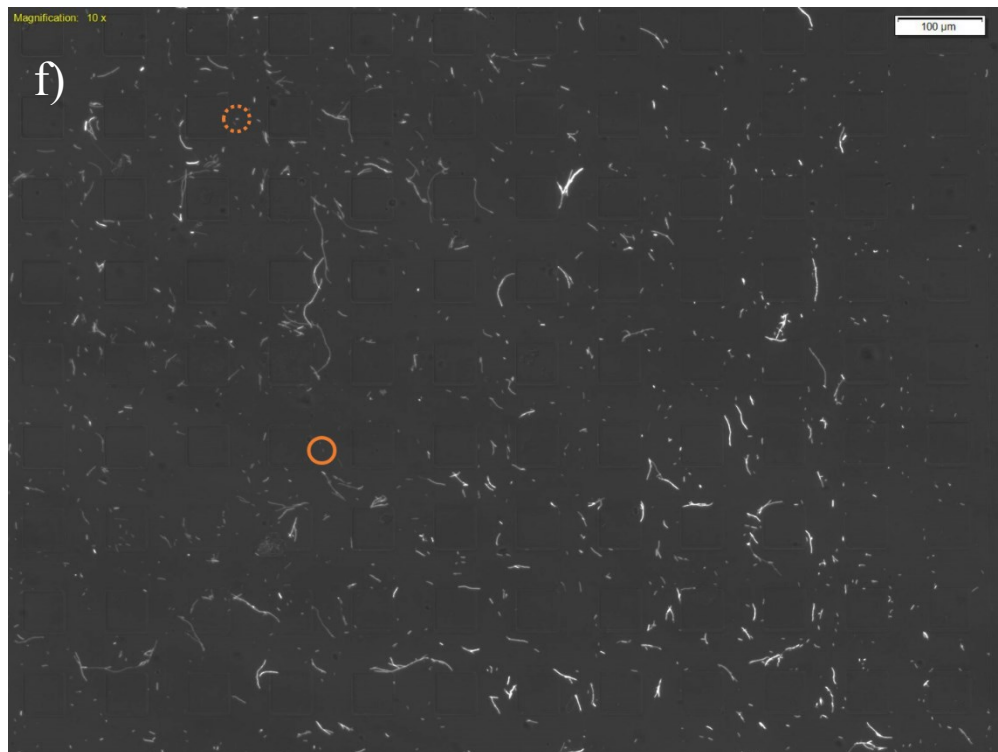
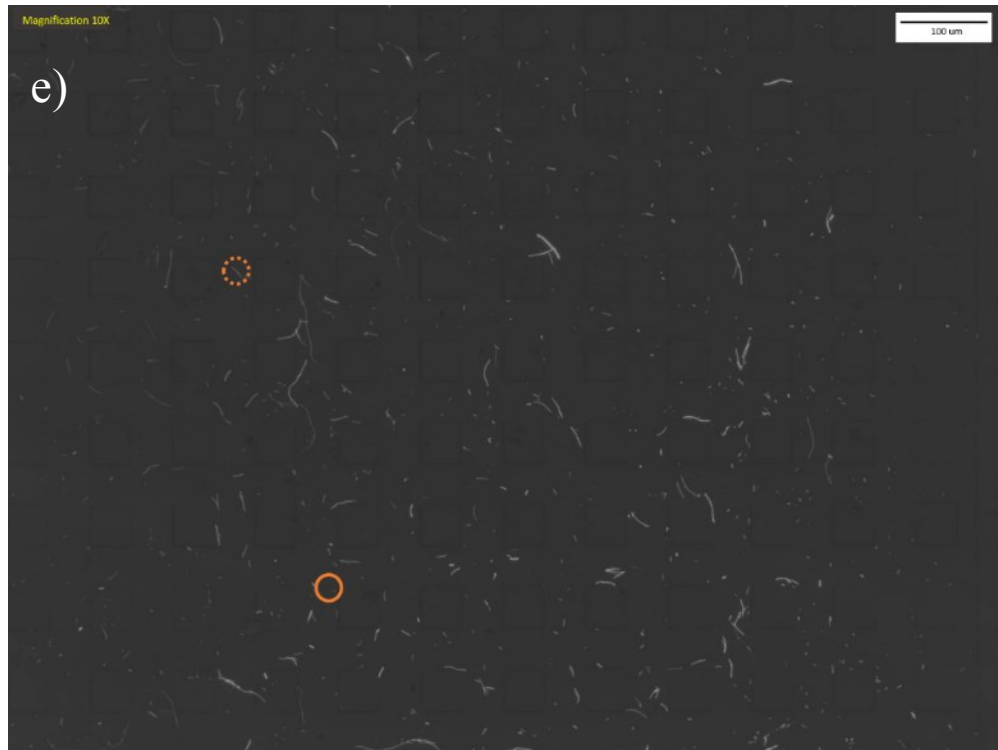
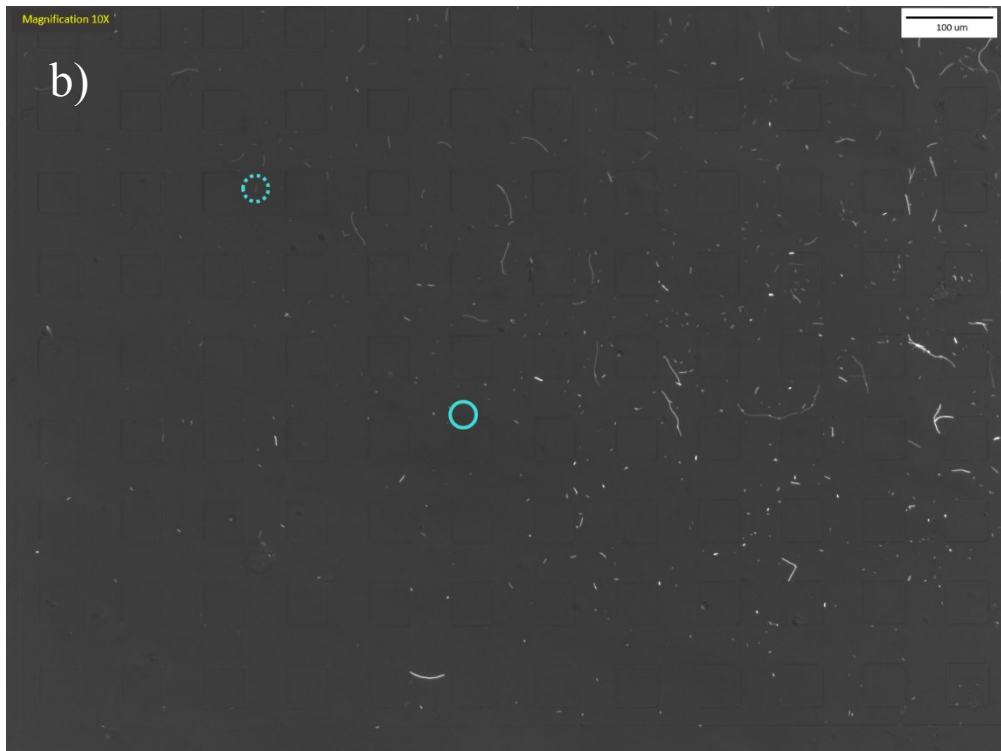
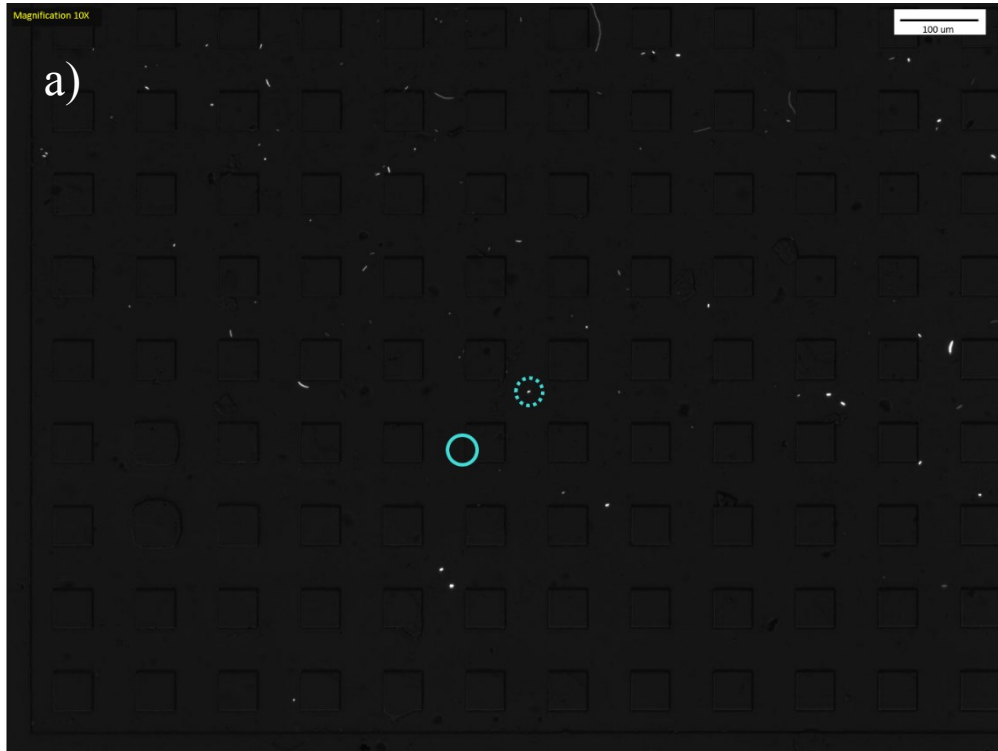
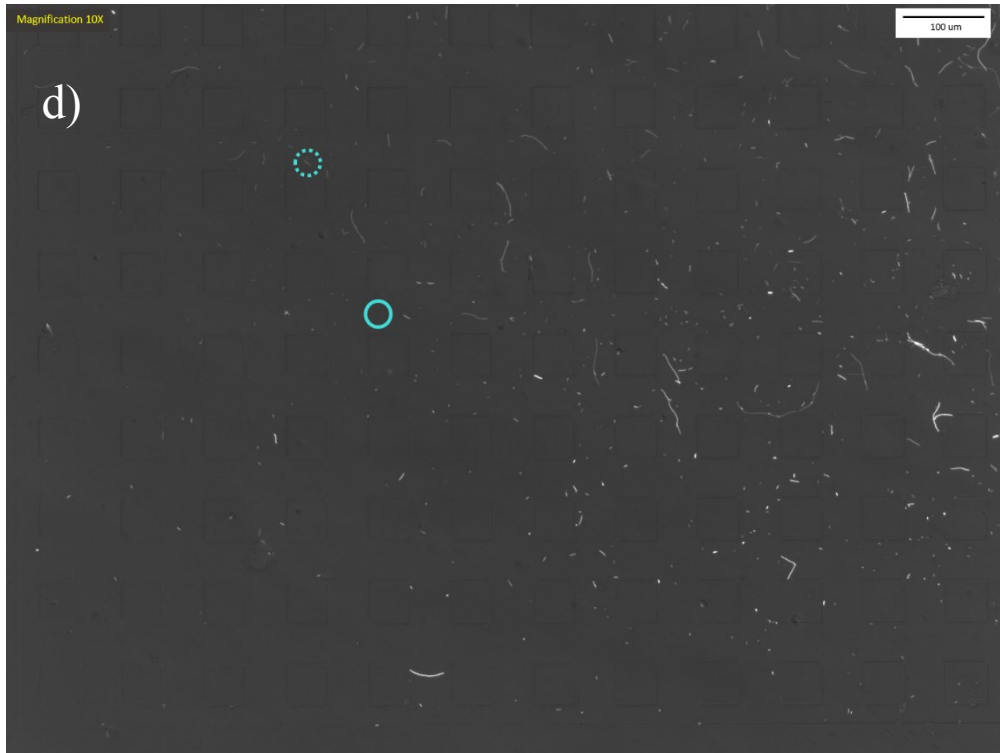
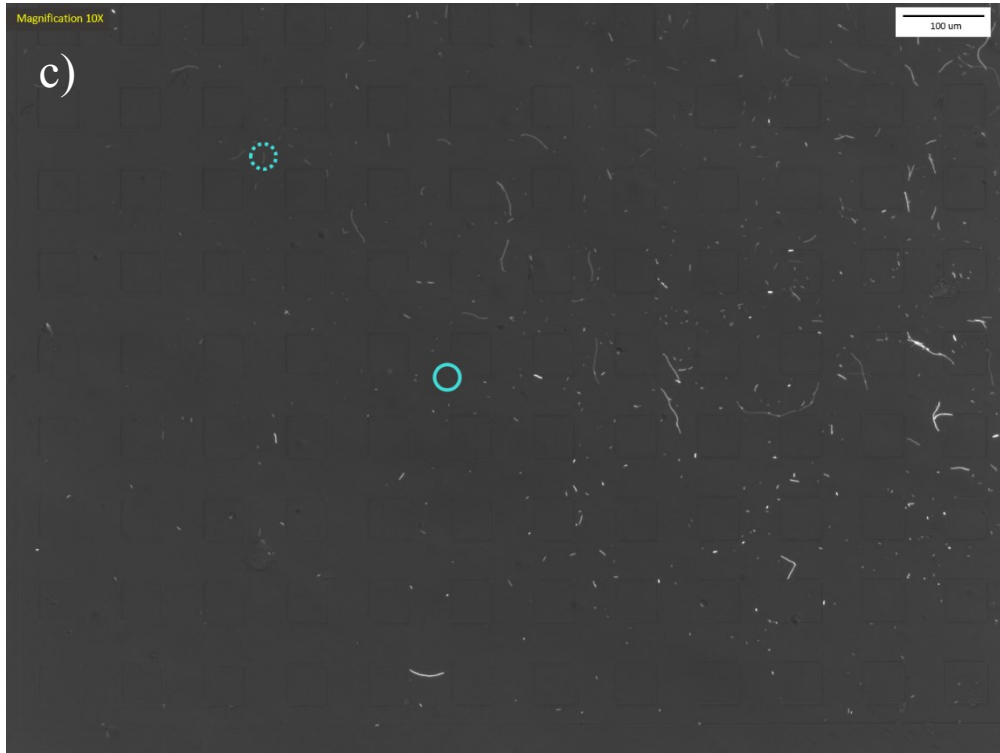


Figure A.3.8. Bacteria total displacement of 6 different analyzed bacteria (images a to f) at the end of 60 minutes for AT_E1 (image a) and AT_E2 (images b to f) at last region at 45°





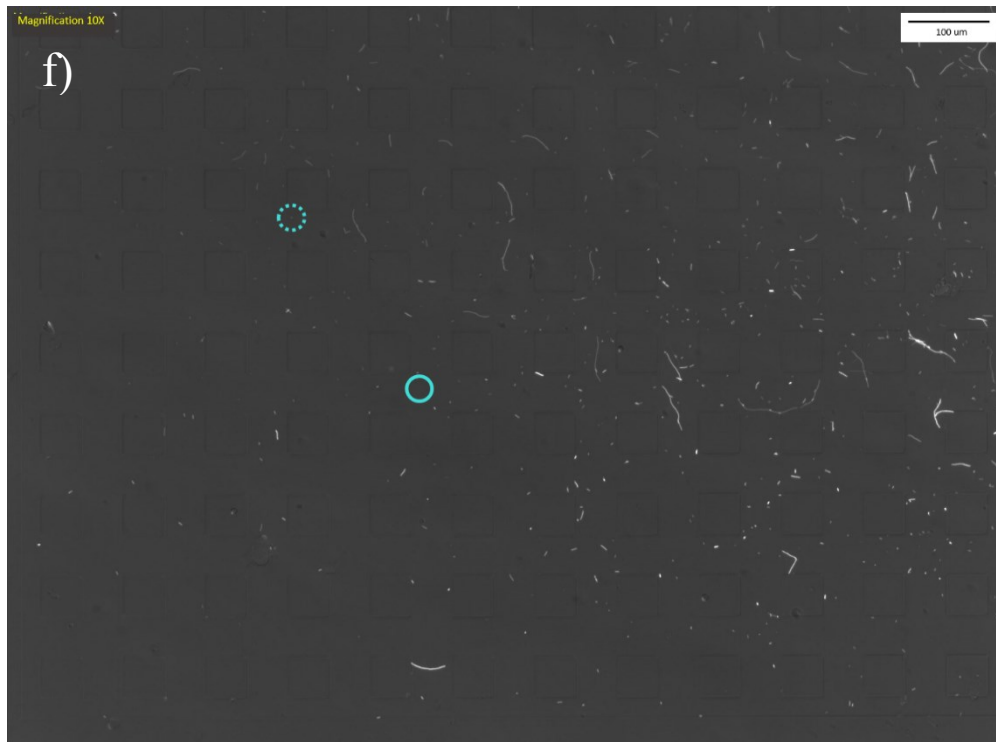
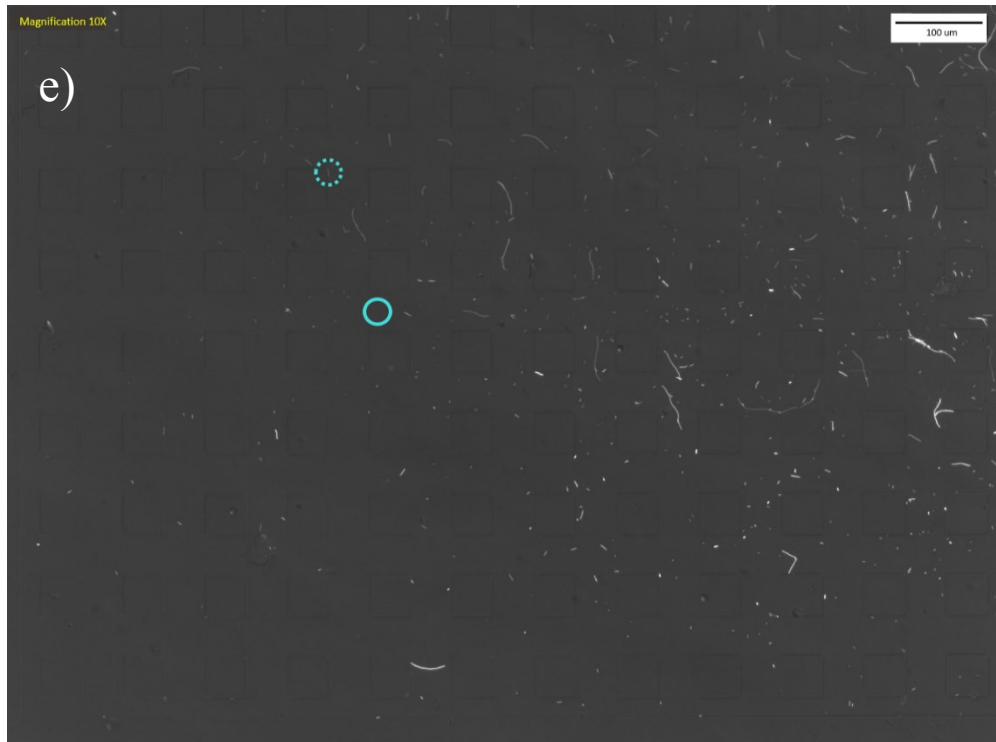
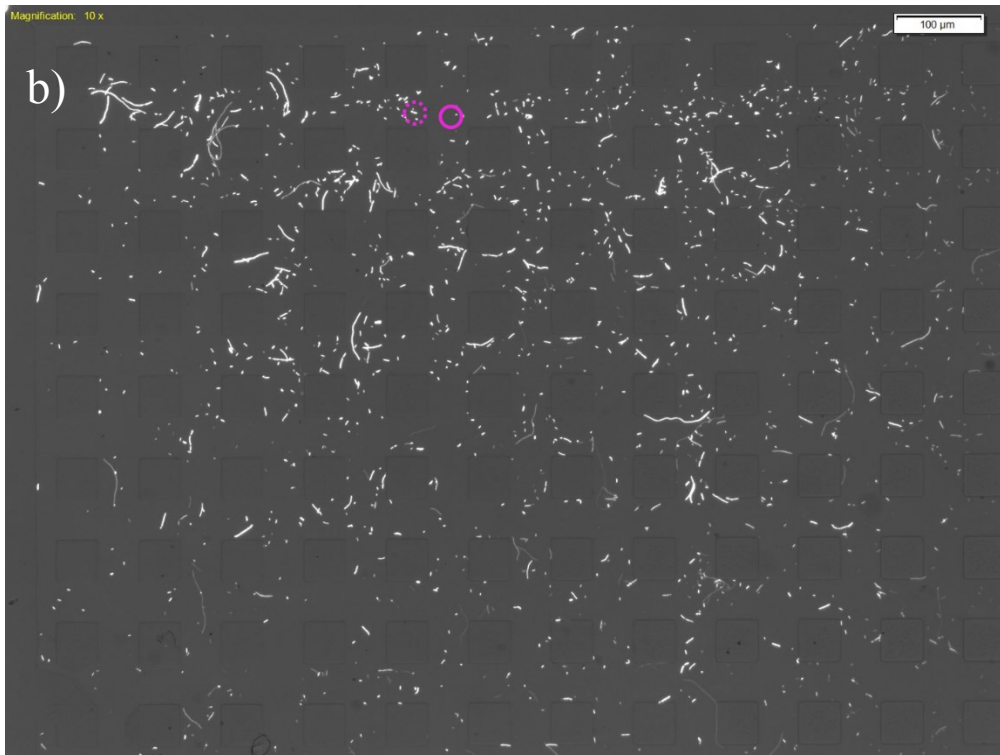
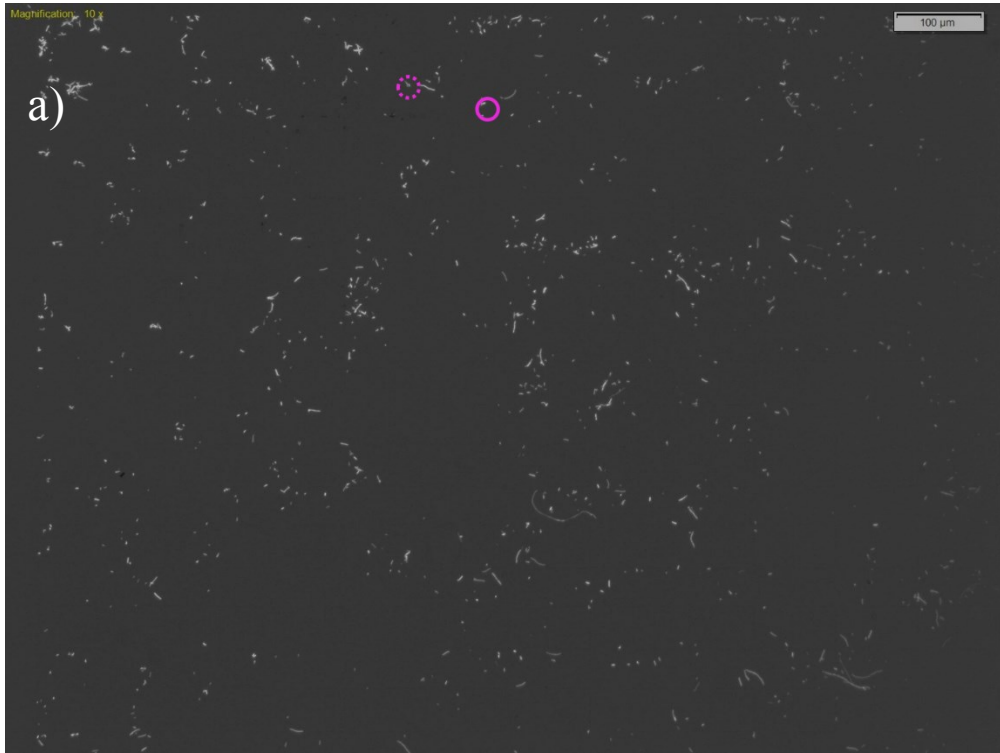


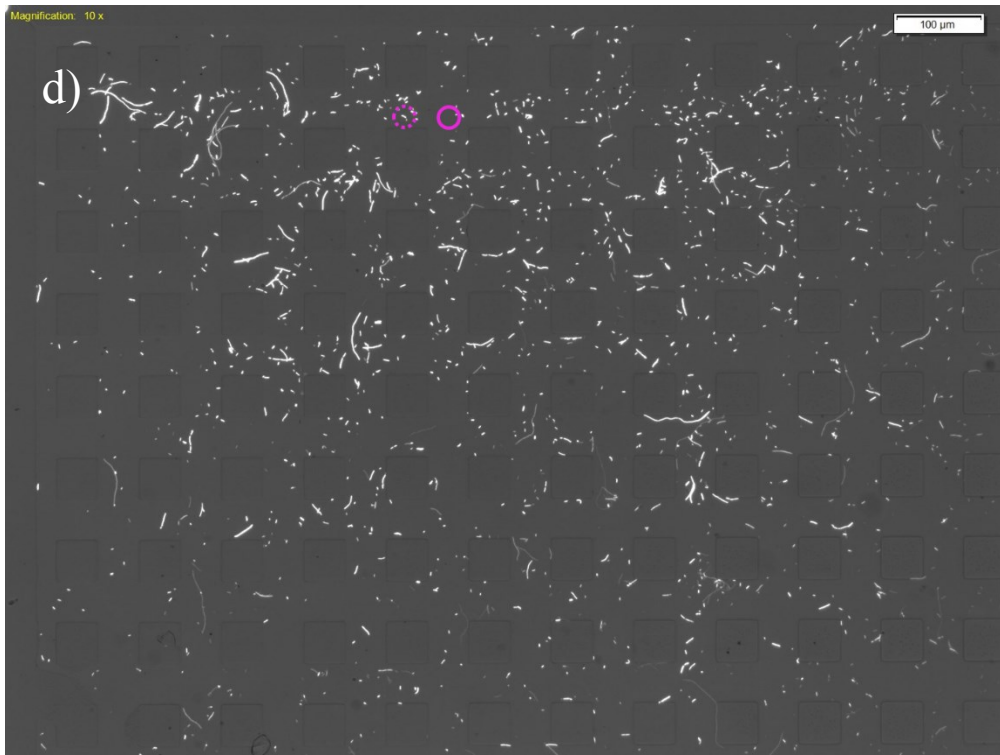
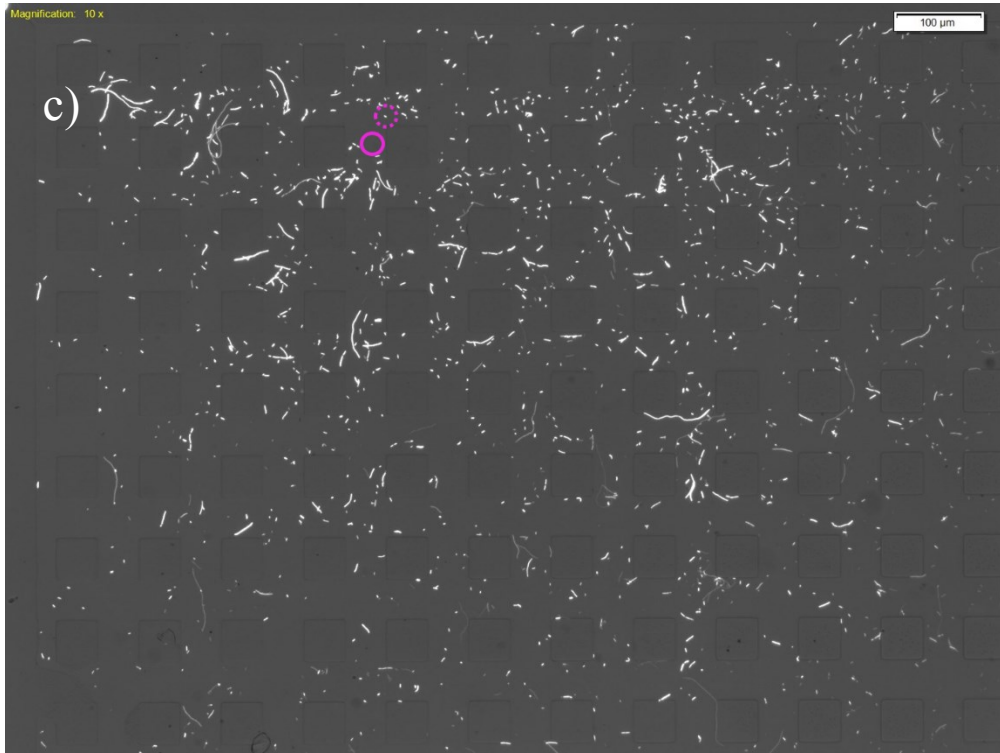
Figure A.3.9. Bacteria total displacement of 6 different analyzed bacteria (images a to f) at the end of 60 minutes for AT_E1 (image a) and AT_E2 (images b to f) at last region at 15°

A.4. Microscopy images of PT_E1 and PT_E2

Figure A.4.1 shows the microscopy images used to measure displacement of 6 bacteria during the 60 minutes of phage treatment experiments. In phage treatment experiments I introduce T4 phage (at concentration of 10^8 PFU/mL) to the loaded bacteria inside the device (flow rate of 0.01 mL/h) and I measured bacteria response to T4 phage during a period of 60 minutes. I repeated the experiment 2 times and the 2 practice of these experiments are abbreviated as PT_E1 and PT_E2 in this text (table 3.1). Figure A.4.1 shows the microscopy images used to measure bacteria displacement with initial position at the first region at 75° (section 1-1 of the imaging areas, see figure 3.4.2). In all images, dashed circles indicate the start position of bacteria and solid circle indicate the final position at that time step.

Figure A.4.2 shows the microscopy images used to measure displacement of 6 bacteria during the 60 minutes of the experiment for PT_E1 and PT_E2, first region at 45° (section 1-1 of the imaging areas, see figure 3.4.2). Figure A.4.3 is in regard to bacteria at first region at 15° , figure A.4.4 is in regard to bacteria at middle region at 75° , figure A.4.5 in regard to middle region at 45° and figure A.4.6 in regard to middle region at 15° . For the last region at 75° , 45° and 15° figures A.4.7, A.4.8 and A.4.9 show microscopy images respectively.





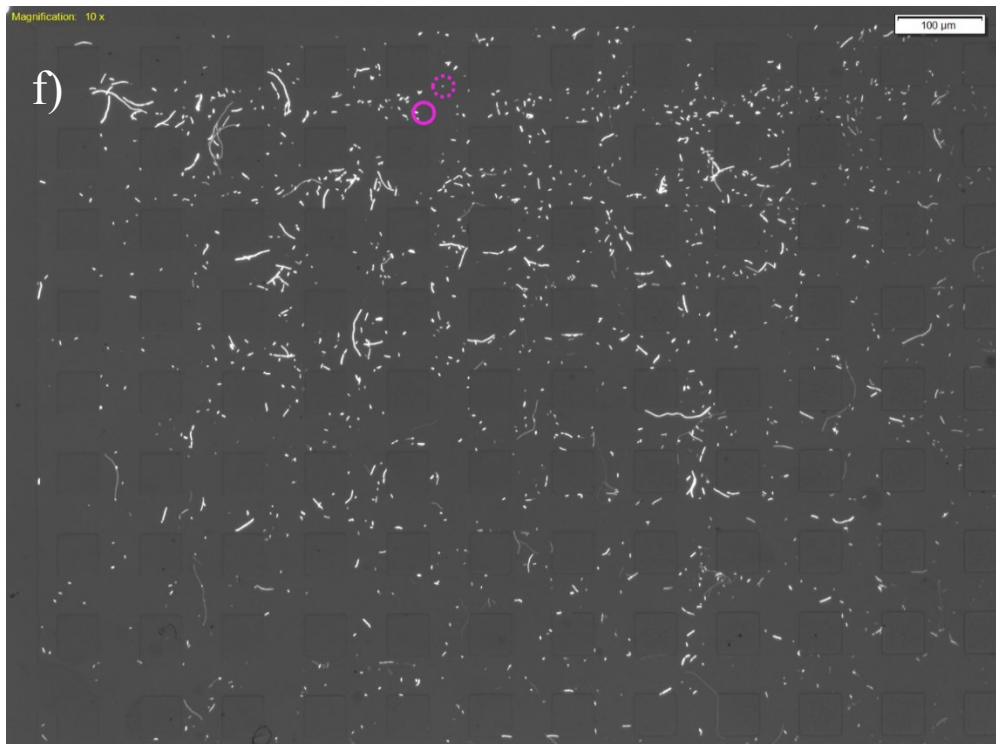
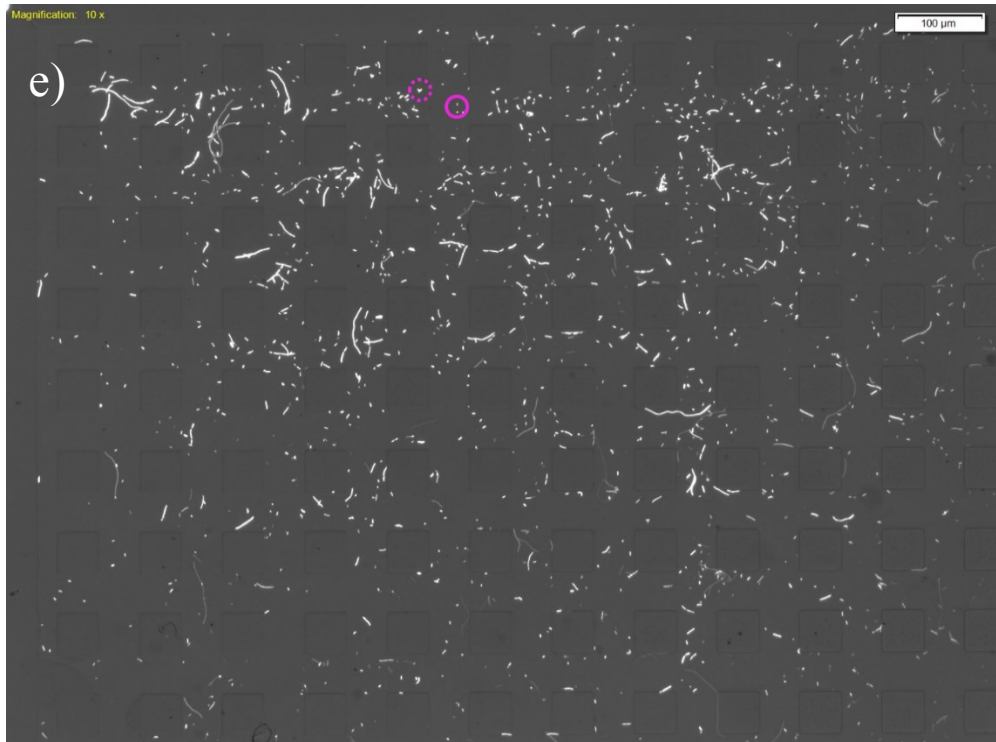
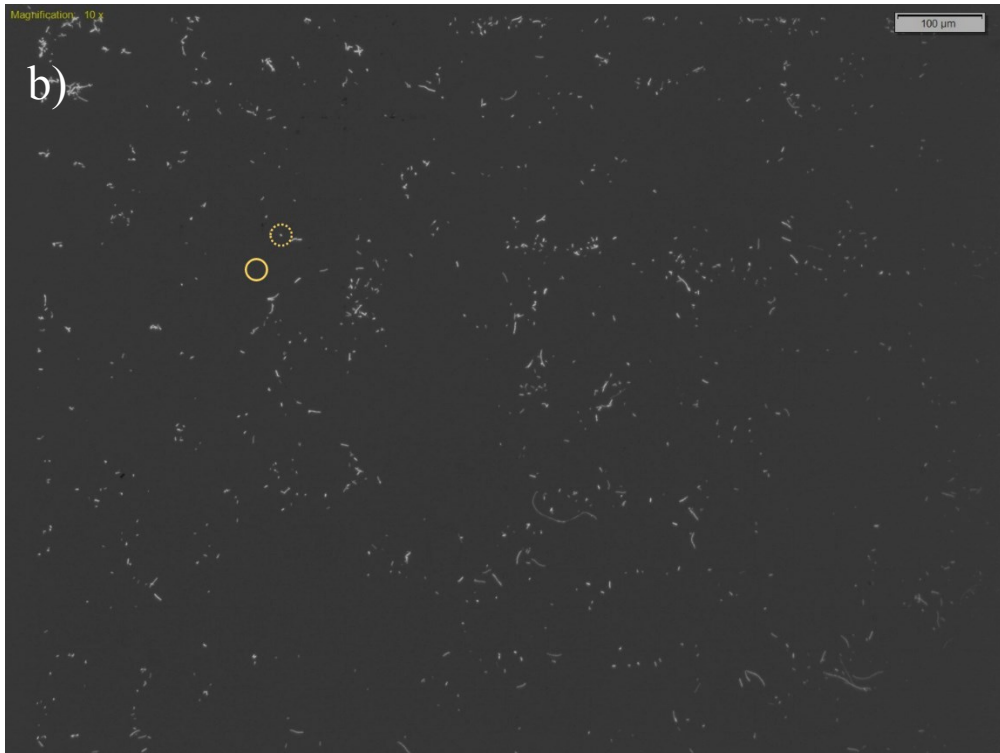
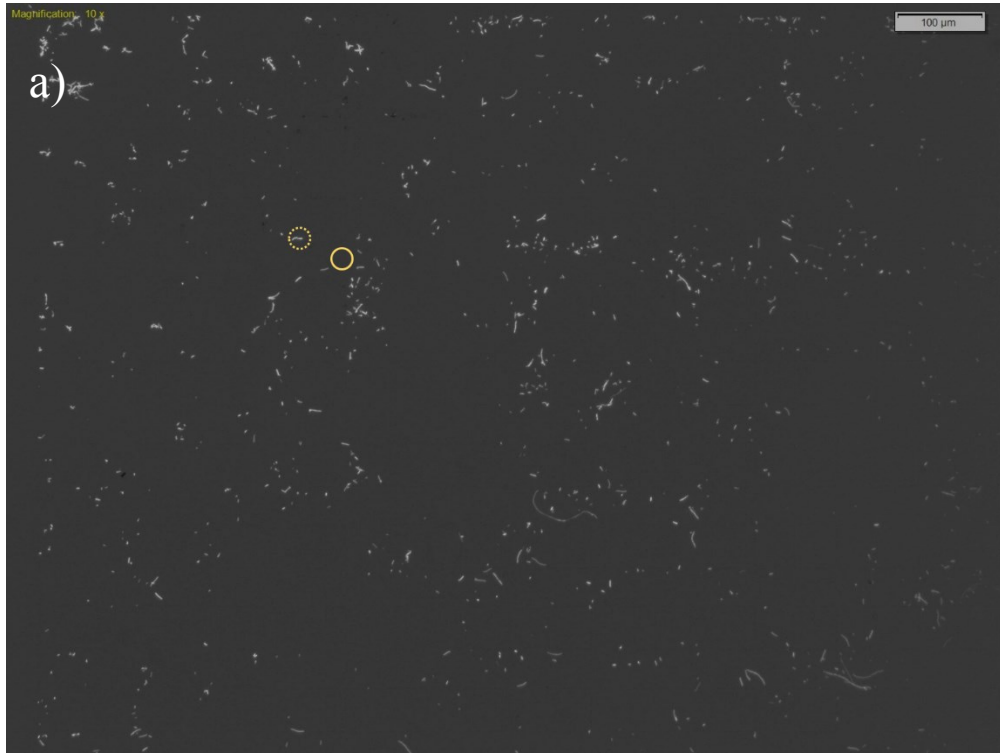
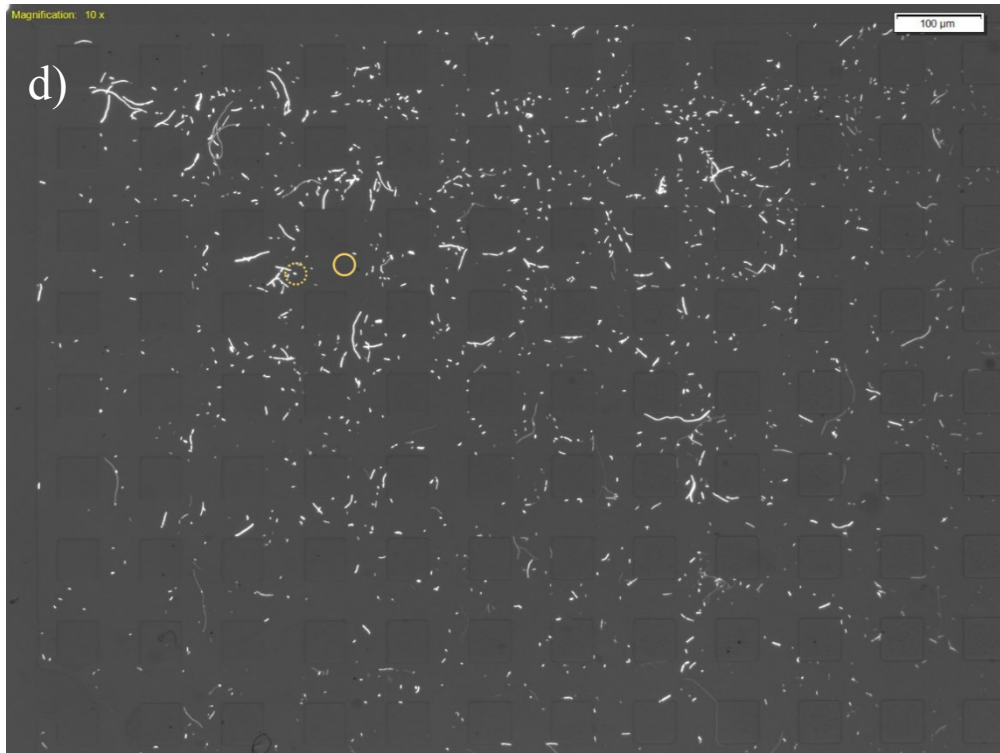
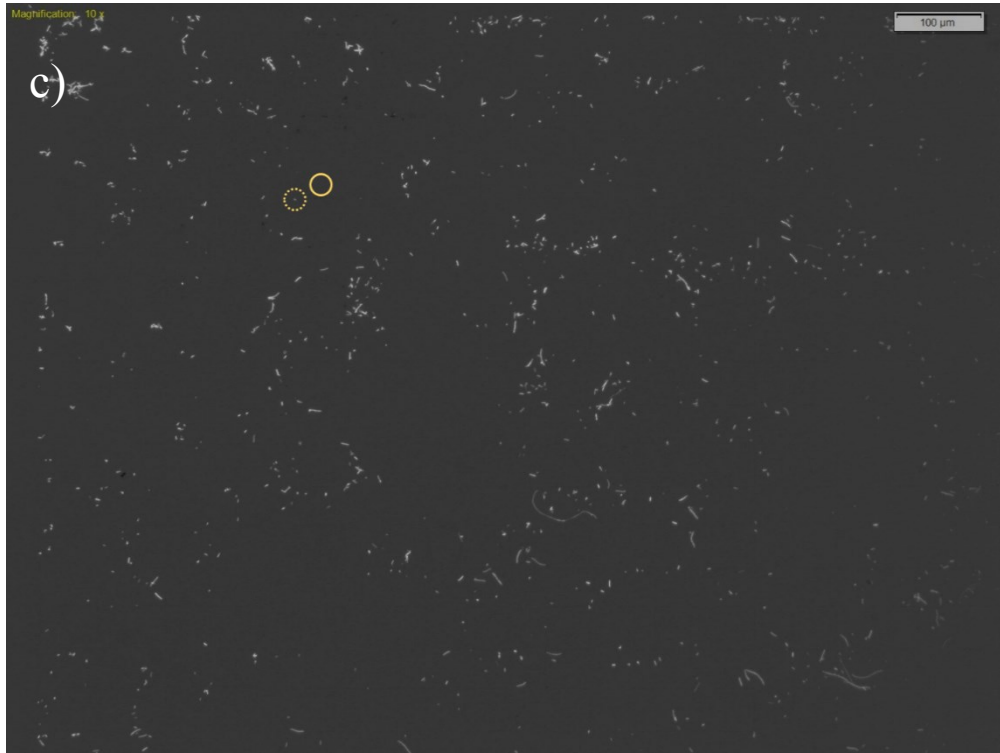


Figure A.4.1. Bacteria total displacement of 6 different analyzed bacteria (images a to f) at the end of 60 minutes for PT_E1 (images a) and PT_E2 (images b to f) at first region at 75°





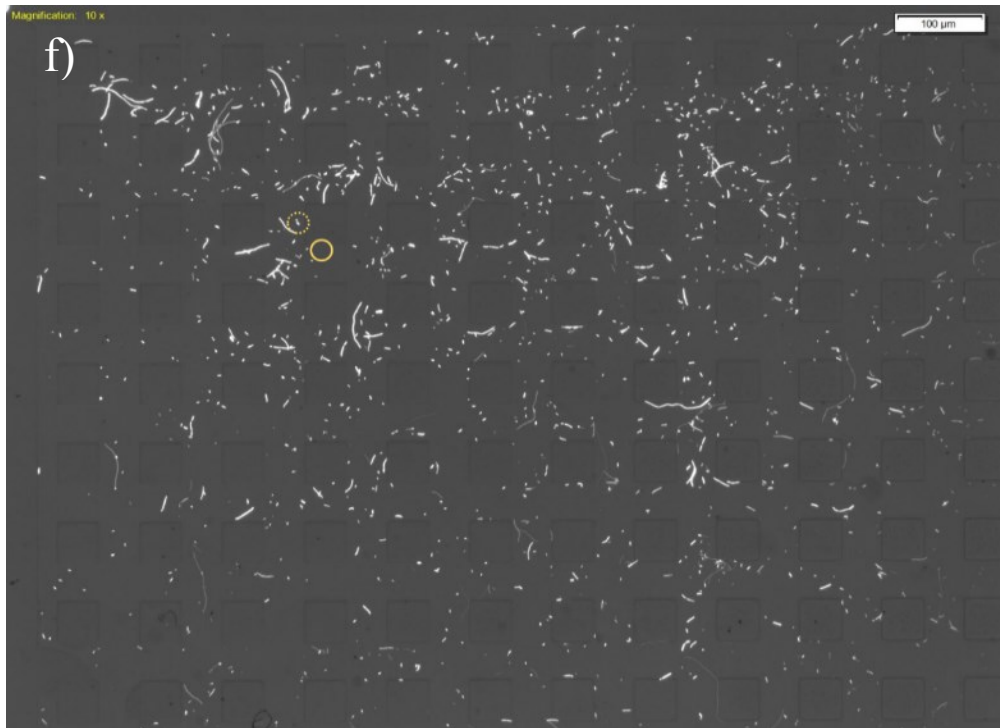
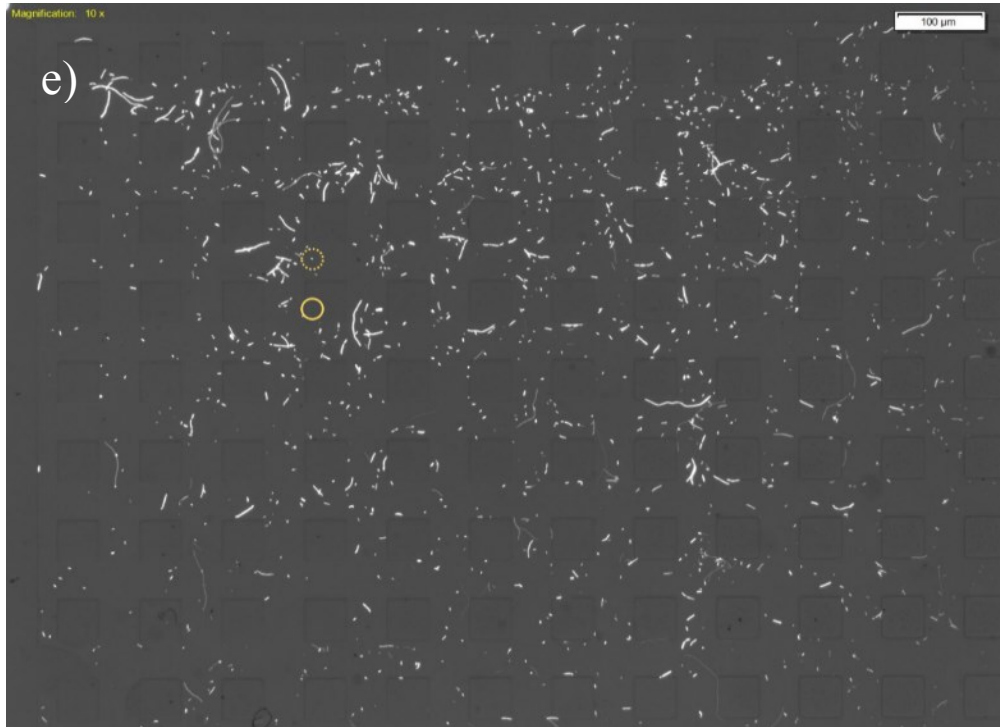
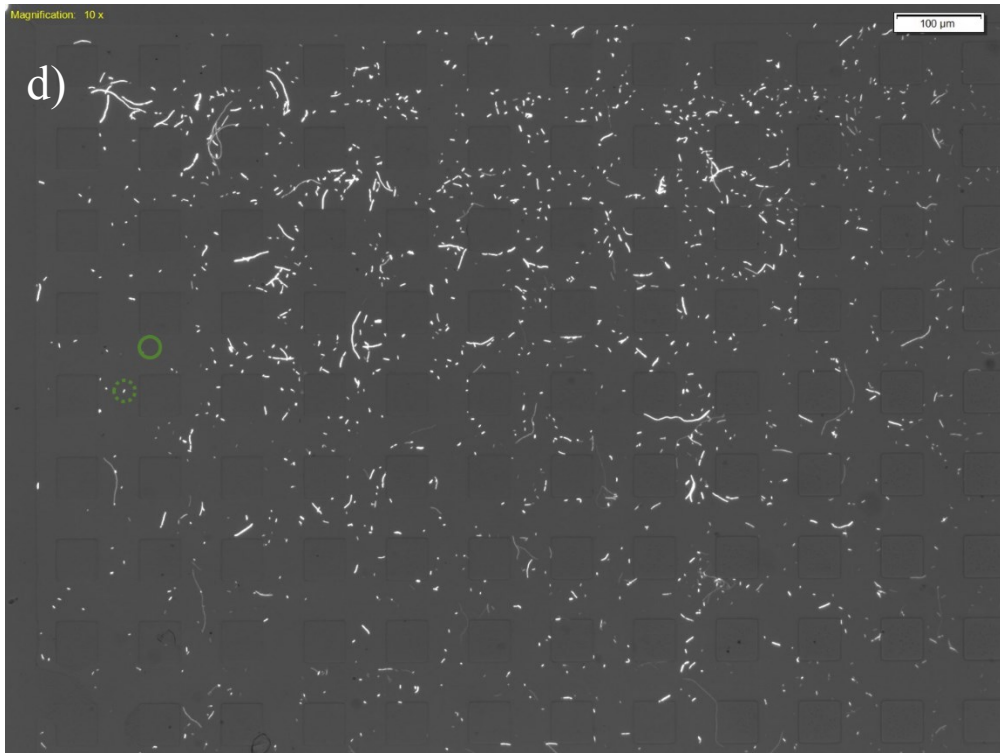


Figure A.4.2. Bacteria total displacement of 6 different analyzed bacteria (images a to f) at the end of 60 minutes for PT_E1 (images a to c) and PT_E2 (images d to f) at first region at 45°





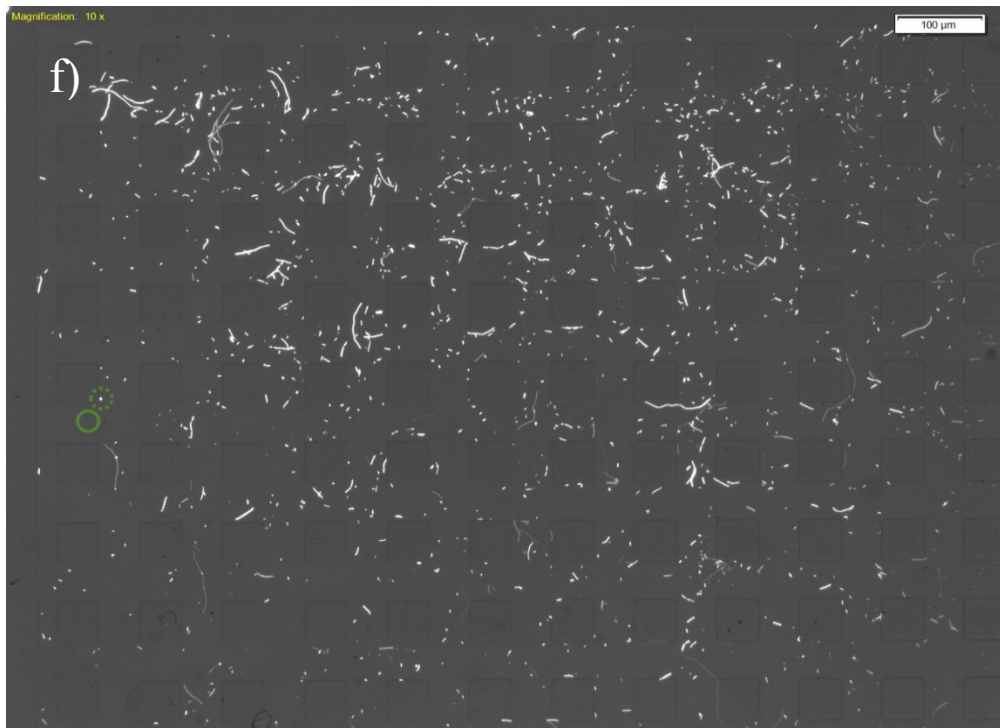
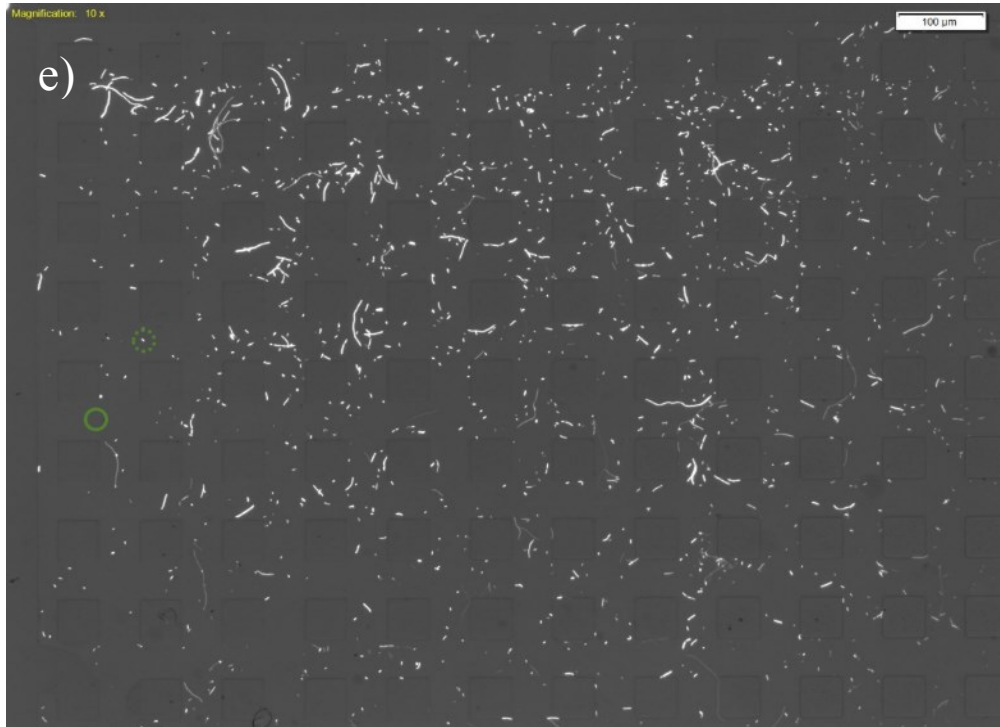
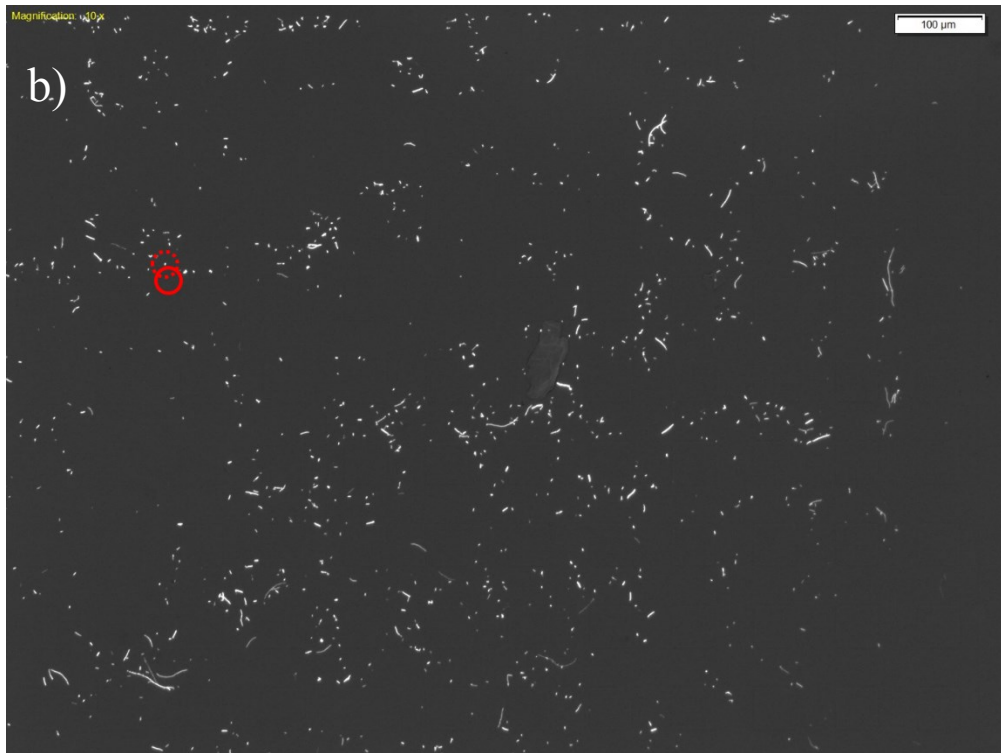
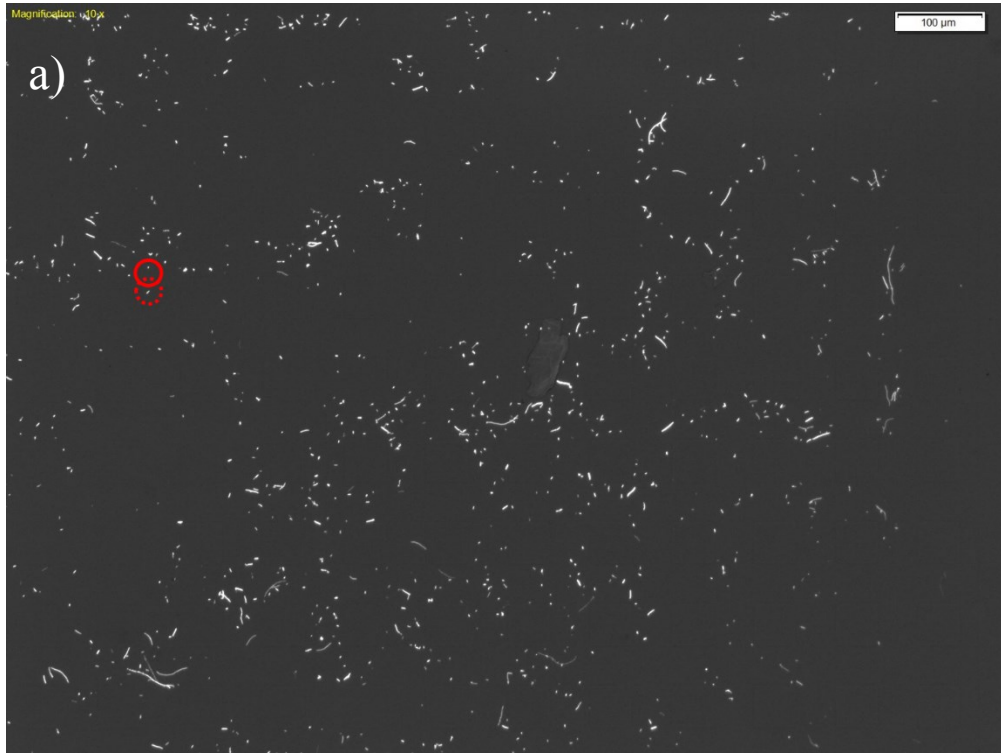
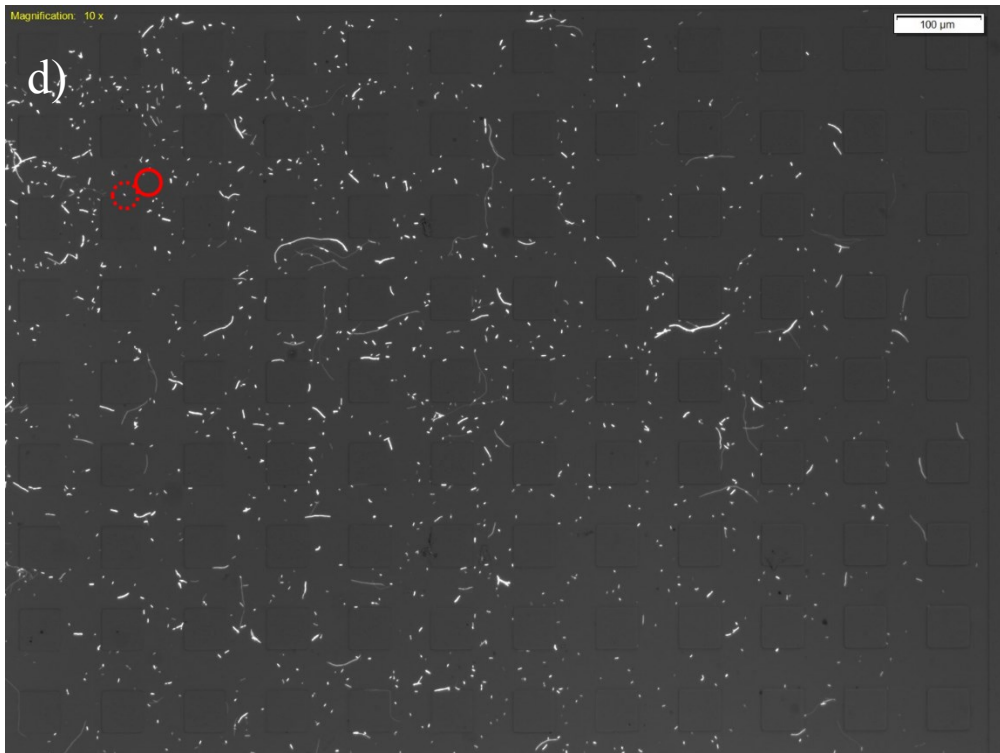
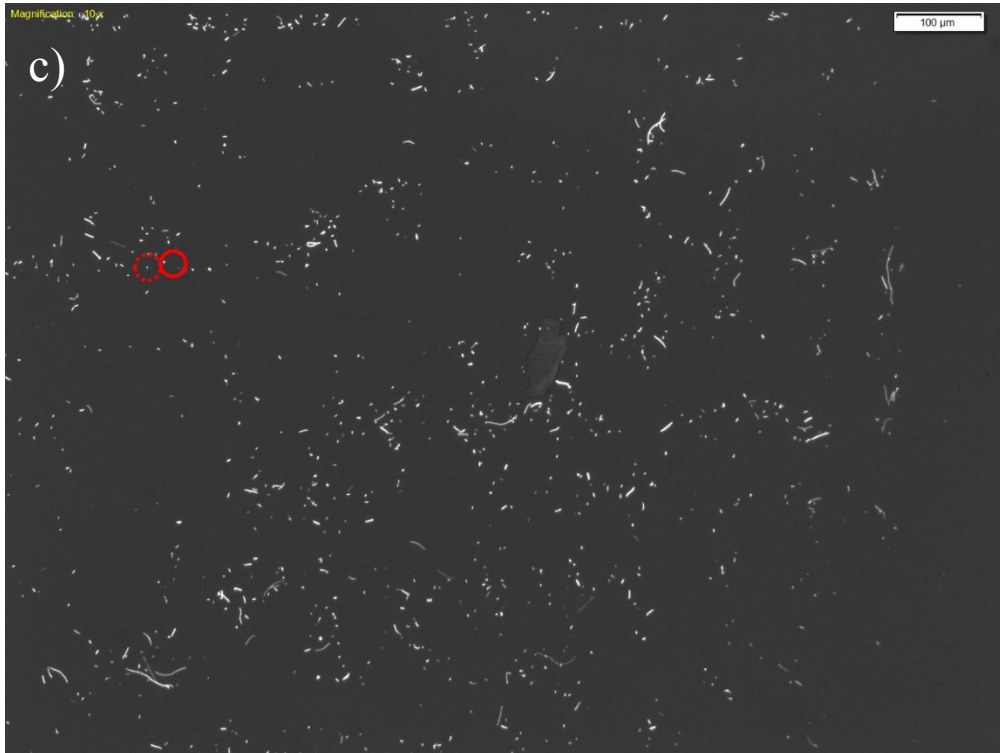


Figure A.4.3. Bacteria total displacement of 6 different analyzed (images a to f) at the end of 60 minutes for PT_E1 (images a to c) and PT_E2 (images d to f) at first region at 15°





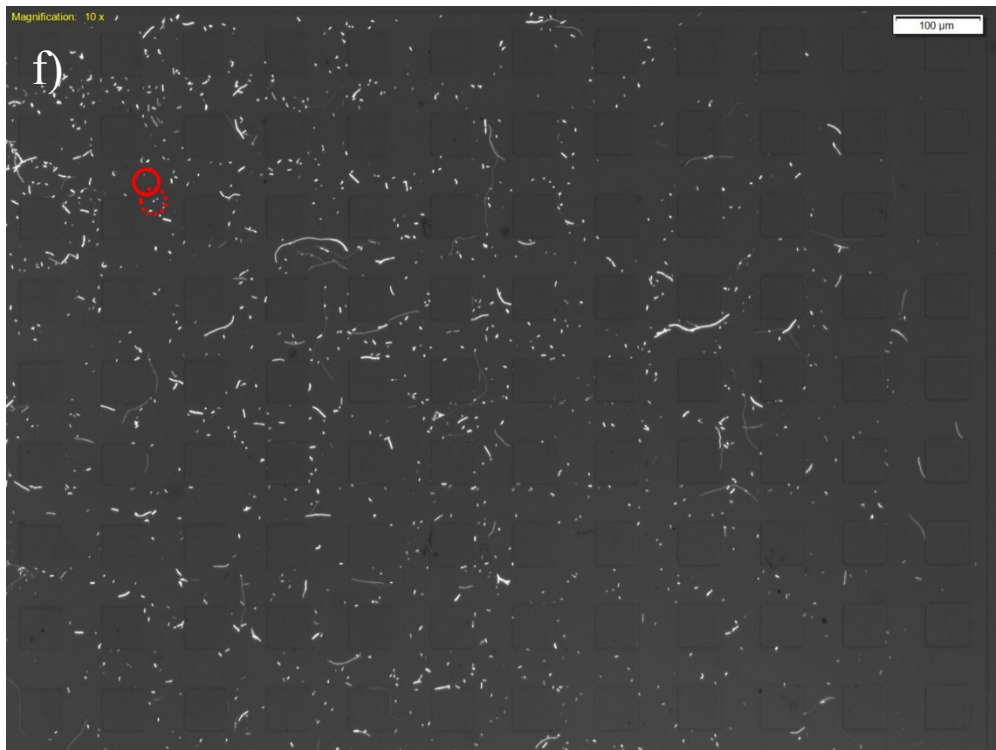
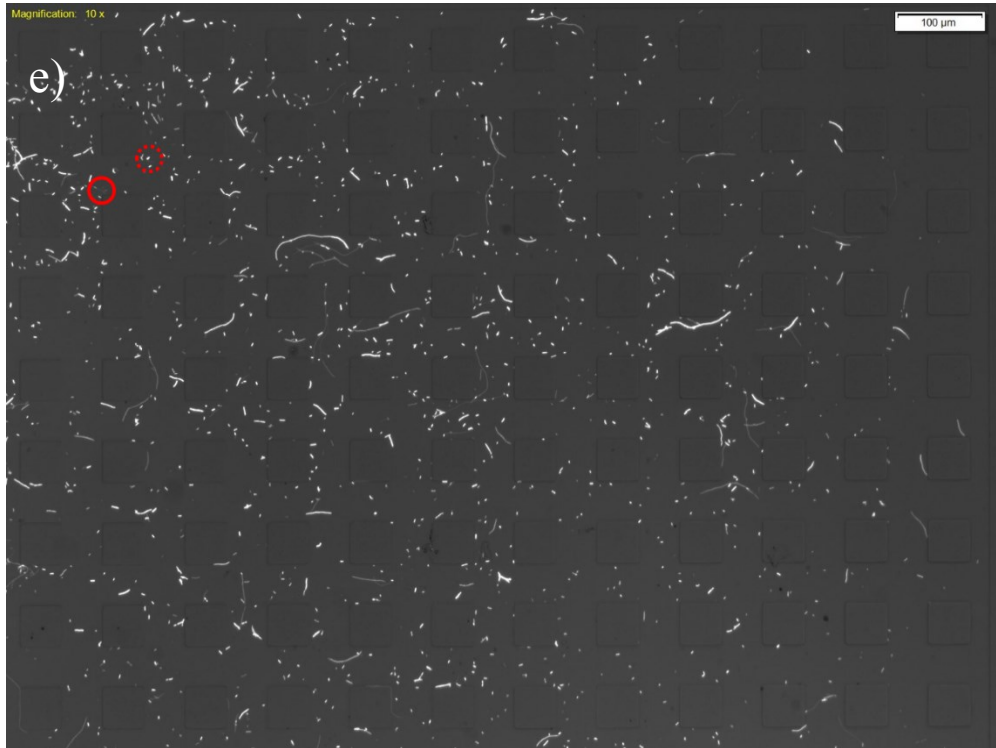
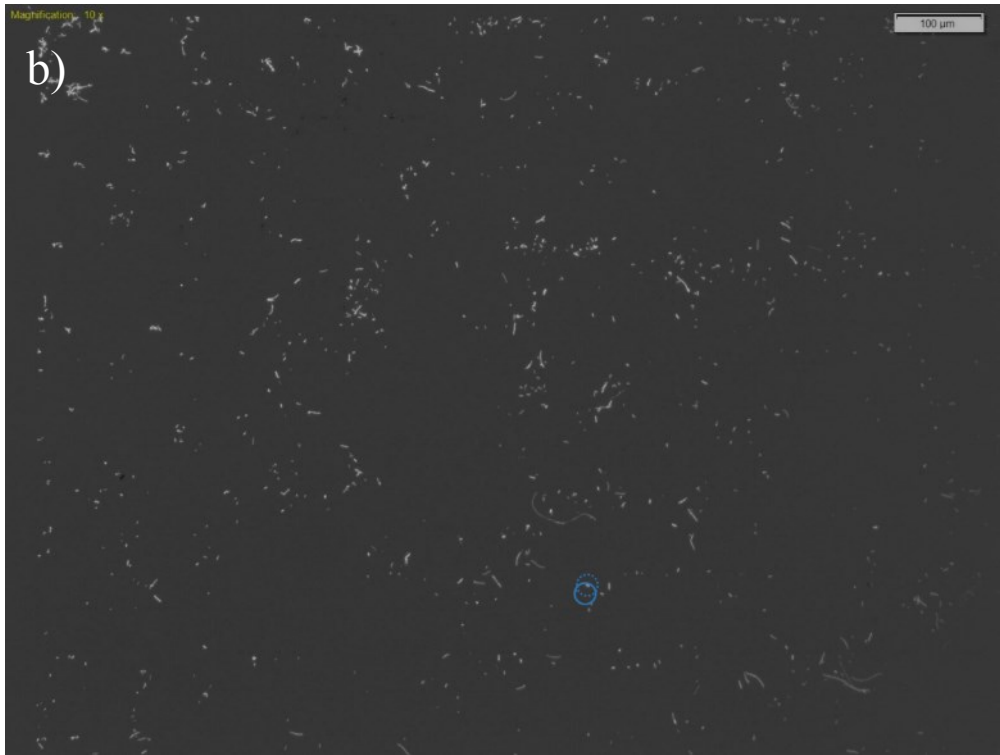
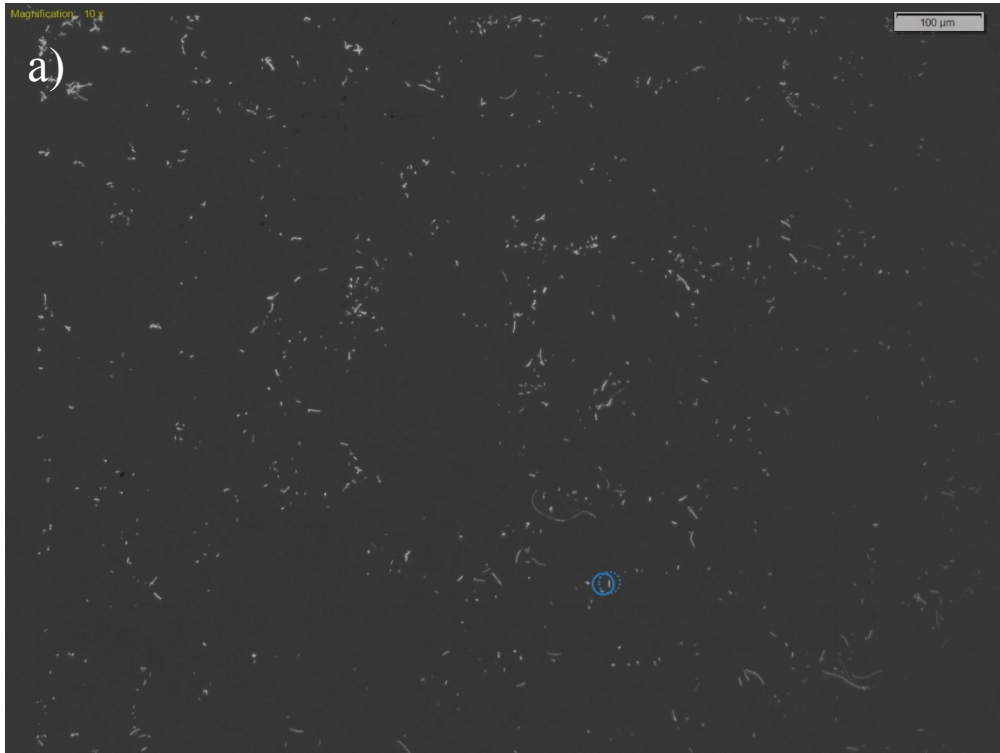
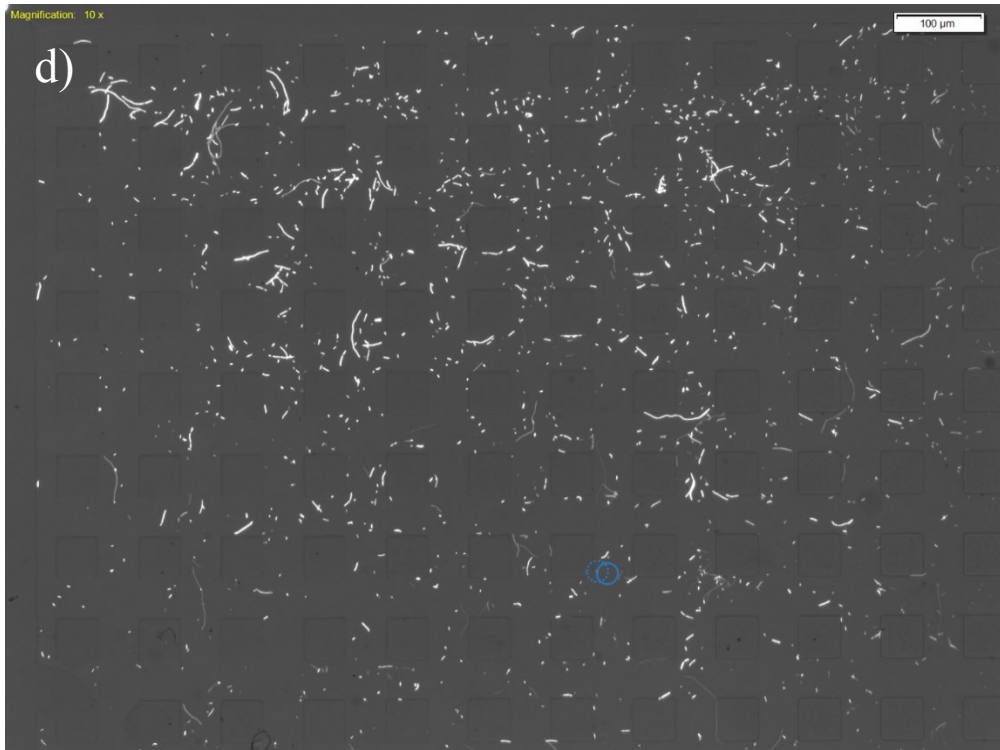
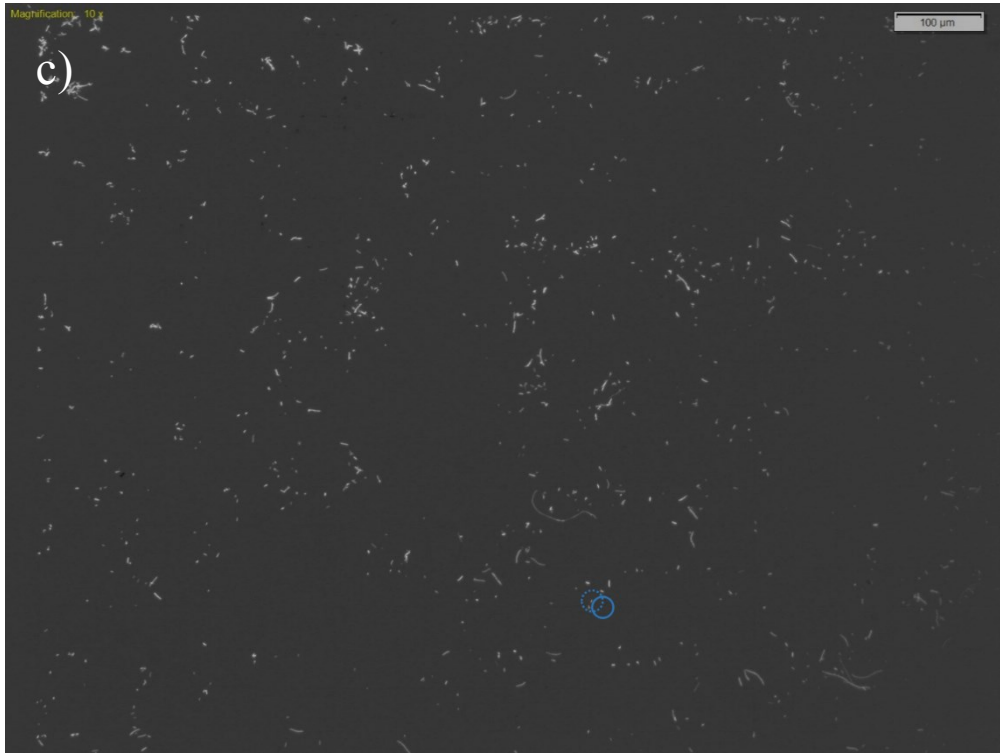


Figure A.4.4. Bacteria total displacement of 6 different analyzed bacteria (images a to f) at the end of 60 minutes for PT_E1 (images a to c) and PT_E2 (images d to f) at middle region at 75°





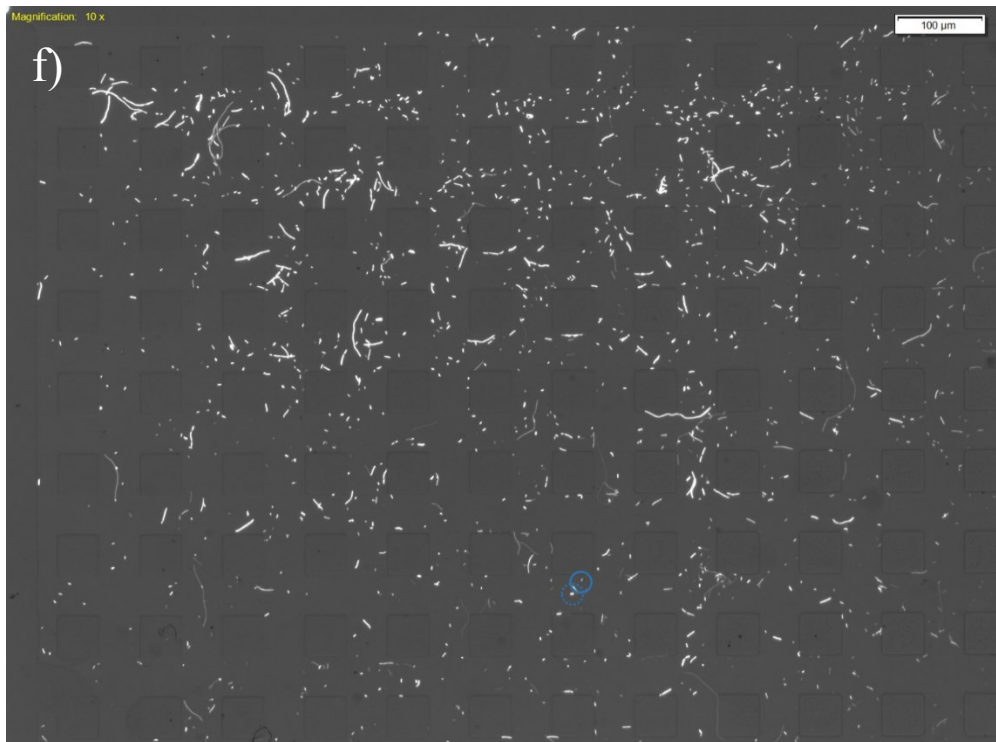
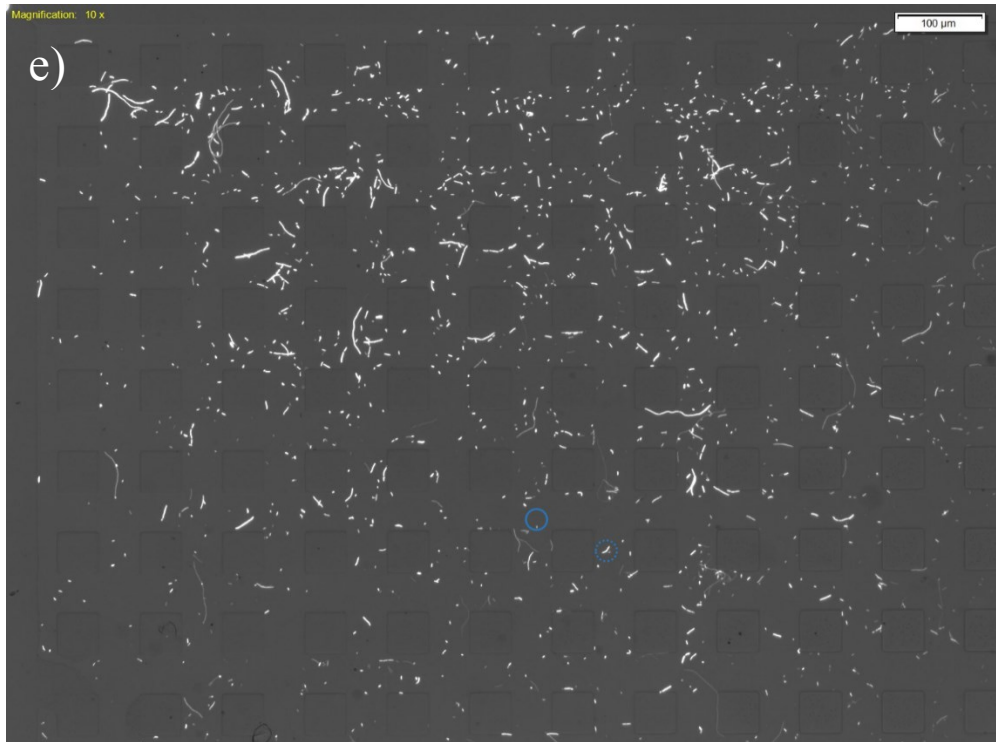
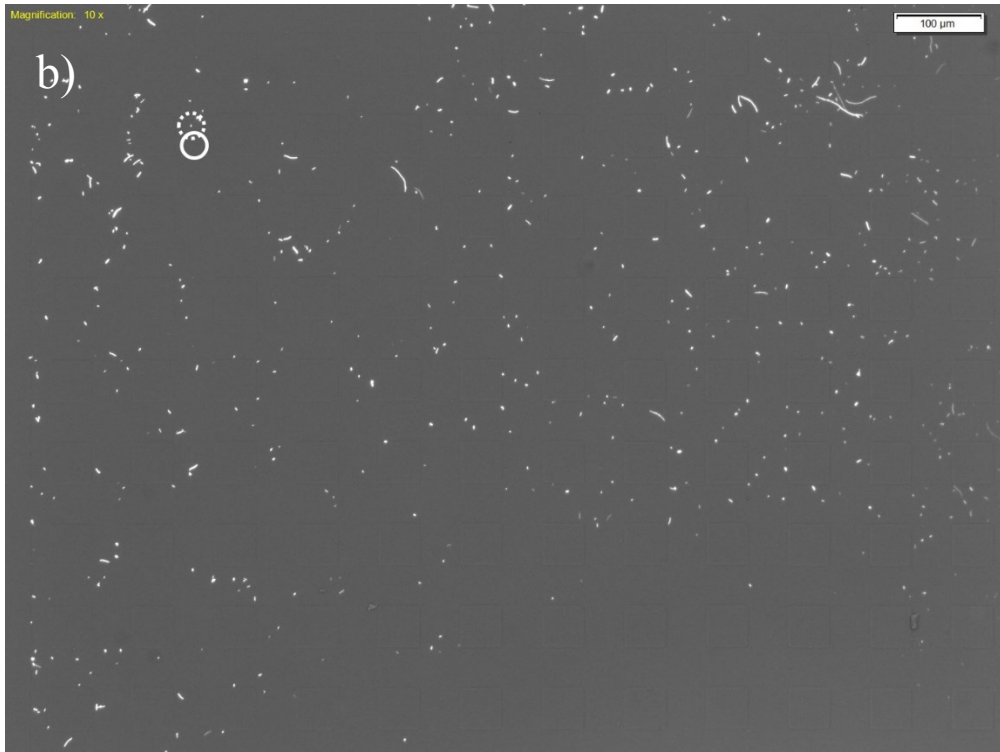
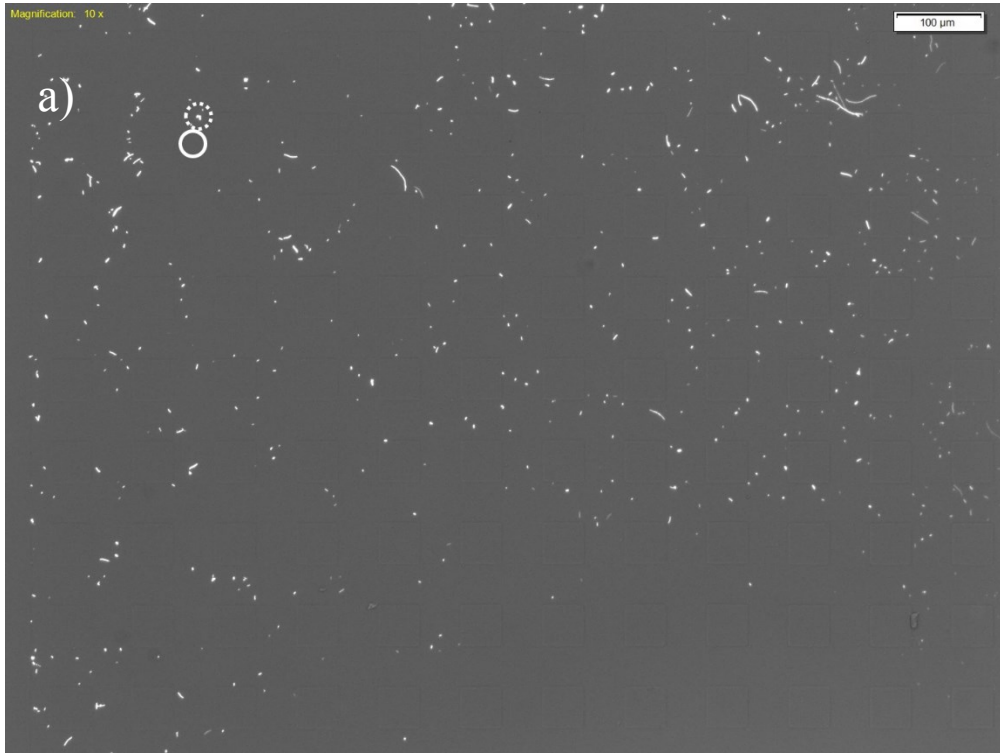
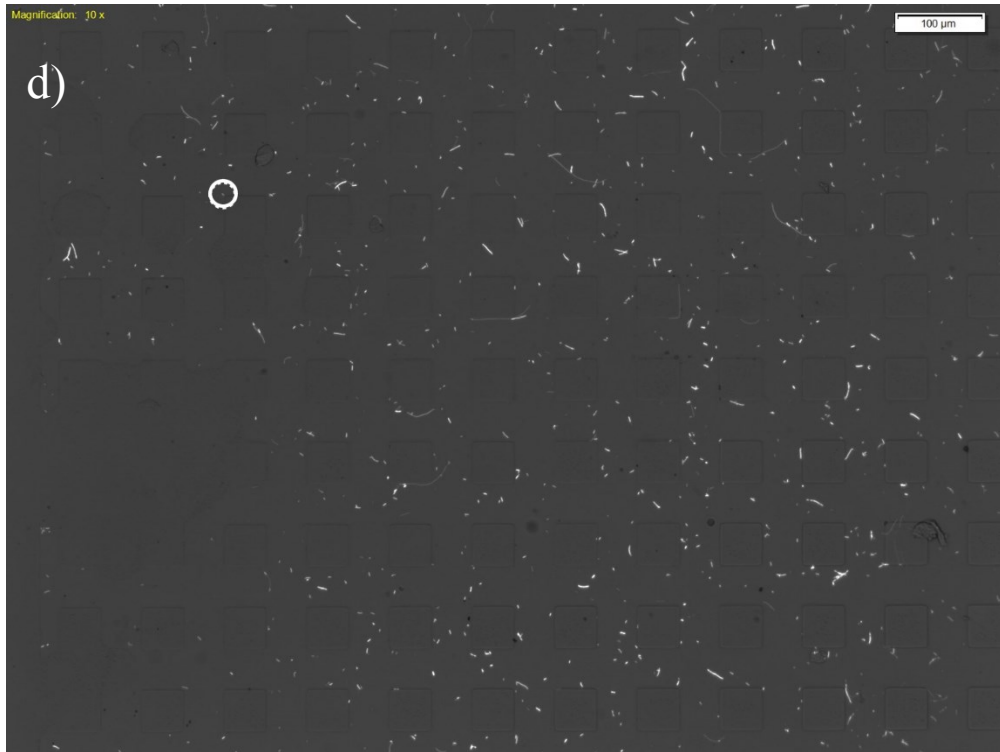
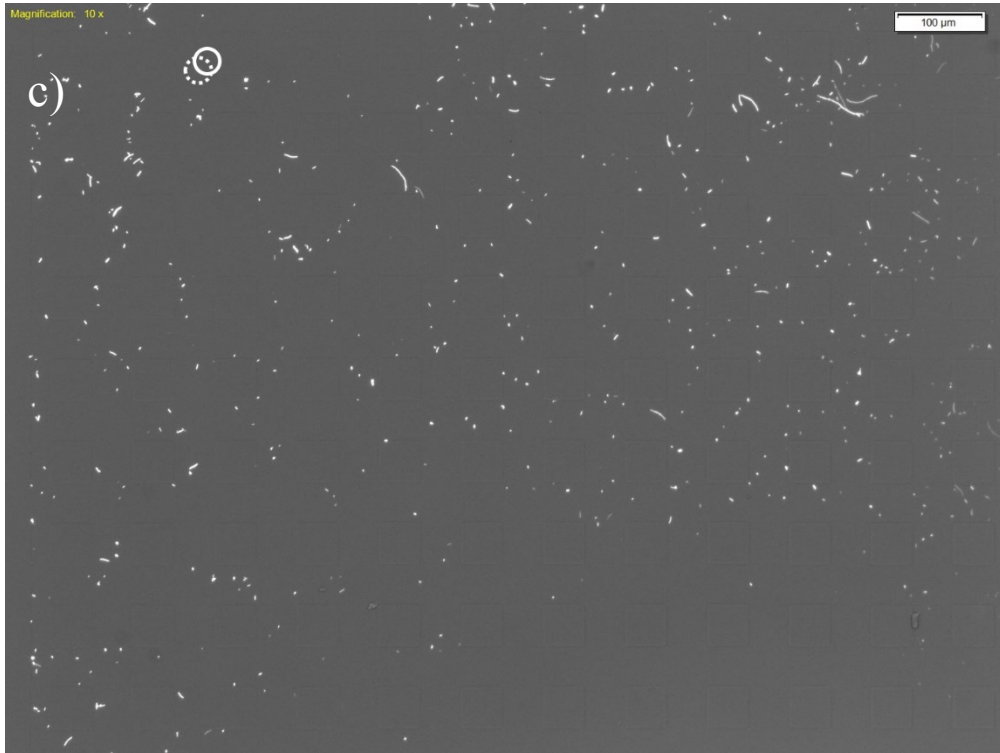


Figure A.4.5. Bacteria total displacement of 6 different analyzed bacteria (images a to f) at the end of 60 minutes for PT_E1 (images a to c) and PT_E2 (images d to f) at middle region at 45°





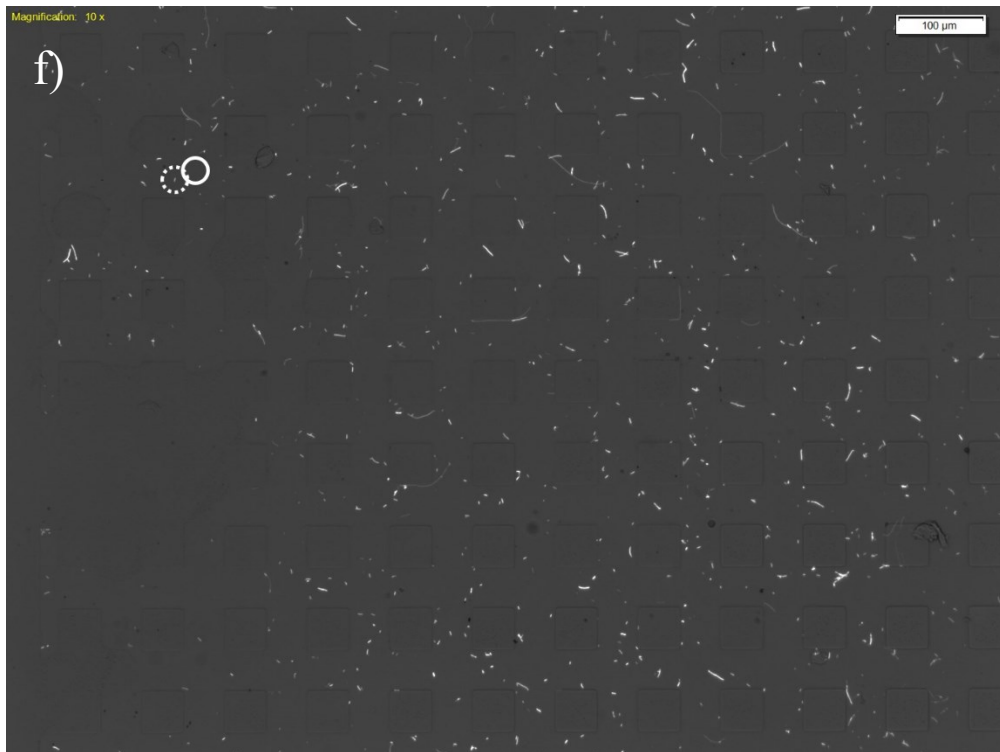
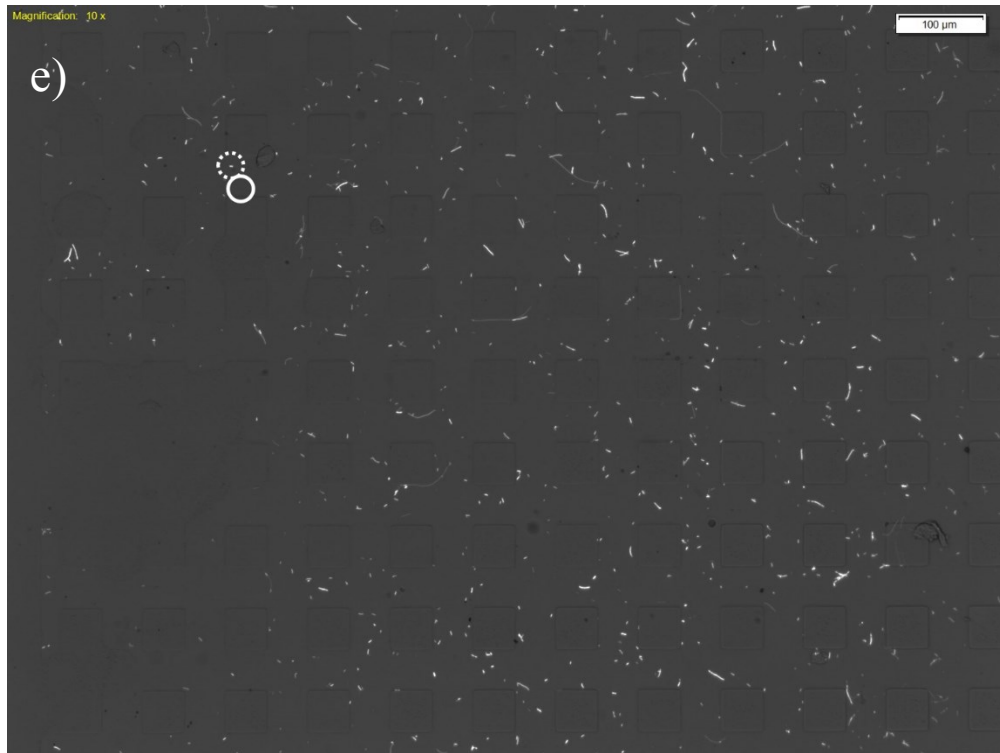
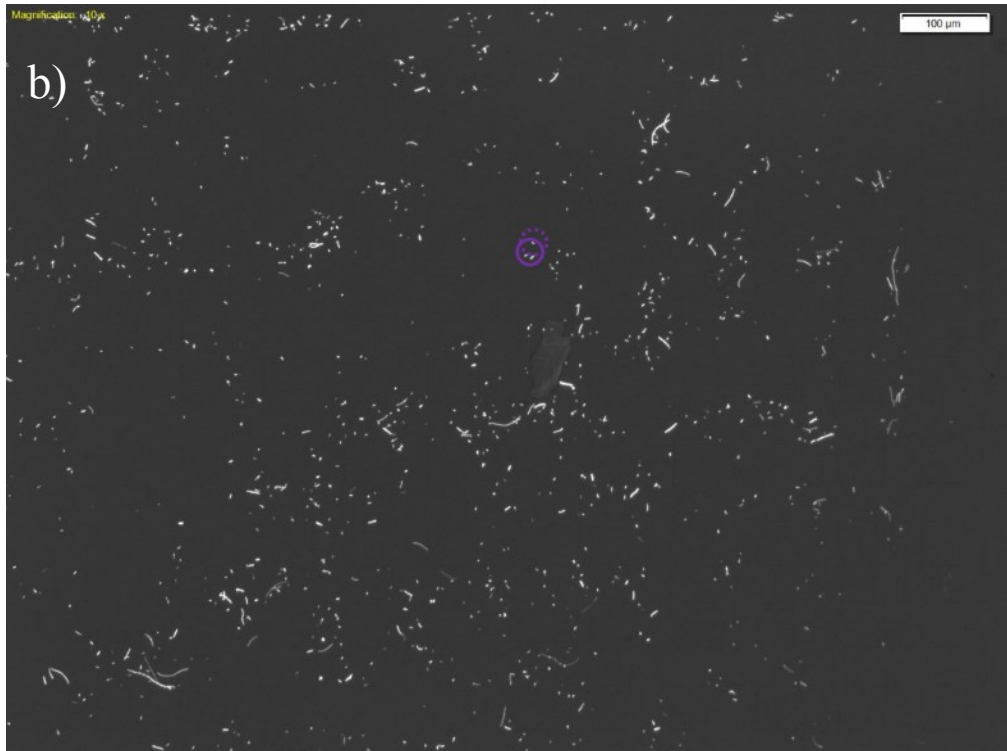
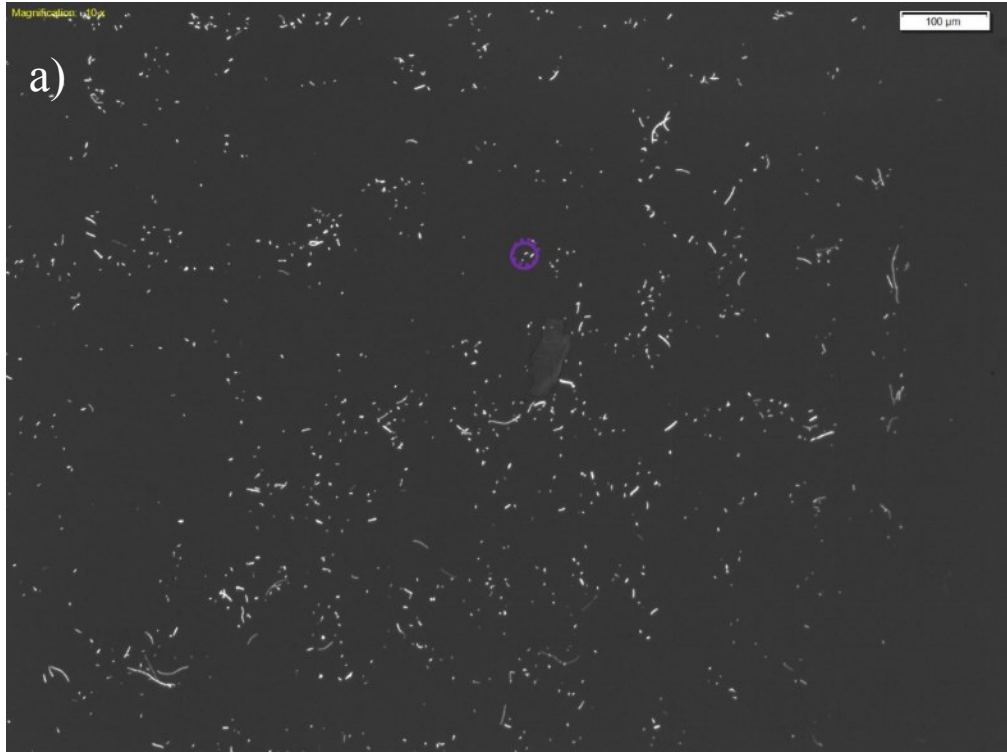
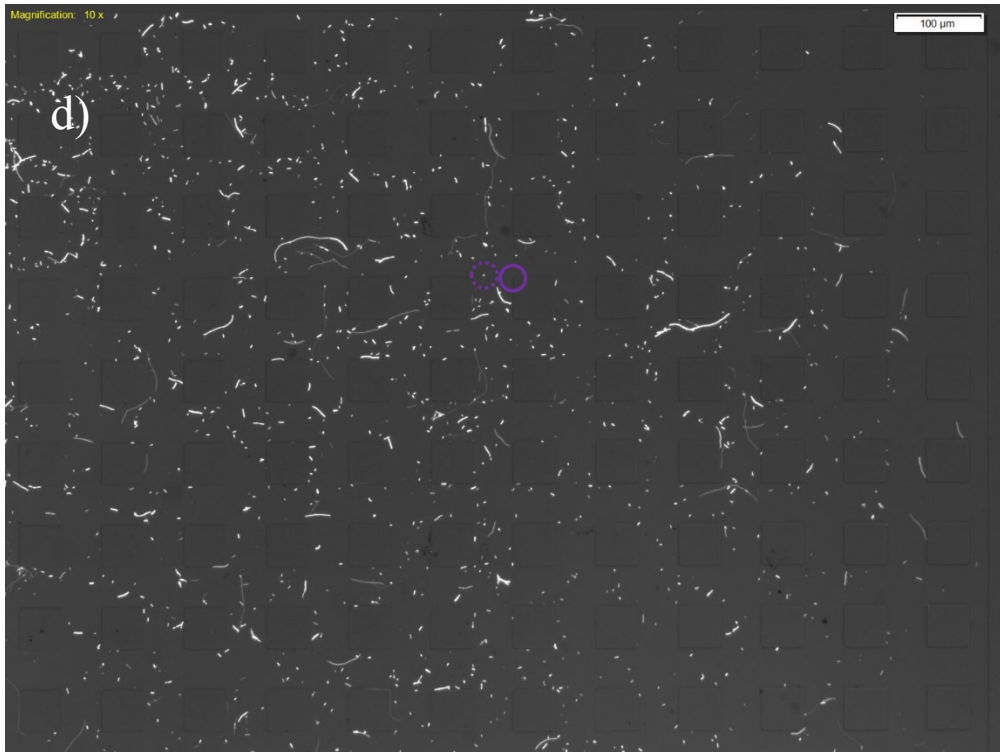
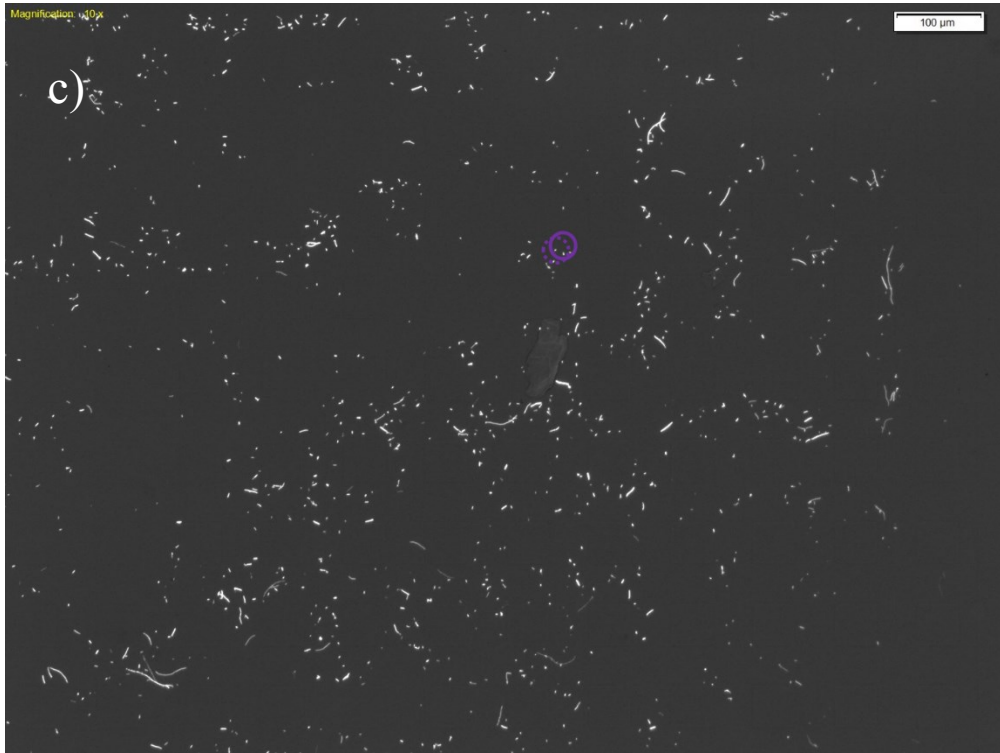


Figure A.4.6. Bacteria total displacement of 6 different analyzed bacteria (images a to f) at the end of 60 minutes for PT_E1 (images a to c) and PT_E2 (images d to f) at middle region at 15°





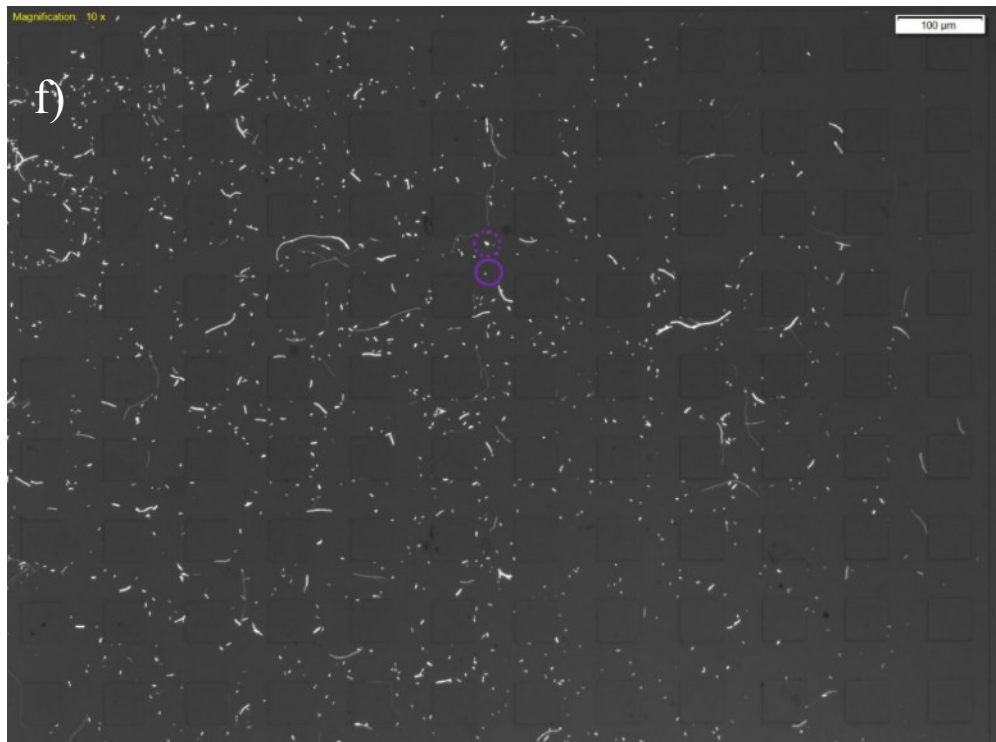
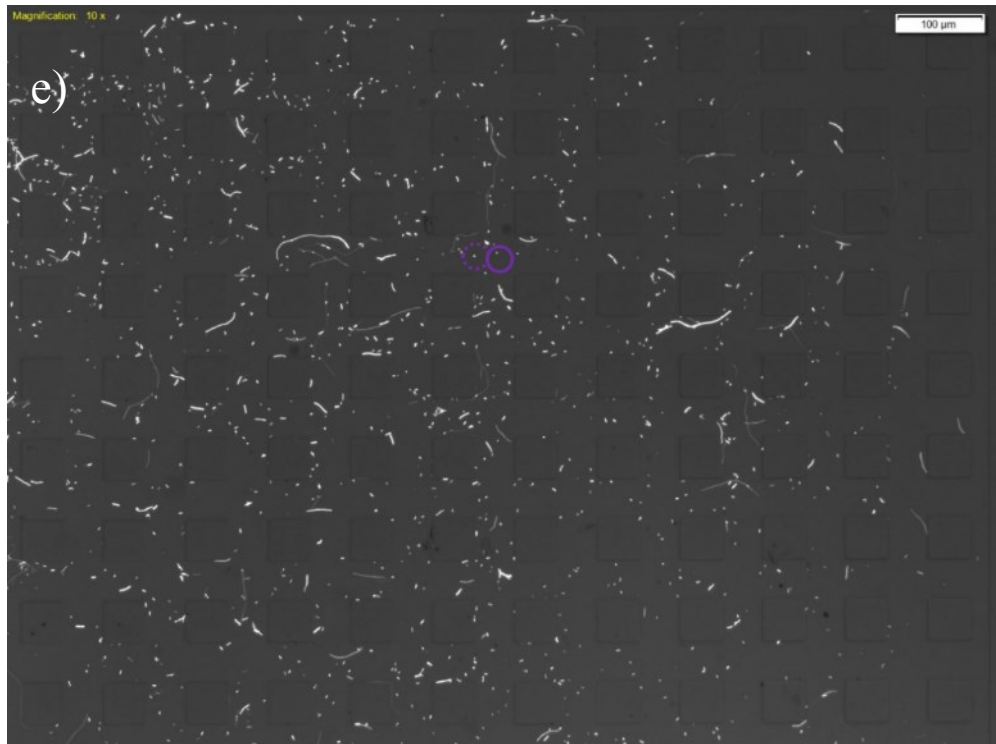
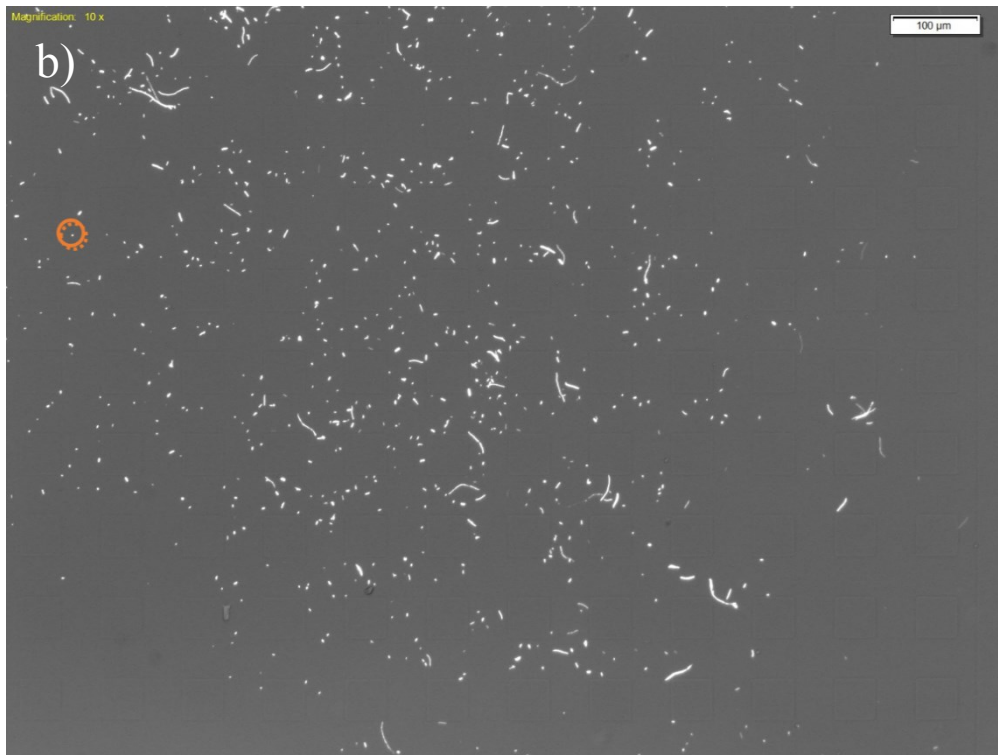
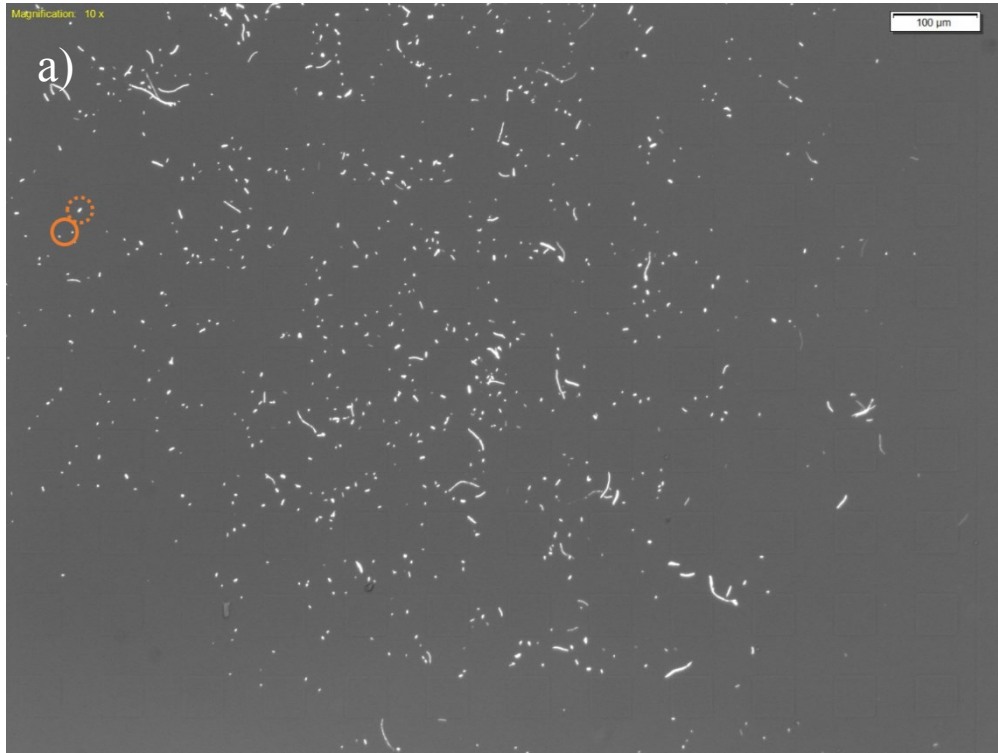
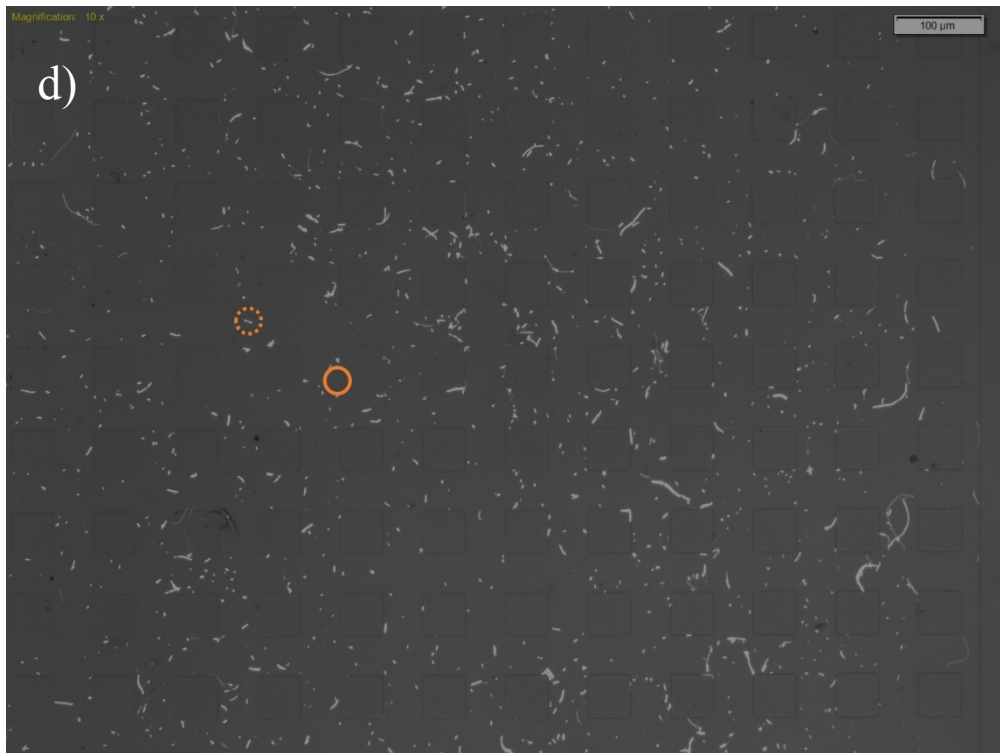
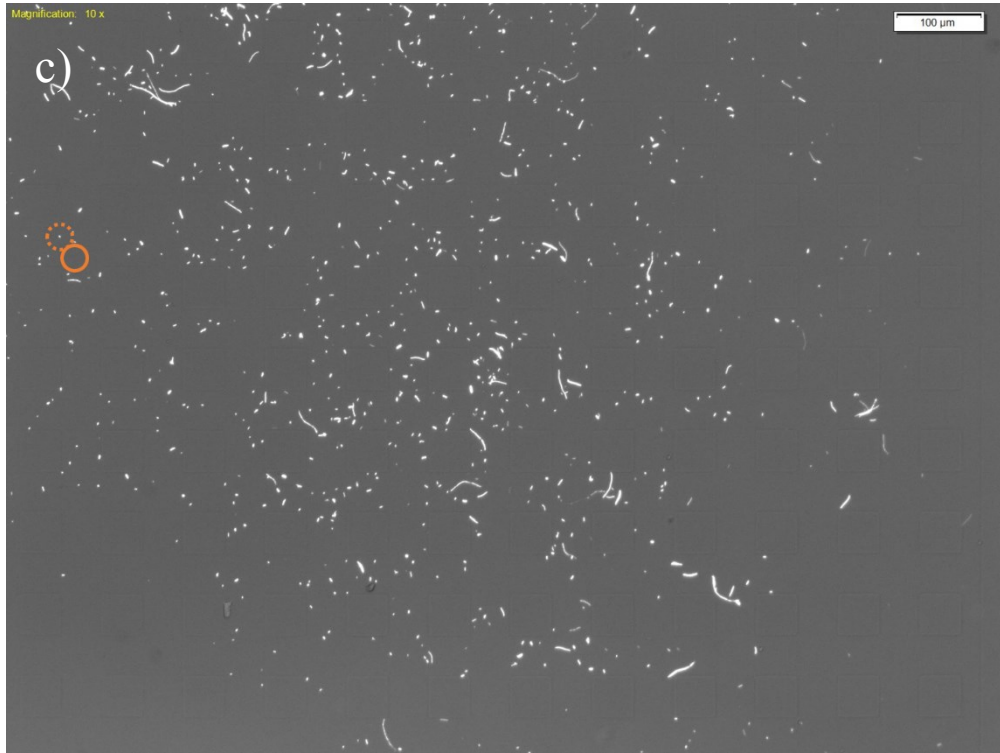


Figure A.4.7. Bacteria total displacement of 6 different analyzed bacteria (images a to f) at the end of 60 minutes for PT_E1 (images a to c) and PT_E2 (images d to f) at last region at 75°





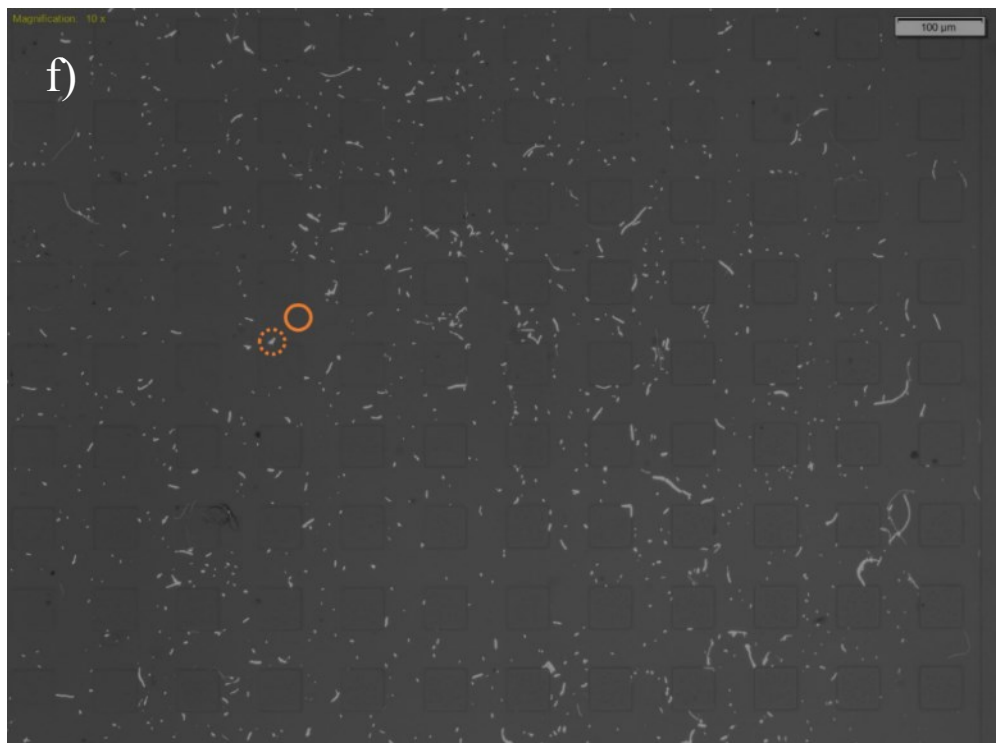
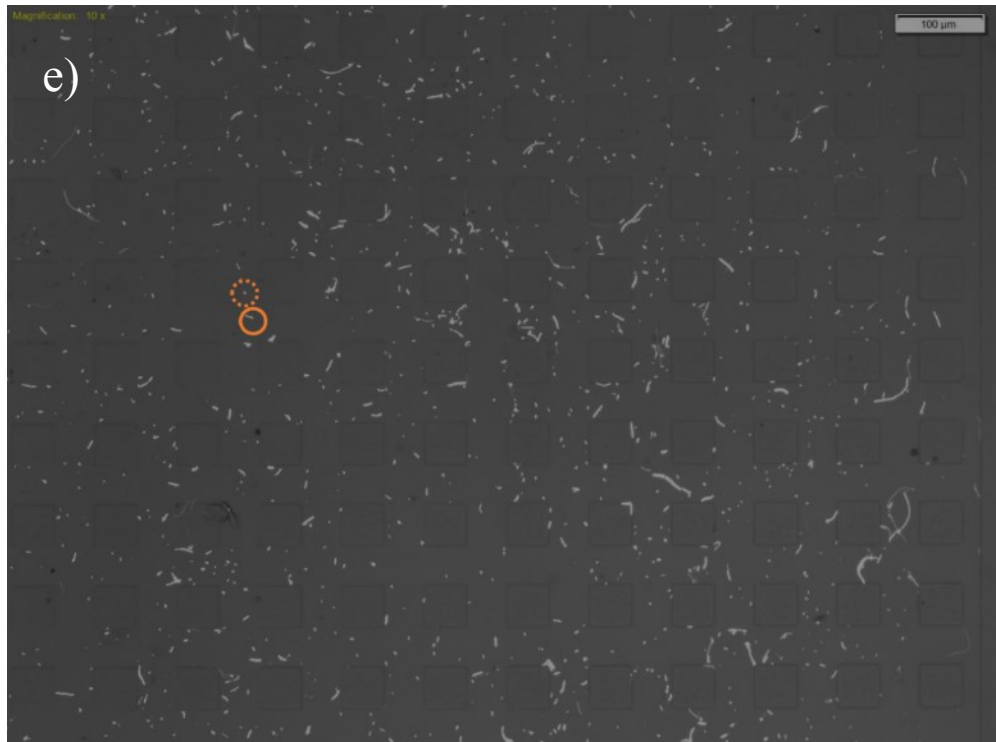
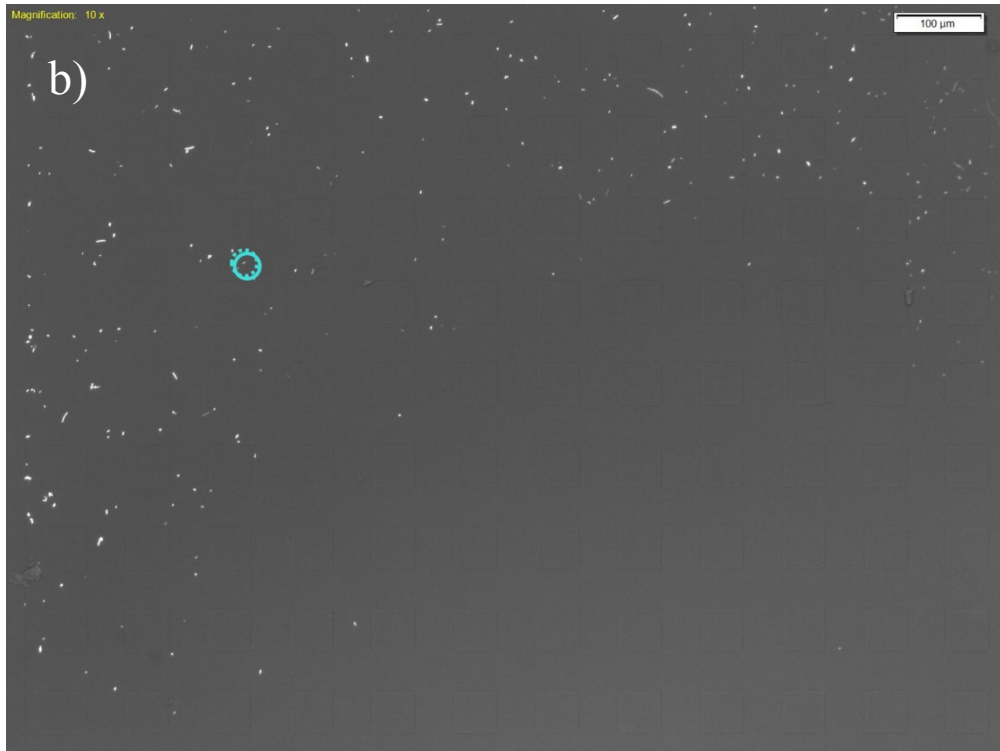
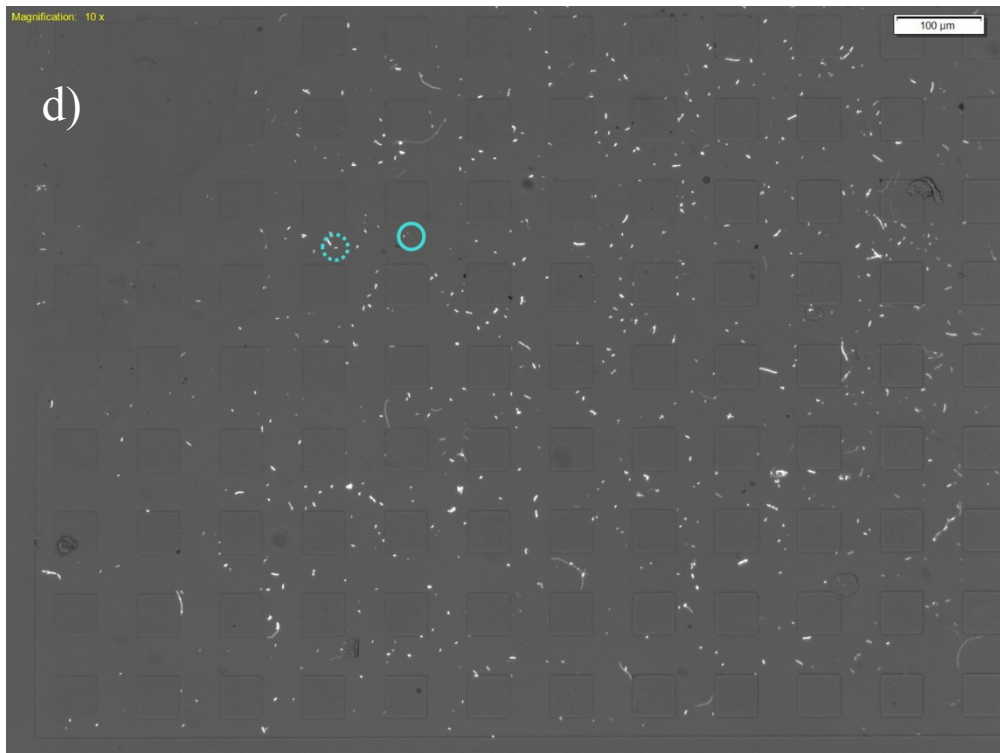


Figure A.4.8. Bacteria total displacement of 6 different analyzed bacteria (images a to f) at the end of 60 minutes for PT_E1 (images a to c) and PT_E2 (images d to f) at last region at 45°





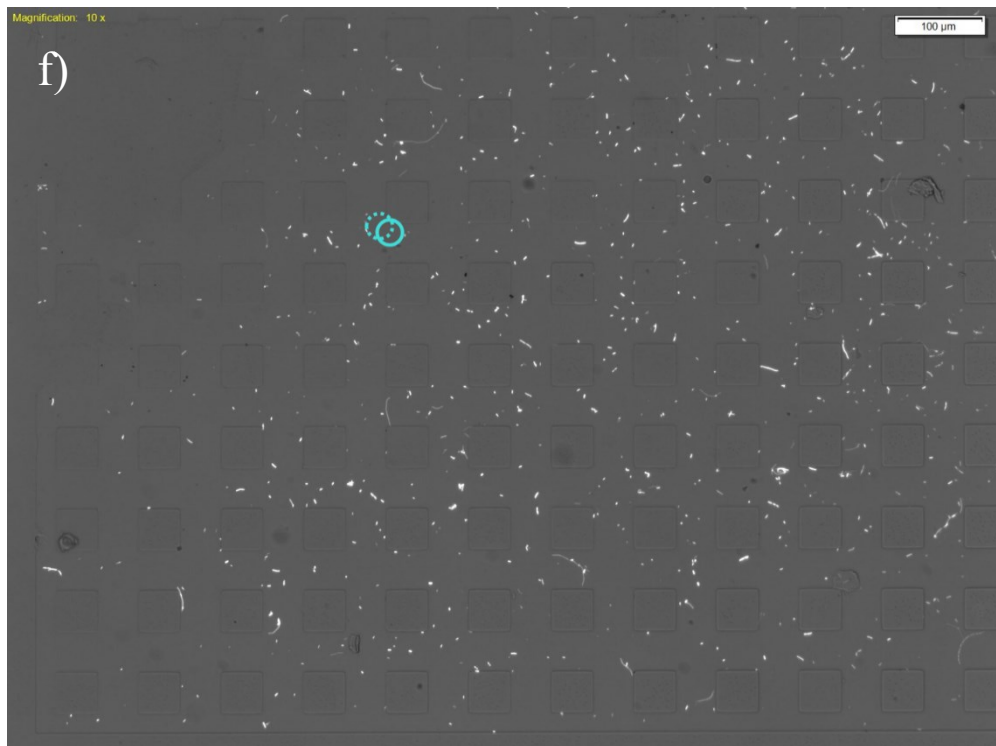
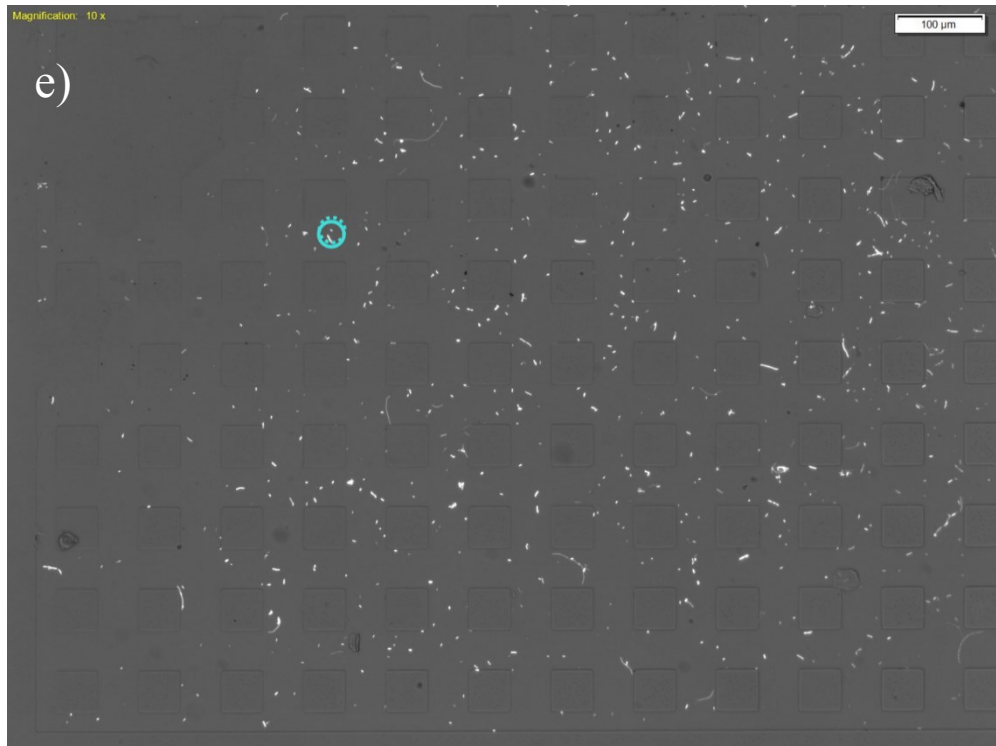


Figure A.4.9. Bacteria total displacement of 6 different analyzed bacteria (images a to f) at the end of 60 minutes for PT_E1 (images a to c) and PT_E2 (images d to f) at last region at 15°

A.5. Governing Equations for the Simulation of Particle Tracing, Transport of Species and Fluid Flow

I used COMSOL default equation for solving a laminar fluid flow in stationary form:

$$0 = \nabla \cdot [-p\mathbf{I} + \mu(\nabla\mathbf{u} + (\nabla\mathbf{u})^T)] + F$$

$$\rho\nabla \cdot (\mathbf{u}) = 0$$

Where P is pressure, μ is dynamic viscosity, \mathbf{u} is velocity field, F is volume force and ρ is density of the fluid. As for the initial conditions, initial magnitude of velocity field in both x and y directions are set to zero and pressure is set to 1 atm since the device is first filled with air and not pressurized. Flow rate into the inlet is set to a constant value of 0.01 ml/h and the outlets are set to atmosphere pressure since they are left open during the filling process.

For the simulation of transport of species, I used general form of convection equation in COMSOL and solved this equation for time frame of $t=0$ to $t=60$ min:

$$\frac{\partial c}{\partial t} + \nabla \cdot (-D\nabla c) + \mathbf{u} \cdot \nabla c = 0$$

$$\mathbf{N} = -D\nabla c + \mathbf{u}c$$

Where c is the concentration of the species, D is diffusion coefficient and \mathbf{u} is velocity field which is calculated from the simulation of laminar flow inside the device. I set the initial concentration of secondary agent to 0 (at $t=0$) and a constant concentration of this agent entering from the inlet.

I solved momentum equation for particles using COMSOL from t=0 to t=60 min to plot their trajectories during this time period:

$$m_p \frac{d\mathbf{v}}{dt} = \mathbf{F}$$

Where m_p is mass of the particle, v is the particle velocity which is calculated from the previous simulations and F is the force applied to a particle. I created a random distribution of the particles with initial velocity of 0 and defined F as a sum of chemotactic force, drag force and a third squeeze force.

A.6. Bacteria Displacement According to Time

Figures A.6.1 to A.6.9 show absolute displacement of bacteria in the first region (5 chambers away from the sub-inlet at 15°, 45°, and 75°) during 10-minutes time frames during the whole 60 minutes duration, for each of the control, antibiotic and phage experiments. In these figures D at t=30, for instance, indicates the displacement of bacteria during the time frame starting at t=20 minutes and ending at t=30 minutes considering t=0 is the moment when introduction of the secondary agent to the bacteria loaded inside the device is initiated. As shown in figures A.6.1 to A.6.9 bacteria displacement in most cases is relatively larger during the first 10 minutes of the experiment compared to any other 10-minutes time steps.

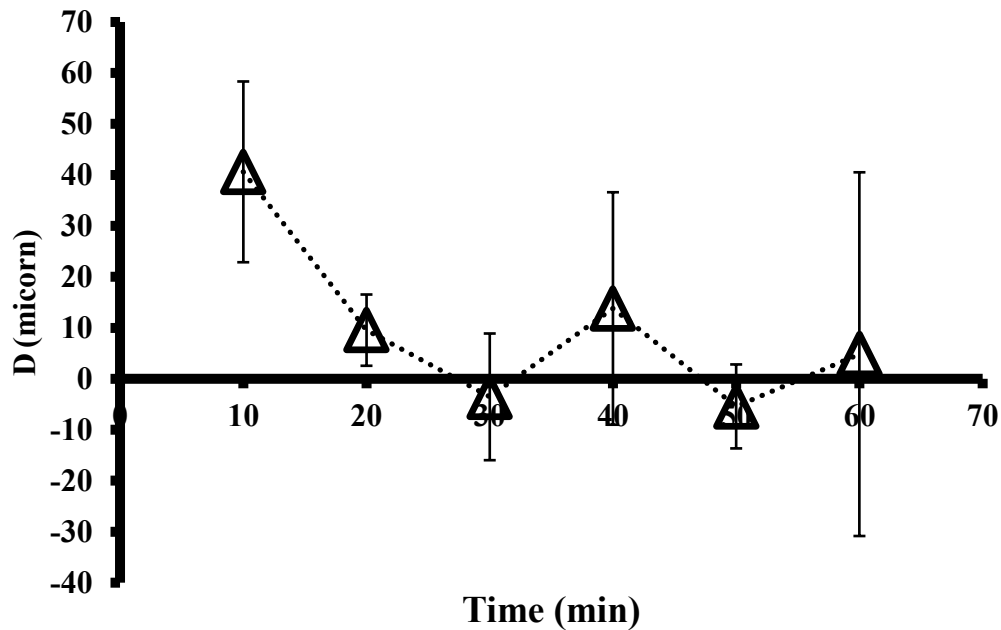


Figure A.6.1. Absolute displacement at time steps of 10 minutes for bacteria at distance of 5 chambers away from sub-inlet at 15° in control experiment

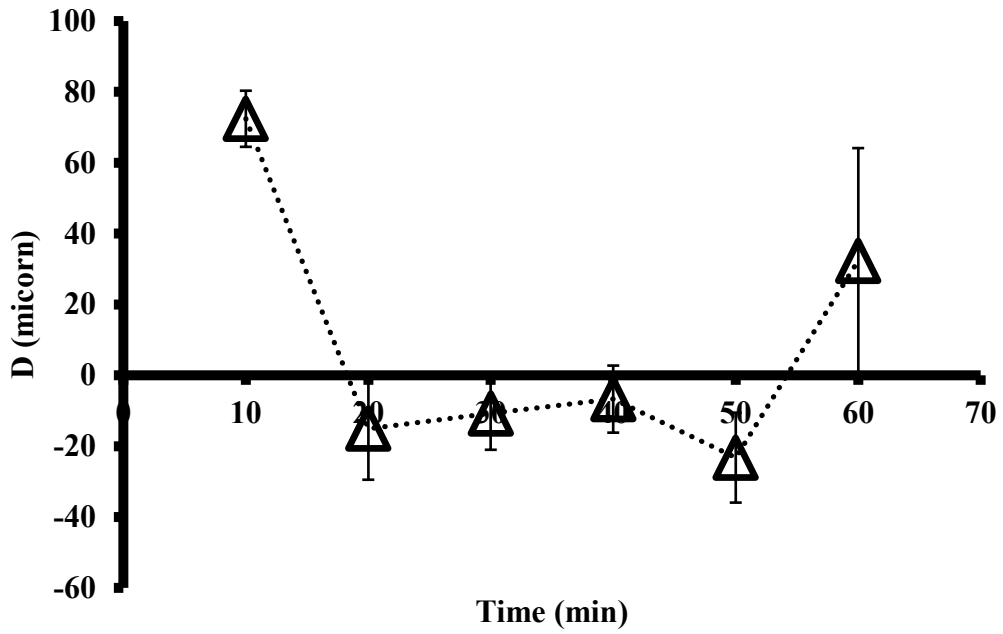


Figure A.6.2. Absolute displacement at time steps of 10 minutes for bacteria at distance of 5 chambers away from sub-inlet at 45° in control experiment

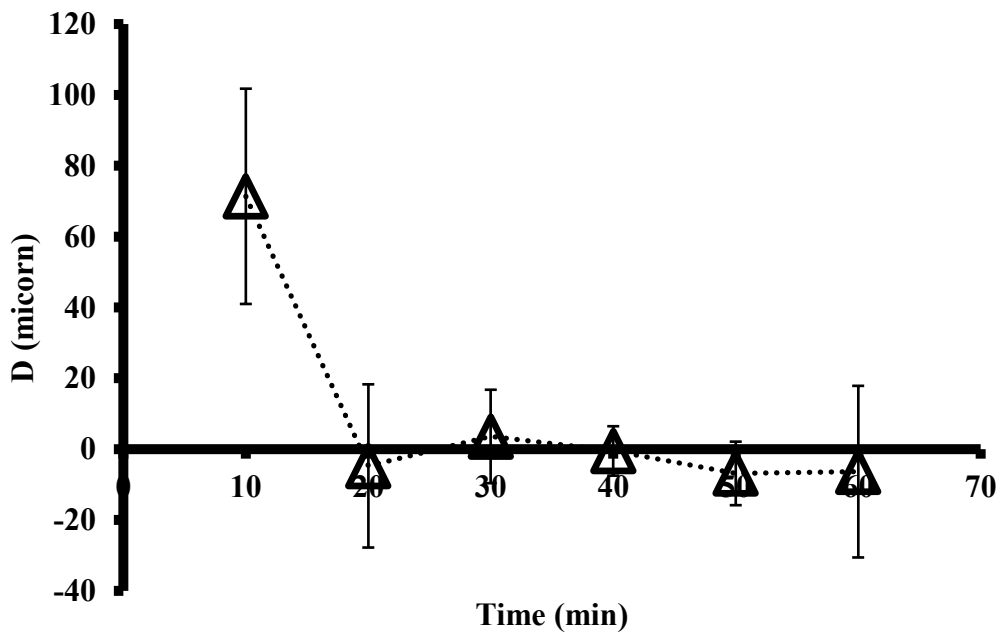


Figure A.6.3. Absolute displacement at time steps of 10 minutes for bacteria at distance of 5 chambers away from sub-inlet at 75° in control experiment

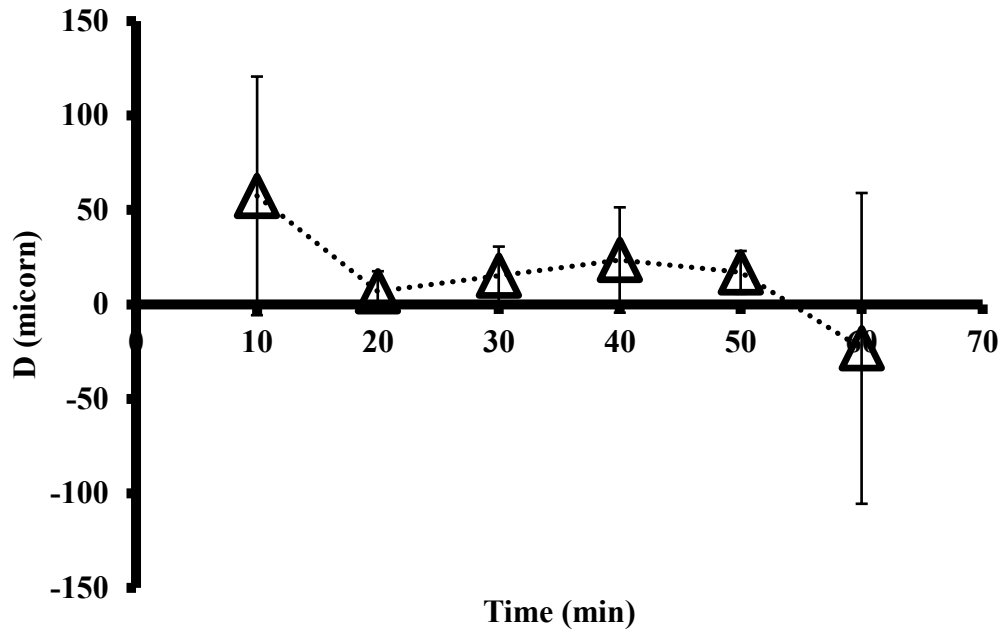


Figure A.6.4. Absolute displacement at time steps of 10 minutes for bacteria at distance of 5 chambers away from sub-inlet at 15° in antibiotic experiment

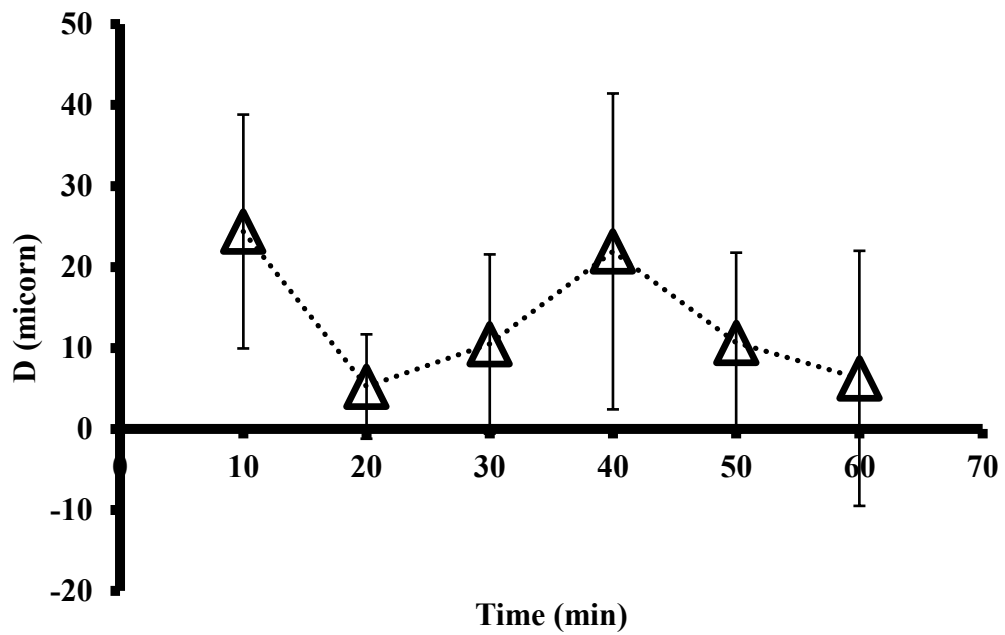


Figure A.6.5. Absolute displacement at time steps of 10 minutes for bacteria at distance of 5 chambers away from sub-inlet at 45° in antibiotic experiment

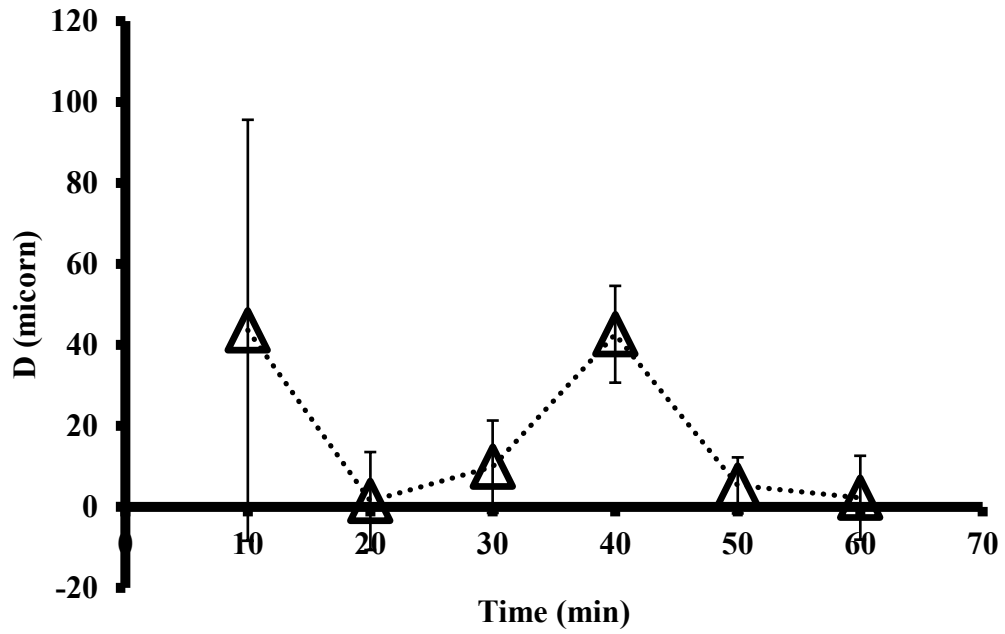


Figure A.6.6. Absolute displacement at time steps of 10 minutes for bacteria at distance of 5 chambers away from sub-inlet at 75° in antibiotic experiment

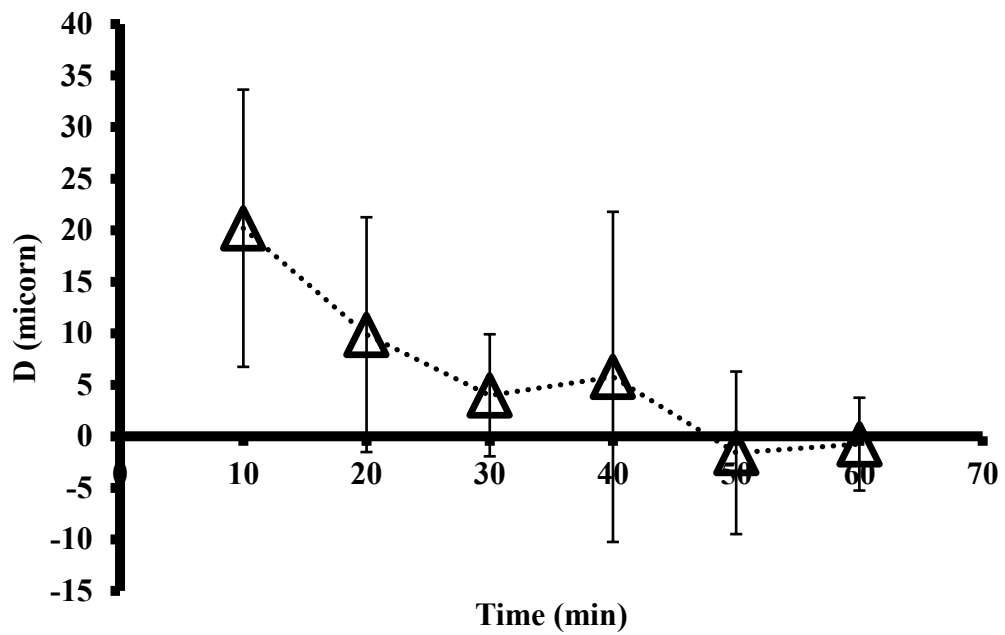


Figure A.6.7. Absolute displacement at time steps of 10 minutes for bacteria at distance of 5 chambers away from sub-inlet at 15° in phage experiment

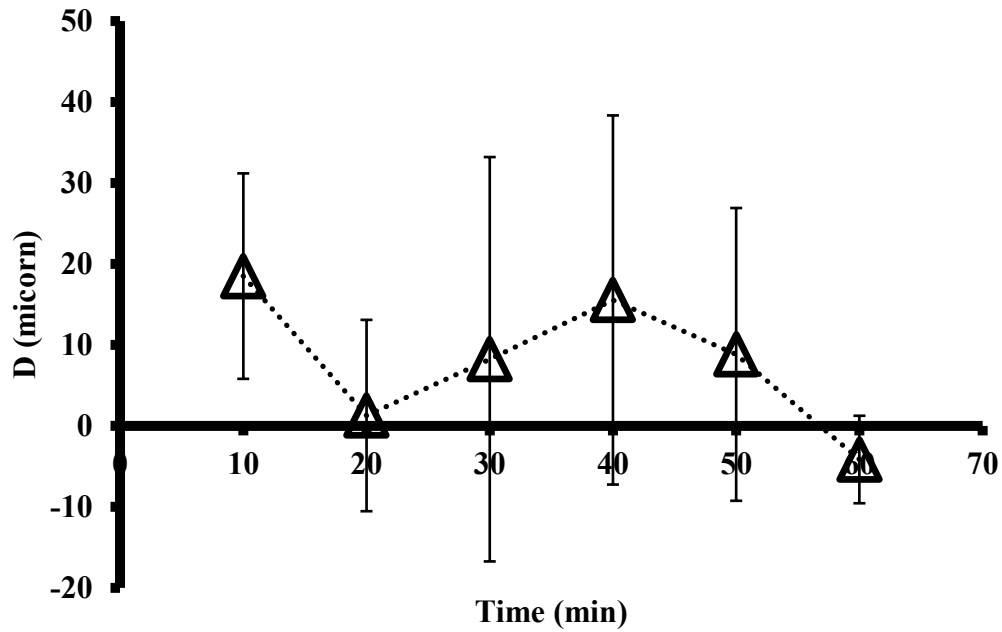


Figure A.6.8. Absolute displacement at time steps of 10 minutes for bacteria at distance of 5 chambers away from sub-inlet at 45° in phage experiment

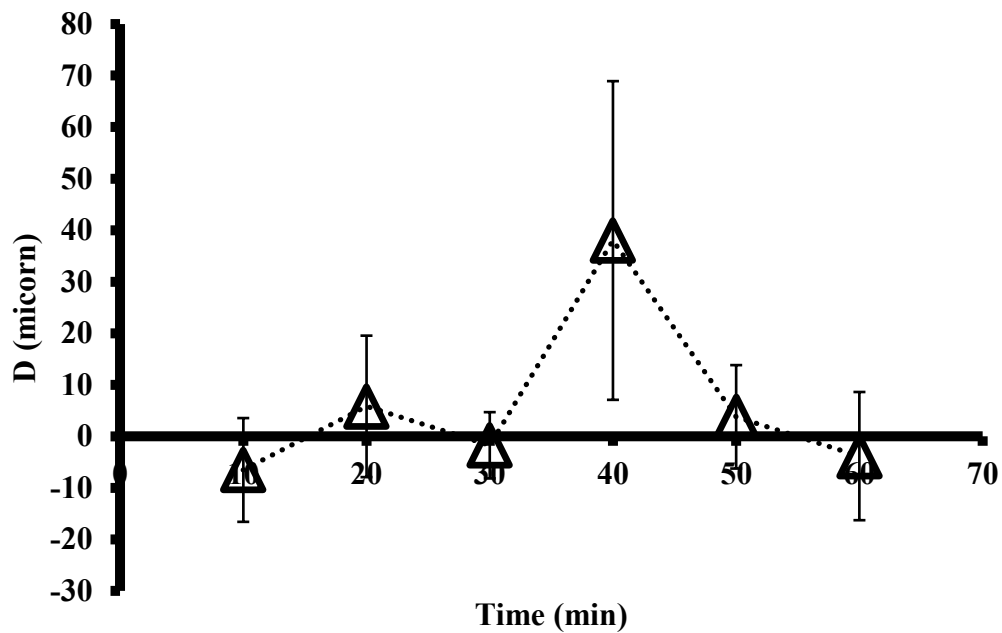


Figure A.6.9. Absolute displacement at time steps of 10 minutes for bacteria at distance of 5 chambers away from sub-inlet at 75° in phage experiment